



HAL
open science

Impact of increasing temperature up to 80 °C on the behaviour of radionuclides in the Callovo-oxfordian formation : application to uranium

Flávia Marina Serafim Maia

► To cite this version:

Flávia Marina Serafim Maia. Impact of increasing temperature up to 80 °C on the behaviour of radionuclides in the Callovo-oxfordian formation : application to uranium. Materials Science [cond-mat.mtrl-sci]. Ecole nationale supérieure Mines-Télécom Atlantique, 2018. English. NNT : 2018IMTA0078 . tel-01950349

HAL Id: tel-01950349

<https://theses.hal.science/tel-01950349>

Submitted on 10 Dec 2018

HAL is a multi-disciplinary open access archive for the deposit and dissemination of scientific research documents, whether they are published or not. The documents may come from teaching and research institutions in France or abroad, or from public or private research centers.

L'archive ouverte pluridisciplinaire **HAL**, est destinée au dépôt et à la diffusion de documents scientifiques de niveau recherche, publiés ou non, émanant des établissements d'enseignement et de recherche français ou étrangers, des laboratoires publics ou privés.

THESE DE DOCTORAT DE

L'ÉCOLE NATIONALE SUPERIEURE MINES-TELECOM ATLANTIQUE
BRETAGNE PAYS DE LA LOIRE - IMT ATLANTIQUE
COMUE UNIVERSITE BRETAGNE LOIRE

ÉCOLE DOCTORALE N° 596

Matière, Molécules, Matériaux

Spécialité : Science des Matériaux

Par

Flávia Marina Serafim MAIA

Impact de l'élévation de la température jusqu'à 80°C sur le comportement des radionucléides dans le Callovo-Oxfordien : application à l'uranium

Thèse présentée et soutenue à Nantes, le 30/05/2018

Unité de recherche : Subatech – Laboratoire de Physique Subatomique et des Technologies Associées

Thèse N° : 2018IMTA0078

Rapporteurs avant soutenance :

Christophe Tournassat HDR, Ing. de Recherche, BRGM

Emmanuel Tertre Professeur, Université de Poitiers

Composition du Jury :

Président : Bernd Grambow

Professeur à IMTA, Subatech

Examineurs : Christophe Tournassat HDR, Ing. de Recherche, BRGM

Emmanuel Tertre Professeur, Université de Poitiers

Bart Baeyens Chercheur Dr., PSI

Gilles Berger HDR, IRAP

Dir. de thèse : Gilles Montavon HDR, Subatech

Co-dir. de thèse : Mireia Grivé Docteur, Amphos21 Consulting S.L. Spain

Invité(s)

Lara Duro Docteur, Amphos21 Consulting S.L.

Thomas Vercouter Chercheur Dr., CEA Saclay

Benoît Madé Docteur, Andra

DOCTORAL THESIS FROM

IMT ATLANTIQUE

COMUE UNIVERSITY OF BRETAGNE LOIRE

DOCTORAL SCHOOL N° 596

Matter Molecules and Material

Specialisation: Material Sciences

by

Flávia Marina Serafim MAIA

Impact of increasing the temperature up to 80 °C on the behaviour of radionuclides in the Callovo-Oxfordian Formation: application to Uranium

Thèse présentée et soutenue à Nantes, le 30/05/2018

Unité de recherche : Subatech – Laboratoire de Physique Subatomique et des Technologies Associées

Thèse N°: 2018IMTA0078

Reviewers before defence:

Christophe Tournassat HDR, Research Eng., BRGM
Emmanuel Tertre Professor, Université de Poitiers

Composition du Jury :

President:	Bernd Grambow	IMTA Professor, Subatech
Reviewers:	Christophe Tournassat	HDR, Research Eng., BRGM
	Emmanuel Tertre	Professor, University of Poitiers
	Bart Baeyens	PhD. Researcher, PSI
	Gilles Berger	HDR, IRAP
Thesis director:	Gilles Montavon	HDR, Subatech
Thesis Co-dir.:	Mireia Grivé	PhD., Amphos21 Consulting S.L.

Inviter(s)

Lara Duro	PhD., Amphos21 Consulting S.L.
Thomas Vercouter	PhD. Researcher, CEA Saclay
Benoît Madé	PhD., Andra

*Aos meus mais que tudo:
Mãe, Pai e a minha querida irmã Cristina*

Acknowledgements

I am not a person of many writing words, I spent most of my time talking and all my thanks were given to each one of you in particular and by person. Although, I want to leave it registered here. Most probably I will forget someone, but no hard feelings on me please! It's already quite difficult to find the right words to describe what each one of you have contributed for this period of my life.

First and foremost, I would like to thank my parent as this thesis came to existence due to their amazing support, not only because they are my parents and gave birth to me but also because of their enthusiastic motivation to always follow my dreams and goals, and especially for their patience for my curiosity and questioning everything!

Thanks go to my supervisors for their support during this project. Mireia Grivé, I want to thank her for first inviting me to start this PhD. Our distance made the communication between us more difficult but in the end, I am thankful to her for being there in the crucial moments of this long journey. To Gilles Montavon, I thank him for all his time, dedication and support during these 3 ½ years. Especially for being there whenever needed, always finding the time among his numerous students and for our long discussions into late Friday afternoons.

This thesis could not have been done without the financial support from Andra. Andra is thanked for the GL-CTEC PhD scholarship which allowed me to undertake this project. I am therefore thankful to Benoît Madé and Eric Giffaut, from Andra, for their supervision and direction.

I must also thank Subatech especially the Radiochemistry group for the warmly welcome. I thank in particular Solange Ribet, Céline Bailly and Axelle Dupont for their help, discussions and technical support. Also, Catherine Landesman for our scientific discussions.

To my AMAZING colleagues and friends at Subatech: Iuliia, Ning, Christophe, Benjamin, Hugues, Andreas, Yahaya, Soumaya, Amaury, Arnaud and Étienne thank all of you guys for our long frenchinglish coffee times and for making my days at work cheerful and very pleasant.

Very special thanks to Ona, Bea, Laurent and Sara for their encouragement and for their emotional support given at the most difficult moments of this journey. Without you guys I would be most probably doing something completely different by now! Not that that would be bad but the feeling of finishing a thesis awesome, without support I would never be able to live this! Oh, additional thanks to Sara for her excellent work on the edition of my manuscript and scientific advice for the writing of this thesis.

And last but not least, I thank the person that stayed by my side during the last period of this journey. I know that we have not known each other for long and we met during the most difficult and hard

phase of the PhD, the moment that I was about to finish it! I am very grateful to Adrien for his patience (sometimes not that much!) during my long days of writing and my mood swings. And most important of all for showing me that life is not only a PhD.

Table of Contents

Acknowledgements	v
List of Figures	xi
List of Tables.....	xvii
Résumé Étendu.....	xxiii
Chaper 1 Introduction	29
1.1. Context	31
1.1.1. Characterisation of the Callovo-Oxfordian Formation System.....	32
1.1.1.1. Chemical composition of the Callovo-Oxfordian porewater	34
1.2. Scopes of the thesis work	35
1.3. References	36
Chaper 2 Speciation of Ca-U(VI)-CO₃ ternary complexes.....	39
2.1. Introduction	39
2.1.1. Ca-U(VI)-CO ₃ system	39
2.1.1. Mg-U(VI)-CO ₃ system	42
2.1.1. Effect of temperature.....	42
2.2. Determination of the thermodynamic data of Ca-U(VI)-CO ₃ aqueous species.....	44
2.2.1. Ionic Exchange Method.....	44
2.2.1.1. Experimental approach.....	45
2.2.1.1.1. Materials and Solutions	45
2.2.1.1.2. Batch experiments	46
2.2.1.2. Conceptual model.....	48
2.2.1.2.1. Numerical approach	49
2.2.1.2.2. Application of the conceptual model on Dong and Brooks (2006) experimental data.....	50
2.3. Results	51
2.3.1. Experimental tests	51
2.3.1.1. Controlling test on temperature and pCO ₂	51
2.3.1.1.1. Controlling test on the initial concentration of U(VI) and electrolyte background.....	52
2.3.1.2. Determination of the stability constants in Ca-U(VI)-CO ₃ -H ₂ O systems at different temperatures ...	54

2.3.1.2.1. In the absence of calcium	54
2.3.1.2.2. In the presence of calcium.....	58
2.3.1.2.2.1. Fitting with PEST	59
2.3.1.2.2.2. Benchmark of fitting using 2D mapping	61
2.3.1.2.3. Evaluation of stability constants and enthalpy of reaction	62
2.3.1.2.4. Comparison with previous literature data.....	65
2.4. Summary	68
2.5. References	69
Chaper 3 Behaviour of Uranium in Callovo-Oxfordian Formation at 20 °C	73
3.1. Introduction	73
3.1.1. Background	74
3.1.1.1. What are clay minerals?	74
3.1.1.2. What are the retention processes?	77
3.1.1.2.1. How to describe the retention processes?.....	77
The retention mechanisms:.....	78
Description and quantification of surface mechanisms:.....	79
3.1.1.2.2. How to interpolate sorption models on natural samples?.....	82
3.2. Experimental work	85
3.2.1. Uranium sorption edge and isotherm experiments	87
3.3. Sorption of U(VI) on illite.....	87
3.3.1. In the absence of carbonate	87
3.3.2. In the presence of carbonate	89
3.3.3. Impact of the presence of Ca-U(VI)-CO ₃	95
3.4. Sorption of U(VI) on Callovo-Oxfordian clay fraction.....	97
3.4.1. In the absence of carbonate	97
3.4.2. In the presence of carbonate	97
3.4.3. Impact of the presence of Ca-U(VI)-CO ₃	98
3.5. Sorption of U(VI) on Callovo-Oxfordian claystone.....	99
3.6. Summary	103
3.7. References	105
Chaper 4 Impact of the temperature on the sorption of U(VI) in the Callovo-Oxfordian Formation.....	109
4.1. Introduction	109
4.1.1. Thermodynamic parameters for sorption processes	110
Protolysis reactions:	110
Ionic exchange and surface complexation reactions:	111
4.1.2. Conceptual approach	111

4.2. Effect of the temperature on the adsorption processes of uranium on clays and clay minerals	112
4.2.1. Experimental approach.....	112
4.2.2. Model Approach.....	113
4.2.3. U(VI)/illite system in temperature up to 80°C.....	116
4.2.3.1. In the absence of carbonate	116
Experimental data:.....	116
Modelling results:.....	117
4.2.3.2. In the presence of carbonate	124
Experimental data:.....	124
Modelling Results:	126
4.2.4. U(VI)/ Callovo-Oxfordian clay fraction system at 80°C.....	128
4.2.5. Impact of Ca-U(VI)-CO ₃ on the retention of U(VI) at 80 °C	130
4.3. Summary	132
4.4. References	134
Chaper 5 Conclusions	137
5.1. Perspectives.....	139
Appendix A: Material and Methods.....	141
A.1. ICP-MS analysis:.....	141
A.1.1. Optimisation method	141
Internal standard solution:	142
Internal standard correction:.....	142
Calibration curve:	142
A.2. TOC Analyser:.....	144
Method of measurement.....	144
Uncertainty of measurement:	145
A.3. Determination of the alkalinity:.....	145
A.4. pH measurements	145
A.5. Stock solutions	146
Calcium, Sodium and carbonate:.....	146
Uranium:.....	146
Synthetic Callovo-Oxfordian porewater:	146
A.6. Solid phases:.....	147
Anion Exchange resin:	147
Callovo-Oxfordian claystone:	147
Callovo-Oxfordian clay fraction:	148
Illite:	149

A.7. Batch experiments procedures.....	150
A.7.1. Open system (atmospheric conditions) procedure:.....	151
A.7.2. Closed system (controlled atmosphere) procedure:.....	151
Appendix B: Auxiliary calculations.....	153
B.1. Calculation of the amount of exchanger considered in the resin.....	153
B.2. Calculation of the sorption parameters of clay minerals.....	153
B.3. Calculation of the concentration of U(VI) sorbed on the solid:.....	154
B.4. Calculation of distribution coefficient of U(VI):.....	154
Appendix C: Experimental results.....	155
C.1. Complementary tests.....	155
C.1.1. Temperature control test:.....	155
C.1.2. Sealing control test:.....	158
C.1.3. Tightness control test:.....	160
C.1.4. PPCO tubes control tests:.....	161
Total Organic Carbon:.....	161
C.2. Chemical composition of stock solutions:.....	164
C.3. Speciation of Ca-U(VI)-CO ₃ species experimental results:.....	164
C.4. Kinetic experiments.....	168
C.4.1. Callovo-Oxfordian claystone:.....	168
C.4.2. Illite:.....	169
C.5. Illite: sorption experiments.....	170
C.5.1. Sorption isotherms:.....	170
C.5.2. Sorption edges:.....	185
C.6. Callovo-Oxfordian clay fraction: sorption isotherm experiments.....	188
C.7. Callovo-Oxfordian claystone samples: isotherm experiments.....	194
Appendix D: Modelling results.....	197
D.1. Geochemical modelling literature data for the Ca-U(VI)-CO ₃ ternary species.....	197
D.2. Ionic exchange method.....	200
D.2.1. Type I experiments ($\Delta S/L$):.....	200
D.2.2. Type II experiments (ΔCa):.....	201
Appendix E: Thermodynamic data.....	205
Appendix F: PEST and Phreeqc files.....	207
PEST input files:.....	207
20 °C and 1% of CO ₂ (g) as a function of S/L ratio.....	207
80 °C and 5% of CO ₂ (g) [U(VI)] as a function of calcium.....	210
Phreeqc input files:.....	213

List of Figures

Figure 1. Schematic representation of deep geological nuclear waste disposal multi-barrier system (1) Callovo-Oxfordian host-rock; (2) engineered barrier for IWL; (3) engineered barrier for HWL; (4) and (5) HWL primary package (e.g. vitrified waste).	30
Figure 2. Schematic pathway for the safety assessment of the nuclear disposal.....	31
Figure 3. Schematic representation of U(VI) controlling processes in radioactive waste disposal system using host-clay rock. The main processes concerning in the present study are highlighted in red.	32
Figure 4. Geological location of the underground research laboratory within the Paris Basin (upper) and cross section of the geological formations surrounding the underground research laboratory. Adapted from Linard et al., 2011.	33
Figure 5. Calculated U(VI) speciation as a function of calcium concentrations between 0 and $5 \cdot 10^{-3}$ M at 25 °C, $[U(VI)]_{\text{total}} = 1 \cdot 10^{-8}$ M, $[CO_3^{2-}]_{\text{total}} = 3 \cdot 10^{-3}$ M, pH = 7.2 and ionic strength of 0.1 M using NaNO ₃ as electrolyte. Calculations performed with ThermoChimie database v9b.....	41
Figure 6. Scheme of the experimental set-up for the closed system experiments.	47
Figure 7. Experimental data originated from supporting information of Dong and Brooks (2006). Fit approach of the a) U(VI) sorbed onto resin as function of U(VI) in equilibrium in solution and b) the distribution of U(VI) as a function of calcium.	50
Figure 8. Mineral saturation index as a function of Ca considered for a) Dong and Brooks (2006) using ThermoChimie database Davies (2009) and b) Endrizzi and Rao (2014) using ThermoChimie database SIT (2014).....	52
Figure 9. Concentration of U(VI) in solution as a function of the concentration of calcium in solution at pH of 7.8 (± 0.1), total $[U(VI)] = 4.7 (\pm 0.3) \cdot 10^{-7}$ M, I = 0.1 (± 0.005) M NaClO ₄ , in atmospheric conditions and 20 °C.	54
Figure 10. Measured pH as a function of S/L ratio in the experiments in the absence of calcium at a) 20 °C in equilibrium with 1% of CO ₂ (g) and b) 80 °C in equilibrium with 5% of CO ₂ (g).....	55
Figure 11. Speciation distribution of U(VI) in the absence of calcium in solution as a function of the temperature.	56
Figure 12. Concentration of U(VI) in the absence of calcium in solution as a function of the solid-liquid ratio (g/L) at a) 20 °C in equilibrium with 1% of CO ₂ (g); b) 40 °C in equilibrium with 1% of CO ₂ (g); c) 60 °C in equilibrium with 3% of CO ₂ (g); and d) 80 °C in equilibrium with 5% of CO ₂ (g). Solid-line: Model fitting of the concentration of U(VI) as a function of the solid-liquid ratio at 20, 40, 60 and 80°C.....	55
Figure 13. Dependency of the calculated $\log_{10}K_{X1}$ value from Reaction 10 with the temperature.	57
Figure 14. Concentration of U(VI) in equilibrium in solution as a function of calcium at different temperatures in 0.1 M of NaNO ₃	58
Figure 15. Symbols: Measured concentration of U(VI) for the Type II experiments as a function of the concentration of calcium at a) 20 °C and b) 40 °C in equilibrium with 1% of CO ₂ (g); c) 60 °C in equilibrium with 3% of CO ₂ (g); and d) 80 °C in equilibrium with 5% of CO ₂ (g). Solid-line: calculated U(VI) concentration using the model proposed in the present work.	59

Figure 16. Symbols: Experimental K_D of U(VI) for the experiments Type II as function of the concentration of calcium at a) 20 °C and b) 40 °C in equilibrium with 1% of CO ₂ (g); c) 60 °C in equilibrium with 3% of CO ₂ (g); and d) 80 °C in equilibrium with 5% of CO ₂ (g). Solid-line: calculated U(VI) concentration using the model proposed in the present work.	60
Figure 17. Temperature effect of the formation of CaUO ₂ (CO ₃) ₃ ²⁻ (left) and Ca ₂ UO ₂ (CO ₃) ₃ (aq) (right).	60
Figure 18. 2D mapping of the stability constants of Ca-U(VI)-CO ₃ aqueous complexes distribution at 20, 40, 60 and 80 °C under respective pCO ₂ . Squares: optimised values using PEST+Phreeqc; Circles: optimised values using Excel+Phreeqc.	61
Figure 19. Dependency of the calculated log ₁₀ β value for Reaction 1 (left) and Reaction 2 (right) with the temperature using PEST-PhreeqC (black circles) and Excel-PhreeqC (white squares).....	62
Figure 20. Variation of CaUO ₂ (CO ₃) ₃ ²⁻ (left) and Ca ₂ UO ₂ (CO ₃) ₃ (aq) (right) stability constants with the temperature. Black: PEST approach. Red: 2D mapping approach. The lines represent least squares fitting following the constant enthalpy of the reaction equation.....	63
Figure 21. Symbols: measured U(VI) concentration as a function of the concentration of calcium in solution for Type II experiments at 20, 40, 60 and 80 °C. Solid line: Calculated uranium concentration using the standard stability constant and enthalpy values from Table 14.....	64
Figure 22. Symbols: experimental K_D value for U(VI) as a function of the concentration of calcium in solution for Type II experiments at 20, 40, 60 and 80 °C. Solid line: Calculated K_D using the standard stability constant and	64
Figure 23. Calculated uranium aqueous speciation of the concentration of calcium in solution for Type II experiments at 20, 40, 60 and 80 °C.....	65
Figure 24. Comparison of the stability constants at 25 °C determined from different studies with the stability constants determined in the present work (p.w.). KAL00: Kalmykov and Choppin (2000); BER01: Bernhard et al. (2001); DON06: Dong and Brooks (2006); LEE13: Lee and Yun (2013); END14: Endrizzi and Rao (2014); JO17: Jo and Yun (2017); p.w.: present work.	66
Figure 25. Calculated U(VI) aqueous speciation at calcium concentrations between 0 and 5·10 ⁻³ M at 25°C. [U] _T = 1·10 ⁻⁸ M, [C] _T = 3·10 ⁻³ M, pH = 7.2 and I = 0.1 M. Left: Calculations performed using the stability constants from Dong and Brooks for Ca-U(VI)-CO ₃ complexes. Right: Calculations performed using the stability constants determined in the present work for Ca-U(VI)-CO ₃ complexes.....	66
Figure 26. Symbols: measured U(VI) concentration as a function of the concentration of calcium in solution for experiments at 20, 40, 60 and 80°C performed in present work. Blue-line: Calculated uranium concentration using the thermodynamic data for Ca-U(VI)-CO ₃ complexes determined in present work. Red-line: calculated uranium concentration using the thermodynamic data for Ca-U(VI)-CO ₃ complexes reported in [1] Endrizzi and Rao (2014).	68
Figure 27. Representation of a) aluminium oxyde octahedra, b) silicium oxyde tetrahedra, c) magnesium oxyde octahedra, plan formed by combination of one tetrahedral sheet with d) one dioctrahedral sheet, and e) one trioctahedral sheet. (Adapted from Ngouana, 2014).	75
Figure 28. Structural elements of phyllosilicates of tetrahedral and octahedral sheets linked to form a 1:1 layer type structure and linked to form 2:1 layer type structure (Adapted from Sposito et al., 1999; http://www.pnas.org/content/96/7/3358).	75
Figure 29. Regular and random interstratified clay minerals. A and B are layers with different periodicity along the c direction (Theng, 2012).....	76
Figure 30. Schematic representation of cation exchange with one uranyl cation and two Na ⁺ cations, and uranyl surface complexation bond to the edge of surface.	79
Figure 31. Schematic representation of the placements of ions, charges (σ) potential (Ψ) and capacitances (C) for different SMCs for surface 0-plane; β-plane and d-plane. Adapted from Goldberg (2013).	81

- Figure 32. a) Callovo-Oxfordian claystone sample: Sorption of $6.8 (\pm 0.2) \cdot 10^{-7}$ M of U(VI) as a function of time in 1% of $\text{CO}_2(\text{g})$, synthetic CO_x porewater, pH of 7.3 (± 0.1) and S/L of 24 g/L. b) Illite: Sorption of $9.8 (\pm 0.8) \cdot 10^{-8}$ M of U(VI) as a function of time in atmospheric pCO_2 , 0.1 M of NaCl, pH 6.3 (± 0.1) and S/L of 0.5 g/L. ...86
- Figure 33. Speciation distribution of the aqueous uranyl species (left) and uranyl hydrolysis surface complexes (right) as function of the pH in the absence of carbonates at 0.1 M of NaNO_3 in contact with illite with S/L of 2 g/L and $\text{U(VI)}_{\text{initial}}$ of $1.1(\pm 0.05) \cdot 10^{-7}$ M.88
- Figure 34. Comparison of the sorption edges of U(VI) on Na-illite in the absence of carbonates between p.w.: present work (0.1 M of NaNO_3 , S/L of 2 g/L and $\text{U(VI)}_{\text{initial}}$ of $1.1(\pm 0.05) \cdot 10^{-7}$ M) and [1] Bradbury and Baeyens (2009) (0.1 M of NaClO_4 , S/L 2.6 g/L and $\text{U(VI)}_{\text{initial}}$ of 10^{-7} M).88
- Figure 35. Sorption isotherm of U(VI) onto Na-illite in the absence of carbonates in $\text{Ar}(\text{g})$ atmosphere at 0.1 M of NaNO_3 , S/L of 2 g/L and pH of 6.4.89
- Figure 36. Sorption isotherms of U(VI) on Na-illite in the absence of carbonates between present work (0.1 M of NaNO_3 in S/L of 2 g/L and pH of 6.4) and work of Bradbury and Baeyens (2005) (0.1 M of NaClO_4 , S/L 2.6 g/L and pH of 5.8).89
- Figure 37. Sorption edges of U(VI) on illite in 0.1 M of NaNO_3 , S/L of 2 g/L and $\text{U(VI)}_{\text{initial}}$ of $1.1(\pm 0.1) \cdot 10^{-7}$ M, in the absence (open circles) and presence (blue circles) of carbonates in equilibrium with atmospheric CO_290
- Figure 38. Speciation distribution of the aqueous uranyl species (left) and uranyl hydrolysis and carbonato surface complexes (right) as function of the pH in the absence of carbonates at 0.1 M.91
- Figure 39. Model approach on sorption edge of U(VI) on illite. Model 0: neither $\equiv\text{SsOUO}_2\text{CO}_3^{2-}$ or $\equiv\text{Ss}_w\text{OUO}_2\text{CO}_3^-$ are considered; Model I: considering the $\log K$ from Montmorillonite; Model II: only $\equiv\text{SsOUO}_2\text{CO}_3^{2-}$ with $\log_{10} K = 17.5 (\pm 0.5)$ is considered; and Model III: the $\equiv\text{SsOUO}_2\text{CO}_3^{2-}$, the $\equiv\text{SsOUO}_2\text{CO}_3^-$ and $\equiv\text{S}_w\text{OUO}_2\text{CO}_3^-$ are considered, with $\log_{10} K$ of 17.5, 9.8 and 9.3, respectively. Error bars that are not visible are smaller than the symbol size.92
- Figure 40. Sorption isotherms of U(VI) onto illite in the absence of carbonates (\circ) at equilibrium pH of 6.4 in 0.1 M of NaCl and presence of carbonates in equilibrium with atmospheric pCO_2 (\bullet) at equilibrium pH of 7.3 in 0.1 M of NaNO_3 . Error bars that are not visible are smaller than the symbol size.93
- Figure 41. Prediction model of sorption of U(VI) onto illite in equilibrium with pCO_2 atmospheric in 0.1 M of NaNO_3 at pH 7.3. a) Model II: only $\equiv\text{SsOUO}_2\text{CO}_3^{2-}$ in considered; b) Model III: U(VI)- CO_3 surface complexation reactions from Table 24. Error bars that are not visible are smaller than the symbol size.93
- Figure 42. Sorption isotherms of U(VI) onto illite in the presence of carbonates in equilibrium with atmospheric pCO_2 , 1% and 5% of $\text{CO}_2(\text{g})$ in 0.1 NaNO_3 , pH fixed at 7.3 (\bullet and \bullet), and 6.6 (\bullet), respectively. Error bars that are not visible are smaller than the symbol size.94
- Figure 43. Model approach for the sorption isotherms of U(VI) onto illite in 0.1 M of NaNO_3 , S/L of 2 g/L at pH 7.3 in equilibrium with 1% of $\text{CO}_2(\text{g})$ (left top and bottom) and pH 6.6 in equilibrium with 5% of $\text{CO}_2(\text{g})$ (right top and bottom). Model II: only $\equiv\text{SsOUO}_2\text{CO}_3^{2-}$ in considered; Model III: U(VI)- CO_3 surface complexation reactions from Table 24. Error bars that are not visible are smaller than the symbol size.95
- Figure 44. Sorption isotherms of U(VI) on illite in the presence of 1% of $\text{CO}_2(\text{g})$ under 0.1 M NaNO_3 at pH 7.3 and synthetic CO_x porewater at pH 7.1. Error bars that are not visible are smaller than the symbol size.96
- Figure 45. Sorption isotherms of U(VI) on illite as a function of the U(VI) in CO_x porewater in equilibrium with 1% of $\text{CO}_2(\text{g})$. Model II: only $\equiv\text{SsOUO}_2\text{CO}_3^{2-}$ in considered taking also in account the thermodynamic data for Ca-U(VI)- CO_3 ternary complexes (see Chapter 2). Error bars that are not visible are smaller than the symbol size.96
- Figure 46. a) Sorption isotherm of U(VI) onto (\circ) illite and (\diamond) Callovo-Oxfordian clay fraction (illite + I/S) in the absence of carbonates in both 2 g/L under 0.1 M NaNO_3 at pH of 6.4 and 7.0 (respectively). b) Sorption isotherm of U(VI) onto (\bullet) illite and (\blacklozenge) Callovo-Oxfordian clay fraction (illite + I/S) in the presence of carbonates in equilibrium with 1% of $\text{CO}_2(\text{g})$ in both 2 g/L under 0.1 M NaNO_3 at pH of 7.3 and 7.2 (respectively). Model approach for illite (solid-line) and for CO_x clay fraction (dash-line). Error bars that are not visible are smaller than the symbol size.98

- Figure 47. a) Sorption isotherms of U(VI) on 2 g/L of CO_x clay fraction (illite + I/S) in equilibrium with 1% of CO₂(g) in 0.1 M of NaNO₃ (♦) and synthetic CO_x porewater (◆). b) Sorption isotherm of U(VI) on (●) 10 g/L of illite and (◆) on 2 g/L of CO_x clay fraction (illite + I/S) in equilibrium with 1% of CO₂(g) in synthetic CO_x porewater conditions. Model approach for illite (solid-line) and for CO_x clay fraction (dash-line). Error bars that are not visible are smaller than the symbol size.....99
- Figure 48. Sorption isotherm of U(VI) onto (●) illite and (◆) CO_x clay fraction (illite + I/S) and (□) Callovo-Oxfordian clays sample in equilibrium with 1% of CO₂(g) in synthetic CO_x porewater conditions. Error bars that are not visible are smaller than the symbol size..... 100
- Figure 49. Model approach (solid line) for sorption isotherm of U(VI) on Callovo-Oxfordian claystone samples in equilibrium with pCO₂ of 1% of CO₂(g) in Callovo-Oxfordian synthetic porewater with pH 7.5. Error bars that are not visible are smaller than the symbol size..... 100
- Figure 50. Experimental and model (black line) data from Hartmann et al. (2008) and the prediction model proposed in the present work (red lines) considering the new stability constant ≡SsOUO₂CO₃23⁻ and its respective uncertainties..... 101
- Figure 51. Comparison of sorption isotherms of U(VI) on the Opalinus clay from [1] Joseph et al. (2011) and Boda clay [2] Marques Fernandes et al. (2015) and [3] Amayri et al. (2016) with the CO_x clayey rock from the [p.w.] present work..... 102
- Figure 52. Model prediction for the sorption isotherms of U(VI) on a) OPA clay from [1] Joseph et al. (2011); b) OPA clay from [2] Marques Fernandes et al. (2015); and c) Boda clay from [2] Marques Fernandes et al. (2015); [p.w.] CO_x clay from present work. Solid-lines: model approach proposed in present work; Dash-line: model uncertainties of the ≡SsOUO₂CO₃23⁻ (log₁₀K = 17.5 ± 0.5)..... 103
- Figure 53. Impact of the temperature on the distribution coefficient of U(VI) as a function of the concentration of U(VI) in equilibrium in CO_x claystone samples. (●) and (□) experimental data from the present work. red-line: model approach at 80°C considering the model approach proposed in Chapter 3 and the thermodynamic parameters of U(VI) aqueous speciation (Chapter 2). 110
- Figure 54. Linear relationship between Log₁₀K^o_x of aqueous species and Log₁₀^SK^o_x of surface complexes for illite and montmorillonite, considering both hydrolysis complexes. Solid-line: correlation of illite surface complexation data; dashed-line: correlation of montmorillonite surface complexation data. 115
- Figure 55. Distribution coefficient for the sorption of U(VI) at 1·10⁻⁷ M of U(VI) onto illite as a function of pH in 0.1 M of NaNO₃ in the absence of carbonates. Error bars that are not visible are smaller than the symbol size. 117
- Figure 56. Temperature effect on the sorption isotherm of U(VI) onto illite in the absence of carbonates at pH of equilibrium of 6.4–6.5 in 0.1 M of NaNO₃. Error bars that are not visible are smaller than the symbol size. . 117
- Figure 57. Distribution of U(VI) aqueous species as a function of the pH at 20°C (solid lines) and 80°C (dashed lines) in the absence of the carbonates..... 118
- Figure 58. Model approach for the distribution coefficient of U(VI) as a function of the pH at a) 20 °C and b) 80 °C in the absence of carbonates. Model II: base model without enthalpy data (see Chapter 3); Model IV: model considering the correlation factor 1 with aqueous and surface complexes for enthalpy values (Table 33). Error bars that are not visible are smaller than the symbol size. 119
- Figure 59. Model approach on sorption of isotherms of U(VI) in the absence of carbonates at a) 20 °C; b) 60 °C; and c) 80 °C. Model II: model approach without enthalpy values (see Chapter 3); Model IV: model approach considering the enthalpy values (see Table 33). Error bars that are not visible are smaller than the symbol size. 119
- Figure 60. Distribution of U(VI) hydrolysis surface complexes of illite at 20°C (solid-lines) and 80°C (dashed-lines) as a function of the pH. Calculations taking the parameters given in Table 33..... 120
- Figure 61. Fitting model for sorption edge experiments (a) at 20 °C and (b) at 80 °C (with ±0.2 log units of uncertainty for the stability constants); for sorption isotherm experiments (c) at 20 °C (with ±0.2 log units of uncertainty for the stability constants); (d) at 60 °C and (e) at 80 °C (with ±0.5 log units of uncertainty for the stability constants). Error bars that are not visible are smaller than the symbol size..... 121

- Figure 62. Relationship between $\text{Log}_{10}K_x^\circ$ of aqueous species and $\text{Log}_{10}^S K_x^\circ$ of surface complexes for illite determined at 20, 60 and 80°C in comparison with the respective standard stability constants at 25°C (solid-line) for illite reported by Bradbury and Baeyens (2009). 122
- Figure 63. Relation of constant of hydrolysis surface complexation (T) and standard constant of hydrolysis surface complexation (T_0) as a function of the $1/T_0 - 1/T$ for the surface species a) $\equiv\text{SsOUO}_2^+$, b) $\equiv\text{SsOUO}_2\text{OH}$, c) $\equiv\text{SsOUO}_2(\text{OH})_2^-$, and d) $\equiv\text{SsOUO}_2(\text{OH})_3^{2-}$. Symbols: experimental data; Dashed-lines: regression line calculated for the enthalpy values. 122
- Figure 64. Symbols: measured experimental data from sorption edge and isotherm of U(VI) at different temperatures. Solid-lines: calculated U(VI) concentration using enthalpy values calculated from Table 35. Dashed-lines correspond to the uncertainty of the enthalpy values. Error bars that are not visible are smaller than the symbol size. 123
- Figure 65. Distribution coefficient of U(VI) as a function of the pH in 0.1 NaCl a) in the absence or presence of carbonates in equilibrium with pCO_2 atmospheric at 80 °C. Error bars that are not visible are smaller than the symbol size. 124
- Figure 66. Sorption isotherms of U(VI) on illite at different temperatures in equilibrium with a) $\text{Ar}(\text{g})$; b) pCO_2 atmospheric; c) pCO_2 of 1% of $\text{CO}_2(\text{g})$; and d) pCO_2 of 5% of $\text{CO}_2(\text{g})$. Error bars that are not visible are smaller than the symbol size. 125
- Figure 67. Distribution of the speciation U(VI) in solution as a function of the pH at 20 (solid-lines) and 80 °C (dashed-lined) in equilibrium with pCO_2 atmospheric. 126
- Figure 68. Sorption edge of U(VI) in equilibrium with pCO_2 atmospheric. Model V: enthalpy values considered only for hydrolysis surface complexation reactions (Table 35). 127
- Figure 69. Model approach considering only the enthalpy of the hydrolysis of surface complexes at different temperatures in the presence of carbonates (see Table 35). Dashed-lines correspond to the uncertainty of the enthalpy values of the hydrolysis surface complexes. 127
- Figure 70. Sorption isotherms of U(VI) on illite and Callovo-Oxfordian clay fraction (illite + I/S) system at 80 °C a) in the absence of carbonates and b) in the presence of carbonates in equilibrium with pCO_2 of 5% of $\text{CO}_2(\text{g})$ 128
- Figure 71. Model approach for describing the sorption isotherms of U(VI) on Callovo-Oxfordian clay fraction (illite + I/S) at 20 and 80 °C a) in the absence and b) in the presence of carbonates in equilibrium with 1% and 5% of $\text{CO}_2(\text{g})$, respectively. Taking the thermodynamic parameters for illite and montmorillonite (see Table 39) the solid-lines correspond to the model prediction at 20°C; and the dashed-lines correspond to the model prediction at 80 °C. 129
- Figure 72. Sorption isotherms of the U(VI) in synthetic porewater performed at 20 and 80 °C for a) U(VI)/illite system; b) U(VI)/ Callovo-Oxfordian clay fraction system; and c) U(VI)/ Callovo-Oxfordian claystone system. Model approach considering thermodynamic data for surface reactions from Table 39 and using the thermodynamic data for Ca-U(VI)- CO_3 aqueous complexes (see Table 14). Solid-line: model at 20 °C; dashed-line: model at 80°C. 131
- Figure 73. Impact of the temperature on the distribution coefficient of U(VI) as a function of the concentration of U(VI) in equilibrium in Callovo-Oxfordian claystone system. (●) and (□) experimental data from the present work. red-line: model approach at 80°C considering the model approach proposed in the present study and the thermodynamic parameters of U(VI) aqueous speciation (Table 14). 131
- Figure A. 1. Schematic representation of the calibration plot of ICP-MS measurements. Black-cross correspond to the measurement of each standard solution; solid-line corresponds to the regression line ($y_{\text{calc}} = bx + c$); dash-lines corresponds to the inferior and superior error of y_{calc} 144
- Figure C. 1. Temperature isolation box. a) internal layer aluminium; b) external layer of Teflon; c) tubes inside isolation box; d) closure of the isolation box. 155

Figure C. 2. Temperature measurements as a function of time at open lid and closed lid with small aperture.	156
Figure C. 3. Temperature measurements as a function of time in presence or absence of the isolation Teflon layer.	156
Figure C. 4. Experimental test of the oxidation of Fe(II) to Fe(III) as gas sealing control.	159
Figure C. 5. pH measured in atmospheric conditions of the CO _x porewater as a function of time.	159
Figure C. 6. Volume of water loss (%) at 80 °C during agitation with tubes with no sealing tape as a function of time.	160
Figure C. 7. Comparison results of the number of washes with ultra-pure water between 3-4 days or 1 days.	161
Figure C. 8. Total organic carbon as function of the number of washing and time of contact. a) washing with ultra- pure water and rinsed with ultra-pure water between each wash; b) first rinsed with 5% of HNO ₃ at 100 °C before washed with ultra-pure water and rinsed with ultra-pure water between washes.	162
Figure D. 1. Left: distribution of the U(VI) (black-lines: Ca ₂ UO ₂ (CO ₃) ₃ (aq); green-lines: UO ₂ (CO ₃) ₃ ⁴⁻); Right: saturation index of Calcite as a function of calcium for: A) <i>I</i> = 0.1 m; B) <i>I</i> = 0.3 m; C) <i>I</i> = 0.5 m; D) <i>I</i> = 0.7 m; E) <i>I</i> = 1 m; and F) <i>I</i> = 3 m from Kalmykov and Choppin (2000) using Thermochemie database SIT (2009). .	197
Figure D. 2. (left) distribution of U(VI) speciation and (right) saturation index of Calcite as a function of the calcium concentration considering the experimental conditions of Bernhard et al. (2001) using Thermochemie database Davies (2014). Solid-line: U(VI) = 1·10 ⁻⁴ M; dash-line: U(VI) = 5·10 ⁻⁵ M; dot-line: U(VI) = 2·10 ⁻⁵ M.....	199
Figure D. 3. Distribution of U(VI) speciation and the saturation index of calcite as a function of the calcium concentration considering the experimental conditions of Lee and Yun (2013) using Thermochemie database Davies (2014).....	199
Figure D. 4. (left) distribution of U(VI) speciation and (right) mineral saturation index as a function of the calcium concentration considering the experimental conditions of Endrizzi and Rao (2006) using Thermochemie database Davies (2014).....	199
Figure D. 5. Distribution of U(VI) speciation at 20°C and 1% of CO ₂ (g) taking the log ₁₀ β ₁₁₃ = 27.4 ± 0.1 and log ₁₀ β ₂₁₃ = 29.8 ± 1.1 (calculated from PEST-Phreeqc).	201
Figure D. 6. Distribution of U(VI) speciation at 40°C and 1% of CO ₂ (g) taking the log ₁₀ β ₁₁₃ = 27.2 ± 0.1 and log ₁₀ β ₂₁₃ = 29.9 ± 0.7 (calculated from PEST-Phreeqc).	202
Figure D. 7. Distribution of U(VI) speciation at 60°C and 3% of CO ₂ (g) taking the log ₁₀ β ₁₁₃ = 26.7 ± 0.03 and log ₁₀ β ₂₁₃ = 29.6 ± 0.1 (calculated from PEST-Phreeqc).	202
Figure D. 8. Distribution of U(VI) speciation at 80°C and 5% of CO ₂ (g) taking the log ₁₀ β ₁₁₃ = 26.5 ± 0.1 and log ₁₀ β ₂₁₃ = 29.7 ± 0.1 (calculated from PEST-Phreeqc).	203

List of Tables

Table 1. Average and extreme values of the mineralogical composition (wt%) of the host layer in borehole EST205 Meure/Haute-Marne site (Gaucher et al., 2004).	34
Table 2. Chemical composition of the Callovo-Oxfordian porewater calculated by geochemical modelling according to the temperature increasing using the reduced mineralogy.	35
Table 3. Chemical composition of the Callovo-Oxfordian porewater calculated by geochemical modelling according to the temperature increasing using the completed mineralogy.	35
Table 4. Summary of the literature analysing the stability constants of Ca-U(VI)-CO ₃ complexes. Data in grey have been superseded by later references of the same authors (2001).	41
Table 5. Summary of the literature on the stability constants for Mg-U(VI)-CO ₃ complexes. Data in grey have been superseded by later references of the same authors.	42
Table 6. Stability constants for Ca-U(VI)-CO ₃ complexes at $I = 0.1M$ and different temperatures suggested by Jo and Yun (2017).	43
Table 7. Summary of the batch experiments performed in the present work.	47
Table 8. Description of the tests performed in different temperatures and in closed system experiments.	51
Table 9. Theoretical and measured parameters from the evaluation of CO ₂ (g) in equilibrium at different temperatures. Theor.: theoretical value in agreement with the initial conditions of the experiments; Exp.: pH and alkanity measured at the end of the experiment, and pCO ₂ calculated according pH and alkanity measurements.	51
Table 10. Estimated values for the Log ₁₀ K _X at different temperatures and pCO ₂ (atm).	57
Table 11. Theoretical and measured pH, alkalinity and pCO ₂ of the batch experiments at different temperatures. Theor.: theoretical values according to the initial conditions of the experiments; Measured pH and alklinity in equilibrium; and calculated pCO ₂ in agreement with pH and alkalinity measured.	58
Table 12. Results of the fitting for the stability constants of Ca-U(VI)-CO ₃ complexes using PEST.	60
Table 13. Stability constants of Ca-U(VI)-CO ₃ complexes calculated by 2D mapping method.	62
Table 14. Thermodynamic data of Ca-U(VI)-CO ₃ ternary complexes determined in this work.	63
Table 15. Calculated UO ₂ ·2H ₂ O(am) solubility and aqueous U(VI) speciation under Callovo-Oxfordian conditions (Tournassat et al., 2008, Table 3)	67
Table 16. Comparison of the thermodynamic parameters of the Ca-U(VI)-CO ₃ ternary complexes reactions. p.w. present work; (1) Endrizzi and Rao (2017); (2) Jo and Yun (2017); n.d. not defined.	67
Table 17. Classification of the planar hydrated phyllosilicates and some examples for each clay mineral species (Theng, 2012). (the higlighted clay minerals are the ones relevant for the present study)	76
Table 18. Sorption parameters for U(VI) onto clay minerals of Callovo-Oxfordian formation (Bradbury and Baeyens, 1997, 2004).	83
Table 19. Cationic exchange and surface complexation reactions used in the sorption model.	83

Table 20. Distribution of surface complexation reactions of U(VI) on illite and montmorillonite in Callovo-Oxfordian formation system (pH = 7.2 and pCO ₂ = 10 ^{-2.1} atm).....	84
Table 21. Description of the experimental cases performed on different phases of Callovo-Oxfordian formation at 20 °C.	85
Table 22. Summary of the experimental conditions for sorption of uranium in different components of Callovo-Oxfordian formation.	86
Table 23. Alkalinity and pH measurements before and after the equilibrium with illite. pCO ₂ calculated from the equilibrium pH/alkalinity.....	90
Table 24. Uranyl carbonate surface complexation reactions proposed for illite in Model III.....	92
Table 25. pH and alkalinity measurements after equilibrium with pCO ₂ atmospheric, 1% and 5% CO ₂ (g).....	94
Table 26. Surface species of U(VI) distribution on illite and montmorillonite for Callovo-Oxfordian formation experimental conditions.	100
Table 27. Comparison of the main chemical parameters for OPA clay, Boda clay and CO _x clay. [1] Joseph et al. (2011); [2] Marques Fernandes et al. (2015); [p.w.] present work. (*) measurements of alkalinity (meq/L). .	102
Table 28. Compilation of the surface reactions for both illite and montmorillonite taken in for the model prediction. (n.a. not applied).....	104
Table 29. Description of the U(VI) sorption experiments carried out on illite, Callovo-Oxfordian clay fraction and clays samples as a function of temperature.....	113
Table 30. Experimental conditions of the sorption experimental cases for the different phases of Callovo-Oxfordian formation at different temperatures. (pw = porewater).....	113
Table 31. Aqueous speciation of U(VI) (Guillaumont et al., 2003) and surface complexation reactions and respective stability constants (Bradbury and Baeyens, 2009; Marques Fernandes et al., 2015) and enthalpy values (unknown: to be determined) used on the predictive model. (n.a.: not applied).....	114
Table 32. pH and alkalinity measured in equilibrium for the sorption isotherms on illite in inert atmosphere at different temperatures.	117
Table 33. Surface complexation constants on strong sites together with the corresponding hydrolysis constants and enthalpy values for illite considered in Model IV.....	118
Table 34. Log ₁₀ ^{OH} K _x ^o fitted based on sorption edges and isotherms experiments performed at different temperatures for illite.	121
Table 35. Enthalpy values calculated from fitting of the stability constants of hydrolysis surface site species at different temperatures. The uncertainty was determined considering only the propagation error of the standard deviation of the stability constants.....	123
Table 36. Alkalinity and pH measurements before and after the equilibrium with illite at 80 °C. pCO ₂ calculated from the equilibrium pH/alkalinity.	125
Table 37. pH of equilibrium and alkalinity measurements in the presence of carbonates at 60 and 80°C.....	126
Table 38. pH and alkalinity measurements in equilibrium for the sorption isotherms on clay fraction at 80 °C in different atmospheres.....	129
Table 39. Enthalpy values for the hydrolysis surface complexation reactions for illite and montmorillonite considered in the present study.	129
Table 40. Experimental pH and alkalinity measurements at 20 and 80 °C for illite, Callovo-Oxfordian clay fraction and claystone samples in synthetic Callovo-Oxfordian porewater in equilibrium with 1% and 5% of CO ₂ (g), respectively.	130
Table 41. Aqueous and surface speciation at 20 and 80°C for the Callovo-Oxfordian formation system in equilibrium with synthetic porewater for [U(VI)] = 10 ⁻⁷ M.....	132

Table 42. Proposed thermodynamic parameters for the surface complexation reactions considered in the model approach.....	133
Table A. 1. Concentration and dilution calculations of the standard solutions for determination of the calibration curve of ICP-MS analysis	142
Table A. 2. Theoretical chemical composition of the Callovo-Oxfordian porewater at 20 °C and 80°C.....	146
Table A. 3. Salt content in g/L used in preparation of synthetic CO _x porewater at 20 and 80°C	147
Table A. 4. Mineral composition of Callovo-Oxfordian claystone	147
Table A. 5. Experimental conditions for the batch experiments. Temp.= temperature; CO _x = Callovo-Oxfordian; I = Ionic strength.....	150
Table B. 1. Amount of exchanger-NO ₃ (mol/L) for the different solid-liquid ratio (χ) considered in the closed system experiments.....	153
Table C. 1. Experimental test of the control of the temperature using an isolation-aluminium box without external layer of Teflon.	156
Table C. 2. Experimental test of the control of the temperature using an isolation-aluminium box with external layer of Teflon.	157
Table C. 3. Experimental test for sealing control.....	159
Table C. 4. Experimental results of the tightness of the tubes without sealing tape.	160
Table C. 5. Uncertainty of the signal of the TOC Analyser determined using standard solution of IC, TC and ultra-pure water.	162
Table C. 6. TOC measurements of the experimental tests.	163
Table C. 7. Chemical composition of the synthetic Callovo-Oxfordian porewater. Uncertainty of k=2	164
Table C. 8. Measurements of the pH for the sorption edge experiments in atmospheric pCO ₂ . ⁽¹⁾ used only in the experiments at 80°C; ⁽²⁾ this solution was not taken for the experiments performed at 20°C.	164
Table C. 9. Alkalinity measurements using H ₂ SO ₄ (0.16 N) in the blank samples of the batch experiments using anionic-exchange resin. *measured	164
Table C. 10. Experimental results of the ionic exchange method at 20°C in atmospheric conditions in the presence of calcium, 0.1 M of NaClO ₄ at fixed solid-liquid ratio adding initially [U(VI)] = 5 · 10 ⁻⁷ M.....	165
Table C. 11. Experimental results of the ionic exchange method at 20°C in closed system at 1% of CO ₂ (g) in the absence of calcium and varying the solid-liquid ration, in 0.1M of NaNO ₃ adding initially [U(VI)] = 5 · 10 ⁻⁷ M. (Ba: blank sample without U(VI); Bb: blank sample without resin with U)	165
Table C. 12. Experimental results of the ionic exchange method at 20°C in closed system at 1% of CO ₂ (g) in the presence of calcium, 0.1 M of NaNO ₃ at fixed solid-liquid ratio adding initially [U(VI)] = 5 · 10 ⁻⁷ M. (blank samples in the absence of calcium (0) or presence of calcium (19) for Ba: without U(VI); and Bb: without resin with U).....	166
Table C. 13. Experimental results of the ionic exchange method at 40°C in closed system at 1% of CO ₂ (g) in the absence of calcium and varying the solid-liquid ration, in 0.1M of NaNO ₃ adding initially [U(VI)] = 5 · 10 ⁻⁷ M. (Ba: blank sample without U(VI); Bb: blank sample without resin with U)	166
Table C. 14. Experimental results of the ionic exchange method at 40°C in closed system at 1% of CO ₂ (g) in the presence of calcium, 0.1 M of NaNO ₃ at fixed solid-liquid ratio adding initially [U(VI)] = 5 · 10 ⁻⁷ M. . (blank samples in the absence of calcium (0) or presence of calcium (19) for Ba: without U(VI); and Bb: without resin with U).....	166

Table C. 15. Experimental results of the ionic exchange method at 60°C in closed system at 3% of CO ₂ (g) in the absence of calcium and varying the solid-liquid ration, in 0.1M of NaNO ₃ adding initially [U(VI)] = 5·10 ⁻⁷ M. (Ba: blank sample without U(VI); Bb: blank sample without resin with U)	167
Table C. 16. Experimental results of the ionic exchange method at 60 °C in closed system at 3% of CO ₂ (g) in the presence of calcium, 0.1 M of NaNO ₃ at fixed solid-liquid ratio adding initially [U(VI)] = 5·10 ⁻⁷ M. . (blank samples in the absence of calcium (0) or presence of calcium (19) for Ba: without U(VI); and Bb: without resin with U).....	167
Table C. 17. Experimental results of the ionic exchange method at 80 °C in closed system at 5% of CO ₂ (g) in the absence of calcium and varying the solid-liquid ration, in 0.1M of NaNO ₃ adding initially [U(VI)] = 5·10 ⁻⁷ M. (Ba: blank sample without U(VI); Bb: blank sample without resin with U)	168
Table C. 18. Experimental results of the ionic exchange method at 80°C in closed system at 5% of CO ₂ (g) in the presence of calcium, 0.1 M of NaNO ₃ at fixed solid-liquid ratio adding initially [U(VI)] = 5·10 ⁻⁷ M. . (blank samples in the absence of calcium (0) or presence of calcium (19) for Ba: without U(VI); and Bb: without resin with U).....	168
Table C. 19. Kinetic results of sorption of U(VI) onto Callovo-Oxfordian claystone at 20 °C in 1% CO ₂ (g), using synthetic Callovo-Oxfordian porewater and initial U(VI) = 6.8(±0.2)·10 ⁻⁷ M.	168
Table C. 20. Kinetic results of sorption of U(VI) onto Callovo-Oxfordian claystone at 80 °C in 5% CO ₂ (g), using synthetic Callovo-Oxfordian porewater and initial U(VI) = 6.8(±0.2)·10 ⁻⁷ M.	169
Table C. 21. Kinetic results of sorption of U(VI) onto Illite at 20 °C in 1% CO ₂ (g), using synthetic Callovo-Oxfordian porewater and initial U(VI) = 9.6(±0.8)·10 ⁻⁸ M.....	169
Table C. 22. Kinetic results of sorption of U(VI) onto illite at 80 °C in 5% CO ₂ (g), using synthetic Callovo-Oxfordian porewater and initial U(VI) = 6.8(±0.2)·10 ⁻⁷ M.....	169
Table C. 23. Alkalinity measurements in sorption isotherms experiments of U(VI)/illite system (2 g/L) at different temperatures. *synthetic Callovo-Oxfordian porewater.	170
Table C. 24. Experimental results of the sorption isotherms of U(VI) onto illite at 20°C in Ar(g) in 0.1 M of NaNO ₃ at fixed solid-liquid ratio. (BF: blank sample filtrated; BNF: blank sample no filtrated).....	171
Table C. 25. Experimental results of the sorption isotherms of U(VI) onto illite at 20°C in atmospheric conditions in 0.1 M of NaCl at fixed solid-liquid ratio. (BF: blank sample filtrated; BNF: blank sample no filtrated)	172
Table C. 26. Experimental results of the sorption isotherms of U(VI) onto illite at 20°C in 1% of CO ₂ (g) in 0.1 M of NaNO ₃ at fixed solid-liquid ratio. (BF: blank sample filtrated; BNF: blank sample no filtrated).....	173
Table C. 27. Experimental results of the sorption isotherms of U(VI) onto illite at 20°C in 5% of CO ₂ (g) in 0.1 M of NaNO ₃ at fixed solid-liquid ratio. (BF: blank sample filtrated; BNF: blank sample no filtrated).....	174
Table C. 28. Experimental results of the sorption isotherms of U(VI) onto illite at 20°C in 1% of CO ₂ (g) in synthetic Callovo-Oxfordian porewater at fixed solid-liquid ratio. (BF: blank sample filtrated; BNF: blank sample no filtrated)	175
Table C. 29. Experimental results of the sorption isotherms of U(VI) onto illite at 60°C in Ar(g) in 0.1 M of NaNO ₃ at fixed solid-liquid ratio. (BF: blank sample filtrated; BNF: blank sample no filtrated).....	176
Table C. 30. Experimental results of the sorption isotherms of U(VI) onto illite at 60°C in atmospheric pCO ₂ in 0.1 M of NaCl at fixed solid-liquid ratio. (BF: blank sample filtrated; BNF: blank sample no filtrated).....	177
Table C. 31. Experimental results of the sorption isotherms of U(VI) onto illite at 60°C in 1% of CO ₂ (g) in 0.1 M of NaNO ₃ at fixed solid-liquid ratio. (BF: blank sample filtrated; BNF: blank sample no filtrated).....	178
Table C. 32. Experimental results of the sorption isotherms of U(VI) onto illite at 60°C in 5% of CO ₂ (g) in 0.1 M of NaNO ₃ at fixed solid-liquid ratio. (BF: blank sample filtrated; BNF: blank sample no filtrated).....	179
Table C. 33. Experimental results of the sorption isotherms of U(VI) onto illite at 80°C in Ar(g) in 0.1 M of NaNO ₃ at fixed solid-liquid ratio. (BF: blank sample filtrated; BNF: blank sample no filtrated).....	180
Table C. 34. Experimental results of the sorption isotherms of U(VI) onto illite at 80°C in atmospheric pCO ₂ in 0.1 M of NaCl at fixed solid-liquid ratio. (BF: blank sample filtrated; BNF: blank sample no filtrated).....	181

Table C. 35. Experimental results of the sorption isotherms of U(VI) onto illite at 80°C in 1% of CO ₂ (g) in 0.1 M of NaNO ₃ at fixed solid-liquid ratio. (BF: blank sample filtrated; BNF: blank sample no filtrated).....	182
Table C. 36. Experimental results of the sorption isotherms of U(VI) onto illite at 80°C in 5% of CO ₂ (g) in 0.1 M of NaNO ₃ at fixed solid-liquid ratio. (BF: blank sample filtrated; BNF: blank sample no filtrated).....	183
Table C. 37. Experimental results of the sorption isotherms of U(VI) onto illite at 80°C in 5% of CO ₂ (g) in synthetic Callovo-Oxfordian porewater at fixed solid-liquid ratio. (BF: blank sample filtrated; BNF: blank sample no filtrated)	184
Table C. 38. pH results of each tube measured before the batch equilibrium at 20 °C in atmospheric pCO ₂	185
Table C. 39. pH results of each tube measured before the batch equilibrium at 80 °C in atmospheric pCO ₂	185
Table C. 40. Experimental results of the sorption edges of U(VI) onto illite at 20°C in Ar(g) in 0.1 M of NaNO ₃ at fixed solid-liquid ratio of 2 g/L with [U(VI)] _{initial} = 1.02(±0.06)·10 ⁻⁷ M. (BF: blank sample filtrated; BNF: blank sample no filtrated)	186
Table C. 41. Experimental results of the sorption edges of U(VI) onto illite at 20°C in atmospheric pCO ₂ in 0.1 M of NaCl at fixed solid-liquid ratio of 0.5-1 g/L with [U(VI)] _{initial} = 1.02(±0.06)·10 ⁻⁷ M. (BF: blank sample filtrated; BNF: blank sample no filtrated)	186
Table C. 42. Experimental results of the sorption edges of U(VI) onto illite at 80 °C in Ar(g) in 0.1 M of NaNO ₃ at fixed solid-liquid ratio of 2 g/L with [U(VI)] _{initial} = 1.02(±0.06)·10 ⁻⁷ M. (BF: blank sample filtrated; BNF: blank sample no filtrated)	187
Table C. 43. Experimental results of the sorption edges of U(VI) onto illite at 80°C in atmospheric pCO ₂ in 0.1 M of NaCl at fixed solid-liquid ratio of 0.5-1 g/L with [U(VI)] _{initial} = 3.07(±0.01)·10 ⁻⁸ M. (BF: blank sample filtrated; BNF: blank sample no filtrated)	187
Table C. 44. Alkalinity measurements in sorption isotherms experiments of U(VI)/clay fraction system at different temperatures. *synthetic Callovo-Oxfordian porewater.	188
Table C. 45. Experimental results of the sorption isotherms of U(VI) onto Callovo-Oxfordian clay fraction at 20°C in Ar(g) in 0.1 M of NaNO ₃ at fixed solid-liquid ratio.	188
Table C. 46. Experimental results of the sorption isotherms of U(VI) onto Callovo-Oxfordian clay fraction at 20 °C in 1% of CO ₂ (g) in 0.1 M of NaNO ₃ at fixed solid-liquid ratio. (BF: blank sample filtrated; BNF: blank sample no filtrated)	189
Table C. 47. Experimental results of the sorption isotherms of U(VI) onto Callovo-Oxfordian clay fraction at 20 °C in 1% of CO ₂ (g) in synthetic Callovo-Oxfordian porewater at fixed solid-liquid ratio. (BF: blank sample filtrated; BNF: blank sample no filtrated)	190
Table C. 48. Experimental results of the sorption isotherms of U(VI) onto Callovo-Oxfordian clay fraction at 80 °C in Ar(g) in 0.1 M of NaNO ₃ at fixed solid-liquid ratio of 2 g/L. (BF: blank sample filtrated; BNF: blank sample no filtrated)	191
Table C. 49. Experimental results of the sorption isotherms of U(VI) onto Callovo-Oxfordian clay fraction at 80 °C in 5% of CO ₂ (g) in 0.1 M of NaNO ₃ at fixed solid-liquid ratio. (BF: blank sample filtrated; BNF: blank sample no filtrated)	192
Table C. 50. Experimental results of the sorption isotherms of U(VI) onto Callovo-Oxfordian clay fraction at 80 °C in 5% of CO ₂ (g) in Callovo-Oxfordian porewater at fixed solid-liquid ratio. (BF: blank sample filtrated; BNF: blank sample no filtrated)	193
Table C. 51. Alkalinity measurements in sorption isotherms experiments of U(VI)/claystone system at 20 and 80°C in synthetic Callovo-Oxfordian porewater.....	194
Table C. 52. Experimental results of the sorption isotherms of U(VI) onto Callovo-Oxfordian claystone at 20 °C in 1% of CO ₂ (g) in Cox porewater at fixed solid-liquid ratio.	194
Table C. 53. Experimental results of the sorption isotherms of U(VI) onto Callovo-Oxfordian claystone samples at 80 °C in 5% of CO ₂ (g) in Callovo-Oxfordian porewater at fixed solid-liquid ratio.	195

Table D. 1. Summary of the main parameters used for determination of stability constants of Ca-U(VI)-CO ₃ complexes using different experimental methods (n.d.: not determined).....	198
Table D. 2. Modelling results using PEST coupled to Phreeqc for experiments as a function of S/L in the absence of Ca at 20 °C and 1% of CO ₂ (g).....	200
Table D. 3. Modelling results using PEST coupled to Phreeqc for experiments as a function of S/L in the absence of Ca at 40 °C and 1% of CO ₂ (g).....	200
Table D. 4. Modelling results using PEST coupled to Phreeqc for experiments as a function of S/L in the absence of Ca at 60 °C and 3% of CO ₂ (g).....	200
Table D. 5. Modelling results using PEST coupled to Phreeqc for experiments as a function of S/L in the absence of Ca at 80 °C and 5% of CO ₂ (g).....	201
Table D. 6. Modelling results using PEST coupled to Phreeqc for experiments as a function of Ca at fixed S/L, 20°C and 1% of CO ₂ (g).....	201
Table D. 7. Modelling results using PEST coupled to Phreeqc for experiments as a function of Ca at fixed S/L, 40°C and 1% of CO ₂ (g).....	202
Table D. 8. Modelling results using PEST coupled to Phreeqc for experiments as a function of Ca at fixed S/L, 60°C and 3% of CO ₂ (g).....	202
Table D. 9. Modelling results using PEST coupled to Phreeqc for experiments as a function of Ca at fixed S/L, 80°C and 5% of CO ₂ (g).....	203
Table E. 1. Thermodynamic data for the aqueous species considered for the calculation of stability constants of Ca-U(VI)-CO ₃ complexes. Note that log ₁₀ β values and enthalpies of reaction are in agreement with the chemical reactions that are included in ThermoChimie database v.9	205
Table E. 2. Thermodynamic data for the solid phases considered for the calculation of stability constants of Ca-U(VI)-CO ₃ complexes. Note that log ₁₀ K and enthalpies of reaction are in agreement with the chemical reactions that are included in ThermoChimie database v.9.....	206

Résumé Étendu

La présence éventuelle de radionucléides dans l'environnement, due à l'utilisation de la production d'énergie nucléaire et à la manipulation généralisée des radio-isotopes dans la recherche, l'industrie, la médecine et l'agriculture, soulève un certain nombre de préoccupations environnementales. Il est essentiel dans ce contexte de comprendre le comportement chimique des radionucléides pour permettre une prévision fiable de leur migration dans le milieu naturel.

En France, la formation argileuse du Callovo-Oxfordien (COx), située en Meuse / Haute-Marne (Est de la France), est à l'étude comme barrière géologique pour le projet de stockage des déchets radioactifs « Cigéo : Centre industriel de stockage géologique ». Cette formation argileuse, de plus de 130 m d'épaisseur et à 500 m de profondeur, est caractérisée par une faible perméabilité ce qui limite la circulation de l'eau, principale cause de la dissémination des radioéléments. De plus, il s'agit d'une zone qui présente une bonne homogénéité sur plusieurs km² (minéralogie, propriétés physico-chimiques) (Andra, 2005). Enfin, elle est caractérisée par un assemblage minéralogique riche en phases argileuses qui jouent un rôle important dans le contrôle des propriétés physico-chimiques et le ralentissement de la migration des radionucléides compte tenu de leurs importantes capacités de rétention.

L'environnement géologique au voisinage d'un stockage de déchets nucléaires sera évidemment soumis à des perturbations (par exemple thermiques, hydrauliques, mécaniques et chimiques, connues sous le nom de THMC) et à différents niveaux de radioactivité au cours du temps. L'une des perturbations primordiales durant les premières années est l'augmentation de la température autour du stockage, favorisée par les désintégrations radioactives au sein des déchets de haute activité à vie longue. Dans la roche argileuse hôte, cet effet peut non seulement modifier la composition chimique de l'eau interstitielle (pH, potentiel d'oxydoréduction et pression du gaz), mais aussi provoquer des processus d'interaction eau-roche-gaz (par exemple : dissolution, précipitation), voire modifier les propriétés de sorption.

Actuellement, dans les installations françaises, le combustible utilisé est composé en plus de la matière fissile (oxydes d'uranium et oxydes mixtes d'uranium et de plutonium) des produits de fission et des actinides mineurs responsables de plus de 98 % de la radioactivité. Ces derniers, considérés comme des déchets, sont séparés pour être conditionnés au sein de matrices de verre par des procédés de vitrification (Andra, 2005). Le combustible utilisé, qui n'est pas retraité, n'est pas considéré comme un déchet. Le degré de radioactivité de ces combustibles utilisés est comparable à celui des déchets vitrifiés. L'interaction du rayonnement α émis par les radio-isotopes avec l'eau peut conduire à des réactions provoquant la corrosion et la dissolution du verre, libérant ainsi les radioéléments (notamment U, Pu, etc...). La mobilité de l'uranium dans la géosphère est intrinsèquement liée à sa solubilité qui dépend de son degré d'oxydation (communément en conditions naturelles U^(IV) ou U^(VI)) et à la stabilité des espèces aqueuses présentes dans l'eau porale de la formation argileuse (Runde, 2000).

Les résultats d'exercices de modélisation géochimique, qui s'appuient sur les données thermodynamiques issues du projet international coordonné par l'Agence de l'Energie Nucléaire (NEA-TDB ; Guillaumont et al., 2003), prédisent l'existence de l'uranium au degré d'oxydation $U^{(IV)}$ dans les conditions physico-chimiques représentatives de l'eau porale des argilites à l'état naturel. Au degré d'oxydation $U^{(IV)}$, l'uranium est peu soluble et les espèces dissoutes associées peuvent réagir fortement avec les surfaces argileuses des argilites du Callovo-Oxfordien ce qui rend cet élément peu mobile. Cependant, des données publiées ont clairement établi l'existence de complexes ternaires $Ca-U(VI)-CO_3$ (Bernhard et al., 1996, 2001 ; Kalmykov et Choppin, 2000 ; Dong et Brooks, 2006 ; Lee et Yun, 2013 ; Endrizzi et Rao., 2014 ; Jo et Yun, 2017) dans les conditions physico-chimiques des argilites ($pH \approx 7,2$ et $Eh \approx -200$ mV). Ainsi, la présence de ces complexes ternaires en solution peut conduire à stabiliser l'uranium au degré d'oxydation $U^{(VI)}$ en solution et donc augmenter la solubilité de l'uranium et une mobilité plus élevée du fait d'une rétention moindre sur les surfaces argileuses (Joseph et al., 2013 ; Vercoouter et al., 2015 ; Tullborg et al., 2017).

Le travail de thèse s'inscrit dans ce contexte et a pour but de mieux comprendre le comportement de l'uranium dans la formation des argilites du Callovo-Oxfordien en prenant en compte de façon exhaustive toutes les données publiées notamment sur la stabilité des complexes ternaires d'uranyle. L'effet de la température (20 à 80 °C) sur ce comportement est particulièrement étudié.

La première partie du travail a pour but d'identifier et de quantifier l'effet de la température sur la formation des complexes ternaires $Ca-U(VI)-CO_3$. Les processus de rétention de l'uranium sont ensuite étudiés à 20 °C, en se concentrant sur la sorption de $U(VI)$ sur des minéraux argileux de référence (illite et montmorillonite), sur la fraction argileuse des argilites du Callovo-Oxfordien (illite et interstratifié illite/smectite) et au contact d'échantillon brut d'argilites du Callovo-Oxfordien. Le modèle de sorption développé à 20 °C, combiné avec les paramètres thermodynamiques qui caractérisent les complexes ternaires, a servi de base pour l'étude de l'effet de la température sur la sorption de $U(VI)$ pour les divers systèmes argileux.

Effet de la température sur la stabilité des complexes ternaires dans le système « $Ca-U(VI)-CO_3$ »

La mesure des constantes de complexation aqueuse à différentes températures est basée sur une méthode de compétition proposée par Dong et Brooks (2006). La méthode a été adaptée pour permettre l'étude en température (*via* l'utilisation d'une résine plus stable) et la concentration en uranium a été ajustée pour éviter tout problème de précipitation. Des tests préliminaires ont été réalisés pour garantir le bon fonctionnement du montage expérimental et pour évaluer l'équilibre entre la pression de $CO_2(g)$ et les solutions aqueuses.

Les résultats indiquent que les deux complexes aqueux ternaires étudiés ont des comportements différents en température. Avec l'augmentation de la température, la formation du complexe anionique ($CaUO_2(CO_3)_3^{2-}$) est défavorisée, alors que celle du complexe neutre ($Ca_2UO_2(CO_3)_3(aq)$) n'est pas influencée.

Ainsi, à partir des données expérimentales, les constantes de stabilité pour $CaUO_2(CO_3)_3^{2-}$ ($\log_{10} \beta_{113}^{\circ} = 27,3 \pm 0,2$) et $Ca_2UO_2(CO_3)_3(aq)$ ($\log_{10} \beta_{213}^{\circ} = 29,7 \pm 0,3$) ont été calculées en suivant deux approches d'ajustement différentes. Les valeurs obtenues sont cohérentes avec celles publiées, ce qui valide la méthode et le modèle conceptuel proposé. De plus, les données d'enthalpie ont été déterminées pour la formation des complexes ternaires $Ca-U(VI)-CO_3$. Les enthalpies de formation de

$\text{CaUO}_2(\text{CO}_3)_3^{2-}$ et $\text{Ca}_2\text{UO}_2(\text{CO}_3)_3(\text{aq})$ sont respectivement égales à $-27,4 \pm 8,2$ et à $0 \pm 1,8$ kJ/mol. La valeur de $\Delta_r H^\circ$ du complexe anionique est négative, comme cela est proposé par Endrizzi et Rao (2014), même si celle-ci est deux fois plus faible dans le cas présent. Cependant, pour le complexe neutre, la valeur de $\Delta_r H^\circ$ est en désaccord avec celle proposée par Endrizzi et Rao (2014) (-47 kJ/mol). Les autres paramètres thermodynamiques (entropie et énergie libre de Gibbs) sont en bon accord avec ceux publiés par Endrizzi et Rao (2014).

Modèle de sorption U(VI)/argilites du Callovo-Oxfordien à 20 °C

La formation des argilites du Callovo-Oxfordien est constituée principalement de quartz, de minéraux carbonatés (comme la calcite, la dolomite), de pyrite et d'une fraction argileuse qui contient en majorité de l'illite et des argiles interstratifiées I/S (illite/smectite). Pour simplifier l'étude, dans une première approche, les hypothèses suivantes sont faites : (i) la fraction argileuse est considérée comme étant à l'origine de la rétention de l'uranium ; (ii) la fraction I/S est décrite comme un mélange d'illite et de smectite et enfin (iii) la réactivité de la phase argileuse est décrite par deux pôles qui sont l'illite et la montmorillonite (comme minéral représentatif des smectites) (Bradbury et Baeyens, 1997, 2005, 2011 ; Chen et al., 2014 ; Marques Fernandes et al., 2015). Le modèle 2SPNE SC/CE proposé par Bradbury et Baeyens (1997) a été utilisé pour décrire les interactions entre U(VI) et les phases argileuses modèles.

Si le système U(VI)/montmorillonite est bien décrit et paramétré (Bradbury et Baeyens, 1999 ; Marques Fernandes et al., 2012 ; Tournassat et al., 2009, 2018), ce n'est pas le cas pour le système U(VI)/illite pour lequel l'influence des carbonates sur la rétention a été très peu étudiée. C'est pourquoi, un travail expérimental a été réalisé avec l'illite, en complément des études réalisées avec la fraction extraite du COx et des argilites du COx.

Le modèle proposé pour l'illite peut relativement bien expliquer les données expérimentales obtenues pour une large gamme de conditions expérimentales (pH = 6 à 7,3 ; $p\text{CO}_2$ de $10^{-3,5}$ à $10^{-2,1}$; NaNO_3 0,1M et composition chimique de l'eau porale synthétique des argilites du Callovo-Oxfordien). Il considère les paramètres de la montmorillonite pour les espèces hydrolysées de surface. Cependant, une nouvelle constante pour le complexe de surface $\equiv\text{SsOUO}_2(\text{CO}_3)_3^{2-}$ est proposée. La valeur de la constante de sorption apparaît plus élevée pour l'illite ($\log_{10} K = 17,5$) que celle proposée pour la montmorillonite ($\log_{10} K = 15,5$, Marques Fernandes et al, 2012).

Le modèle permet également de décrire de manière convenable le comportement de U(VI) en présence de la fraction argileuse des argilites du Callovo-Oxfordien (illite et I/S), bien qu'un léger décalage ait pu être observé entre l'expérience et le calcul en absence de carbonates. Dans la mesure où le modèle proposé fonctionne correctement dans les conditions physico-chimiques représentatives de la formation du Callovo-Oxfordien (présence de carbonates), aucun changement de paramètre n'a été effectué et l'hypothèse de décrire I/S comme deux pôles d'illite et de montmorillonite est considérée comme valable.

Enfin, le modèle proposé a été appliqué avec succès pour décrire les données de sorption obtenues pour le système U(VI)/argilites du Callovo-Oxfordien. Il permet également de décrire le comportement de U(VI) en présence d'autres roches argileuses, telles que les argiles de l'Opalinus (Amayri et al., 2016 ; Joseph et al., 2013 ; Marques Fernandes et al., 2015) et de Boda (Marques Fernandes et al., 2015). Les résultats obtenus indiquent que la fraction argileuse gouverne la rétention de U(VI). De manière simplifiée, la spéciation en solution est contrôlée par les complexes ternaires de U(VI)

alors que la spéciation à la surface est dominée par le complexe $\equiv\text{SsOUO}_2(\text{CO}_3)_3^{2-}$. Au-delà de ce schéma simplifié, il est important de noter que le modèle prend en compte un nombre important d'équilibres, tels que les réactions d'échange cationique ou celles qui décrivent les propriétés acido-basiques des sites de surface. Il est donc difficile d'évaluer l'incertitude du modèle par rapport à ces capacités prédictives, bien que des études préliminaires de sensibilité indiquent que l'incertitude sur le complexe carbonaté de surface influence fortement les résultats de calcul dans les conditions du CO_x.

Modèle de sorption U/argilites du Callovo-Oxfordien en température (20 à 80 °C)

Le comportement de la sorption de U(VI) en température a été étudié en partant du système le plus simple (illite) vers le système le plus complexe (assemblage minéralogique argileux de la formation du Callovo-Oxfordien) en suivant l'approche mise en place pour l'étude à 20 °C. Les paramètres clés étudiés sont le pH, la pression partielle de CO₂(g) et la composition de la solution.

L'une des principales conclusions de cette étude est que l'effet de la température sur la sorption de U(VI) sur l'illite est négligeable en présence de NaNO₃ ou NaCl ; les valeurs de K_d obtenues dans des conditions expérimentales similaires (pH, force ionique...) ne sont pas influencées dans la gamme de température étudiée (20–80 °C). Ceci est en contradiction avec l'analyse quantitative des données. En effet, la formation des complexes aqueux (et notamment les complexes d'hydrolyse) est favorisée lorsque la température augmente (base de données ThermoChimie, Giffaut et al., 2014), ce qui devrait alors conduire à une diminution de la rétention. Pour permettre une interprétation quantitative des données, il est donc nécessaire de considérer également un effet endothermique pour décrire les phénomènes de sorption afin de contrebalancer l'effet observé en phase aqueuse. Les données ne peuvent pas être décrites en appliquant directement les valeurs d'enthalpie connues des espèces aqueuses aux espèces de surface correspondantes, car le modèle global surestime systématiquement les données expérimentales. Ainsi, les valeurs d'enthalpie pour les complexes de surface ont dû être ajustées à partir des données expérimentales en suivant une approche progressive en considérant un effet négligeable de la température pour le mécanisme d'échange ionique et en prenant en compte deux contraintes pour les complexes de surfaces : l'équation de Van't Hoff doit être respectée et une corrélation linéaire doit s'appliquer entre les valeurs pour la spéciation aqueuse et pour la spéciation de surface. Un modèle de complexation de surface a ainsi pu être construit pour permettre d'expliquer de manière satisfaisante les données expérimentales. Dans le modèle, seules les valeurs d'enthalpie pour les espèces hydrolysées de surface ont dû être ajustées. Avec l'augmentation de la température, les espèces carbonatées de surface ne sont plus majoritaires pour les valeurs de pH inférieures à 7.

Le modèle développé pour l'illite peut s'appliquer de manière satisfaisante aux échantillons naturels (fraction argileuse et échantillon brut des argilites du Callovo-Oxfordien) en absence ou en présence des complexes ternaires Ca-U(VI)-CO₃.

Le modèle proposé, avec les nouveaux paramètres obtenus, peut donc être utilisé pour évaluer le comportement de U(VI) dans la formation argileuse du Callovo-Oxfordien pour une gamme de température variant entre 20 et 80 °C. Si l'uranium reste majoritairement sous le degré d'oxydation (VI) dans la solution porale du fait de la formation des complexes ternaires, la présence éventuelle de complexes de surface faisant intervenir l'uranium au degré d'oxydation U(IV) demeure une possibilité. Cela peut être étudié si l'on est capable de contrôler expérimentalement le potentiel redox du système dans les conditions physico-chimiques représentatives des argilites à l'état naturel.

References

- Amayri, S., Fröhlich, D. R., Kaplan, U., Trautmann, N., and Reich, T.. (2016). Distribution Coefficients for the Sorption of Th, U, Np, Pu, and Am on Opalinus Clay. *Radiochimica Acta* **104** (1): 33–40.
- Andra. (2005). *Dossier 2005 Argile - Synthèse Evaluation de La Faisabilité Du Stockage Géologique En Formation Argileuse*. 240p. Andra, Châtenay-Malabry (France).
- Bernhard, G., Geipel, G., Brendler, V., and Nitsche, H. (1996). Speciation of Uranium in Seepage Waters of a Mine Tailing Pile Studied by Time-Resolved Laser-Induced Fluorescence Spectroscopy (TRLFS). *Radiochimica Acta* **74**: 87–91.
- Bernhard, G., Geipel, G., Reich, T., Brendler, V., Amayri, S., and Nitsche, H. (2001). Uranyl(VI) Carbonate Complex Formation: Validation of the $\text{Ca}_2\text{UO}_2(\text{CO}_3)_3(\text{aq.})$ Species. *Radiochimica Acta* **89**: 511–518.
- Bradbury, M. H., and Baeyens, B. (1997). A Mechanistic Description of Ni and Zn Sorption on Na-Montmorillonite. Part II: modelling. *Journal of Contaminant Hydrology* **27** (3–4): 223–248.
- Bradbury, M. H., and Baeyens, B. (1999). Modelling the Sorption of Zn and Ni on Ca-Montmorillonite. *Geochimica et Cosmochimica Acta* **63** (3–4): 325–336.
- Bradbury, M. H., and Baeyens, B. (2005c). Modelling the Sorption of Mn(II), Co(II), Ni(II), Zn(II), Cd(II), Eu(III), Am(III), Sn(IV), Th(IV), Np(V) and U(VI) on Montmorillonite: Linear Free Energy Relationships and Estimates of Surface Binding Constants for Some Selected Heavy Metals and Actinide. *Geochimica et Cosmochimica Acta* **69** (4): 875–892.
- Bradbury, M. H., and Baeyens, B. (2011). Predictive Sorption Modelling of Ni(II), Co(II), Eu(III), Th(IV) and U(VI) on MX-80 Bentonite and Opalinus Clay: A ‘Bottom-Up’ Approach. *Applied Clay Science* **52** (1–2): 27–33.
- Chen, Z., Montavon, G., Guo, Z., Wang, X., Razafindratsima, S., Robinet, J. C., and Landesman, C.. (2014a). Approaches to Surface Complexation Modeling of Ni(II) on Callovo-Oxfordian Clayrock. *Applied Clay Science* **101**: 369–380.
- Dong, W. and Brooks, S. C. (2006). Determination of the Formation Constants of Ternary Complexes of Uranyl and Carbonate with Alkaline Earth Metals (Mg^{2+} , Ca^{2+} , Sr^{2+} , and Ba^{2+}) Using Anion Exchange Method. *Environmental Science & Technology* **40** (15): 4689–4695.
- Endrizzi, F. and Rao, L. (2014). Chemical Speciation of Uranium (VI) in Marine Environments: Complexation of Calcium and Magnesium Ions with $[(\text{UO}_2)(\text{CO}_3)_3]^{4-}$ and the Effect on the Extraction of Uranium from Seawater. *Chemistry-A European Journal* **20** (44): 14499–14506.
- Giffaut, E., Grivé, M., Blanc, P., Vieillard, P., Colàs, E., Gailhanou, H., Gaboreau, S., Marty, N., Madé, B., and Duro, L. (2014). Andra Thermodynamic Database for Performance Assessment: ThermoChimie. *Applied Geochemistry* **49**: 225–236.
- Guillaumont, R., Fanghänel, T., Neck, V., Fuger, J., Palmer, D. A., Grenthe, I., and Rand, M. (2003). *Update on the Chemical Thermodynamics of Uranium, Neptunium, Plutonium, Americium and Technetium*. 2nd ed. 919p. OECD Nuclear Energy Agency, Data Bank, Issy-les-Moulineaux (France).
- Jo, Y. and Yun, J. (2017). Spectroscopic Properties and Formation Constants of Ternary Ca-UO₂-CO₃ Complexes at High Temperatures. p. 34–35 in 6th *Asia-Pacific Symposium on Radiochemistry*. Jeju Island (South Korea).
- Joseph, C., Van Loon, L. R., Jakob, A., Stuedtner, R., Schmeide, K., Sachs, S., and Bernhard, G. (2013). Diffusion of U(VI) in Opalinus Clay: Influence of Temperature and Humic Acid. *Geochimica et Cosmochimica Acta* **109**: 74–89.

- Joseph, C. (2013). *'The Ternary System U(VI) / Humic Acid / Opalinus Clay'*. Ph. Dissertation Helmholtz-Zentrum Dresden-Rossendorf (Germany).
- Kalmykov, S. N. and Choppin, G. R. (2000). Mixed $\text{Ca}^{2+}/\text{UO}_2^{2+}/\text{CO}_3^{2-}$ Complex Formation at Different Ionic Strengths. *Radiochimica Acta* **88** (9–11): 603-606.
- Lee, J-Y and Yun, J. (2013). Formation of Ternary $\text{CaUO}_2(\text{CO}_3)_3^{2-}$ and $\text{Ca}_2\text{UO}_2(\text{CO}_3)_3(\text{aq})$ Complexes under Neutral to Weakly Alkaline Conditions. *Dalton Transactions* **42** (27): 9862-9869.
- Marques Fernandes, M., Baeyens, B., Dähn, R., Scheinost, A. C., and Bradbury, M. H. (2012). U(VI) Sorption on Montmorillonite in the Absence and Presence of Carbonate: A Macroscopic and Microscopic Study. *Geochimica et Cosmochimica Acta* **93**: 262–277.
- Marques Fernandes, M., Vér, N., and Baeyens, B.. (2015). Predicting the Uptake of Cs, Co, Ni, Eu, Th and U on Argillaceous Rocks Using Sorption Models for Illite. *Applied Geochemistry* **59**: 189–199.
- Runde, W. (2000). The Chemical Interactions of Actinides in the Environment. *Los Alamos Science* **26** (26) : 392–411.
- Tournassat, C., Blanc, P., and Gaucher, E.C. (2008). *Estimation de La Composition de L'eau Porale Du Callovo-Oxfordien À 50, 70, 80 et 90 °C*. BRGM Report RP-5617. 41p. Orléans (France)
- Tournassat, C., Tinnacher, R. M., Grangeon, S., and Davis, J. A. (2018). Modeling uranium(VI) Adsorption onto Montmorillonite under Varying Carbonate Concentrations: A Surface Complexation Model Accounting for the Spillover Effect on Surface Potential. *Geochimica et Cosmochimica Acta* **220**: 291–308.
- Tullborg, E. L., Suksi, J., Geipel, G., Krall, L., Auqué, L., Gimeno, M., and Puigdomenech, I. (2017). The Occurrences of $\text{Ca}_2\text{UO}_2(\text{CO}_3)_3$ Complex in Fe(II) Containing Deep Groundwater at Forsmark, Eastern Sweden. *Procedia Earth and Planetary Science* **17** (li): 440–443.
- Vercouter, T., Reiller, P. E., Ansoborlo, E., Février, L., Gilbin, R., Lomenech, C., and Philippini, V. (2015). A Modelling Exercise on the Importance of Ternary Alkaline Earth Carbonate Species of uranium(VI) in the Inorganic Speciation of Natural Waters. *Applied Geochemistry* **55** (Vi): 192–198.

Chapter 1

Introduction

The possible existence of radionuclides (RN) in nature, due to the increasing use of nuclear power generation and the widespread use of radioisotopes for beneficial purposes in research, industry, medicine and agriculture, raises a number of environmental concerns. Therefore, it is essential to understand the chemical behaviour of these radioelements for reliable prediction of their migration.

The disposal of radioactive waste has been discussed for many decades because of the special status that it has with the public, leading to implementation and development programmes that are typically mobilised by research and development efforts, resulting in a number of alternative disposal options. The options reflect the specifics of national legislations, geological differences and variations in the amount and characteristics of different waste types (IAEA, 2016).

Countries such as Argentina, Belgium, Canada, Czech Republic, Finland, France, Japan, the Netherlands, Republic of Korea, Russia, Spain, Sweden, Switzerland, the UK, and the USA have chosen to dispose of radioactive waste in deep geological underground repositories. The usage of these repositories is generally reserved for intermediate- and high-level waste (ILW and HLW) and for long half-life radionuclides. The waste is mostly generated by the nuclear fuel cycle, mainly in the form of spent fuel and a variety of other waste types, as a consequence of the reprocessing cycle (such as vitrified waste and bituminous wastes). The rationale behind deep geological disposals is based on storing the waste packages in specifically engineered facilities located deep underground (often 400m to 600 m deep) in geological contexts. The main types of host-rock formations used are sedimentary (e.g. claystones), crystalline (e.g. granite) and salt domes (Altmann, 2008).

Many countries have chosen to use claystone formations (e.g. Opalinus Clay in Switzerland; Boda Claystone Formation in Hungary; Boom Clay in Belgium; Callovo-Oxfordian Clay Formation in France) as deep geological repositories and these are the ones we are interested in the present work. These countries have dedicated large research efforts on choosing an optimal type of rock (e.g. through the analysis of mineralogy and physical–chemical and mechanical properties) and a favourable geological context (e.g. depth, tectonic stability and groundwater systems). Moreover, research has also characterised the properties of the host-rock which determine its capacity to limit radionuclides transfer to the geosphere (such as hydraulic permeability, solute diffusion characteristics and retention processes).

The deep repository allows the confinement of the radioactive waste in a facility that ensures long-term safety through a multiple-barrier system to isolate the waste from the hydrosphere and biosphere.

As a result, future generations are protected from radioactive risk and toxicity. The multi-barrier system includes from the single-waste container to the near- and far-field: spent fuel disposal cells; concrete/metal canisters; backfill materials composed by cements and engineered swelling clays as bentonite; and natural host-rock as geological barrier (see example in Figure 1, showing the Andra disposal concept in claystone host-rock). The safety of radioactive disposal results from the performance assessment simulations that are based on modelling the processes that govern the radionuclide speciation and migration in natural systems (McKinley and Alexander, 2007).

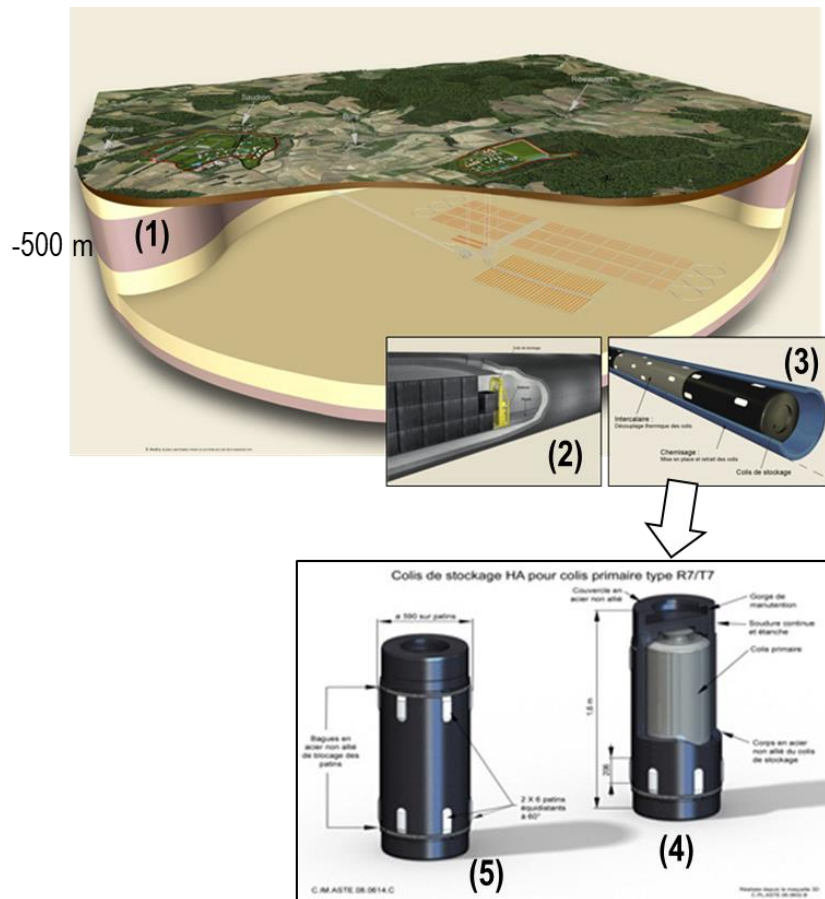


Figure 1. Schematic representation of deep geological nuclear waste disposal multi-barrier system (1) Callovo-Oxfordian host-rock; (2) engineered barrier for IWL; (3) engineered barrier for HWL; (4) and (5) HWL primary package (e.g. vitrified waste).

The quantitative description of the radionuclides migration relies on a detailed knowledge of the system's geochemistry across the potential migration pathways (e.g. aqueous speciation, sorption, incorporation, precipitation) (Figure 2). Here, two main parameters have to be considered: the mobility of the radionuclides in solution and the retention that describes the affinity of radionuclides to the mineral surface, which also help in limiting their mobility.

The geological environment in a nuclear waste repository will also be subjected to disturbances (e.g. thermal, hydraulic, mechanical and chemical, known as THMC) and different levels of radioactivity over time. One of the consequences of this is the increase in temperature of all repository promoted by the radioactivity of the long half-life HLW. In the host-rock, this effect may not only change the porewater chemical composition (aqueous speciation, pH, redox potential and gas pressure) but also the water-rock interaction processes (dissolution, precipitation and sorption).

For this reason, it is essential to understand the processes of retention, through the analysis of sorption, and determine the stability of the surface complexes over a wide range of temperatures in order to predict the mobility of the radionuclides (Halter, 1999).

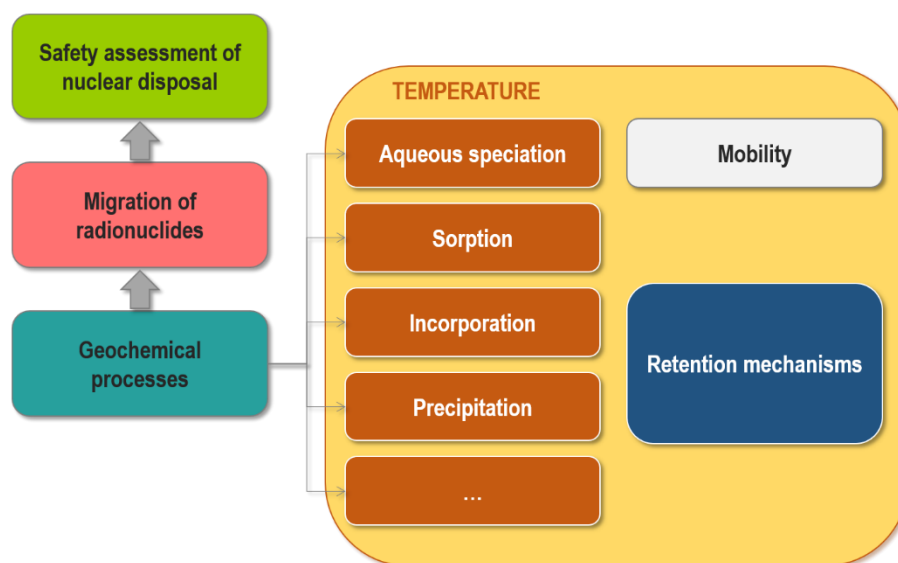


Figure 2. Schematic pathway for the safety assessment of the nuclear disposal.

1.1. Context

In France, the Callovo-Oxfordian claystone formation (so-called COx) is under study as a geological barrier in the “Cigéo” (Centre Industriel de Stockage Géologique) radioactive waste disposal project, located in Meuse/Haute-Marne site (Eastern France). This argillaceous formation is characterised by low permeability, mineralogical homogeneity and low variation of other physicochemical properties in a large extension (Andra, 2005a).

The Callovo-Oxfordian claystone, together with an engineered barrier system (EBS), comprises a mineralogical assemblage that plays an important role on the physical-chemical control and retardation of radionuclides migration to the natural environment.

At present, in French facilities the spent fuel is composed by uranium oxides and mixed uranium-plutonium oxides, which are conditioned in glass matrices by vitrification processes. The diffusion of α -radiation promoted by radioisotopes and water causes corrosion and dissolution of the spent fuel releasing radionuclides.

Uranium is one of the main components of the radioactive waste and it is usually found in its fourth oxidation state mainly in solid form in the repository’s surrounding. Its mobility in the environment is intrinsically related to its solubility, which is limited by a) the stability of the solubility-controlling mineral, and b) the stability of the aqueous species (Runde, 2000).

In the surrounding environments of the repository, in contact with the groundwater, U(IV) may oxidise to U(VI), which results in stable and mobile complexes. The U(VI) may be present even under reducing conditions as a result of the formation of the ternary calcium-uranyl- carbonate aqueous complexes (Ca-U(VI)-CO₃). As shown in Figure 3, the uranium released from vitrified waste in

uranyl form will be controlled by the retention properties of the host-rock minerals (clay fraction) and by the chemical composition of the claystone porewater. In this study, we will focus on the sorption processes and the aqueous complexation of U(VI) in solution.

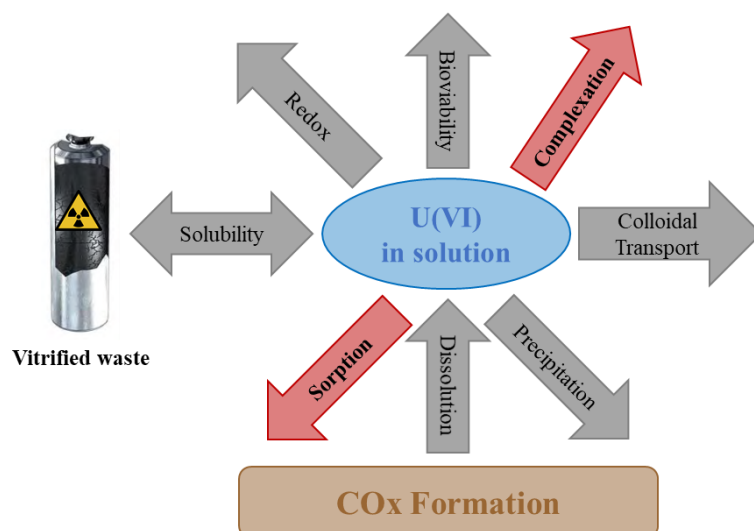


Figure 3. Schematic representation of U(VI) controlling processes in radioactive waste disposal system using host-clay rock. The main processes concerning in the present study are highlighted in red.

The processes described in Figure 3 are important for the performance assessment of nuclear waste disposal under clay rock conditions. According to the scenarios developed for the Cigéo project, the temperature of the Callovo-Oxfordian formation must reach 90 °C in the short-term and not more than 70 °C in the long-term (for at least 1000 years) (Andra, 2005b). Changes in temperature can potentially induce changes in uranium behaviour (e.g. solubility, retention and mobility) through physical-chemical changes of the host-clay rock and porewater composition.

Thus, it becomes relevant to evaluate the effect of temperature on the chemical behaviour of U(VI).

1.1.1. Characterisation of the Callovo-Oxfordian Formation System

The Callovo-Oxfordian claystone is a geological formation belonging to the Paris Basin (Figure 4). The Paris basin is composed of alternating claystone and limestone layers in a simple and regular geometric structure, deposited during a stable marine environment in the Jurassic period. The Callovo-Oxfordian unit is surrounded by massive carbonate units (Dogger and Oxfordian limestones) and is a predominantly clay-rich layer, 130m to 160m thick and located between 500m and 630m deep in the transition zone. The unit is divided in three sedimentary sequences: the central part is the most clayey zone (up to 60% clay minerals); whereas the top and bottom are characterised by a carbonate enrichment, related with the transition to the limestone units. At the transition zone and beyond, the unit shows very little lateral variation in lithology.

In terms of mineralogy, the Callovo-Oxfordian claystone formation is composed of phyllosilicates (20-60 wt%, mainly illite and interstratified illite/smectite, kaolinite, micas and chlorite),

tectosilicates (10-40 wt%, mainly quartz and feldspars), carbonates (15-75wt%, mainly calcite and dolomite) and sulphides (0-3wt%, mainly pyrite). An example of a mineralogical composition of a borehole crossing Meuse/Haute-Marne site is provided in Table 1.

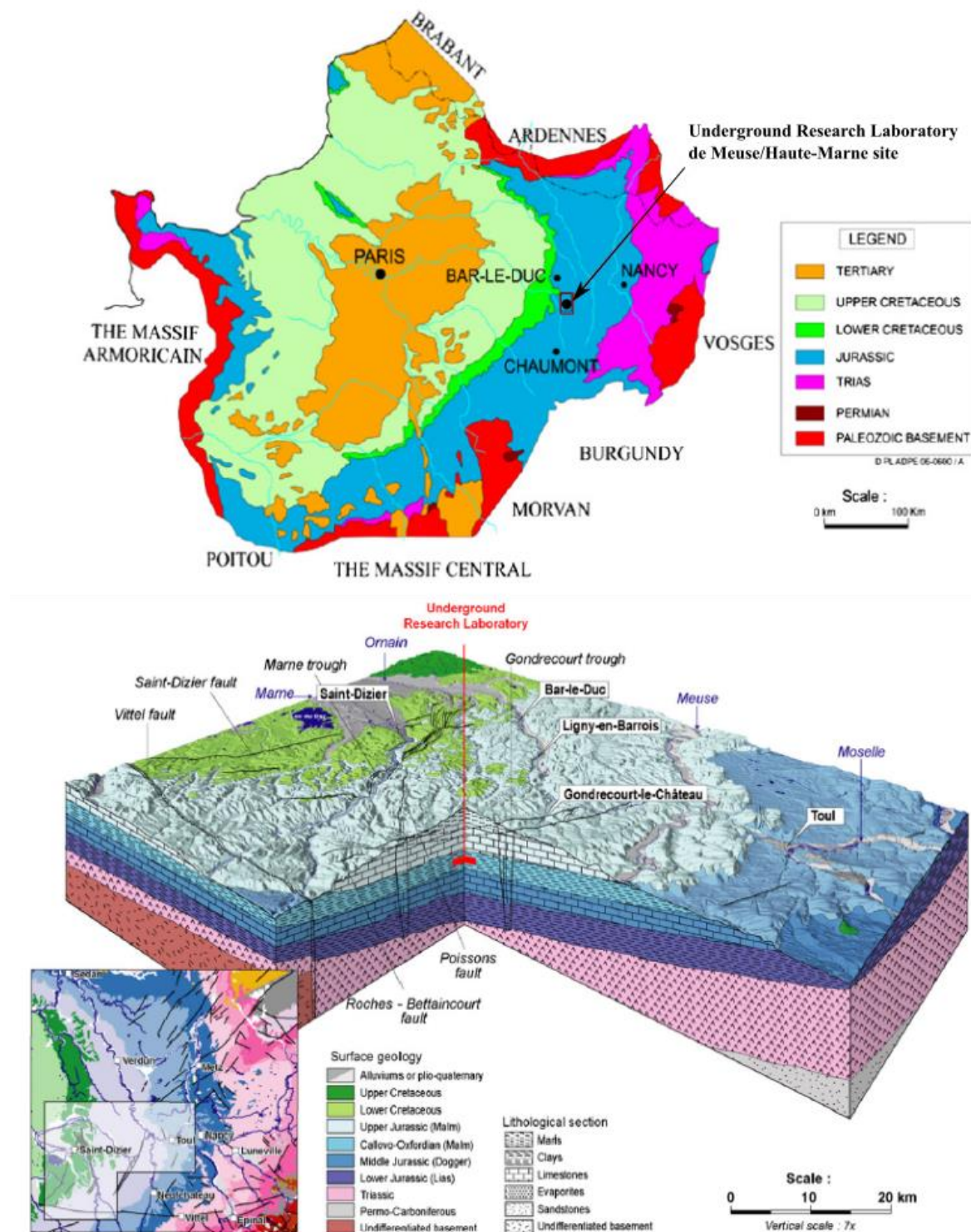


Figure 4. Geological location of the underground research laboratory within the Paris Basin (upper) and cross section of the geological formations surrounding the underground research laboratory. Adapted from Linard et al., 2011.

Table 1. Average and extreme values of the mineralogical composition (wt%) of the host layer in borehole EST205 Meure/Haute-Marne site (Gaucher et al., 2004).

Minerals	wt%	max	min
Illite group	12.9	21	2
Interstratified illite-smectite (I/S)	11.6	33	0
Kaolinite	1.7	5	0
Chlorite	1.9	2.7	0
Quartz (silicates)	9.5	43	0.9
Calcite (carbonates)	15.3	75	2
Pyrite	0.7	0.9	0.2
Siderite + ferriferous minerals	1.5	2.7	0.5
Titanium minerals	0.2	0.4	0
Phosphate minerals	0.2	0.6	0.2

1.1.1.1. Chemical composition of the Callovo-Oxfordian porewater

The chemical composition of the claystone porewater is essential to assess the chemical and diffusive behaviour of the radionuclides, as well as the stability of the materials present in the nuclear waste disposal. Knowing the main chemical conditions of the clay-host rock porewater is thus an important step in predicting how the clay-host rock barrier will behave over time (Altmann, 2008).

The chemical composition of the Callovo-Oxfordian porewater has been determined by *in situ* measurements and by complementary geochemical calculations taking into account the mineralogical composition. The latter is done due to the difficulty of sampling directly the porewater of COx claystone (or any other type of clay rock), where only small volumes can usually be obtained to allow a quantitative representation of the *in situ* conditions. However, improvements in characterisation techniques have made it feasible and, as a result, representative porewater samples have been obtained, as shown by Vinsot et al. (2008). The comparison of the chemical composition measured *in situ* and that calculated validates the geochemical model proposed by Gaucher et al. (2009), taking into account the mineral's solubility and cationic exchange reactions (using ThermoChimie database, Giffaut et al., 2014 and Grivé et al., 2015).

As previously mentioned, the temperature increase originated from the radioactivity of the HLW will change the porewater chemistry. This temperature effect was experimentally studied by using different mineralogy assemblages (Beaucaire et al., 2012; Tournassat et al., 2008). Two systems were defined: a) complete mineralogical composition, representative of COx claystone, composed of quartz, illite, chlorite, carbonates (calcite, dolomite and siderite), pyrite and celestine; and b) reduced mineralogical composition characterised only by carbonates and sulphates (calcite, dolomite, siderite and celestine). The results of the chemical composition of the different *in situ* porewaters (25°C) and at different temperatures considering both mineralogy assemblages are provided in Table 2 and Table 3 (Tournassat et al., 2008).

Table 2. Chemical composition of the Callovo-Oxfordian porewater calculated by geochemical modelling according to the temperature increasing using the reduced mineralogy.

Temp	pH	pCO ₂	Cl ⁻	SO ₄ ²⁺	TIC	Na ⁺	K ⁺	Ca ²⁺	Mg ²⁺	Sr ²⁺	Si ⁴⁺
°C		atm					mM				
25	7.2	10 ^{-2.1}	41	14.7	2.4	43.2	1.04	8.5	5.4	0.21	0.18
50	6.86	10 ^{-1.7}	41	14	2.3	42	1.00	9.7	4	0.2	0.18
70	6.66	10 ^{-1.4}	41	12	2.1	40	0.98	9.8	3	0.18	0.18
80	6.57	10 ^{-1.3}	41	11	2.1	39	0.95	9.7	2.7	0.16	0.18
90	6.5	10 ^{-1.2}	41	10	2.0	38	0.93	9.5	2.3	0.15	0.18

Table 3. Chemical composition of the Callovo-Oxfordian porewater calculated by geochemical modelling according to the temperature increasing using the completed mineralogy.

Temp	pH	pe	pCO ₂	Cl ⁻	SO ₄ ²⁺	TIC	Na ⁺	K ⁺	Ca ²⁺	Mg ²⁺	Sr ²⁺	Fe _{total}	Al ³⁺	Si ⁴⁺
°C			atm					mM						
25	7.2	-3	10 ^{-2.1}	41	15	2.4	43	1.0	8.5	5.4	0.21	47	2.9·10 ⁻⁶	0.18
50	6.66	-2.9	10 ^{-1.3}	41	14	3.8	42	1.0	9.9	4.1	0.2	0.05	2	0.35
70	6.31	-2.8	10 ^{-0.8}	41	12	5.9	41	0.99	10	3.2	0.19	0.05	4	0.56
80	6.15	-2.8	10 ^{-0.5}	41	11	7.6	40	0.98	10	2.8	0.18	0.05	6	0.69
90	6.01	-2.8	10 ^{-0.3}	41	10	10	39	0.96	10	2.5	0.17	0.05	8	0.84

1.2. Scopes of the thesis work

In the past, geochemical modelling exercises applied to nuclear waste disposal usually predicted U(IV) as the most important redox state when using thermodynamic data sets, such as NEA-TDB (Guillaumont et al., 2003). Recent published data have clearly established the existence of Ca-U(VI)-CO₃ ternary complexes (Bernhard et al., 1996, 2001; Kalmykov and Choppin, 2000; Dong and Brooks, 2006; Lee and Yun, 2013; Endrizzi and Rao, 2014; Jo and Yun, 2017). The presence of these complexes leads to an increase of the predicted uranium mobility (greater solubility and lower retention) (Joseph et al., 2013; Vercouter et al., 2015; Tullborg et al., 2017). For this reason, a special care is taken for uranium, since it is considered to be the most mobile actinide in the performance assessment.

Therefore, the aim of the present work is to better understand the behaviour of U(VI) in Callovo-Oxfordian formation, including how it is affected by temperature changes.

This work is divided into three main parts. In Chapter 2 we aim to identify and understand the dominating uranyl aqueous species at different temperatures, with a special focus on the thermodynamic properties of Ca-U(VI)-CO₃ ternary complexes. In Chapter 3 we aim to understand the retention processes of uranium at 20°C, focusing on the U(VI) sorption in the most relevant clay minerals (illite and interstratified illite/smectite) of the Callovo-Oxfordian claystone system. In the last Chapter (Chapter 4), we used the model proposed at 20 °C for the retention mechanisms of U(VI) to further study the effect of temperature on U(VI) sorption on Callovo-Oxfordian claystone systems at different temperatures.

1.3. References

- Altmann, S. (2008). “Geo”chemical Research: A Key Building Block for Nuclear Waste Disposal Safety Cases. *Journal of Contaminant Hydrology* **102** (3–4): 174–179.
- Andra. (2005a). *Dossier 2005: Andra Research on the Geological Disposal of High-Level Long-Lived Radioactive Waste*. 4p. Andra, Châtenay-Malabry (France).
- Andra. (2005b). *Dossier 2005 Argile - Synthèse Evaluation de La Faisabilité Du Stockage Géologique En Formation Argileuse*. 240p. Andra, Châtenay-Malabry (France).
- Beaucaire, C., Tertre, E., Ferrage, E., Grenut, B., Pronier, S., and Madé, B. (2012). A Thermodynamic Model for the Prediction of Pore Water Composition of Clayey Rock at 25 and 80°C - Comparison with Results from Hydrothermal Alteration Experiments. *Chemical Geology* **334**: 62–76.
- Bernhard, G., Geipel, G., Brendler, V., and Nitsche, H. (1996). Speciation of Uranium in Seepage Waters of a Mine Tailing Pile Studied by Time-Resolved Laser-Induced Fluorescence Spectroscopy (TRLFS). *Radiochimica Acta* **74**: 87–91.
- Bernhard, G., Geipel, G., Reich, T., Brendler, V., Amayri, S., and Nitsche, H. (2001). Uranyl(VI) Carbonate Complex Formation: Validation of the $\text{Ca}_2\text{UO}_2(\text{CO}_3)_3(\text{aq.})$ Species. *Radiochimica Acta* **89**: 511–518.
- Dong, W. and Brooks, S. C. (2006). Determination of the Formation Constants of Ternary Complexes of Uranyl and Carbonate with Alkaline Earth Metals (Mg^{2+} , Ca^{2+} , Sr^{2+} , and Ba^{2+}) Using Anion Exchange Method. *Environmental Science & Technology* **40** (15): 4689–4695.
- Endrizzi, F. and Rao, L. (2014). Chemical Speciation of Uranium (VI) in Marine Environments: Complexation of Calcium and Magnesium Ions with $[(\text{UO}_2)(\text{CO}_3)_3]^{4-}$ and the Effect on the Extraction of Uranium from Seawater. *Chemistry-A European Journal* **20** (44): 14499–14506.
- Gaucher, E., Robelin, C., Matray, J. M., Négrel, G., Gros, Y., Heitz, J., Vinsot, A., Rebours, H., Cassagnabère, A., and Bouchet, A. (2004). ANDRA Underground Research Laboratory: Interpretation of the Mineralogical and Geochemical Data Acquired in the Callovian–Oxfordian Formation by Investigative Drilling. *Physics and Chemistry of the Earth, Parts A/B/C* **29** (1): 55–77.
- Giffaut, E., Grivé, M., Blanc, P., Vieillard, P., Colàs, E., Gailhanou, H., Gaboreau, S., Marty, N., Madé, B., and Duro, L. (2014). Andra Thermodynamic Database for Performance Assessment: ThermoChimie. *Applied Geochemistry* **49**: 225–236.
- Grivé, M., Duro, L., Colàs, E., and Giffaut, E. (2015). Thermodynamic Data Selection Applied to Radionuclides and Chemotoxic Elements: An Overview of the ThermoChimie-TDB. *Applied Geochemistry* **55**: 85–94.
- Guillaumont, R., Fanghänel, T., Neck, V., Fuger, J., Palmer, D. A., Grenthe, I., and Rand, M. (2003). *Update on the Chemical Thermodynamics of Uranium, Neptunium, Plutonium, Americium and Technetium*. 2nd ed. 919p. OECD Nuclear Energy Agency, Data Bank, Issy-les-Moulineaux, France.
- Halter, W. E. (1999). Surface Acidity Constants of $\alpha\text{-Al}_2\text{O}_3$ between 25 and 70°C. *Geochimica et Cosmochimica Acta* **63** (19): 3077–3085.
- IAEA. (2016). Waste Technology Section. *Nuclear Fuel Cycle & Waste Technology*.
- Jo, Y. and Yun, J. (2017). Spectroscopic Properties and Formation Constants of Ternary Ca-UO₂-CO₃ Complexes at High Temperatures. p. 34–35 in *6th Asia-Pacific Symposium on Radiochemistry*. Jeju Island (South Korea).

- Joseph, C., Van Loon, L. R., Jakob, A., Steudtner, R., Schmeide, K., Sachs, S., and Bernhard, G. (2013). Diffusion of U(VI) in Opalinus Clay: Influence of Temperature and Humic Acid. *Geochimica et Cosmochimica Acta* **109**: 74–89.
- Kalmykov, S. N. and Choppin, G. R. (2000). Mixed $\text{Ca}^{2+}/\text{UO}_2^{2+}/\text{CO}_3^{2-}$ Complex Formation at Different Ionic Strengths. *Radiochimica Acta* **88** (9–11): 603–606.
- Lee, J-Y. and Yun, J. (2013). Formation of Ternary $\text{CaUO}_2(\text{CO}_3)_3^{2-}$ and $\text{Ca}_2\text{UO}_2(\text{CO}_3)_3(\text{aq})$ Complexes under Neutral to Weakly Alkaline Conditions. *Dalton Transactions* **42** (27): 9862-9869.
- Linard, Y., A. Vinsot, B. Vincent, J. Delay, S. Wechner, R. De La Vaissière, E. Scholz, B. Garry, M. Lundy, M. Cruchaudet, S. Dewonck, and G. Vigneron. (2011). Water Flow in the Oxfordian and Dogger Limestone around the Meuse/Haute-Marne Underground Research Laboratory. *Physics and Chemistry of the Earth* **36** (17–18): 1450–1468.
- McKinley, L. E. and Alexander, W. R. (2007). *Deep Geological Disposal of Radioactive Waste*. Radioactivity in the Environment, vol. 9. 273p. Elsevier
- Runde, W. (2000). The Chemical Interactions of Actinides in the Environment. *Los Alamos Science* **26** (26): 392–411.
- Tournassat, C., Blanc, P., and Gaucher, E. C. (2008). *Estimation de La Composition de L'eau Porale Du Callovo-Oxfordien À 50, 70, 80 et 90 °C*. BRGM Report RP-5617. 41p. Orléans (France)
- Tullborg, E. L., Suksi, J., Geipel, G., Krall, L., Auqué, L., Gimeno, M., and Puigdomenech, I. (2017). The Occurrences of $\text{Ca}_2\text{UO}_2(\text{CO}_3)_3$ Complex in Fe(II) Containing Deep Groundwater at Forsmark, Eastern Sweden. *Procedia Earth and Planetary Science* **17** (li): 440–443.
- Vercouter, T., Reiller, P. E., Ansoborlo, E., Février, L., Gilbin, R., Lomenech, C., and Philippini, V. (2015). A Modelling Exercise on the Importance of Ternary Alkaline Earth Carbonate Species of uranium(VI) in the Inorganic Speciation of Natural Waters. *Applied Geochemistry* **55** (Vi): 192–198.

Chapter 2

Speciation of Ca-U(VI)-CO₃ ternary complexes

2.1. Introduction

The evaluation of the migration of actinide elements from a deep underground repository requires reliable thermodynamic stability data on complex formation of actinide ions. The existence of ternary calcium-uranyl-carbonate aqueous complexes (Ca-U(VI)-CO₃), and their impact on aqueous systems, has been studied extensively (Bernhard et al., 1996, 2001; Steward et al., 1996; Kalmykov and Chopin, 2000; Zheng et al., 2003; Dong and Brooks, 2006; Kelly et al., 2007; Meleshyn et al., 2009; Prat et al., 2009; Joseph et al., 2011, 2012, 2013; Lee and Yun, 2013; Endrizzi and Rao, 2014; Vercouter et al., 2015; Jo and Yun, 2017; Tullborg et al., 2017).

Recently, predictive modelling performed by Vercouter et al. (2015) indicated that alkaline earth ternary carbonate species of M(II)-U(VI)-CO₃ (where M(II) = Mg or Ca) dominate the uranyl speciation in natural water and clay conditions. Geochemical calculations carried out by Joseph (2013) and Tullborg et al. (2017) also indicated that the formation of calcium uranyl carbonates can stabilise uranium in solution and increase its mobility. Moreover, among the different actinides present in the radioactive waste, uranium is the most mobile. Therefore, the study of these complexes, and of their behaviour at temperatures higher than 25 °C, is highly relevant for the knowledge of uranium behaviour in nuclear waste disposal. In this context, a brief overview of literature data on the system Ca/Mg-U(VI)-CO₃ is provided below.

2.1.1. Ca-U(VI)-CO₃ system

The Ca-U(VI)-CO₃ complexes were primarily identified by Bernhard and co-workers (1996) in seepage waters with high content of calcium and carbonates. TRLFS (Time-resolved laser induced fluorescence) spectroscopy analysis was used to identify these complexes. The authors detected that in the presence of calcium the fluorescence intensity of uranyl carbonates increases, while the uranyl carbonate species itself exhibits poor fluorescence, suggesting the formation of calcium-uranyl-

carbonate aqueous species under such chemical conditions. The identification of these species and the uncertainty of the calculations have led to the on-going investigation of a better understanding of Ca-U(VI)-CO₃ species formation. Consequently, different studies were developed to identify and validate the presence of Ca-U(VI)-CO₃ aqueous species in different experimental conditions (Kalmykov and Choppin, 2000; Bernhard et al., 2001; Dong and Brooks, 2006; Lee and Yun, 2013; Endrizzi and Rao, 2014; Jo and Yun, 2017).

The stability constants for Ca₂UO₂(CO₃)₃(aq) and CaUO₂(CO₃)₃²⁻ can be described by Reaction 1 and Reaction 2 and a summary of the literature that includes the data is provided in Table 4.

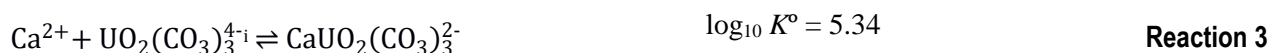


Table 4. Summary of the literature analysing the stability constants of Ca-U(VI)-CO₃ complexes. Data in grey have been superseded by later references of the same authors (2001).

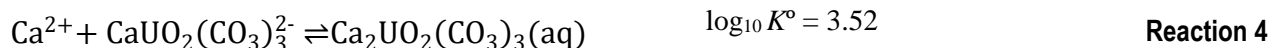
Reference	log ₁₀ β ^o ₁₁₃ CaUO ₂ (CO ₃) ₃ ²⁻	log ₁₀ β ^o ₂₁₃ Ca ₂ UO ₂ (CO ₃) ₃ (aq)	Ionic strength correction	Technique
Bernard et al. (1996)	-	26.80±0.70 (I=0.1)	n.a.	TRLFS
Kalmykov and Choppin (2000)	-	29.80 ± 0.70	SIT	fluorescence
Bernhard et al. (2001)	25.40 ± 0.25	30.45 ± 0.35	Davies	TRLFS
Dong and Brooks (2006)	27.18 ± 0.06	30.70 ± 0.05	Davies	Anion exchange resin
Lee and Yun (2013)	27.27 ± 0.14	29.81 ± 0.19	SIT	TRLFS
Endrizzi and Rao (2014)	26.99 ± 0.72	30.84 ± 0.72	SIT	selective electrode and UV/VIS
Jo and Yun (2017)	26.13 ± 0.20	30.64 ± 0.20	SIT	TRLFS

In the NEA (Nuclear Energy Agency) chemical thermodynamics update for uranium (Guillaumont et al., 2003), a review on the available publications up to 2003 for those species was made. The authors analysed the studies from Bernhard et al. (2001) and Kalmykov and Choppin (2000). Guillaumont et al. (2003) pointed out some shortcomings in those experimental works, especially in relation to the ionic strength control of the system. For this reason, Guillaumont et al. (2003) did not support the selected stability constants for the formation of CaUO₂(CO₃)₃²⁻ and Ca₂UO₂(CO₃)₃(aq). However, the NEA review stated that *the constant proposed in Kalmykov and Chopin (2000) and Bernhard et al. (2001) may be used as a guidance*. For further information, a detailed discussion of these studies can be found in Appendix A in Guillaumont et al. (2003).

Later in 2006, Dong and Brooks determined the formation constants from anionic-exchange experiments with a calcium concentration range of 0 to 5 mM at pH = 8.1 and 0.1 M ionic strength by using NaNO₃ as background electrolyte under room conditions. The authors pointed out that the constants agree with the expected trend: the binding constant of Ca²⁺ to UO₂(CO₃)₃⁴⁻ (Reaction 3) is larger than Ca²⁺ binding constant to CaUO₂(CO₃)₃²⁻ (Reaction 4).



ⁱ Note: UO₂²⁺ + 3CO₃²⁻ ⇌ UO₂(CO₃)₃⁴⁻, Logβ^o₀₁₃ = 21.84 according to data selection in Guillaumont et al. (2013).



In 2013, Lee and Yun studied the chemical behaviour of $\text{CaUO}_2(\text{CO}_3)_3^{2-}$ and $\text{Ca}_2\text{UO}_2(\text{CO}_3)_3(\text{aq})$ species under atmospheric $\text{CO}_2(\text{g})$ in weakly alkaline conditions using TRLFS measurements. Endrizzi and Rao (2014) studied the Ca-U(VI)-CO₃ system by ion selective electrode potentiometry in 0.1 M of NaCl at pH 10 and Jo and Yun (2017) are studying spectroscopic properties and formation constants of the ternary Ca-U(VI)-CO₃ complexes using TRLFS measurements. Although all these authors used different experimental approaches, the stability constants suggested for the formation of $\text{CaUO}_2(\text{CO}_3)_3^{2-}$ and $\text{Ca}_2\text{UO}_2(\text{CO}_3)_3(\text{aq})$ are in agreement with the ones reported by Dong and Brooks (2006) (see Table 4).

Besides the investigation of their thermodynamic properties, some studies have analysed the structure of Ca-U(VI)-CO₃ complexes using EXAFS (Extended X-Ray Absorption Fine Structure) (Bernhard et al. 2001; Kelly et al., 2007) or molecular dynamic simulations (Kerisit and Liu, 2010).

Finally, some works used the stability constants from Dong and Brooks (2006) in order to explain U(VI) sorption, mobility and speciation in different systems. For example, Meleshyn et al. (2009) evaluated the influence of Ca-U(VI)-CO₃ complexes on uranium sorption on bentonites; Prat et al. (2009) included Ca-U(VI)-CO₃ complexes in their studies for U(VI) speciation in drinking water; and Stewart et al. (2010) studied the impact of Ca-U(VI)-CO₃ complexes on uranium adsorption to synthetic and natural sediments.

The Ca-U(VI)-CO₃ ternary complexes and their associated stability constants (as reported in 2006 by Dong and Brooks) have already been included in the ThermoChimie database version 9.b (Giffaut et al., 2014, www.thermochimie-tdb.com). Using this thermodynamic database, we were able to calculate the distribution of the aqueous speciation of uranium under specific geochemical conditions (Figure 5). From these results, it is possible to evaluate the importance of such aqueous species on the behaviour of U(VI) under neutral pH and in the presence of calcium and carbonates systems as clay systems, relevant for nuclear waste disposal.

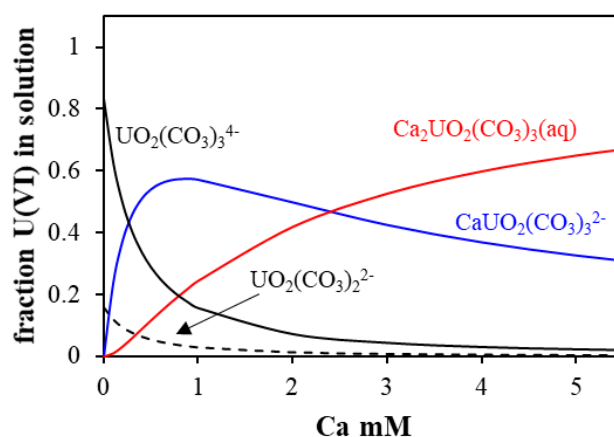


Figure 5. Calculated U(VI) speciation as a function of calcium concentrations between 0 and $5 \cdot 10^{-3}$ M at 25 °C, $[\text{U(VI)}]_{\text{total}} = 1 \cdot 10^{-8}$ M, $[\text{CO}_3^{2-}]_{\text{total}} = 3 \cdot 10^{-3}$ M, pH = 7.2 and ionic strength of 0.1 M using NaNO_3 as electrolyte. Calculations performed with ThermoChimie database v9b.

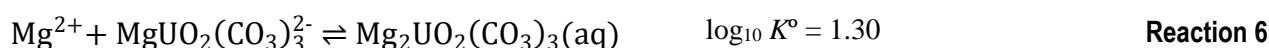
2.1.1. Mg-U(VI)-CO₃ system

Besides the stability of Ca-U(VI)-CO₃ complexes, only a few studies have been published concerning the stability of Mg-U(VI)-CO₃ aqueous complexes (Dong and Brooks, 2008; Geipel et al. 2008; Endrizzi and Rao, 2014; Lee et al. 2017). The stability of MgUO₂(CO₃)₃²⁻ has been experimentally studied using different analytical techniques (see a summary in Table 5); the resulting values seem to be in reasonable agreement. On the other hand, the stability of Mg₂UO₂(CO₃)₃(aq), to the best of our knowledge, has only been reported recently by Lee et al. (2017).

Table 5. Summary of the literature on the stability constants for Mg-U(VI)-CO₃ complexes. Data in grey have been superseded by later references of the same authors.

Reference	$\log_{10} \beta^{o}_{113}$ MgUO ₂ (CO ₃) ₃ ²⁻	$\log_{10} \beta^{o}_{213}$ Mg ₂ UO ₂ (CO ₃) ₃ (aq)	Ionic strength correction	Technique
Dong and Brooks (2006)	26.11 ± 0.04		Davies	Anion exchange resin
Dong and Brooks (2008)	25.02 ± 0.08		SIT	Anion exchange resin
Dong and Brooks (2008)	25.80 ± 0.50		Davies	Anion exchange resin
Geipel et al. (2008)	26.24 ± 0.13		Davies	TRLFS
Endrizzi and Rao (2014)	26.25 ± 0.07		SIT	Selective electrode and UV/VIS
Lee et al. (2017)	25.80 ± 0.30	27.10 ± 0.60	SIT	TRLFS

The constants provided by Lee et al. (2017), as also reported by Dong and Brooks (2006) for the Ca-counterpart, agree with the expected trend: the binding constant of Mg²⁺ to UO₂(CO₃)₃⁴⁻ (Reaction 5) is larger than the Mg²⁺ binding constant to MgUO₂(CO₃)₃²⁻ (Reaction 6).



Besides the investigation of their thermodynamic properties, Lee et al. (2017) have also investigated the structure of Mg-U(VI)-CO₃ complexes using EXAFS.

According to Endrizzi and Rao (2014) and Lee et al. (2017), the main difficulty in determining the Mg₂UO₂(CO₃)₃(aq) stability constants is caused by its lower stability compared with the corresponding stability constant of Ca₂UO₂(CO₃)₃(aq).

2.1.1. Effect of temperature

Although the formation behaviour of the calcium-uranyl-carbonate ternary complexes is widely studied at room temperature conditions, there is a lack of thermodynamic data in conditions of increased temperature. The effect of temperature on Ca-U(VI)-CO₃ complexes is not clear. Only one study (Endrizzi and Rao 2014) is published and Jo and Yun (2017) have shown preliminary results using a different experimental approach.

In 2014, Endrizzi and Rao determined the enthalpy of $\text{CaUO}_2(\text{CO}_3)_3^{2-}$ and $\text{Ca}_2\text{UO}_2(\text{CO}_3)_3(\text{aq})$ using microcalorimetry at ionic strength (I) 0.1 M of NaCl. The experimental data were fitted using HypDeltaH software; the enthalpy data were not corrected to infinite dilution ($I = 0$) since the effect of the media in the ionic strength ranged between 0 and 0.1 M, which was considered to be negligible. The reported enthalpy data are shown in Reaction 7 and Reaction 8.



The authors used an initial concentration of uranium of 20 mM at pH 10 –10.3 in NaCl 0.1 M. The high uranium concentrations are probably required for the correct performance of the microcalorimeter, however, it may lead to precipitation of U(VI) solids. Although the presence of solids is not reported in the original article, PhreeqC calculations performed in the context of the present work indicate that sodium uranate (as Clarkeite) may be oversaturated under those conditions (see in Appendix 4 Figure D. 4).

Jo and Yun (on-going) have been working on the spectroscopic properties and formation constants of the ternary Ca-U(VI)-CO₃ complexes at different temperatures. Their work consists in determining the complexes' thermodynamic data, including stability constants and enthalpy values, using TRLFS measurements at a range of temperatures between 10 and 80°C. Recently, Jo and Yun (2017) showed preliminary data relative to the stability constants (at $I = 0.1$ M) for Reaction 1 and Reaction 2 at different temperatures. Their results are shown in Table 6.

Table 6. Stability constants for Ca-U(VI)-CO₃ complexes at $I = 0.1$ M and different temperatures suggested by Jo and Yun (2017).

T°C	log ₁₀ <i>K</i> (Reaction 1)	log ₁₀ <i>K</i> (Reaction 2)
10 ± 0.1	2.46 ± 0.3	5.59 ± 0.7
25 ± 0.2	3.01 ± 0.2	6.0 ± 0.3
40 ± 0.5	2.86 ± 0.3	6.22 ± 0.3
55 ± 0.6	3.17 ± 0.2	6.41 ± 0.6
70 ± 1.0	-	6.72 ± 0.2

In the calculation of the stability constants there is a clear temperature effect, where increasing the temperature leads to an increase of the stability constants; however, these results should be taken with caution as the work is still on-going and exhaustive experimental data are not available yet.

Based on TRLFS analysis, the authors suggested that uranyl hydrolysis was observed at low concentrations of calcium, where $\text{CaUO}_2(\text{CO}_3)_3^{2-}$ is predominant. For this reason, the authors only suggested enthalpy values for the $\text{Ca}_2\text{UO}_2(\text{CO}_3)_3(\text{aq})$ species (Jo and Yun, 2017). The stability constant corrected for infinite dilution using SIT was determined as an average value of 30.64 ± 0.17 for Reaction 2, and the enthalpy of reaction was -35 ± 18 kJ/mol.

ⁱ Note: $\text{UO}_2^{2+} + 3\text{CO}_3^{2-} \rightleftharpoons \text{UO}_2(\text{CO}_3)_3^{4-}$, $\Delta_r H^\circ = -39.20$ according to data selection in Guillaumont et al. (2013).

Following the discussion above, and the relevance of the Ca-U(VI)-CO₃ complexes for nuclear waste disposal in clay conditions, it seems necessary to further study the effect of temperature in the formation of these species.

2.2. Determination of the thermodynamic data of Ca-U(VI)-CO₃ aqueous species

From the discussion in the previous section, the existence and stability of the Ca-U(VI)-CO₃ aqueous species at 25 °C is confirmed. Nevertheless, the effect of temperature on the formation of these complexes is not yet clear.

Stability constants are mostly determined by equilibrium methods, where it is assumed that the activity coefficients of all species is effectively constant by the use of a suitable ionic medium, so that the law of mass action can be applied to the concentrations of reacting species (Rossotti and Rossotti, 1961).

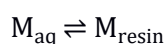
Most aqueous complexes form reaching the equilibrium rapidly and their stability constants can be determined by direct or indirect methods. In direct methods, such as TRLFS or potentiometry, the aqueous species of interest is directly measured. For the case of the indirect methods, the stability constants are determined based on the analysis of the variation of element concentration on a biphasic system (such as solubility, ionic exchange and partition experiments) as a function of different parameters (*e.g.* temperature, solid-liquid ratio) that change the chemical system.

The objectives of the present work are:

- 1) To design an experimental method for the ionic exchange experiments performed in a different range of temperatures, where the control of temperature and partial pressure of CO₂ of the system are our main concern;
- 2) To evaluate the reliability of the stability of Ca-U(VI)-CO₃ aqueous species at 25°C by corroborating it with the literature data and to provide confidence to the experimental methodology and modelling approach.
- 3) To study the effect of temperature between 20 and 80°C on the formation and stability of Ca-U(VI)-CO₃ complexes.

2.2.1. Ionic Exchange Method

In the present work, the ionic exchange method was used to determine the stability constants of the Ca-U(VI)-CO₃ complexes and the effect of temperature on their stability. This indirect method was previously used by Dong and Brooks (2006) to determine the stability constants of the Ca-U(VI)-CO₃ system at 25°C under atmospheric conditions. The approach is based on the distribution of a metal (uranium in this case) between an ionic-exchange resin and the aqueous phase (Reaction 9).



Reaction 9

In this reaction, M is the solute, M_{aq} represents the solute dissolved in the aqueous phase (mol/mL) and M_{resin} corresponds to the solute adsorbed into the ionic-exchange resin (mol/g). The ratio between the adsorbed solute and the solute that remained in solution is normally described as the distribution coefficient K_D (Equation 1).

$$K_D = \frac{[M]_{\text{resin}}}{[M]_{\text{aq}}} \quad \text{Equation 1}$$

In this equation, $[M]_{\text{aq}}$ represents the concentration of all dissolved species (mol/mL) and $[M]_{\text{resin}}$ represents the concentration of all adsorbed species of M (mol/g). The K_D value is very sensitive to the chemical conditions and special care should be taken to the pH of the solution, concentration of solute, the ionic strength of the media, number of exchanging sites and temperature.

To achieve the stability constants, batch experiments at different temperatures using an anionic-exchange resin in the absence or presence of calcium were performed followed by the fitting of a geochemical model to the experimental data. The details are provided below.



In this reaction, M is the solute, M_{aq} represents the solute dissolved in the aqueous phase (mol/mL) and M_{resin} corresponds to the solute adsorbed into the ionic-exchange resin (mol/g). The ratio between the adsorbed solute and the solute that remained in solution is normally described as the distribution coefficient K_D (Equation 1).

$$K_D = \frac{[M]_{\text{resin}}}{[M]_{\text{aq}}} \quad \text{Equation 2}$$

In this equation, $[M]_{\text{aq}}$ represents the concentration of all dissolved species (mol/mL) and $[M]_{\text{resin}}$ represents the concentration of all adsorbed species of M (mol/g). The K_D value is very sensitive to the chemical conditions and special care should be taken to the pH of the solution, concentration of solute, the ionic strength of the media, number of exchanging sites and temperature.

To achieve the stability constants, batch experiments at different temperatures using an anionic-exchange resin in the absence or presence of calcium were performed followed by the fitting of a geochemical model to the experimental data. The details are provided below.

2.2.1.1. Experimental approach

The distribution of U(VI) between an anionic-exchange resin and the aqueous phase was monitored as a function of different parameters to study the stability of the Ca-U(VI)-CO₃ complexes. Further details of the materials and a description of the different methods used in the present study are provided in Appendix A.

2.2.1.1.1. Materials and Solutions

The anionic-exchange resin used in the experiments is the gel-type Dowex 1x2 strong base anion exchange resin, stable up to 99°C. In contrast, the resin used by Dong and Brooks (2006) (Amberlite

IRA-410) is not stable at temperature above 40 °C, and thus, it is not appropriate to study the effect of temperature in the Ca-U(VI)-CO₃ system.

The background electrolyte used in the experiments was 0.1 M NaNO₃, and initial U(VI) concentrations were in the order of 5·10⁻⁷ M (except when stated).

2.2.1.1.2. Batch experiments

Sorption batch experiments were carried out at different temperatures by following, as abovementioned, the experimental procedure proposed by Dong and Brooks (2006).

Before performing these experiments, different types of preliminary tests were performed in order to confirm the correct performance of the experimental set-up. The preliminary tests included:

- To verify if CO₂(g) is in equilibrium with the solution at the different temperatures and pressures studied
- To test if sampling procedures affect the temperature of the solution in a significant way
- To check if there is a significant leaching of organic material from the plastic tubes at the different temperatures studied

After the preliminary experiments were completed, the final experimental set-up used is shown in Figure 6. The experimental set-up consisted in firstly degassing ultrapure water and weight all samples at room conditions and transfer it into the glove-box with controlled CO₂(g) (whose concentration depends on the temperature studied). Once inside the glove-box, the stock solutions of calcium and sodium nitrate, sodium carbonate and uranium nitrate solution were prepared and added to each tube. The tubes were sealed with Teflon tape, closed and transferred outside of the glove-box. The samples were then conditioned in vacuum (20 mbar) using an aluminium-foil bag, transferred to an incubator coupled with a reciprocate shaker and left in equilibrium at the temperature of interest. Once the samples were equilibrated (in this case, after 5 days of contact), the aluminium-foil bag was opened, and the tubes were introduced in an isolated Teflon/aluminium-box, especially prepared to maintain the temperature of the tubes, followed by rapid transfer into the glove-box. In the glove-box, the sampling was done, and the pH was measured at the temperature of interest. The pH meter was previously calibrated with pH 4.0 and pH 7.0 buffer standards at the temperature of interest by using a duo dry-bath system. After cooling the samples at room temperature, the alkalinity of the remaining samples was analysed.

Additional experimental tests were also performed to ensure the viability of the Dowex 1x2 resin for the sorption of U(VI), the initial concentration of U(VI) in solution and the influence of the electrolyte background. These experimental tests were performed in atmospheric conditions at 20°C, following the procedure proposed by Dong and Brooks (2006).

Two types of batch experiments were performed in controlled atmosphere. These were performed at constant ionic strength, pH, carbonate content and initial concentration of U(VI):

Experiment Type I: Batch experiments at different temperatures in the absence of calcium as a function of the solid-liquid ratio (1–25 g/L). The objective of these experiments is to establish the distribution coefficient of U(VI) in the absence of calcium.

Experiment Type II: Batch experiments at different temperatures as a function of the concentration of calcium (0–5 mM) at fixed solid-liquid ratio of 2.5 g/L. The upper limit of calcium concentration was calculated in order to avoid calcite oversaturation in the experiments. The objective of these experiments is to study the stability and the effect of temperature on Ca-U(VI)-CO₃ complexes.

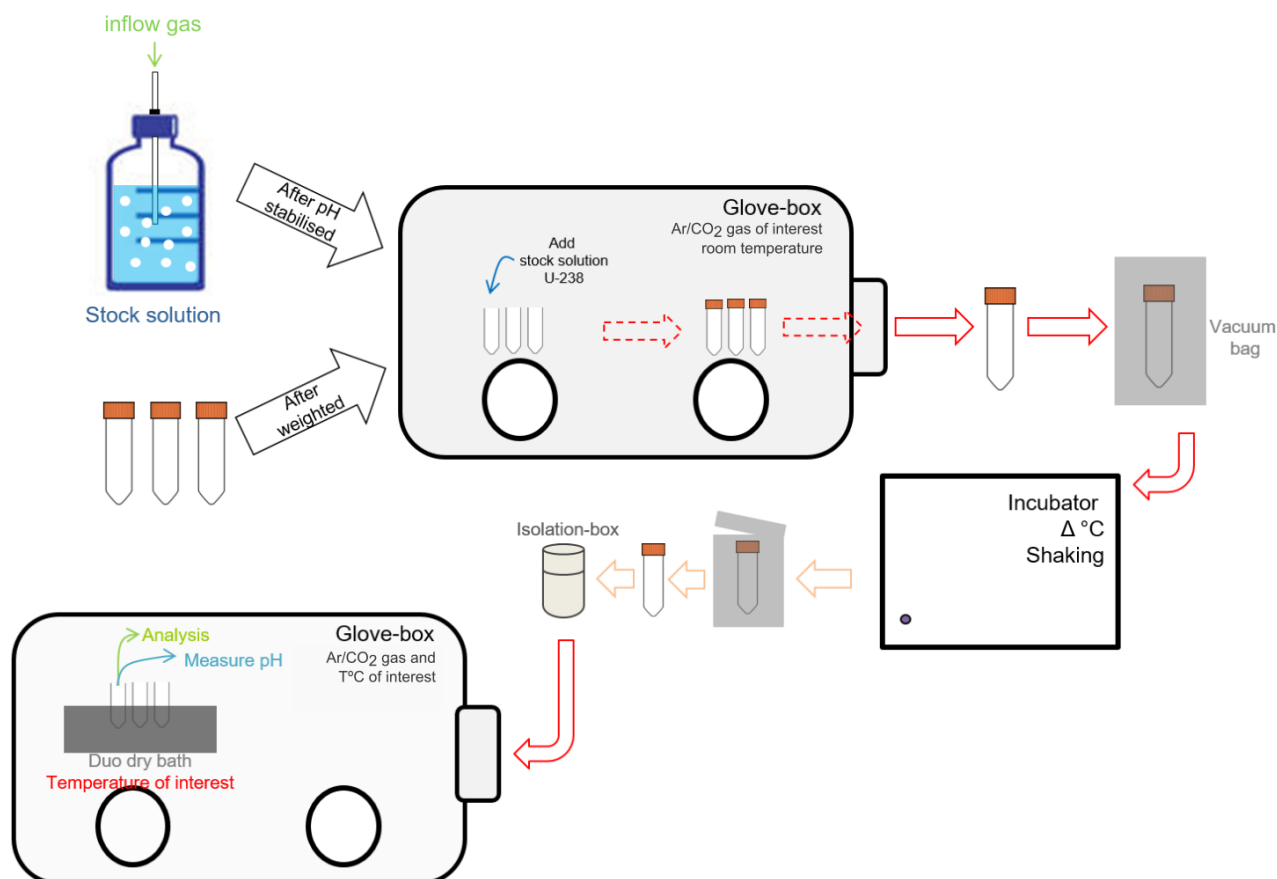


Figure 6. Scheme of the experimental set-up for the closed system experiments.

The different experiments performed are summarized in Table 7. In Callovo-Oxfordian formation conditions (section 1.1.1.1), the increase of temperature is expected to lead to changes in the pH and on the CO₂(g) equilibrium of the system (see a description in Tournassat et al., 2008). The theoretical pH and % CO₂(g) of each experiment was established taking this effect into account.

For each experimental set, two series of blank samples were used to control the uranyl sorption in the tubes and filters and to control for the possible precipitation of uranium. Further details on these experiments are provided in Appendix A.7.

Table 7. Summary of the batch experiments performed in the present work.

Type	NaNO ₃ M	S/L g/L	[Ca] nM	[U(VI)] _{initial} M	Temperature °C	pH	CO ₂ (g) %
I	0.1	1 – 25	0	≈ 5·10 ⁻⁷	20	7.2	1
					40	7.0	1
					60	6.8	3
					80	6.6	5

Type	NaNO ₃	S/L	[Ca]	[U(VI)] _{initial}	Temperature	pH	CO ₂ (g)
	M	g/L	nM	M	°C		%
II	0.1				20	7.2	1
	0.1				40	7.0	1
	0.1	2.5	0 – 5	≈ 5·10 ⁻⁷	60	6.8	3
	0.087 ⁱ				80	6.6	5

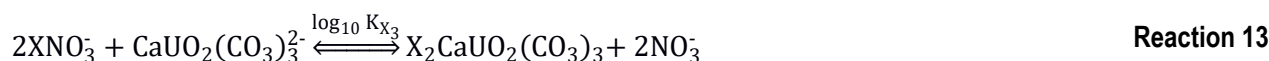
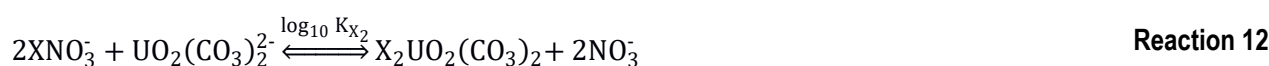
2.2.1.2. Conceptual model

The geochemical model approach has been defined to simulate the ionic exchange processes between the resin and the anionic species of U(VI) formed in a solution rich in carbonates, in the absence or presence of calcium, at different temperatures. The calculations aim to determine the stability constants of the aqueous Ca-U(VI)-CO₃ species based on the distribution coefficient of U(VI) after equilibration. The solutions were defined according to the equilibrium conditions of batch experiments as a function of the concentration of calcium in solution.

In the conceptual model, each batch is considered as a single system in which each solution is assumed to be in equilibrium with the resin.

In this specific case, the resin is an anionic-exchange resin in the nitrate form (XNO₃) and the amount of exchange sites in the resin is calculated based on the density and the exchange capacity of the resin, as described in Appendix B.1.

Different anions present in the solution can exchange with the nitrate in the resin. The overall chemical reactions that may be involved in the exchanger are defined according to the aqueous speciation as follows:



From the reactions above, only Reaction 11 has been considered for the present system. This reaction corresponds to the exchange of UO₂(CO₃)₃⁴⁻, a highly charged species. Thus, its sorption is expected to be more relevant than the sorption of other less charged species, for example UO₂(CO₃)₂²⁻, and as such Reaction 12 will not be taken into consideration. According to Dong and Brooks (2006), sorption of CaUO₂(CO₃)₃²⁻ (Reaction 13) on the resin is expected to be minor. Sorption of Ca₂UO₂(CO₃)₃(aq), which is a non-charged species, is expected to be negligible. Finally, the sorption of HCO₃⁻ or CO₃²⁻

ⁱ Concentration set up to 0.087 due to an experimental error. This has been taken into account in the modelling and calculations.

(Reaction 14 and Reaction 15, respectively) is considered to play a minor role and will not be taken into account in the calculations.

The concentration of carbonates in the model is controlled by the pCO₂ of the system, when no information of its concentration is known. When carbonate concentration is known, the pCO₂ of the system will be allowed to be free, where the measured alkalinity and pH will be the main agents that control carbonate concentration.

The conceptual model will be tested by taking into account the experimental data from Dong and Brooks (2006). In this exercise, atmospheric pCO₂ will be considered since the concentration of carbonates is known to be in equilibrium with atmospheric pCO₂.

2.2.1.2.1. Numerical approach

All simulations were conducted by Phreeqc code version 3.1.4 (Parkhurst and Appelo, 2013) which includes chemical equilibrium reactions and gas-aqueous phase equilibria.

The determination of the stability constants of CaUO₂(CO₃)₃²⁻ and Ca₂UO₂(CO₃)₃(aq) (log₁₀β₁₁₃ and log₁₀β₂₁₃, respectively) considering the experimental distribution coefficient of U(VI) at different temperatures was done using Parameter ESTimation code PEST (Doherty, 2010). PEST is an open-source, public-domain software suite that allows model-independent parameter estimation and parameter/predictive-uncertainty analysis. Subsequently, PEST was coupled to the batch version of Phreeqc.

A benchmark was also performed by using a complementary approach with the aim of fitting the model to the experimental data. This was achieved by designing a matrix with Microsoft Excel[®] where two variables (log₁₀β₁₁₃ and log₁₀β₂₁₃) are defined simultaneously. The PhreeqC input file is defined to run all combination possibilities within a reasonable and equally spaced values range. The sum of squared differences (SSD) and then calculated in Microsoft Excel[®] between the model and the experimental data. The OriginLab[®] software was used to represent graphically the variations of the SSD values as a function of both variables. The lower SSD value is taken as the best approach and it is within the darkest zone of the 2D mapping. To reduce the uncertainties of the variables, the previous routine can be applied to a more limited range of values.

All calculations were performed using ThermoChimie Database v9b with a Davies approach for ionic strength correction, unless otherwise mentioned. The database already contains the stability constants for the CaUO₂(CO₃)₃²⁻ and Ca₂UO₂(CO₃)₃(aq) complexes, based on the work by Dong and Brooks (2006). These data have not been used in the calculations as one of the objectives of the present work is to confirm those values. On the other hand, the thermodynamic data for UO₂(CO₃)₂²⁻ and UO₂(CO₃)₃⁴⁻ is also included in this database, where the stability constants and enthalpy values originate from the work of Guillaumont et al. (2003). These U(VI)-CO₃ complexes are the most relevant U(VI) complexes expected to be formed in the absence of calcium under the conditions of the study, and that data has been included in the calculations.

An extensive listing of aqueous and solid species included in the database relevant for the study is provided in Appendix E.

2.2.1.2.2. Application of the conceptual model on Dong and Brooks (2006) experimental data

According to the conceptual model proposed in the present study, the distribution coefficient of U(VI) in the absence or presence of calcium is calculated based on the sum of its speciation distribution between the aqueous and resin phase. The model approach that we applied takes into consideration the isotherm of U(VI) onto the anionic exchange resin in the absence of calcium in solution to determine the stability constant of the anionic-exchange reaction (Reaction 11). Furthermore, a model approach using the stability constant determined previously and the experimental K_D of U(VI) as a function of calcium in solution is applied to determine the stability constants of the Ca-U(VI)-CO₃ ternary complexes. The results of both model approaches are shown in Figure 7. All constants were fitted by PEST.

The model approach in both cases reproduces well the experimental data, both the U(VI) sorbed onto the resin (Figure 7a) and the K_D of U(VI) as a function of calcium (Figure 7b). The results of the fitting approach indicate that the $\log_{10} \beta_{113}^{\circ}$ and $\log_{10} \beta_{213}^{\circ}$ for the Reaction 1 and Reaction 2 are respectively $27.29 (\pm 0.07)$ and $30.02 (\pm 0.63)$. These results differ slightly from those proposed by Dong and Brooks (2006) in which $\log_{10} \beta_{113}^{\circ} = 27.18 (\pm 0.07)$ and $\log_{10} \beta_{213}^{\circ} = 30.7 (\pm 0.06)$, although they are in the same range. The most important issue that should be pointed out is the uncertainty of the resultant stability constant. Special concern should be taken on the calculation of the uncertainty of $\log_{10} \beta_{213}^{\circ}$, which seems to be very small in the case of the work by Dong and Brooks (2006).

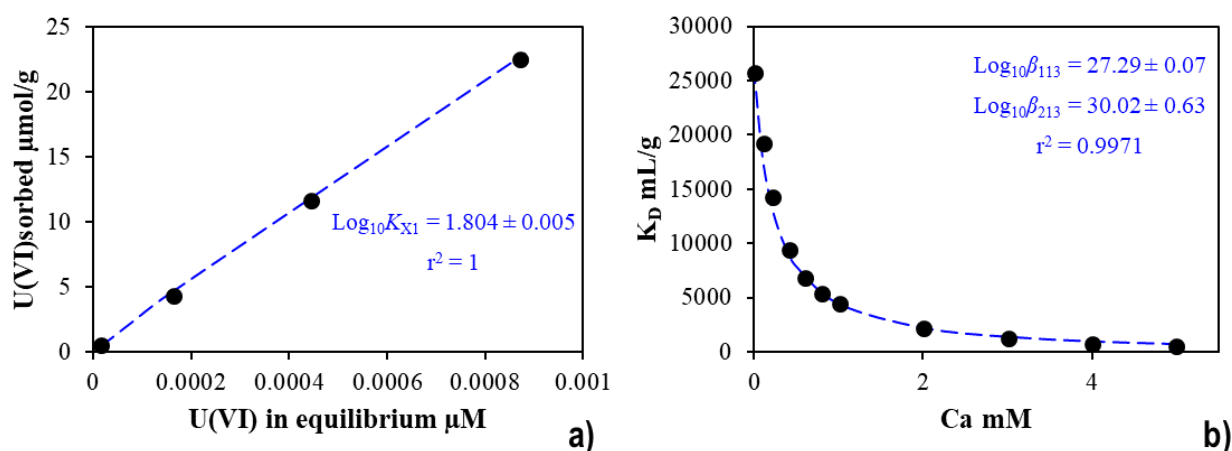


Figure 7. Experimental data originated from supporting information of Dong and Brooks (2006). Fit approach of the a) U(VI) sorbed onto resin as function of U(VI) in equilibrium in solution and b) the distribution of U(VI) as a function of calcium.

In conclusion, the conceptual model here presented can be validated based on the application of the model approach on the data of Dong and Brooks (2006). However, with an increase in the temperature of the system some considerations must be taken:

Not all species or solids have enthalpy of reaction values, which will be considered zero for the modelling calculations. This assumption must be taken carefully, since the behaviour of some species might change with an increase in temperature.

2.3. Results

2.3.1. Experimental tests

Extensive details of the experimental test results are available in Appendix C.1.

2.3.1.1. Controlling test on temperature and pCO₂

Different preliminary tests were performed to guarantee the correct performance of the experimental set-up (Figure 6). A summary of the experimental tests and results obtained are described in Table 8.

Table 8. Description of the tests performed in different temperatures and in closed system experiments.

Challenge	Task	Actions
Equilibrium with CO ₂ (g) is difficult to reach in solutions at T > 25°C	Study carbonates concentration at the different temperatures and pressures studied.	pH will be measured inside the glovebox at the temperature of the experiments. Alkalinity will be measured at room temperature inside the glovebox.
Temperature may change during sampling procedures	Verify if the temperature is maintained when sampling	An isolation box will be used to control the temperature
Degradation of PPCO tubes at high temperatures	Verify by TOC analysis the concentration of organic carbon released in time at different temperatures	Washing 3 times the tubes with ultra-pure water at respective temperature before each batch experiment.

Some insights from the results of the CO₂(g) equilibrium experiment (first test) will be provided here, since they are essential for the interpretation and modelling of the experimental data.

The equilibrium of CO₂(g) with the solution may be difficult to achieve, and can be a challenge at temperatures higher than 25°C (Giffaut, 1994). In order to evaluate this, alkalinity measurements were done following the procedure described in Appendix A.3. The results are shown in Table 9. The results show that the equilibrium between the chemical system and the pCO₂ is not reached during the time of the experiment. The major differences are observed at higher temperatures (60 and 80°C). To minimise the uncertainty of the calculated pCO₂ values, it is crucial to measure the pH and the alkalinity for all experimental cases. These parameters will be further used in the simulation/fitting to obtain correct interpretation and modelling data.

Table 9. Theoretical and measured parameters from the evaluation of CO₂(g) in equilibrium at different temperatures. Theor.: theoretical value in agreement with the initial conditions of the experiments; Exp.: pH and alkalinity measured at the end of the experiment, and pCO₂ calculated according pH and alkalinity measurements.

Temperature	20 °C		40°C		60 °C		80 °C	
	Theor.	Exp.	Theor.	Exp.	Theor.	Exp.	Theor.	Exp.
pH	7.2	7.3	7.0	7.4	6.8	7.0	6.6	7.0
Alkalinity (meq/L)	2.0	2.5	2.0	2.5	1.8	2.3	1.8	2.3
pCO ₂ (atm)	10 ^{-2.1}	10 ^{-2.2}	10 ^{-2.0}	10 ^{-2.2}	10 ^{-1.5}	10 ^{-1.8}	10 ^{-1.3}	10 ^{-1.7}

2.3.1.1.1. Controlling test on the initial concentration of U(VI) and electrolyte background

Besides the lack of information on the control of carbonates in the system, another issue that is almost as disregarded in all published studies is the lack of evaluation of the possible precipitation of U(VI)-bearing minerals, such as clarkeite and calcite. Bernhard and co-workers (2001) and Dong and Brooks (2006) were the only ones monitoring the concentration of uranium and calcium to check the possible precipitation of mineral phases. In both works, it was reported that no solids were observed. In all experimental data published (see details in Appendix D. 1), the initial concentration of U(VI) in solution ($2 \cdot 10^{-5}$ and $4.7 \cdot 10^{-4}$ M) is high enough to precipitate some U-mineral phases. Not only uranium plays an important role on the solubility of U-bearing minerals but also the concentration of sodium and calcium are relevant for the solubility of such mineral phases. For example, clarkeite (Na-Uranate) easily precipitates even at low ionic strength solutions (0.01 M) (Giammar and Hering, 2004). Another example is the possible precipitation of becquerelite (Ca-U(VI) hydroxide mineral), which solubility is below $1.5 \cdot 10^{-8}$ M of U(VI) (Casas et al., 1997; Rai et al., 2002; Sandino and Grambow, 1994). Consequently, using concentration of U(VI) above this value can lead to an oversaturation of becquerelite. However, the possible precipitation of mineral phases should be merely speculative as the formation of these type of phases is not controlled by concentration of U(VI) in solution but also by its kinetics. For this reason, assuming the precipitation of such mineral phases in the geochemical calculations may lead to misinterpretation of the experimental data because the equilibrium is always assumed.

Predictive calculations using ThermoChimie Database v9b (Giffaut et al., 2014) performed taking the experimental data reported by Dong and Brooks (2006) and Bernhard et al. (2001) show that calcite, clarkeite and becquerelite seem to be oversaturated despite the observations reported by the authors. Dong and Brooks (2006) indicated that calcite may precipitate at concentrations of calcium above 3 mM (as also observed in these predictive calculations); although in case of the U(VI)-bearing minerals would be undersaturated under their experimental conditions (Figure 8a). On the other hand, Bernhard and co-workers (2001) reported that even after one year no precipitation or other chemical changes were detected. The same results were observed using the experimental data reported by Endrizzi and Rao (2014) (Figure 8b).

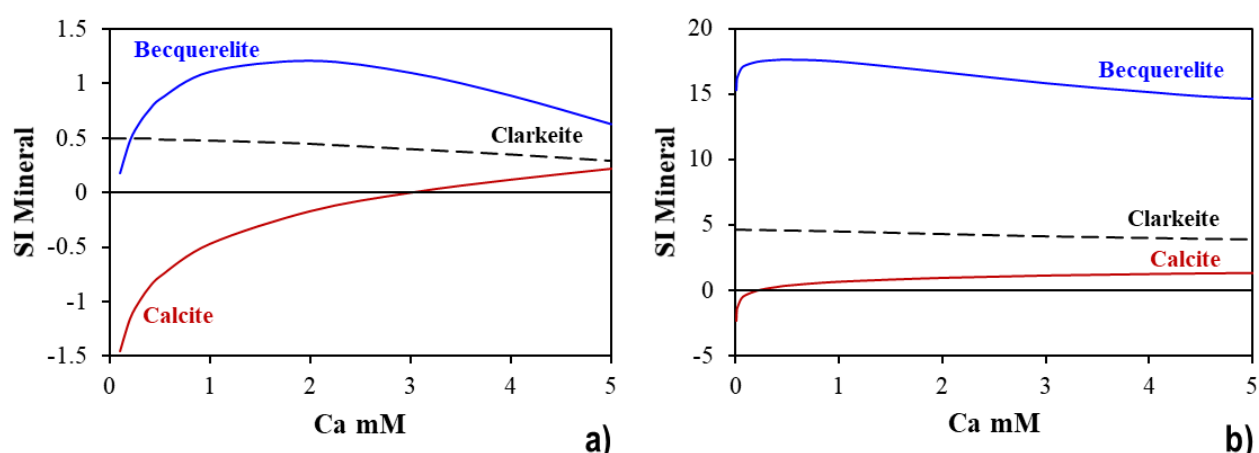


Figure 8. Mineral saturation index as a function of Ca considered for a) Dong and Brooks (2006) using ThermoChimie database Davies (2009) and b) Endrizzi and Rao (2014) using ThermoChimie database SIT (2014).

Details of all modelling results of the experimental conditions for all works described in Table 4 are provided in Appendix D.1.

Except for the works of Endrizzi and Rao (2014) and Lee and Yun (2013), most published work mentions that no mineral precipitation was observed, and a careful filtration of the samples was taken. Even though the authors did not mention the possibility of precipitation it does not mean that they did not consider this issue. Most probably they did not observe any perturbation of the system and realised that it was not worth mentioning it.

It should also be noted that the solubility of the U(VI) solids is not only dependent on the initial concentration of U(VI), but also on other chemical parameters such as pH, temperature and concentration of carbonates. Following the discussion above, the batch experiments carried out in the present study were performed using $5 \cdot 10^{-7}$ M of initial concentration of U(VI) (this means two orders of magnitude lower than reported by Dong and Brooks work (2006)). According to geochemical calculations, no U(VI) phases are expected to be oversaturated, at least at temperatures below 25°C, under the experimental conditions envisaged for the present work. If they are, this will be taken into account on the calculations of the stability constants.

The composition of the electrolyte background is a relevant parameter to consider in this kind of studies. It is well known, that the composition of electrolyte media is important due to its interaction with the uranium in solution. For this reason, a less complexing electrolyte media should be used. Except for Dong and Brooks (2006) and Endrizzi and Rao (2014), that used NaNO₃ and NaCl (respectively) as electrolyte background, other experimental works used sodium perchlorate, which is a less complexing agent in its relation to uranium.

For this reason, to test the impact of taking sodium perchlorate as electrolyte background instead of sodium nitrate as proposed by Dong and Brooks (2006), a batch experimental test was performed with 0.1 M NaClO₄.

Special care must be taken upon using NaClO₄ as electrolyte background in experiments, as it is well known that pH measurements under perchlorate conditions can affect the pH electrode due to precipitation of KClO₄ at the junction of the electrode. Moreover, the pH electrode used in this experimental test is very sensitive to reference electrode solution changes, thus the reference solution was not changed. The pH measurements during this test were performed as quickly as possible to avoid the precipitation of KClO₄. Another issue that should be considered, besides the impact of the perchlorate solution in pH measurements at room temperature, concerns the increase of the temperature in the system. This increase may lead to an increase in the solubility of the salt solution, which will also interfere with pH measurements.

Nonetheless, the ionic exchange batch experiments using sodium perchlorate were performed at room temperature and atmospheric conditions for practical reasons. The resin was previously changed for perchlorate form (as for the nitrate form, see Appendix A.6). The pH of the equilibrium was measured at the end of the experiment and found to be an average of 7.8 (± 0.1). The details of the experimental results are provided in Appendix C.3. The results of the concentration of U(VI) in solution are shown in Figure 9. The sorption of U(VI) in the anionic exchange resin is almost negligible, showing a strong selectivity coefficient of the perchlorate with respect to the anionic species of U(VI) present in solution. The same effect was observed in Gu et al. (2005) when different types of anion-exchange resins were tested with both U(VI) and perchlorate. The authors show that the resin's functional group plays

an important role on the selectivity of the anionic species, and that approximately 34 % of perchlorate can be desorbed from gel-type resins (such as Dowex 1x2) after rinsed with HCl diluted acid.

In the present study, the perchlorate is hardly desorbed from the resin. Consequently, the distribution coefficient of U(VI) is constant and the formation of Ca-U(VI)-CO₃ ternary complexes cannot be studied. As a result, the use of perchlorate as counter-ion on the anionic-exchange resin and as electrolyte media was dismissed and all ionic exchange batch experiments were performed using sodium nitrate as performed in Dong and Brooks (2006).

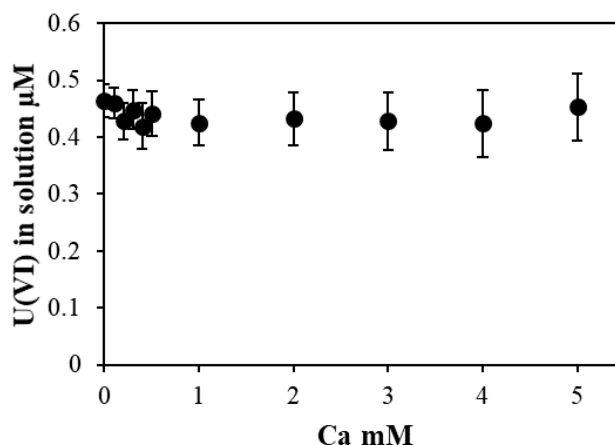


Figure 9. Concentration of U(VI) in solution as a function of the concentration of calcium in solution at pH of 7.8 (± 0.1), total [U(VI)] = $4.7 (\pm 0.3) \cdot 10^{-7}$ M, $I = 0.1 (\pm 0.005)$ M NaClO₄, in atmospheric conditions and 20 °C.

2.3.1.2. Determination of the stability constants in Ca-U(VI)-CO₃-H₂O systems at different temperatures

After validation of the proposed experimental procedure, we studied the aqueous behaviour of U(VI) under a controlled atmosphere at different temperatures. The study consists in changing the pCO₂ of the system according to the temperature of interest (20, 40, 60 or 80 °C). The experimental conditions try to reproduce as closely as possible the chemical system of CO_x formation (section 1.1.1). The resultant K_D further allows the determination of thermodynamic properties of the Ca-U(VI)-CO₃ aqueous species. The details of the experimental results are provided in Appendix C.3, and the modelling results and the input files can be found in Appendix D. 2 and F, respectively.

2.3.1.2.1. In the absence of calcium

Batch experiments in the absence of calcium (Type I, Table 7) were carried out to determine the distribution coefficient of U(VI) in the absence of Ca-U(VI)-CO₃ complexes.

U(VI) initial concentrations in the experiments are ca. $5 \cdot 10^{-7}$ M. No precipitation was visible in the tubes, neither before nor after filtration and this was confirmed by measure the blanks and afterwards by Phreeqc calculations. The alkalinity measured in the blank samples led to a total concentration of dissolved inorganic carbon in solution of around 2 meq/L.

The experiments were performed as a function of the solid-liquid ratio (1–25 g/L). An increase of the solid-liquid ratio promotes a pH decrease (Figure 10) probably related to changes on the gas/solution volume. This has been taken into account in the modelling calculations.

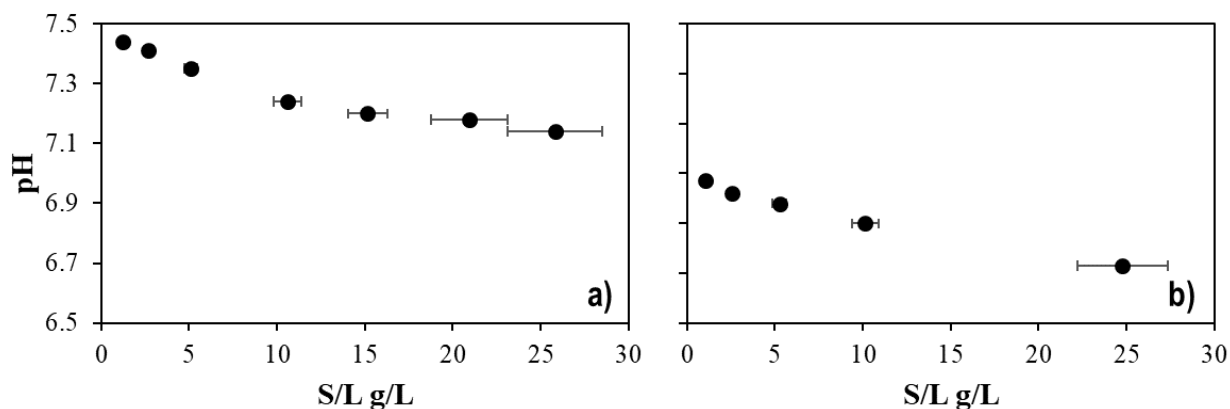


Figure 10. Measured pH as a function of S/L ratio in the experiments in the absence of calcium at a) 20 °C in equilibrium with 1% of CO₂(g) and b) 80 °C in equilibrium with 5% of CO₂(g).

As explained previously (section 2.2.1.1), at temperatures higher than 25 °C it is difficult to reach an equilibrium between the solution and the CO₂(g) atmosphere. Thus, the measured alkalinity values shown in Table 9 have been used for the interpretation of the results obtained (Figure 11).

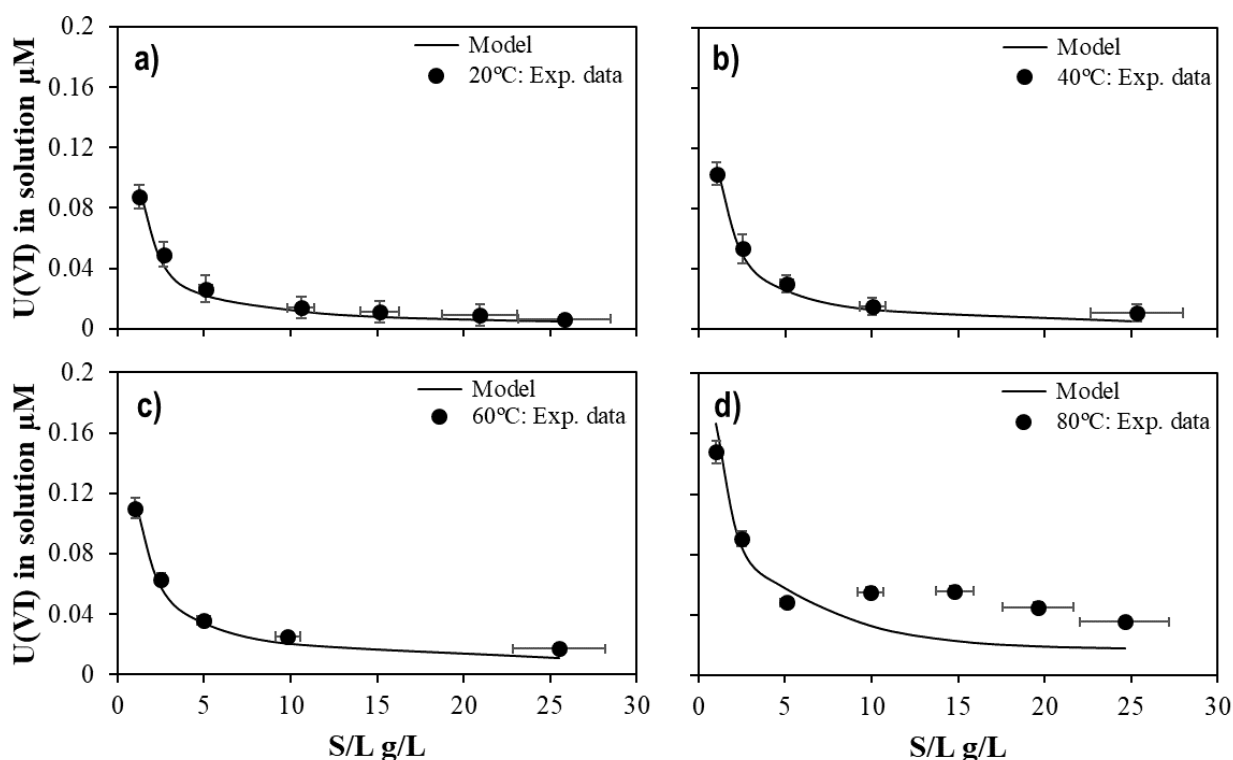


Figure 11. Concentration of U(VI) in the absence of calcium in solution as a function of the solid-liquid ratio (g/L) at a) 20 °C in equilibrium with 1% of CO₂(g); b) 40 °C in equilibrium with 1% of CO₂(g); c) 60 °C in equilibrium with 3% of CO₂(g); and d) 80 °C in equilibrium with 5% of CO₂(g). Solid-line: Model fitting of the concentration of U(VI) as a function of the solid-liquid ratio at 20, 40, 60 and 80°C.

The results obtained in Type I experiments show that the concentration of U(VI) in solution (symbols in Figure 11) decreases as the amount of resin increases. The effect of temperature on the

concentration of equilibrium of U(VI) is directly controlled by the thermodynamic properties of water and simultaneously by the thermodynamic properties of the speciation of U(VI) (Appendix E), assuming that there are no changes on resin properties. The speciation of U(VI) in the presence of carbonates in temperatures between 20 and 80 °C is controlled mainly by $\text{UO}_2(\text{CO}_3)_3^{4-}$ and $\text{UO}_2(\text{CO}_3)_2^{2-}$ (Figure 12). At 80 °C, the hydrolysis of the $\text{UO}_2(\text{OH})_3^-$ and $\text{UO}_2(\text{OH})_2(\text{aq})$ are expected but can be considered negligible. These changes of the speciation of U(VI) in solution, due to the changes in temperature, may lead to changes of the $\text{Log}_{10}K_X$. At 20 °C, the system can be simple, since there is only one predominant species that may compete in adsorption to the resin. However, with increasing temperature the complexity of the chemical system increases, and two aqueous species may compete for the adsorption of U(VI). The experiment proposed here cannot distinguish which aqueous species will control the sorption of U(VI) onto the resin, therefore it is not possible to determine two different $\text{Log}_{10}K_X$ at the same time (Reaction 11 and Reaction 12). Thus, the experimental data have been modelled using PEST in order to determine a constant for $\text{UO}_2(\text{CO}_3)_3^{4-}$ sorption (Reaction 11) at each temperature studied.

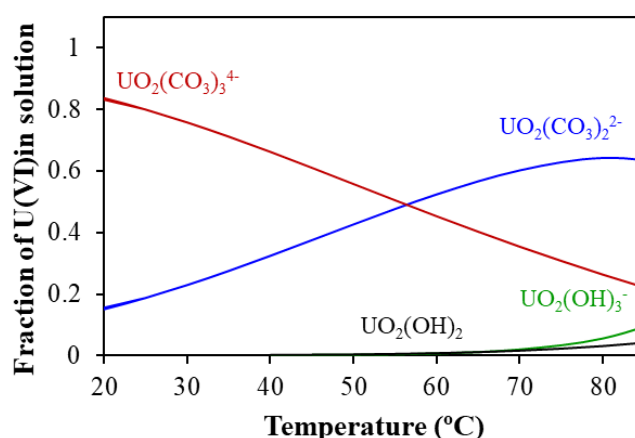


Figure 12. Speciation distribution of U(VI) in the absence of calcium in solution as a function of the temperature.

It should be pointed out that these experiments have been performed to quantify the U(VI) adsorbed to the resin in the absence of calcium, which will be used as a reference state when calcium is present and the formation of Ca-U(VI)- CO_3 ternary complexes are favoured. In fact, description of the real mechanism of the anionic-exchange processes is not of concern to this work. Thus, as a simplification of the geochemical model, it will be assumed that the $\text{UO}_2(\text{CO}_3)_3^{4-}$ will be the only species adsorbed to the anionic-exchange resin. This is assumed as these species are present in all cases and also have high anionic charge, more likely to be adsorbed to the resin, in contrast to the lower anionic charge species.

The agreement between the experimental data and the calculated values at 20, 40 and 60 °C is excellent (solid-lines in Figure 11). In contrast, the fit between the estimated and experimental observations at 80 °C and 5 % of $\text{CO}_2(\text{g})$ is less satisfactory. Although some deviation is noticed in the experiments at 80 °C, the agreement between the model and the experiments at $\text{S/L} = 2.5 \text{ g/L}$ (which is the ratio that will be used afterwards in the experiments in the presence of calcium, see further Section 2.3.1.2.2) is excellent.

The results show that there is a clear effect of temperature on the anionic-exchange resin, following a linear trend, in which the complexation of $\text{UO}_2(\text{CO}_3)_3^{4-}$ onto the anionic-exchange resin is favoured

with a temperature increase (Figure 13). The $\log_{10} K_{X1}$ values for Reaction 11 obtained from the fitting procedure at each temperature are provided in Table 10.

Table 10. Estimated values for the $\log_{10} K_X$ at different temperatures and $p\text{CO}_2$ (atm).

Case	Experimental conditions	Estimated value		
		$\log_{10} K_{X1}$	\pm	corr. Coef.
A	20 °C; $p\text{CO}_2 = 10^{-2.0}$ atm	1.08	0.06	0.995
B	40 °C; $p\text{CO}_2 = 10^{-2.0}$ atm	1.19	0.06	0.999
C	60 °C; $p\text{CO}_2 = 10^{-1.7}$ atm	1.53	0.06	0.998
D	80 °C; $p\text{CO}_2 = 10^{-1.5}$ atm	1.68	0.16	0.966

The dependency of the $\log_{10} K_{X1}$ values with temperature is shown in Figure 13. The results indicate that the dependence of the stability constants with $\frac{1}{T_0} - \frac{1}{T}$ is a straight line. The slope of this line can be correlated with an “apparent” enthalpy of reaction for the process represented in Reaction 11 using the Van’t Hoff equation (Equation 3), assuming that the standard heat capacity is constant.

$$\log_{10} K^\circ(T) = \log_{10} K^\circ(T_0) + \frac{\Delta H_r^\circ(T_0)}{R \ln(10)} \left(\frac{1}{T_0} - \frac{1}{T} \right) \quad \text{Equation 3}$$

In Equation 3, R is the gas constant ($8.31451 \text{ JK}^{-1} \cdot \text{mol}^{-1}$).

Thus, using the fitted data for the $\log_{10} K_{X1}$ (25 °C) values at different temperatures and applying the Equation 3, it is possible to calculate the standard stability constant and an “apparent enthalpy” ($\Delta_r H^{\text{app}}$) value for Reaction 11. The resultant $\log_{10} K_{X1}$ is $1.1 (\pm 0.06)$ and the $\Delta_r H^{\text{app}}$ is $21.2 (\pm 3.3)$ kJ/mol.

From the results of the batch experiments of anionic exchange of U(VI) in the absence of calcium it is possible to: quantify the U(VI) sorption to the resin; verify that the simplified conceptual model proposed in the present work is able to explain the experimental results obtained and; determine the standard stability constant and the “apparent” enthalpy values for the Reaction 11 to be used in modelling calculations in the presence of calcium.

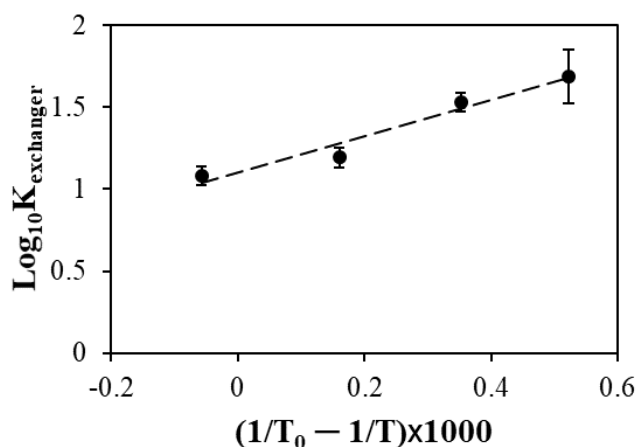


Figure 13. Dependency of the calculated $\log_{10} K_{X1}$ value from Reaction 11 with the temperature.

2.3.1.2.2. In the presence of calcium

We performed batch experiments of sorption of U(VI) on resin as a function of calcium concentration (Type II, see Table 7) at different temperatures in order to study the formation of Ca-U(VI)-CO₃ complexes.

The initial concentration of U(VI) was set as ca. $5 \cdot 10^{-7}$ M. As before, no precipitation was visible in the tubes neither before nor after filtration. The average pH and alkalinity measured in the blank samples are shown in Table 11. There is good agreement between the pH calculated and the one measured (compare values described in Table 11). This means that the equilibrium of pCO₂/pH/temperature of the present system is relatively well controlled.

Table 11. Theoretical and measured pH, alkalinity and pCO₂ of the batch experiments at different temperatures. Theor.: theoretical values according to the initial conditions of the experiments; Measured pH and alkalinity in equilibrium; and calculated pCO₂ in agreement with pH and alkalinity measured.

Temp.	CO ₂ (g)	pH theor.	Alkalinity Theor.	pCO ₂ theor.	pH measured	Alkalinity measured	pCO ₂ calculated
20 °C	1 %	7.2	2.0 meq/L	10 ^{-2.1} atm	7.18	2.5 meq/L	10 ^{-2.1} atm
40 °C	1 %	7.0	1.8 meq/L	10 ^{-2.0} atm	7.16	2.5 meq/L	10 ^{-2.0} atm
60 °C	3 %	6.8	1.8 meq/L	10 ^{-1.5} atm	6.90	2.2 meq/L	10 ^{-1.6} atm
80 °C	5 %	6.6	1.6 meq/L	10 ^{-1.3} atm	6.87	2.2 meq/L	10 ^{-1.5} atm

The results obtained in Type II experiments show that the concentration of U(VI) in solution (Figure 14) increases as the calcium concentration in the system increases. This behaviour is related to the formation of Ca-U(VI)-CO₃ complexes, according to the conceptual model described in Section 2.2.1.2. Contrary to the observed behaviour of the U(VI) in the absence of calcium, the retention of U(VI) in the resin decreases when the temperature increases. In Figure 14, two sets of data can be clearly distinguished: a) data at 20 and 40 °C and b) data at 60 and 80 °C. The concentration of uranium in equilibrium is higher at 20 and 40 °C than at 60 or 80 °C. The change of concentration can be related to the changes of the speciation of uranyl-carbonate complexes as observed in Figure 12. This means that the formation of UO₂(CO₃)₃⁴⁻ and CaUO₂(CO₃)₃²⁻ is strongly affected by the temperature of the system.

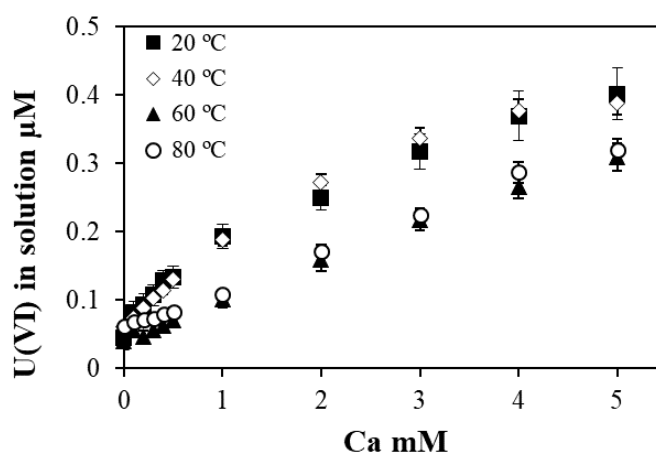


Figure 14. Concentration of U(VI) in equilibrium in solution as a function of calcium at different temperatures in 0.1 M of NaNO₃.

The respective stability constants for the Reaction 1 and Reaction 2 are calculated as shown in the following Equation 4.

$$\beta_{x13} = \frac{[\text{Ca}_x\text{UO}_2(\text{CO}_3)_3]^{2x-4}}{[\text{Ca}^{2+}]^x[\text{UO}_2^{2+}][\text{CO}_3^{2-}]^3} \quad \text{Equation 4}$$

In Equation 4, $x = 1$ or 2 . The $\log_{10} K^{\circ}_{X1}$ and the “apparent” enthalpy determined previously were used to fit the experimental data of concentration of U(VI) as a function of calcium at the different temperatures. The best fit line followed a non-linear model since two species $\text{CaUO}_2(\text{CO}_3)_3^{2-}$ and $\text{Ca}_2\text{UO}_2(\text{CO}_3)_3$ are formed. The results obtained in the fitting of the experimental data are provided in the following sections.

2.3.1.2.2.1. Fitting with PEST

In a first approach, the fitting of the stability constants has been performed with PEST coupled to Phreeqc. The results of the model approach for each experimental data are shown in Figure 15 and Figure 16. The agreement between the model approach and the experimental data is excellent for each experimental set. The $\log_{10} \beta_{113}$ and $\log_{10} \beta_{213}$ for each temperature obtained from the fitting are provided in Table 12. The details of the fitting are provided in Appendix D.2 and F.

The fit of the model approach with increasing temperature and respective pCO₂ of the chemical system, with the experimental data is good (solid-lines in Figure 15). The model approach also reproduces well the K_D of U(VI) for all experimental cases (solid-lines in Figure 16) except at 40 °C, since the calculated values are slightly overestimated at low concentrations of calcium with respect to the experimental data (Figure 15b and Figure 16b).

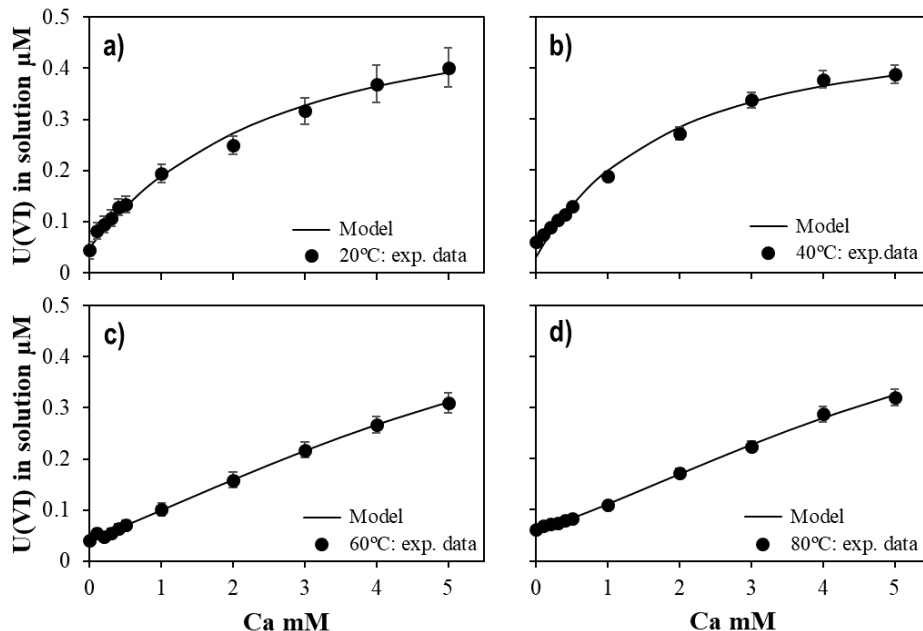


Figure 15. Symbols: Measured concentration of U(VI) for the Type II experiments as a function of the concentration of calcium at a) 20 °C and b) 40 °C in equilibrium with 1% of CO₂(g); c) 60 °C in equilibrium with 3% of CO₂(g); and d) 80 °C in equilibrium with 5% of CO₂(g). Solid-line: calculated U(VI) concentration using the model proposed in the present work.

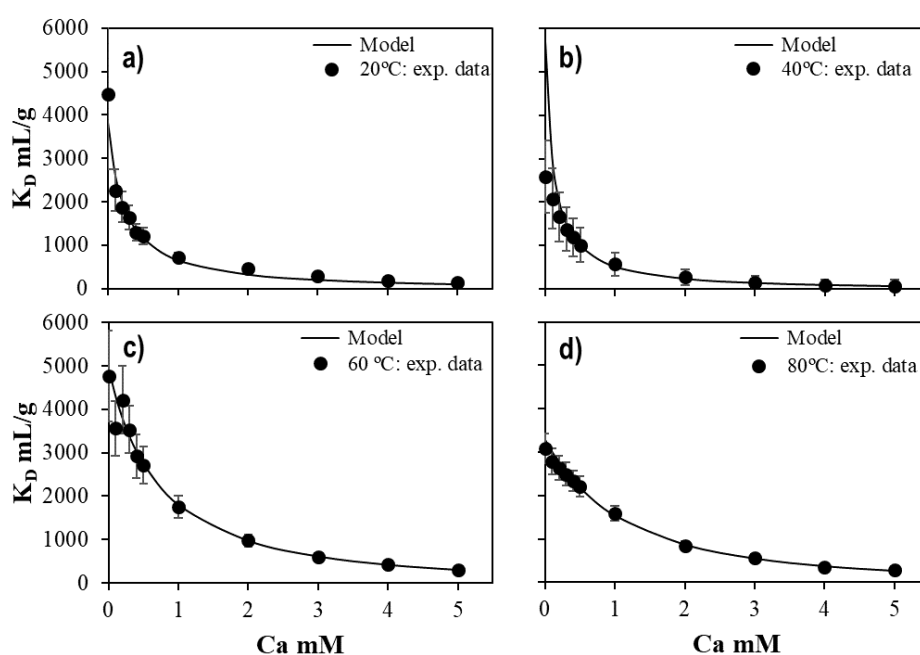


Figure 16. Symbols: Experimental K_D of U(VI) for the experiments Type II as function of the concentration of calcium at a) 20 °C and b) 40 °C in equilibrium with 1% of $\text{CO}_2(\text{g})$; c) 60 °C in equilibrium with 3% of $\text{CO}_2(\text{g})$; and d) 80 °C in equilibrium with 5% of $\text{CO}_2(\text{g})$. Solid-line: calculated U(VI) concentration using the model proposed in the present work.

Table 12. Results of the fitting for the stability constants of Ca-U(VI)- CO_3 complexes using PEST.

Estimated	20 °C		40 °C		60 °C		80 °C	
	value	±	value	±	value	±	value	±
$\log_{10} \beta_{213}$	29.81	1.08	29.90	0.73	29.64	0.09	29.73	0.10
$\log_{10} \beta_{113}$	27.43	0.11	27.23	0.12	26.68	0.03	26.49	0.06

The dependency of temperature on the stability constants of $\text{CaUO}_2(\text{CO}_3)_3^{2-}$ and $\text{Ca}_2\text{UO}_2(\text{CO}_3)_3(\text{aq})$ is shown in Figure 17. From the model results, it is possible to observe that both constants do not exhibit the same behaviour, as $\log_{10} \beta_{113}$ clearly decreases with temperature and $\log_{10} \beta_{213}$ is not affected by temperature changes.

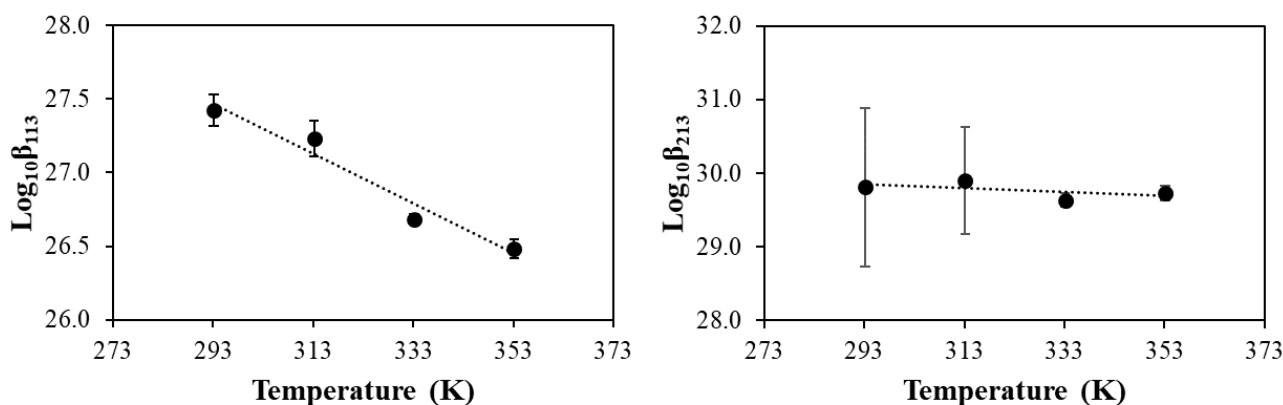


Figure 17. Temperature effect of the formation of $\text{CaUO}_2(\text{CO}_3)_3^{2-}$ (left) and $\text{Ca}_2\text{UO}_2(\text{CO}_3)_3(\text{aq})$ (right).

2.3.1.2.2. Benchmark of fitting using 2D mapping

Even though the use of PEST was successful for the parameterisation of the stability constants, this software can lead to high uncertainty, as the definition of the global minimum in non-linear systems is difficult to achieve. For this reason, a complementary numerical approach was performed by using Phreeqc as a geochemical model software, Excel for the sample standard deviation (SSD) and OriginLab© to evaluate the range of stability constants by 2D mapping.

With this method, the best fit for the stability constants is defined by the difference of SSD by means of colour grades. The lightest colour corresponds to the lower probability of the stability constants values (higher SSD) and the darkest correspond to the higher probability that can occur in a pair of stability constants (lower SSD). The best pair of stability constants lies within the darkest zone of the 2D mapping. The results of 2D mapping for each Type II experiment are shown in Figure 18. The circle- and square-sign represent the optimised value of the stability constants for each fitting method; i.e. the circle-sign corresponds to the best fit determined from matrix defined by Excel coupled with Phreeqc, and the square-sign corresponds to the best fit provided by PEST coupled with Phreeqc.

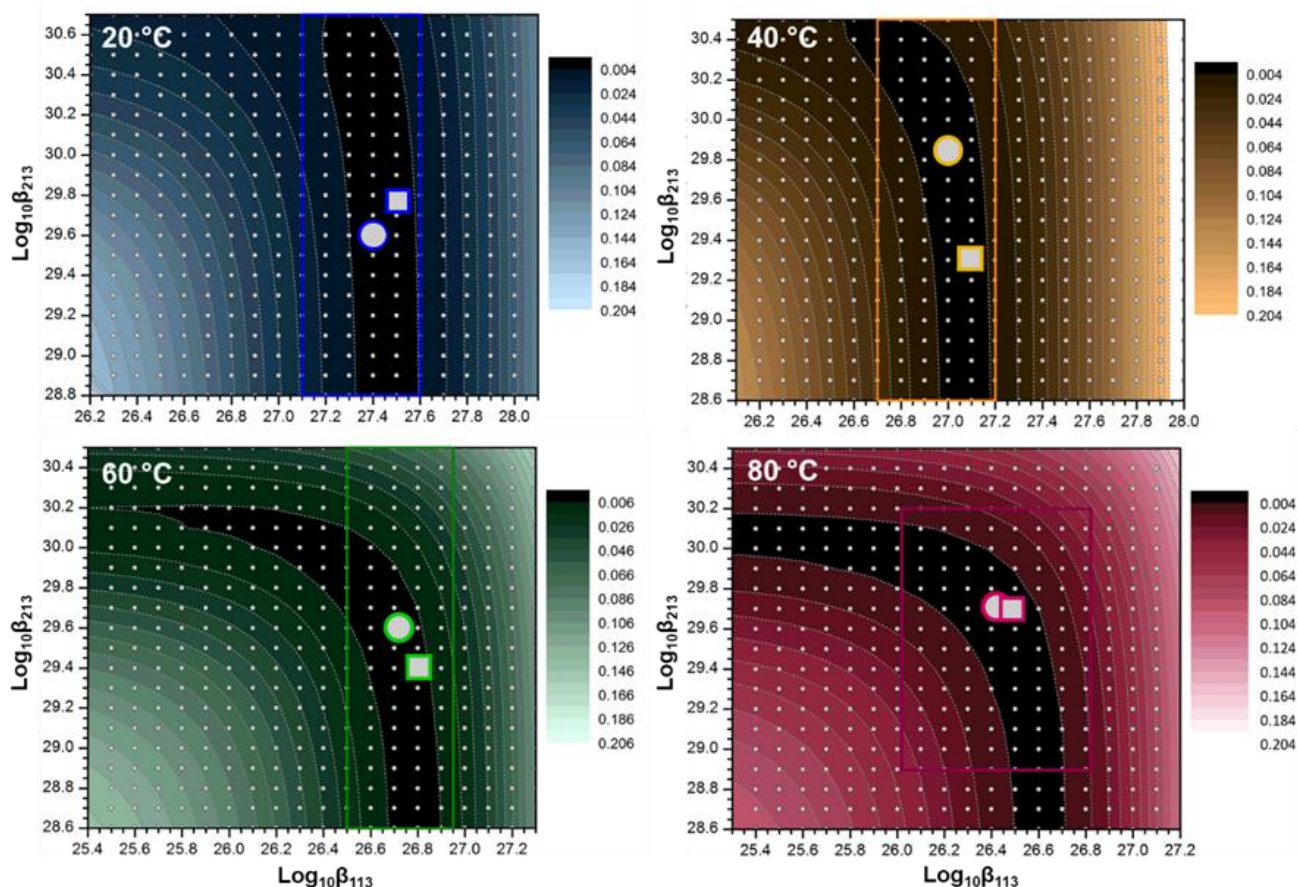


Figure 18. 2D mapping of the stability constants of Ca-U(VI)-CO₃ aqueous complexes distribution at 20, 40, 60 and 80 °C under respective pCO₂. Squares: optimised values using PEST+Phreeqc; Circles: optimised values using Excel+Phreeqc.

The results shown in Figure 18 indicate that the constants for Ca-U(VI)-CO₃ complexes seem to be inversely correlated; for higher values of $\log_{10}\beta_{213}$, lower values of $\log_{10}\beta_{113}$ are calculated. For the experiments at 20 °C and 40 °C, 2D mapping indicates that the best fit is strongly dependent on the

stability constant of $\text{Ca}_2\text{UO}_2(\text{CO}_3)_3(\text{aq})$. This is probably related to the fact that this complex may play a minor role in the experiments at those temperatures (see further Figure 23).

The optimised values of the stability constants for the Ca-U(VI)- CO_3 ternary complexes at different temperatures and pCO_2 are described in Table 13.

Table 13. Stability constants of Ca-U(VI)- CO_3 complexes calculated by 2D mapping method.

	20 °C	40 °C	60 °C	80 °C
Estimated	value	value	value	value
$\log_{10} \beta_{213}$	29.35	29.9	29.6	29.72
$\log_{10} \beta_{113}$	27.41	26.99	26.72	26.41

A further comparison of the calculated stability constants as a function of temperature using PEST or using 2D mapping are provided in Figure 19. The results obtained with both approaches are in good agreement and, in most cases, they are within the uncertainty range calculated with PEST. Highest deviations are observed in the case of data obtained at 20 and 40 °C.

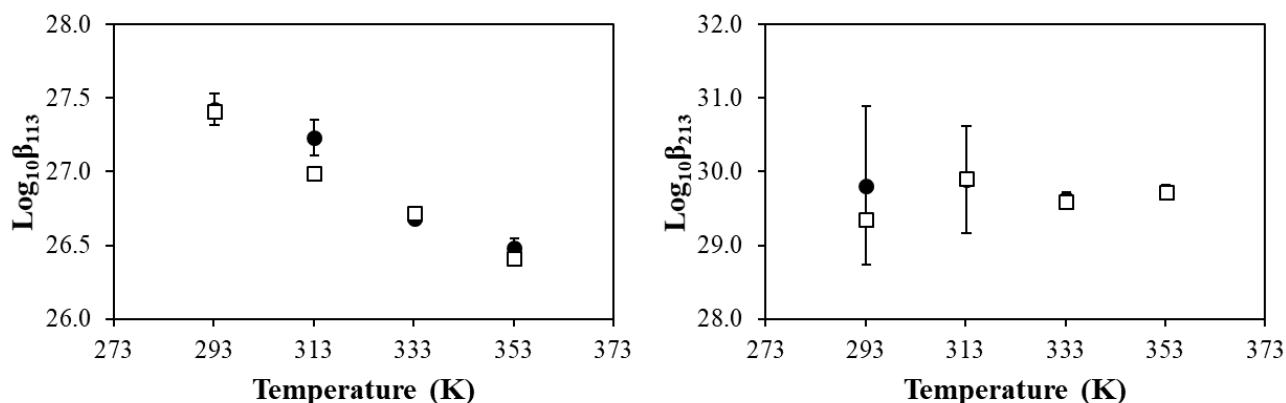


Figure 19. Dependency of the calculated $\log_{10}\beta$ value for Reaction 1 (left) and Reaction 2 (right) with the temperature using PEST-PhreeqC (black circles) and Excel-PhreeqC (white squares).

2.3.1.2.3. Evaluation of stability constants and enthalpy of reaction

All stability constants determined by PEST or 2D mapping are calculated at infinite dilution (zero ionic strength) and corrected using the Davies equation for each temperature stated; values are plotted as a function of $\frac{1}{T} - \frac{1}{T_0}$ in Figure 20. PEST and 2D mapping results are in excellent agreement in the case of $\text{CaUO}_2(\text{CO}_3)_3^{2-}$ although the stability constants for $\text{Ca}_2\text{UO}_2(\text{CO}_3)_3(\text{aq})$ have a higher uncertainty (Figure 20).

From the experiments undertaken at different temperatures, we determined the thermodynamic data needed to understand and model the U(VI) behaviour under temperature elevation. One can write the temperature dependence of the equilibrium constants as a function of the enthalpy, since the range of temperatures is small enough that the enthalpy can be assumed constant and assuming that the heat capacity change of reaction is zero at all temperatures (Equation 5). The enthalpy of reaction and the standard stability constants (at 298.15 K) were calculated following Equation 3.

Knowing the standard stability constant and the enthalpy of reaction, we further can determine the Gibbs free energy by its isotherm equation (Equation 5) and the entropy (Equation 6).

$$\Delta_r G^\circ = -RT \ln K^\circ(T_0) \quad \text{Equation 5}$$

$$\Delta_r G^\circ = \Delta_r H^\circ - T \Delta_r S^\circ \quad \text{Equation 6}$$

In Equation 5 and Equation 6, R is the gas constant (8.31451 JK⁻¹·mol⁻¹).

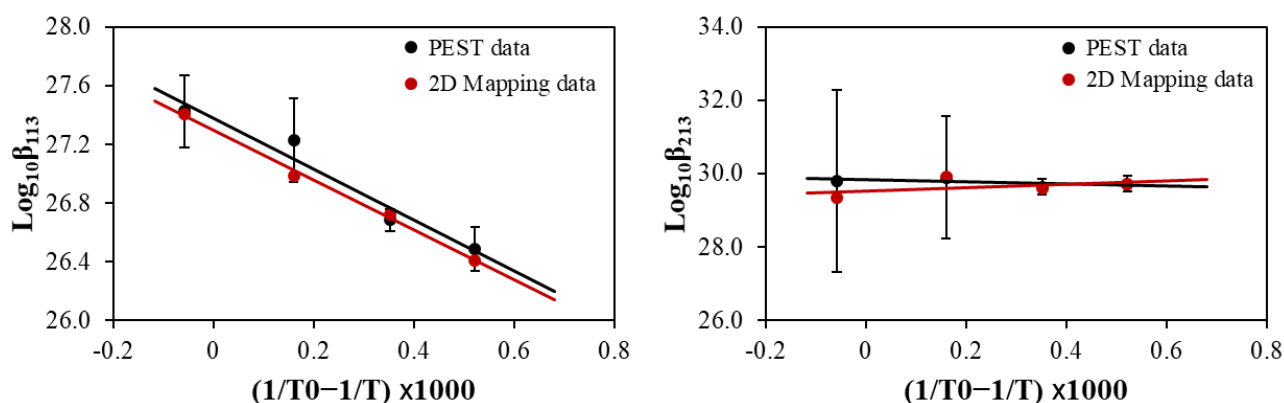


Figure 20. Variation of CaUO₂(CO₃)₃²⁻ (left) and Ca₂UO₂(CO₃)₃(aq) (right) stability constants with the temperature. Black: PEST approach. Red: 2D mapping approach. The lines represent least squares fitting following the constant enthalpy of the reaction equation.

We obtained the thermodynamic data for both uranyl-calcium-carbonate complexes, based on these calculations. The results summarized in Table 14 are the average values from both the PEST and 2D mapping approaches.

Table 14. Thermodynamic data of Ca-U(VI)-CO₃ ternary complexes determined in this work.

Reaction	log ₁₀ β° ± σ	Δ _r H° ± σ (kJ/mol)	Δ _r S° ± σ (kJ/K·mol)	Δ _r G° ± σ (kJ/mol)
Ca ²⁺ + UO ₂ ²⁺ + 3CO ₃ ²⁻ ⇌ CaUO ₂ (CO ₃) ₃ ²⁻	27.3 ± 0.2	-27.4 ± 8.2	0.41 ± 0.004	-150.8 ± 8.2
2Ca ²⁺ + UO ₂ ²⁺ + 3CO ₃ ²⁻ ⇌ Ca ₂ UO ₂ (CO ₃) ₃ (aq)	29.7 ± 0.3	1.3 ± 1.8	0.59 ± 0.03	-177.1 ± 13

As observed in the literature, the stepwise constants determined in the present work agree with the expected trend: the binding constant of Ca²⁺ to UO₂(CO₃)₃⁴⁻ (Reaction 16) is larger than the Ca²⁺ binding constant to CaUO₂(CO₃)₃²⁻ (Reaction 17).



The slope of the linear correlation between the stability constants and the temperature indicate that the enthalpy of reaction is different for each uranyl-calcium-carbonate ternary complex. The formation of the anionic species is not favoured with the increase of temperature controlled by an exothermic reaction; whereas the formation of the neutral species is not significantly affected by the changes of temperature. The enthalpy of reaction of the neutral species is slightly positive, although

ⁱ Note: UO₂²⁺ + 3CO₃²⁻ ⇌ UO₂(CO₃)₃⁴⁻, LogK⁰ = 21.84 according to data selection in Guillaumont, 2003.

its uncertainty is very high, so it can be assumed that there is no impact of the temperature on the formation of the $\text{Ca}_2\text{UO}_2(\text{CO}_3)_3(\text{aq})$. We obtained the calculations shown in Figure 21 and Figure 22 using the stability constants and enthalpy of reaction provided in Table 14 and observed a good agreement between experimental and calculated data.

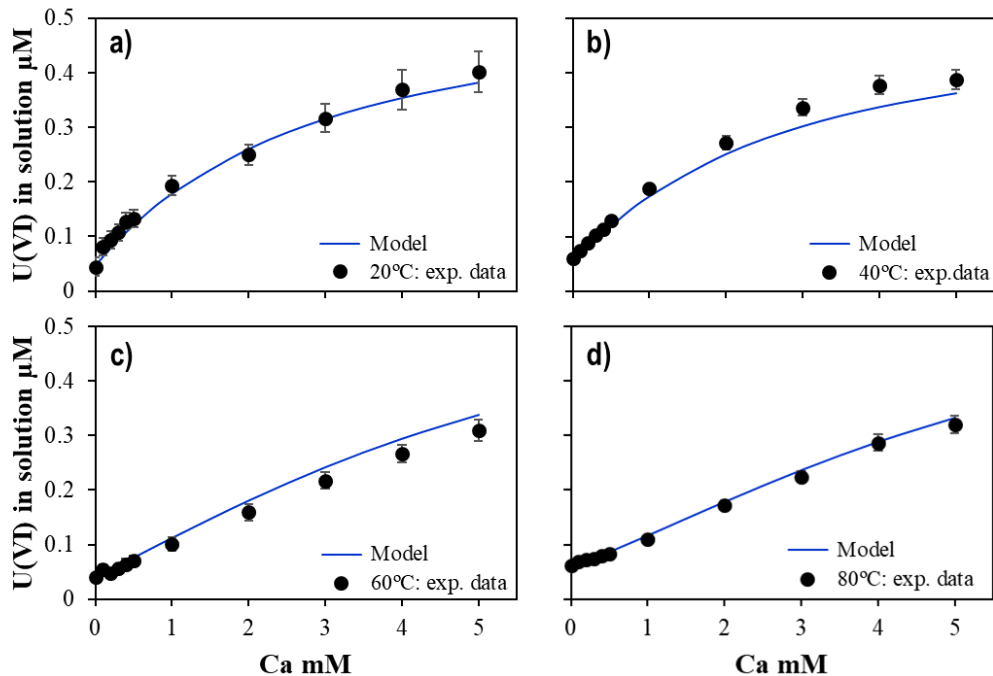


Figure 21. Symbols: measured U(VI) concentration as a function of the concentration of calcium in solution for Type II experiments at 20, 40, 60 and 80 °C. Solid line: Calculated uranium concentration using the standard stability constant and enthalpy values from Table 14.

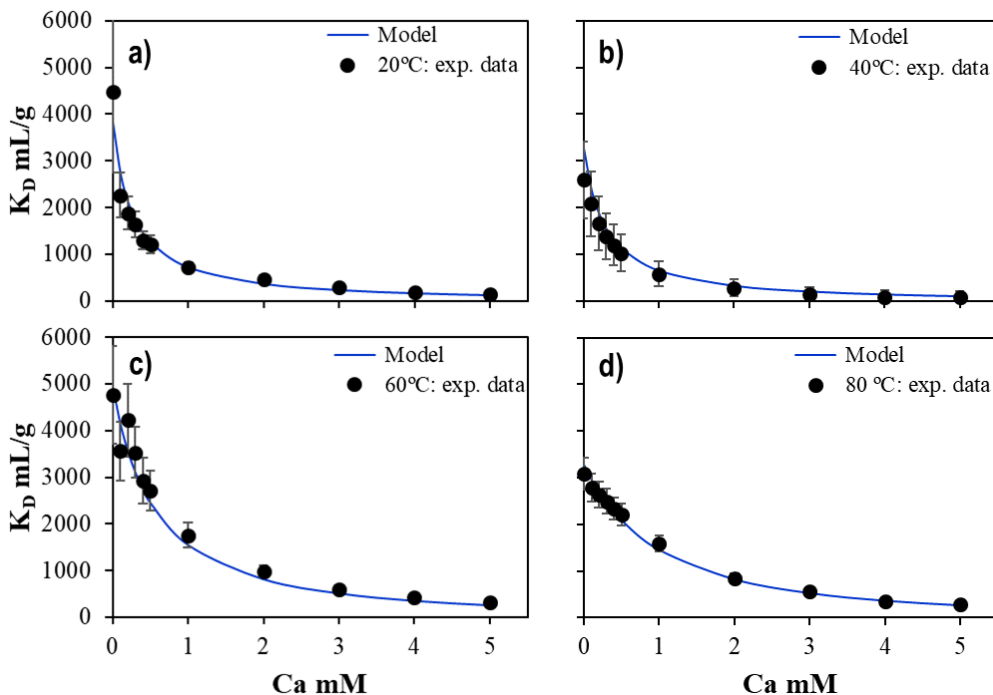


Figure 22. Symbols: experimental K_D value for U(VI) as a function of the concentration of calcium in solution for Type II experiments at 20, 40, 60 and 80 °C. Solid line: Calculated K_D using the standard stability constant and standard stability constant and enthalpy values from Table 14.

The uranium aqueous speciation values calculated for the experiments at the different temperatures are shown further in Figure 23. The aqueous speciation results indicate that $\text{CaUO}_2(\text{CO}_3)_3^{2-}$ is the main aqueous U(VI) species at all temperatures for Ca concentrations above 1mM. The fraction of $\text{Ca}_2\text{UO}_2(\text{CO}_3)_3(\text{aq})$ increases with Ca concentrations and in temperature, but this species is not the main one in any case. This is linked to the higher uncertainty found in the determination of its stability constant.

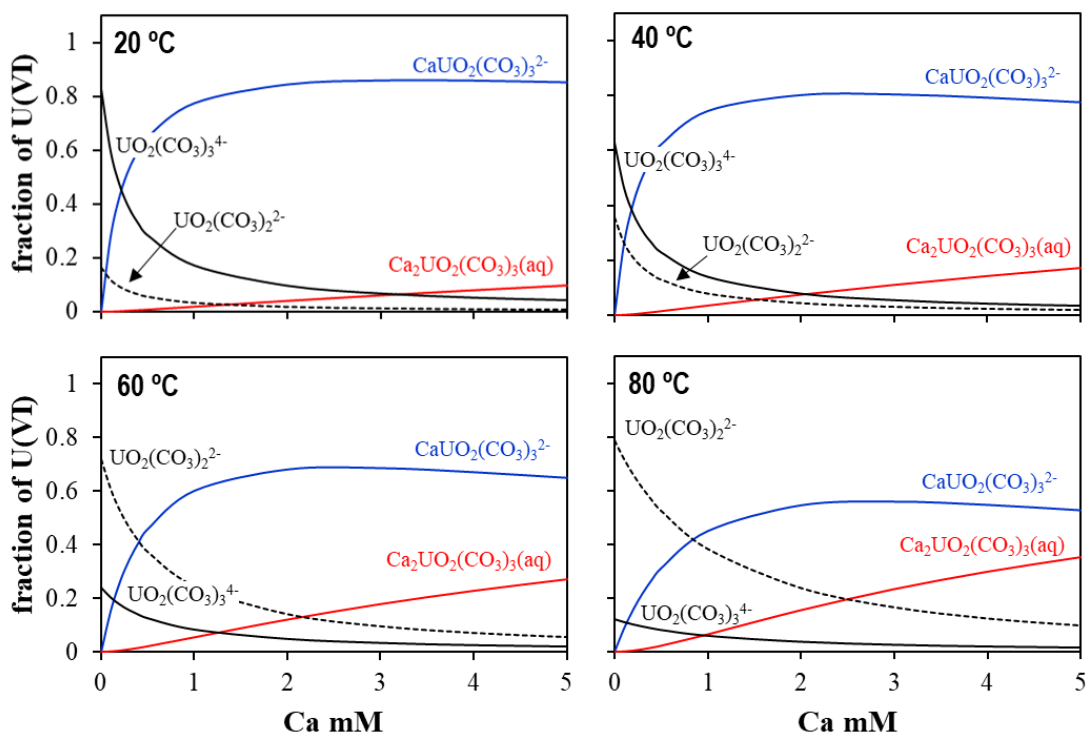


Figure 23. Calculated uranium aqueous speciation of the concentration of calcium in solution for Type II experiments at 20, 40, 60 and 80 °C.

2.3.1.2.4. Comparison with previous literature data

The stability constants for $\text{CaUO}_2(\text{CO}_3)_3^{2-}$ and $\text{Ca}_2\text{UO}_2(\text{CO}_3)_3(\text{aq})$ obtained as an average of PEST and 2D mapping fitting are $\log_{10} \beta_{113}^{\circ} = 27.3 (\pm 0.2)$ and $\log_{10} \beta_{213}^{\circ} = 29.7 (\pm 0.3)$. These values obtained from ionic exchange methods at different temperatures are consistent with the values previously found (Figure 24). The stability constant $\log_{10} \beta_{113}^{\circ}$ agrees with the recent works of Dong and Brooks (2006), Endrizzi and Rao (2014) and Lee and Yun (2013). The values for $\log_{10} \beta_{213}^{\circ}$ are in agreement with the published literature values within the range of uncertainty.

Although the stability constants obtained here for both complexes are in agreement with the published literature values within the range of uncertainty, taking as example the Callovo-Oxfordian geochemical conditions ($\text{pH} = 7.2$, $\text{pCO}_2 = 10^{-2.1}$ atm and $[\text{U(VI)}] = 10^{-8}$ M) we can evaluate the impact of the stability constants of those complexes. Comparing the stability constants proposed in the present work with those reported by Dong and Brooks (2006), we can observe significant changes on the speciation of U(VI) as a function of calcium in solution (Figure 25). The predictive modelling results at 25 °C indicate that $\text{CaUO}_2(\text{CO}_3)_3^{2-}$ plays an important role on the U(VI) speciation with the increase of the concentration of calcium in solution at the expense of $\text{Ca}_2\text{UO}_2(\text{CO}_3)_3(\text{aq})$.

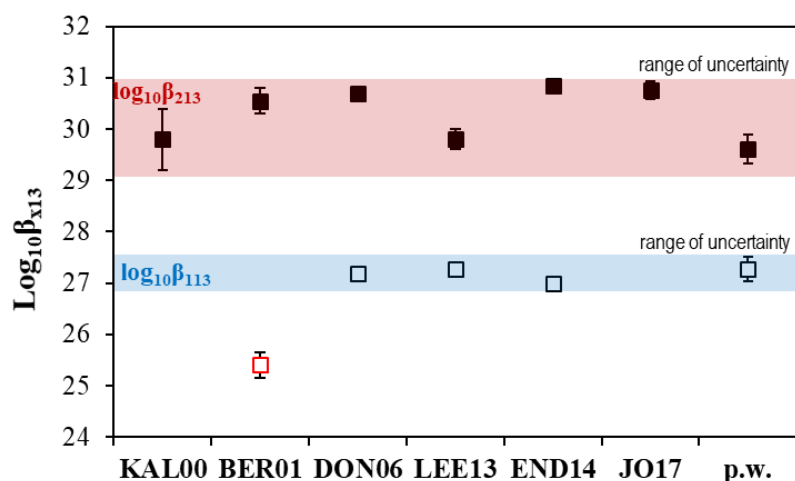


Figure 24. Comparison of the stability constants at 25 °C determined from different studies with the stability constants determined in the present work (p.w.). KAL00: Kalmykov and Choppin (2000); BER01: Bernhard et al. (2001); DON06: Dong and Brooks (2006); LEE13: Lee and Yun (2013); END14: Endrizzi and Rao (2014); JO17: Jo and Yun (2017); p.w.: present work.

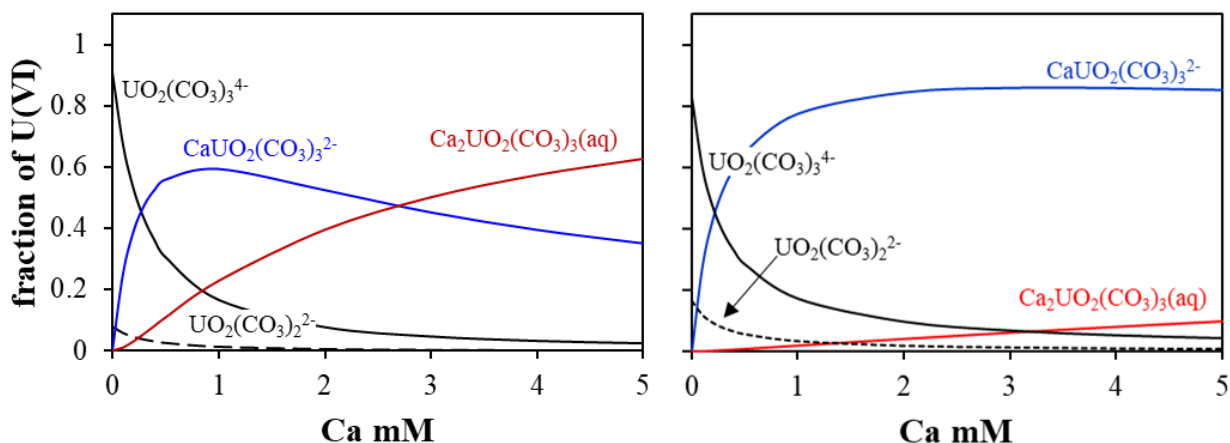


Figure 25. Calculated U(VI) aqueous speciation at calcium concentrations between 0 and $5 \cdot 10^{-3}$ M at 25°C. $[U]_T = 1 \cdot 10^{-8}$ M, $[C]_T = 3 \cdot 10^{-3}$ M, pH = 7.2 and $I = 0.1$ M. Left: Calculations performed using the stability constants from Dong and Brooks for Ca-U(VI)-CO₃ complexes. Right: Calculations performed using the stability constants determined in the present work for Ca-U(VI)-CO₃ complexes.

Even if the change in calculated speciation is significant, the impact on uranium solubility is more limited, as shown below. The solid exerting a solubility control of uranium in clay porewater conditions (Callovo-Oxfordian porewater, Table 3, see Section 1.1.1.1) at 25 °C is expected to be UO₂·2H₂O(am). The calculated aqueous uranium speciation under Callovo-Oxfordian conditions in equilibrium with UO₂·2H₂O(am) is shown in Table 15.

Two different calculations, using two different sets for the stability constants of Ca-U(VI)-CO₃ complexes, have been performed: using the stability constants from Dong and Brooks (2006); and using the stability constants determined in the present work. As seen in Table 15, even if the calculated U(VI) speciation is very different, the calculated uranium solubility is similar in both cases.

The enthalpy of reaction for CaUO₂(CO₃)₃²⁻ determined in the present work is almost two times smaller than the one reported by Endrizzi and Rao (2014). The most important difference is observed in the case of Ca₂UO₂(CO₃)₃(aq) thermodynamic data, although it must be kept in mind that the

uncertainty associated with the formation of this complex is also high (see the discussion above). One reason behind those differences may be the possible uranium precipitation in the experiments by Endrizzi and Rao (2014), due to the high uranium initial concentration needed in the microcalorimetry experiments.

Table 15. Calculated UO₂·2H₂O(am) solubility and aqueous U(VI) speciation under Callovo-Oxfordian conditions (Tournassat et al., 2008, Table 3)

Solid phase	Ca-U(VI)-CO ₃ stability constants	
	Dong and Brooks (2006)	Present work
	UO ₂ ·2H ₂ O(am)	UO ₂ ·2H ₂ O(am)
U concentration	1.9·10 ⁻⁶ M	7.7·10 ⁻⁷ M
	CaUO ₂ (CO ₃) ₃ ²⁻	18 %
Speciation	Ca ₂ UO ₂ (CO ₃) ₃ (aq)	78 %
	UO ₂ (CO ₃) ₃ ⁴⁻	2 %

The overall thermodynamic data of the Ca₂UO₂(CO₃)₃(aq) and CaUO₂(CO₃)₃²⁻ from the present work and the data of Endrizzi and Rao (2014) can be compared in the following Table 16.

Table 16. Comparison of the thermodynamic parameters of the Ca-U(VI)-CO₃ ternary complexes reactions. p.w. present work; (1) Endrizzi and Rao (2017); (2) Jo and Yun (2017); n.d. not defined.

Reaction	log ₁₀ β° ±σ	Δ _r H° ±σ (kJ/mol)	Δ _r S° ±σ (kJ/K·mol)	Δ _r G° ±σ (kJ/mol)	Ref.
Ca ²⁺ + UO ₂ ²⁺ + 3CO ₃ ²⁻ ⇌ CaUO ₂ (CO ₃) ₃ ²⁻	27.3 ±0.2	-27.4 ±8.2	0.43 ±0.01	-155.8 ±8.2	p.w.
	27.0 ±0.04	-47 ±6	0.36 ±0.01	-154.1 ±0.2	(1)
2Ca ²⁺ + UO ₂ ²⁺ + 3CO ₃ ²⁻ ⇌ Ca ₂ UO ₂ (CO ₃) ₃ (aq)	29.7 ±0.3	0 ± 1.8	0.57 ±0.02	-169.5 ±1.8	p.w.
	30.84 ±0.04	-47 ±7	0.43 ±0.01	-176.0 ±0.2	(1)
	30.75 ±0.2	-37 ±18	n.d.	n.d.	(2)

Finally, we tested if the previous literature data could be used to explain the experimental measurements obtained in the present work. In this context, the results obtained in the ionic exchange experiments in the presence of calcium have been modelled using the thermodynamic data for Ca-U(VI)-CO₃ complexes, available in Endrizzi and Rao (2014), since both stability constants and enthalpy data are reported.

The comparison of modelling with the thermodynamic data of the present work and with data from Endrizzi and Rao (2014) is shown in Figure 26. The modelling results indicate that the thermodynamic data for CaUO₂(CO₃)₃²⁻ and Ca₂UO₂(CO₃)₃(aq) using the data from Endrizzi and Rao (2014) provide reasonable results at low temperatures, but a higher deviation is observed when the temperature increases.

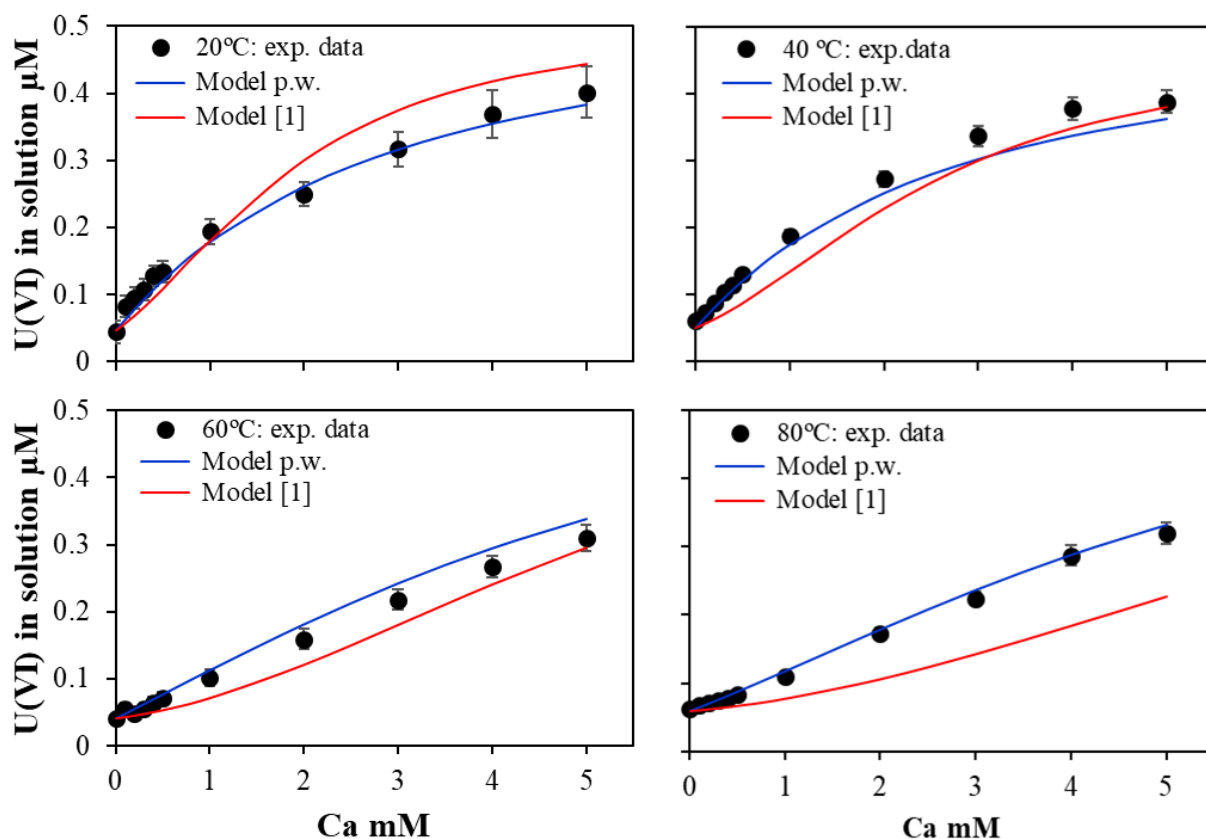


Figure 26. Symbols: measured U(VI) concentration as a function of the concentration of calcium in solution for experiments at 20, 40, 60 and 80°C performed in present work. Blue-line: Calculated uranium concentration using the thermodynamic data for Ca-U(VI)-CO₃ complexes determined in present work. Red-line: calculated uranium concentration using the thermodynamic data for Ca-U(VI)-CO₃ complexes reported in [1] Endrizzi and Rao (2014).

2.4. Summary

In conclusion, the experimental method proposed here, in which we determined the stability constants of the Ca-U(VI)-CO₃ ternary complexes at different temperatures, and consequently their thermodynamic parameters, was successful.

The anionic-exchange experimental method performed in the present study was adapted from the one proposed by Dong and Brooks (2006), where the main modifications were attributed to the changes of anionic-exchange resin more stable in temperature, and the initial concentration of U(VI). Furthermore, preliminary experiments were performed to guarantee the correct performance of the experimental set-up and to evaluate the equilibrium between CO₂(g) and the solutions.

The main issue found for this experimental method was the difficulty in controlling the changes of pH/carbonates of the system in temperature during the batch experiments. To achieve the control of all parameters in this type of systems was challenging. Initially, the experimental tests show that the pH and alkalinity (control of the carbonate concentration) were slightly higher than expected. Besides these less accurate results during the anionic-exchange batch experiments, the measured pH and alkalinity of the solution were in good agreement with those from the theoretical data.

The batch experiments in the absence of calcium aiming to quantify the sorption of uranyl-carbonate complexes on the resin at different temperatures (20, 40, 60 and 80 °C) and controlled atmospheres were successfully accomplished. Moreover, we also performed batch experiments in the presence of calcium adapted from Dong and Brooks (2006) to study the formation of Ca-U(VI)-CO₃ complexes at different temperatures (20, 40, 60 and 80 °C) and controlled atmospheres.

We determined the stability constants of Ca-U(VI)-CO₃ complexes by fitting a geochemical model, previously evaluated and validated using the Dong and Brooks (2006) experimental data, to the experimental data obtained from the anionic batch experiments performed at different temperatures. The fitting was performed by two different parameterisation/optimisation software (PEST and Excel©). The results show that both aqueous complexes studied here show different behaviours in temperature. The formation of the anionic complex (CaUO₂(CO₃)₃²⁻) is not favoured with the increase of temperature, though the formation of the neutral complex (Ca₂UO₂(CO₃)₃(aq)) is independent of the changes in temperature (Figure 20).

From these data, the standard stability constants for CaUO₂(CO₃)₃²⁻ and Ca₂UO₂(CO₃)₃(aq) were obtained and are consistent with those previously published, which provides confidence on the methodology used and the conceptual model proposed. Furthermore, we also determined the enthalpy data for the formation of Ca-U(VI)-CO₃ complexes (Table 14). The enthalpy of reaction of the formation of CaUO₂(CO₃)₃²⁻ and Ca₂UO₂(CO₃)₃(aq) are -27.4 ± 8.2 and 0 ± 1.8 kJ/mol, respectively. The $\Delta_r H^\circ$ of the anionic complex is negative as proposed by Endrizzi and Rao (2014), although it is two times lower. However, for the neutral complex, the $\Delta_r H^\circ$ contradicts the value proposed by Endrizzi and Rao (2014) (-47 kJ/mol). Besides the high uncertainty of $\Delta_r H^\circ$ of the Ca₂UO₂(CO₃)₃(aq) reaction, there is no impact of the temperature on its formation, in which we can assume that the ΔH is zero.

The other thermodynamic parameters of CaUO₂(CO₃)₃²⁻ and Ca₂UO₂(CO₃)₃(aq) formation (entropy and Gibbs free energy) are in good agreement with those published by Endrizzi and Rao (2014) (Table 16).

2.5. References

- Bernhard, G., Geipel, G., Brendler, V., and Nitsche, H. (1996). Speciation of Uranium in Seepage Waters of a Mine Tailing Pile Studied by Time-Resolved Laser-Induced Fluorescence Spectroscopy (TRLFS). *Radiochimica Acta* **74**: 87–91.
- Bernhard, G., Geipel, G., Reich, T., Brendler, V., Amayri, S., and Nitsche, H. (2001). Uranyl (VI) Carbonate Complex Formation: Validation of the Ca₂UO₂(CO₃)₂(aq.) Species. *Radiochimica Acta* **89**: 511–518.
- Casas, I., Bruno, J., Cera, E., Finch, R. J., and Ewing, R. C. (1997). Characterization and Dissolution Behavior of a Becquerelite from Shinkolobwe, Zaire. *Geochimica et Cosmochimica Acta* **61** (18): 3879–3884.
- Doherty, J. (2010). *PEST Model-Independent Parameter Estimation User Manual*. 5th ed. Watermark Numerical Computing. 122 p. Corinda (Australia)
- Dong, W. and Brooks, S. C. (2006). Determination of the Formation Constants of Ternary Complexes of Uranyl and Carbonate with Alkaline Earth Metals (Mg²⁺, Ca²⁺, Sr²⁺, and Ba²⁺) Using Anion Exchange Method. *Environmental Science & Technology* **40** (15): 4689–4695.
- Dong, W. and Brooks, S. C. (2008). Formation of Aqueous MgUO₂(CO₃)₃²⁻ Complex and Uranium Anion

- Exchange Mechanism onto an Exchange Resin. *Environmental Science & Technology* **42** (6): 1979–1983.
- Endrizzi, F. and Rao, L.. (2014). Chemical Speciation of uranium(VI) in Marine Environments: Complexation of Calcium and Magnesium Ions with $[(\text{UO}_2)(\text{CO}_3)_3]^{4-}$ and the Effect on the Extraction of Uranium from Seawater. *Chemistry - A European Journal* **20** (44): 14499–51406.
- Fox, P. M., Davis, J. A., and Zachara, J. M. (2006). The Effect of Calcium on Aqueous uranium(VI) Speciation and Adsorption to Ferrihydrite and Quartz. *Geochimica et Cosmochimica Acta* **70** (6): 1379–1387.
- Geipel, G., Amayri, S., and Bernhard, G.. (2008). Mixed Complexes of Alkaline Earth Uranyl Carbonates: A Laser-Induced Time-Resolved Fluorescence Spectroscopic Study. *Spectrochimica Acta - Part A: Molecular and Biomolecular Spectroscopy* **71** (1): 53–58.
- Giammar, D. E. and Hering, J. G. (2004). Influence of Dissolved Sodium and Cesium on Uranyl Oxide Hydrate Solubility. *Environmental Science and Technology* **38** (1): 171–179.
- Giffaut, E. (1994). ‘*Influence Des Ions Chlorure Sur La Chimie Des Actinides Effects de La Raiolyse et de La Température*’. PhD Thesis l’Université Paris XI Orsay (France)
- Gu, B., Ku, Y. K., and Brown, G. M. (2005). Sorption and Desorption of Perchlorate and U(VI) by Strong-Base Anion-Exchange Resins. *Environmental Science and Technology* **39** (3): 901–907.
- Guillaumont, R., Fanghänel, T., Neck, V., Fuger, J., Palmer, D. A., Grenthe, I., and Rand, M. (2003). *Update on the Chemical Thermodynamics of Uranium, Neptunium, Plutonium, Americium and Technetium*. 2nd ed. 919 p. OECD Nuclear Energy Agency, Data Bank, Issy-les-Moulineaux (France).
- Jiang, J-Q and Zeng, Z. (2003). Comparison of Modified Montmorillonite Adsorbents Part II: The Effects of the Type of Raw Clays and Modification Conditions on the Adsorption Performance. *Chemosphere* **53**: 53–62.
- Jo, Y and Yun, J. (2017). Spectroscopic Properties and Formation Constants of Ternary Ca-UO₂-CO₃ Complexes at High Temperatures. p. 34–35 in *6th Asia-Pacific Symposium on Radiochemistry*. Jeju Island, (South Korea).
- Joseph, C., Schmeide, K., Sachs, S., Brendler, V., Geipel, G., and Bernhard, G.. (2011). Sorption of uranium(VI) onto Opalinus Clay in the Absence and Presence of Humic Acid in Opalinus Clay Pore Water. *Chemical Geology* **284** (3–4): 240–50.
- Joseph, C., Steudtner, R., Schemid, K., Sachs, S., Bernhard, G., Van Loon, L. R., and Jakob, A. (2012). Do Elevated Temperatures and Organic Matter Influence the U(VI) Diffusion through Argillaceous Rock? in *Clay in natural engineered barriers for radioactive waste confinement*. Montpellier (France).
- Joseph, C. (2013). ‘*The Ternary System U(VI) / Humic Acid / Opalinus Clay*’. PhD thesis Helmholtz-Zentrum Dresden-Rossendorf (Germany).
- Kalmykov, S. N. and Choppin, G. R. (2000). Mixed Ca²⁺/UO₂²⁺/CO₃²⁻ Complex Formation at Different Ionic Strengths. *Radiochimica Acta* **88** (9–11_2000): 603-606.
- Kelly, S. D., Kemner, K. M., and Brooks, S. C. (2007). X-Ray Absorption Spectroscopy Identifies Calcium-Uranyl-Carbonate Complexes at Environmental Concentrations. *Geochimica et Cosmochimica Acta* **71** (4): 821–834.
- Kerisit, S. and Liu, C.. (2010). Molecular Simulation of the Diffusion of Uranyl Carbonate Species in Aqueous Solution. *Geochimica et Cosmochimica Acta* **74** (17): 4937–4952.
- Lee, J-Y. and Yun, J. (2013). Formation of Ternary CaUO₂(CO₃)₃²⁻ and Ca₂UO₂(CO₃)₃(aq) Complexes under Neutral to Weakly Alkaline Conditions. *Dalton Transactions* **42** (27): 9862-9869.

- Lee, J.-Y., Vespa, M., Gaona, X., Dardenne, K., Rothe, J., Rabung, T., Altmaier, M., and Yun, J. (2017). Formation, Stability and Structural Characterization of Ternary MgUO₂(CO₃)₃²⁻ and Mg₂UO₂(CO₃)₃(aq) Complexes. *Radiochimica Acta* **105** (3): 171–185.
- Meleshyn, A., Azeroual, M., Reeck, T., Houben, G., Riebe, B., and Bunnenberg, C. (2009). Influence of (Calcium-)Uranyl-Carbonate Complexation on U(VI) Sorption on Ca- and Na-Bentonites. *Environmental Science and Technology* **43** (13): 4896–4910.
- Parkhurst, D. L. and Appelo, C. A. J. (2013). *Description of Input and Examples for PHREEQC Version 3 — A Computer Program for Speciation, Batch-Reaction, One-Dimensional Transport, and Inverse Geochemical Calculations*. U.S. Geological Survey Techniques and Methods, Chapter A43, 497 p.
- Prat, O., Vercouter, T., Ansoborlo, E., Fichet, P., Perret, P., Kurttio, P., Salonen, L. (2009). Uranium Speciation in Drinking Water from Drilled Wells in Southern Finland and Its Potential Links to Health Effects. *Environmental Science & Technology* **43** (10): 3941–3946.
- Rai, D., Felmy, A. R., Hess, N. J., Legore, V. L., and Mccready, D. E. (2002). Thermodynamics of the U(VI)–Ca²⁺–Cl⁻–OH–H₂O System: Solubility Product of Becquerelite. *Radiochimica Acta* **90**: 495–503.
- Sandino, A. and Grambow, B. (1994). Solubility Equilibria in the U(VI)-Ca-K-Cl-H₂O System: Transformation of Schoepite into Becquerelite and Compreignacite. *Radiochimica Acta* **66**: 37–43.
- Stewart, B. D. and Mayes, M. A. (2010). Impact of Uranyl-Calcium-Carbonate Complexes on Uranium(VI) Adsorption to Synthetic and Natural Sediments. *Environmental Science & Technology* **44** (3): 928–934.
- Tullborg, E. L., Suksi, J., Geipel, G., Krall, L., Auqué, L., Gimeno, M., and Puigdomenech, I. (2017). The Occurrences of Ca₂UO₂(CO₃)₃ Complex in Fe(II) Containing Deep Groundwater at Forsmark, Eastern Sweden. *Procedia Earth and Planetary Science* **17** (li): 440–43.
- Vercouter, T., Reiller, P. E., Ansoborlo, E., Février, L., Gilbin, R., Lomenech, C., and Philippini, V. (2015). A Modelling Exercise on the Importance of Ternary Alkaline Earth Carbonate Species of uranium(VI) in the Inorganic Speciation of Natural Waters. *Applied Geochemistry* **55** (Vi): 192–198.
- Zheng, Z., Tokunaga, T. K., and Wan, J. (2003). Influence of Calcium Carbonate on U (VI) Sorption to Soils. *Environmental Science & Technology* **37** (24): 5603–5608.

Chapter 3

Behaviour of Uranium in Callovo-Oxfordian Formation at 20 °C

3.1. Introduction

The development of reliable predictive sorption models is essential to accurately evaluate the long-term fate of radionuclides in real geochemical conditions. The aim of this chapter is to describe the retention mechanisms of U(VI) in Callovo-Oxfordian formation at 20 °C. The model here proposed for the retention mechanisms of U(VI) will be further used as a basis for studying the temperature effect on the sorption of U(VI) on Callovo-Oxfordian systems at different temperatures (see further Chapter 4).

One of the difficulties of the present work lies on the complexity of the Callovo-Oxfordian claystone (carbonated clayed facies) mineral assemblage (see Table 1, Gaucher et al., 2004). In general, the clay fraction of COx claystone corresponds to 20–50 wt% of the total mass of the formation, where illite and interstratified illite/smectite (disordered I/S_{R0} and ordered I/S_{R1}) are the main components. This argillaceous rock is well known for its high content of carbonates, such as calcite and dolomite that can correspond to 20 to 40 wt%, responsible for buffering the system from neutral to weakly alkaline conditions. The minor content of pyrite present in the COx formation (< 1 wt%) allows the maintenance of the redox potential as reductive (Vinsot et al., 2008, 2017). The presence of clay minerals, in addition to a neutral pH environment and reducing aqueous conditions, are relevant parameters for the safety of nuclear waste, since all favour a high sorption of radionuclides and a low solubility of most radionuclides of interest, such as uranium, by limiting radionuclide migration through the geosphere (Bruno et al., 2002)

The present study aims to answer the following questions: what mineral phases contribute for the retention of metal/radionuclides ions and which retention mechanisms should be considered in the model to describe the retention of U(VI) under Callovo-Oxfordian conditions?

We propose a three-step methodology:

- 1) A description of the main phases that could be involved in the retention processes;

- 2) A literature review to select and define a retention model and to identify possible missing parameters with respect to Callovo-Oxfordian formation conditions;
- 3) The definition of the experimental parameters to be measured during the laboratory experiments will be discussed in light of the literature review.

3.1.1. Background

In the following section, we provide a brief description of the main solid phases that contribute for the retention of radionuclides in Callovo-Oxfordian claystone systems as well as the mechanisms of retention involved at the water-minerals interface and we will discuss how these can be interpolated for natural systems.

3.1.1.1. What are clay minerals?

The clay minerals are hydrated phyllosilicates composed by tetrahedral and octahedral sheets separated or not by interlayer cation and/or water molecules. They are classified according to: (1) the thickness between the tetrahedral and octahedral sheets; (2) the anisotropy of the layers or particles; (3) the existence of several types of surfaces (planar or basal and edges); (4) the ability to which the external (and internal) surface can be modified by e.g. adsorption and ionic exchange; (5) plasticity; and (6) hardening by heat (Brigatti et al., 2006).

The clay minerals contain continuous tetrahedral (T) and octahedral (O) sheets. Each tetrahedron consists of a cation (Si^{4+} , Al^{3+} and Fe^{3+}) coordinated to four oxygen atoms (Figure 27b) and linked to adjacent tetrahedral through shared basal oxygen atoms. The octahedron consists of a cation (Al^{3+} , Fe^{3+} , Mg^{2+} and Fe^{2+}) coordinated to six oxygen atoms (Figure 27a, c) and linked to the next octahedral sheet by sharing edges. The combination of several tetrahedra across basal oxygen atoms leads to the formation of a basal surface, while for the octahedral sheets the individual octahedra are connected by sharing edges. When Al^{3+} is the central cation, only two of every three octahedra are occupied to maintain electrical neutrality resulting in a so-called dioctahedral structure (Figure 27d). On the other hand, when Mg^{2+} is the cation, all three octahedra are filled forming a so-called trioctahedral structure (Figure 27e).

The combination of one tetrahedral sheet and one octahedral sheet results in a 1:1 (TO) layer structure (Figure 28a). The edges of the tetrahedral sheets project into a hydroxyl plane of the octahedral sheet, replacing 2/3 of the hydroxyl ions and forming one basal plane of oxygen atoms from the tetrahedral sheet while the other plane is made of hydroxyls from the octahedral sheet (Bergaya et al., 2013). The combination of one octahedral sheet sandwiched between two tetrahedral sheet results in a 2:1 (TOT) layer structure (Figure 28b). Here both basal planes of individual layers are composed by oxygen atoms (belonging to the tetrahedral sheets).

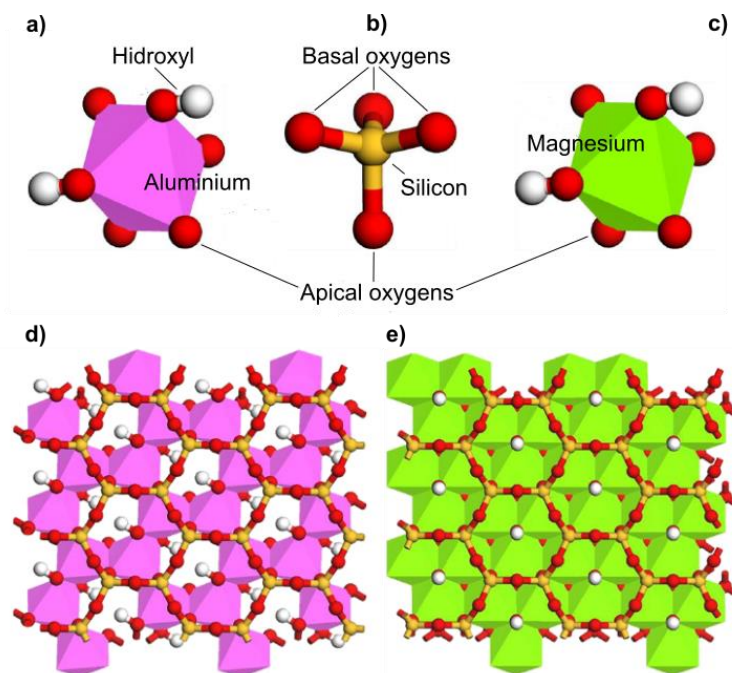


Figure 27. Representation of a) aluminium oxide octahedra, b) silicon oxide tetrahedra, c) magnesium oxide octahedra, plan formed by combination of one tetrahedral sheet with d) one dioctahedral sheet, and e) one trioctahedral sheet. (Adapted from Nguouana, 2014).

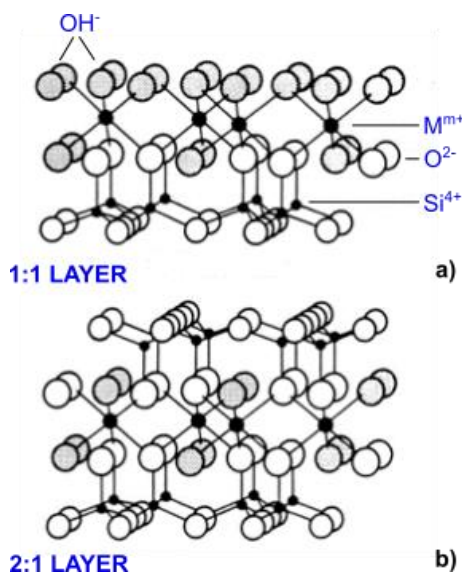


Figure 28. Structural elements of phyllosilicates of tetrahedral and octahedral sheets linked to form a 1:1 layer type structure and linked to form 2:1 layer type structure (Adapted from Sposito et al., 1999; Copyright (1999) National Academy of Sciences <http://www.pnas.org/content/96/7/3358>).

Isomorphous substitutions may occur in these layer structures. The isomorphous substitutions are characterised by replacing the Si⁴⁺ in tetrahedral positions by cations of a similar size and coordination but of lower valency, or/and through substitutions of Al³⁺ in octahedral positions. As a result, the layer structure acquires permanent negative charge. The isomorphous substitutions are typical of 2:1 layer structures in which the net layer charge is balanced by hydrated or non-hydrated-cations occupying interlayer positions. When the interlayer space is filled with a hydroxide sheet a 2:1:1 layer structure is formed. Based on these parameters, we can distinguish different groups of clay minerals.

In Table 17, we show some examples of different types of clay minerals, highlighting the most relevant for the present work.

Table 17. Classification of the planar hydrated phyllosilicates and some examples for each clay mineral species (Brigatti et al., 2006). (the highlighted clay minerals are the ones relevant for the present study)

Layer type	Interlayer composition	Net layer charge	Group	Octahedral character	Example
1:1	None or H ₂ O	≈ 0	Serpentine–Kaolin	Tri	Amesite
				Di	Kaolinite
				Di–Tri	Odinite
2:1	None	≈ 0	Talc–pyrophyllite	Tri	Talc
				Di	Pyrophyllite
	Hydrated exchangeable cation	0.2–0.6	Smectite	Tri	Saponite
				Di	Montmorillonite
	Hydrated exchangeable cation	0.6–0.9	Vermiculite	Tri	Vermiculite
				Di	Vermiculite
	Exchangeable monovalent cation	0.85–1.0	Micas	Tri	Phlogopite
				Di	Muscovite
	Exchangeable mono- and di-valent cation	0.6–0.85	Illite	Tri	Biotite
				Di	Illite
Hydroxide sheet	variable	Chlorite	Tri	Clinochlore	
			Di	Donbassite	
				Di–Tri	Cookeite

So far, we described the clay mineral as a single unit cell. When considering all unit cells, the planar phyllosilicates are formed by a finite number of either 1:1 or 2:1 type layer structures that are continuous along the layer planes and stacked perpendicularly. This kind of arrangement leads to the possibility of layer displacements by rotation and/or translation, which provides several polytypes or structures with different layer stacking sequences. The packing of the different types of layers can be randomly or regularly interstratified in a so-called mixed-layer structural arrangement. The interstratified clay minerals can be classified based on their stacking as ordered, random or partially ordered. In Figure 29, we show a schematic example of the stacking of interstratified clay minerals.

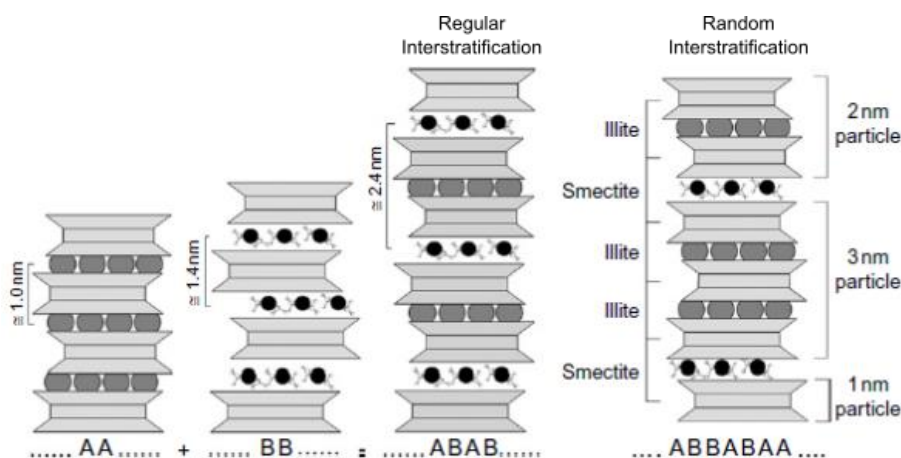


Figure 29. Regular and random interstratified clay minerals. A and B are layers with different periodicity along the c direction (Brigatti et al., 2006).

3.1.1.2. What are the retention processes?

The retention processes can be classified as reversible or irreversible. In the reversible retention processes, there are sorption processes such for example: ion exchange and surface complexation. On the other hand, irreversible retention is associated generally with immobilisation processes (in which in some cases can be reversible in very slow equilibrium processes) such as surface precipitation, co-precipitation, surface substitution or diffusion on the minerals (NEA, 2002),.

In real geochemical conditions, all retention processes should be included in prediction models. However, due to the complexity of most natural systems, simplifications must be made by neglecting, in some cases, some of these processes. For instance, in predictive models most irreversible processes are not considered due to a lack of relevant data, and the presence of uncertainties associated to the slowness and complexity of such processes (NEA, 2002). The understanding of irreversible processes has been improved due to the recent development of high-quality laboratory surface-specific analyses such as Surface Nuclear Magnetic Resonance (NMR) or Extended X-ray Adsorption Fine Structure (EXAFS), but both qualitative and quantitative data are still needed. In contrast, the reversible processes are easier to describe and are the subject of an important number of studies leading to data that is available and can be used for the prediction of retention processes. Moreover, most reversible processes, such as surface sorption processes, are kinetically faster and are generally the main processes controlling the concentration of the elements in the porewater, *i.e.* the elements which are mobile. In this work we will, therefore, focus on reversible surface retention processes, in which the surface processes are strictly related to a complex formation reaction between dissolved metal ions and the surface functional groups present at the surface of minerals.

3.1.1.2.1. How to describe the retention processes?

Adsorption, in which the ion of interest makes a chemical bond at the surface of the mineral, is one of the most relevant reversible processes responsible for the retention of radionuclides. There are two distinct models describing the equilibria of adsorption-desorption mechanisms at the mineral surface: (1) empirical adsorption models, that are based on partitioning relationships with no predictive character; and (2) mechanistic adsorption models that describe the details of chemical species formation at mineral surfaces using thermodynamic formalisms; in this last case such models have predictive character but also require a better characterization of the system.

In the empirical model, the adsorption is often described by law of mass action and by simple distribution coefficients or Langmuir and Freundlich isotherms. The simplest distribution coefficients (K_D) models (see example of Equation 1 in Chapter 2) describe the partitioning of solutes between the aqueous phase and the surface in a given set of experimental conditions. The K_D is then constant according to the solid-to-liquid ratio in a given concentration range where the site saturation does not occur.

In more sophisticated empirical models, such as the Langmuir and Freundlich isotherms model, the sites of interaction are considered without specifying the type of species formed at the surface. Such models can explain the sites saturation (not possible with the K_D model) and can therefore describe sorption isotherms in concentration. These models are widely used due to their conceptual and numerical simplicity, although they are seriously constrained as they are not able to describe chemical

and physical perturbations in the geochemical system, such as the pH effect (Hochella and White, 1990).

The mechanistic models are essentially extensions of the ion association models in aqueous chemistry that make the following assumptions: a) the surface functional groups react with dissolved solutes to form surface complexes; b) the physical-chemical equilibrium is described via mass action law equations with correlation factors applied for variable electrostatic conditions and boundaries; c) the surface charge is treated as a chemical reaction of the functional group and d) the apparent binding constants determined for the mass law equations are empirical parameters constrained by thermodynamic properties of the activity coefficients of the surface species (references in Davis and Kent, 1990).

In this study, we will concentrate our attention only on mechanistic models focusing on three questions: What are the retention mechanisms to be considered? How to describe and quantify them and what are their limitations? How to interpolate the sorption mechanisms to environmental samples?

The retention mechanisms:

The main retention mechanisms occur at the surface of all mineral phases by the presence of surface hydroxide groups. They result from the hydroxylation of the surface upon exposure to water molecules and can be seen, by analogy with what happens in solution, as hydroxide surface sites. According to the type of mineral, they have different reactivities depending on the metal to which the OH group is bound, e.g. iron for hydroxides or silicon for silicates surfaces.

The adsorption of ions on the hydroxide surface sites is known as surface complexation. The ions can then interact with these sites leading to outer- (the ion keeps its first hydration sphere) or inner- (one or several water molecules in the first coordination sphere are replaced by atoms belonging to the reacting surface group) sphere complexes. For the clay minerals of interest in this work (e.g. 2:1 layer type structure), the hydroxide surface sites are located on the edges and can be identified as strong and weak sites. Such sites will be better described later.

In addition to the classical “surface complexation” mechanism, one has also to consider the ion exchange (Figure 30) that occurs in clay materials. The ion exchange comes from the permanent charge originated from isomorphous substitutions during the formation of the clay mineral. To compensate for the negative charge, cations are bonded by electrostatic interaction, and can be exchanged according to the composition of the solution. These cations are normally bounded at one type of sites denominated “basal sites”. A schematic representation of the cation exchange sites existing at the basal and edge surfaces is given in Figure 30.

Besides the permanent negatively charged character, the charge of the mineral can either be positive or negative depending on the pH of the suspension due to the amphoteric nature of the surface functional groups. In acidic conditions, the edge surface becomes positive due to protonation of the functional groups, whereas in alkaline conditions the edge surface deprotonates and becomes negatively charged.

For clay materials, the combination of this pH-dependence charge with the permanent charge at the basal surface hinders the description of surface mechanisms, notably in terms of surface potential (Ferrage et al., 2005; Tournassat et al., 2013).

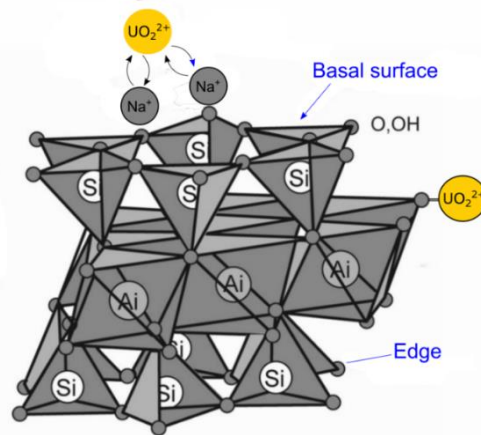


Figure 30. Schematic representation of cation exchange with one uranyl cation and two Na⁺ cations, and uranyl surface complexation bond to the edge of surface.

Description and quantification of surface mechanisms:

Cation exchange process

The cation exchange process is in most cases pH-independent (in normal environmental conditions) but it is strongly dependent on the ionic strength and chemical composition of the solution. Typically, a cation exchange reaction of metal ion B with valency z exchanging with a metal ion A with valency y on a clay mineral surface X is generically defined according to Reaction 18.



Reaction 18 is defined by the selectivity coefficient $K_{A/B}^X$ according to law mass action relationship (Equation 7).

$$K_{A/B}^X = \frac{[AX(\text{s})]^z \cdot \gamma_B [B]^y}{[B^zX(\text{s})]^y \cdot \gamma_A [A]^z} \quad \text{Equation 7}$$

In Equation 6, $\gamma_{A,B}$ is the activity of the solute A and B (mol/L), the square brackets correspond to the concentration of A and B sorbed per unit mass divided by CEC (Cationic Exchange Capacity, eq/kg) or in solution (mol/L). For exchange metal ions, different conventions may be used as there is no unifying theory to calculate the activity coefficients (Gaines and Thomas, 1953; Gapon, 1933; Vanselov, 1932). Amongst such conventions, the Gaines-Thomas convention is the most widely used. Due to no unifying theory for the activity coefficient of the exchanger, the reference state of the activity coefficient of the adsorbed ions normally stands for 1, assuming that the exchanger is totally occupied by the same cation. This simplified assumption should be taken with caution since the selectivity coefficient can change according to the solution composition, as the activities coefficient are highly dependent on the ionic strength and the type of exchange sites occupied (McBride, 1980). Therefore, the selectivity coefficient must be chosen carefully according to the system of interest (Tournassat et al., 2009). Recently, there are models under development where the correction of activity for the different sites is considered (Reinoso-Maset and Ly, 2014, 2016; Stammose et al., 1992). In this work, the Gaines-Thomas convention is used.

Surface complexation models and application to clay minerals

In contrast to the cationic exchange, the surface complexation is strongly dependent on the pH and weakly dependent on the ionic strength of the solution. In environmental conditions (pH approx. 7 and metal trace concentrations), surface complexation is the main process governing the retention of metals present in trace concentrations.

In the last decades different surface complexation models (SCM) have been proposed. The different models can be distinguished based on specific interfacial structures, resulting in various kinds of surface reactions and electrostatic correction factors to mass law equations. These models were originally developed to describe the surface reaction on oxides minerals, but they have been widely used to any mineral that develops an amphoteric surface charge, such as clay minerals (Davis and Kent, 1990). In SCM models, as for the empirical models, the parameters must be determined in a wide range of solution compositions in order to reproduce the natural conditions as closely as possible (Parks, 1990).

The SCM models can be described as chemical equilibrium approaches defined by surface species, chemical reactions, equilibrium constants, mass balances and charge balances (Goldberg, 2013). Different models have been defined in the literature based on the reactive surface function group, that undergoes both protonation and deprotonation reactions, with common characteristics and adjustable parameters. In acidic conditions, there is protonation of the functional groups (Reaction 19), with a release of H⁺ ions to the solution changing the pH of the media. In more alkaline conditions the deprotonation of the functional groups is favoured (Reaction 20).



The equilibrium constants of the protonation and deprotonation reactions are shown, respectively, in Equations 7 and 8 below,

$$K_+^{\equiv\text{SOH}} = \left(\frac{[\equiv\text{SOH}_2^+]}{[\equiv\text{SOH}] \cdot \{\text{H}^+\}} \right) \cdot e^{(F\Psi/RT)} \quad \text{Equation 8}$$

$$K_-^{\equiv\text{SOH}} = \left(\frac{[\equiv\text{SO}^-] \cdot \{\text{H}^+\}}{[\equiv\text{SOH}]} \right) \cdot e^{-(F\Psi/RT)} \quad \text{Equation 9}$$

In Equation 8 and Equation 9, the F is the Faraday constant (96485 C·mol⁻¹), Ψ is the surface potential, R the molar gas constants, and T the absolute temperature. The squared brackets correspond to the concentration of the respective surface functional group and the curly brackets correspond to the aqueous activities. The aqueous activities are calculated as a function of the ionic strength of the solution according to the Extended Debye-Hückel, Davies, SIT or Pitzer models (Grenthe et al. 1997). The best known for this type of models is the Davies equation, which is suitable for ionic strength below 0.1 M and will be the one considered hereafter.

Moreover, different models were proposed to describe the surface potential. These models differ on the structural representation of the solution-surface interface: CCM— Constant Capacitance Model (Schindler and Kamber, 1968; Hohl and Stumm, 1976; Sposito, 1984; Schindler and Stumm, 1987); DLM— Diffuse Layer Model (Stumm et al., 1970; Huang and Stumm, 1973) and TLM— Triple Layer

Model (Hayes, 1987). When the surface functional group is characterised by either one or two protons, the SCM model is developed from the Stern Model based on one layer at surface, so-called Stern layer. The expansion of the TLM models is known as Charge Distribution Multi-Site Complexation (CD-MUSIC), which considers charge distribution bond valence principles and identifies different types of surface sites based on their crystallographic structure. The location and surface configuration of the adsorbed ions for the different SCMs models are schematically shown in Figure 31.

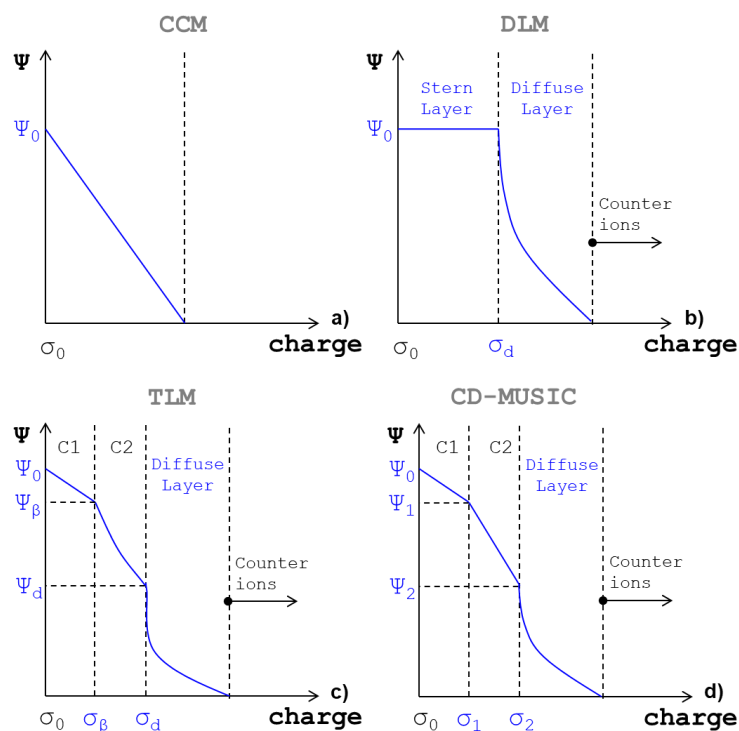


Figure 31. Schematic representation of the placements of ions, charges (σ) potential (Ψ) and capacitances (C) for different SMCs for surface 0-plane; β -plane and d-plane. Adapted from Goldberg (2013).

In the case of clay minerals, specially 2:1 type clay minerals, even though SCM model approaches can describe sorption experimental data the thermodynamic parameters obtained have no real significance as the correction of the electrostatic potential is not correct as the potential arises from two types of charges that are not located structurally in the same place (i.e. at the basal and edge surfaces). For this reason, specific models are being developed for surface complexation on clay minerals, and recently a model considering the spill-over effect on the surface potential was applied successfully for describing the retention of U(VI) on montmorillonite (Tournassat et al., 2018). However, this research is still in progress and this type of model cannot yet be used in this work due to the limitation of thermodynamic data available for the other clay minerals.

An alternative approach is to ignore the electrostatic parameter and use Non-electrostatic surface complexation models (references in Parks, 1990; Bradbury and Baeyens, 1997, 2005c; Marques Fernandes et al., 2008, 2012; Poinssot et al., 1999; Turner et al., 1996). In clay mineral systems, non-electrostatic models were originally developed for Zn/Ni-montmorillonite systems as the electrostatic term was not required for describing titration experiments. Such models have been widely used by Bradbury and Baeyens (1997, 2000, 2005, 2009) for different metal cations and radionuclides in clay systems. In 1997, Bradbury and Baeyens proposed a non-electrostatic model approach and they defined two protolysis sites (protonation/deprotonation sites) to describe the surface reactivity as a

function of the pH for 2:1 clay minerals. Besides the protolysis sites, an additional strong surface site of low capacity had also to be defined to describe the surface complexation of metal ions. Moreover, cation-exchange processes were also required to describe the sorption behaviour mainly at low pH, high equilibrium metal concentration or low ionic strength. This model approach is called the 2 Sites Protolysis Non-Electrostatic Surface Complexation and Cation Exchange (2SPNE SC/CE) sorption model. Since the development of this model, numerous parameters have been obtained for several elements (e.g. Eu, Th, U). In 2005 and 2009, Bradbury and Baeyens demonstrated a linear free energy relationship (LFER model) between the equilibrium constant of the surface complexation and the hydrolysis stability constants for different cations for the strong sites of the surface of montmorillonite (Bradbury and Baeyens, 2005c) and illite (Bradbury and Baeyens, 2009a). The combination of the non-electrostatic surface models and the LFER allows the prediction of all cations' adsorption on most clay minerals considering the competitive sorption of co-existing cations as well (Bradbury and Baeyens, 2011; Marques Fernandes et al., 2012).

In this work, we will use the 2SPNE SC/CE model to describe the sorption behaviour of U(VI).

3.1.1.2.2. How to interpolate sorption models on natural samples?

The quantification of adsorption processes in natural systems can be done through two approaches: the component additivity (CA) and the generalised composite (GC) approach (Davis et al., 1998; Waite et al., 2000).

The CA approach, known also as bottom-up approach, attempts to model the sorption processes taking into account all minerals constituting the natural system and assumes that each mineral has unique surface sites with characteristic sorption properties. In this case, the characterisation of the surface of each single mineral is necessary. For practical reasons, this approach requires the simplification of the system in order to consider only the most important interacting phases. However, in some cases, the CA approach can lead to an over simplification of the systems, where the sorption is controlled only by one mineral-phase (NEA, 2005; Payne et al., 2013).

In the semi-empirical model (GC approach), it is assumed that the mechanistic description of surface composition of the mineral assemblage is inherently too complex to evaluate the contributions of individual phases. Instead, generic surface functional groups are assigned to the mineral mixture, in which the stoichiometry and formation constants for each sorption equilibrium and site capacities are determined by fitting experimental data. The GC approach is merely a fitting rather than a predicting procedure (Davis et al., 1998; Marques Fernandes et al., 2015; Waite et al., 2000). These kind of model approaches have been widely used to predict the behaviour of different cations in different mineral-phases (e.g. Marques Fernandes et al., 2015; Chen et al., 2014).

For clay rock systems, bottom-up approach has been applied considering the 2SPNE SC/CE model. The bottom-up approach was applied successfully on Opalinus clay (Bradbury et al., 2011; Hartmann et al., 2008; Van Loon et al., 2009) for several metals (Ni(II), Co(II), Eu(III), Th(IV) and U(VI)). It was also possible to describe Cs/COx clay (Chen et al., 2014) and Ni/COx clay (Chen et al., 2014a) considering that the clay fraction was characterised as illite and interstratified I/S, where I/S is mixture of illite and montmorillonite as proposed in Tournassat et al., 2009. For the latter case, Chen et al.

(2014a) observed some limitations in the interpolation for natural systems (COx claystone) highlighting the difficulty of generalising the quantitative description of mineral reactivity.

At this stage, and considering the objective of this work, we propose to use the 2SPNE SC/CE model with the bottom-up approach. The simplifications and assumptions correspond to those already published (Tournassat et al., 2009; Bradbury et al., 2011; Chen et al., 2014, 2014a; Marques Fernandes et al., 2015, Jin et al., 2016) and are as follows:

- i. 2:1 clay minerals control the retention; this corresponds to a content of 30–40% in COx formation (mainly composed by illite and interstratified I/S layers).
- ii. I/S mixed layers should be treated as sorption phase separately, although due to a lack of data and sorption models, here, the I/S interstratified layers will be assumed as two phases, where each phase corresponds to 50 % wt of illite and smectite, respectively.
- iii. Montmorillonite will be used as a proxy for smectite phases since it is a well-known and studied smectite.
- iv. The potential contributions of chlorite and kaolinite will not be taken into account on the overall sorption of uranium.

The sorption parameters for both illite and montmorillonite are summarised in Table 18, and the surface complexation reactions and their respective selective coefficients are provided in Table 19. For both clay minerals, the number of surface and exchange sites and their respective mass are detailed in Appendix B.2. The thermodynamic data of the aqueous speciation and solids are included in the Thermochemie database and a summary of the most relevant data is described in Appendix E. Concerning the aqueous Ca-U(VI)-CO₃ ternary complexes, the new thermodynamic data presented in the previous chapter will be used in the geochemical model (Table 14 in Chapter 2). In COx systems, Mg-U(VI)-CO₃ ternary complexes (Lee et al., 2017) were also taken into account in the model.

Table 18. Sorption parameters for U(VI) onto clay minerals of Callovo-Oxfordian formation (Bradbury and Baeys, 1997, 2004).

	Montmorillonite	Illite
CEC (eq/kg)	0.87	0.25
Specific surface area (m ² /g)	39	20
Sites capacities (mol/kg)		
≡S _s OH	2·10 ⁻³	2·10 ⁻³
≡S _{w1,w2} OH	4·10 ⁻²	4·10 ⁻²

Table 19. Cationic exchange and surface complexation reactions used in the sorption model.

	Illite	Montmorillonite
CATIONIC EXCHANGE REACTIONS		log₁₀ K
2XNa + Ca ²⁺ ⇌ X ₂ Ca + 2Na ⁺	1.04	0.61
2XNa + UO ₂ ²⁺ ⇌ X ₂ UO ₂ ²⁺ + 2Na ⁺	0.65 ^{a)}	0.15 ^{b)}
2XNa + Mg ²⁺ ⇌ X ₂ Mg + 2Na ⁺	1.04	0.34
2XNa + Fe ²⁺ ⇌ X ₂ Fe + 2Na ⁺	0.8	0.8
2XNa + Sr ²⁺ ⇌ X ₂ Sr + 2Na ⁺	0.8	1.0
XNa + K ⁺ ⇌ XK + Na ⁺	1.1	0.6
PROTOLYSIS REACTIONS		log₁₀ K

	Illite	Montmorillonite
$\equiv S^sOH + H^+ \rightleftharpoons \equiv S^sOH_2^+$	4.0 ^{a)}	4.5 ^{b)}
$\equiv S^sOH \rightleftharpoons \equiv S^sO^- + H^+$	-6.2 ^{a)}	-7.9 ^{b)}
$\equiv S^{w1}OH + H^+ \rightleftharpoons \equiv S^{w1}OH_2^+$	4.0 ^{a)}	4.5 ^{b)}
$\equiv S^{w1}OH \rightleftharpoons \equiv S^{w1}O^- + H^+$	-6.2 ^{a)}	-7.9 ^{b)}
$\equiv S^{w2}OH + H^+ \rightleftharpoons \equiv S^{w2}OH_2^+$	8.5 ^{a)}	6.0 ^{b)}
$\equiv S^{w2}OH \rightleftharpoons \equiv S^{w2}O^- + H^+$	-10.5 ^{a)}	-10.5 ^{b)}
SURFACE COMPLEXATION REACTIONS		
	log₁₀ K	
Hydrolysis reactions		
$\equiv S^sOH + UO_2^{2+} \rightleftharpoons \equiv S^sOUO_2^+ + H^+$	2.0 ^{a)}	3.1 ^{e)}
$\equiv S^sOH + UO_2^{2+} + H_2O \rightleftharpoons \equiv S^sOUO_2OH + 2H^+$	-3.5 ^{a)}	-3.4 ^{e)}
$\equiv S^sOH + UO_2^{2+} + 2H_2O \rightleftharpoons \equiv S^sOUO_2(OH)_2 + 3H^+$	-10.6 ^{a)}	-11 ^{e)}
$\equiv S^sOH + UO_2^{2+} + 3H_2O \rightleftharpoons \equiv S^sOUO_2(OH)_3 + 4H^+$	-19 ^{a)}	-20.5 ^{e)}
$\equiv S^{w1}OH + UO_2^{2+} \rightleftharpoons \equiv S^{w1}OUO_2^+ + H^+$	0.1 ^{d)}	0.7 ^{e)}
$\equiv S^{w1}OH + UO_2^{2+} + H_2O \rightleftharpoons \equiv S^{w1}OUO_2OH + 2H^+$	-5.3 ^{d)}	-5.7 ^{e)}
Carbonato reactions		
$\equiv S^sOH + UO_2^{2+} + CO_3^{2-} \rightleftharpoons \equiv S^sOUO_2CO_3^- + 2H^+$	unknown	9.8 ^{d)}
$\equiv S^sOH + UO_2^{2+} + 2CO_3^{2-} \rightleftharpoons \equiv S^sOUO_2(CO_3)_2^{3-} + H^+$	unknown	15 ^{d)}
$\equiv S^{w1}OH + UO_2^{2+} + CO_3^{2-} \rightleftharpoons \equiv S^{w1}OUO_2CO_3^- + 2H^+$	unknown	9.3 ^{d)}

- a) Bradbury and Baeyens, 2009
b) Bradbury and Baeyens, 2005b
c) Bradbury and Baeyens, 2005a
d) Marques Fernandes et al., 2012
e) Bradbury and Baeyens, 2011

Based on the 2SPNE SC/CE model (Table 18 and Table 19) and taking the CO_x formation chemical conditions into account (pH = 7.2 and pCO₂ = 10^{-2.1} atm, see Table 2 in Chapter 1), it is interesting to notice that the surface complexation is controlled mainly by the sorption of carbonato complexes of U(VI) on montmorillonite (Table 20) while the corresponding constants for illite are unknown.

Table 20. Distribution of surface complexation reactions of U(VI) on illite and montmorillonite in Callovo-Oxfordian formation system (pH = 7.2 and pCO₂ = 10^{-2.1} atm)

Surface complexation	Illite	Montmorillonite
Hydrolysis reactions	4.1 %	3.1 %
Carbonato reactions	-	91.3 %

The importance of the carbonate complexes on the sorption process was observed on different model phases from hydro(oxides) to different clay minerals and clay rocks. These modelling studies predict that U(VI) adsorption decreases at alkaline pH when carbonate anions are present due to the formation of strong aqueous uranyl-carbonate complexes (Davis et al., 2004). However, the impact of the aqueous carbonate complexes on U(VI) sorption depends on whether these complexes adsorb on the surface of clay minerals. In Marques Fernandes et al. (2012), the authors found necessary to include ternary uranyl-carbonate-surface (U(VI)-CO₃-S) complexation reactions to describe their experimental data on the sorption of U(VI) onto montmorillonite, as a function of different carbonate contents. The formation of such ternary surface complexes was also suggested by Waite et al. (1994) for describing the sorption of U(VI) on ferrihydrite. However, the existence of ternary U(VI)-CO₃ surface complexes has been questioned due to a lack of strong spectroscopic evidences (Tournassat et al., 2018). Tournassat and co-workers (2018) have been developing a model that integrates the

electrostatic correction and have recently suggested that such surface complexes are not necessary to describe U(VI)/montmorillonite systems.

Most studies have focussed on U(VI)/montmorillonite systems whereas only a few works have been reported on the sorption mechanisms of U(VI) on illite (Bradbury et al., 2005c; Gao et al., 2015; Marques Fernandes et al., 2015) and to our knowledge no studies have been published concerning the effect of carbonates on the sorption of U(VI) on illite. Therefore, if carbonate surface complexation on illite surface exists, the only parameter missing in the model is the stability constants of the U(VI)-CO₃ surface complexation reactions, and in case these are needed they will be fitted according to the experimental data.

3.2. Experimental work

The objective of the present work is to apply the bottom-up approach proposed by Bradbury and Baeyens (1997, 2011) on Callovo-Oxfordian formation by following a stepwise approach:

- The first step is to generate experimental data for illite in order to test the model and fit, if necessary, any surface parameters, particularly in the presence of carbonates.
- The second step is to test the model on the CO_x clay fraction, where illite and I/S are the main phases responsible for the retention of radionuclides on CO_x formation.
- The third and final step is to test the model on a “real system” using the CO_x claystone natural samples.

The parameters of interest for solution characterisation are the pH, alkalinity and the initial concentration of calcium. The experimental cases defined in the present study are described in Table 21. As proposed in Chapter 2, for all modelling exercises both the pH and the alkalinity were fixed to those experimentally measured. The pCO₂ was let free accordingly to the pH/alkalinity measured.

Table 21. Description of the experimental cases performed on different phases of Callovo-Oxfordian formation at 20 °C.

Case	Methods	Material	Observations
A	Sorption pH edge experiments in the absence and in the presence of carbonates	Illite	Validate the parameters describing the surface complexation of hydrolysis and carbonate surface species
B	Sorption isotherm experiments in the absence of carbonates	Illite and CO _x clay fraction	Sorption capacity of clay minerals for U-hydrolysis and U-carbonate surface species
C	Sorption isotherms experiments in CO _x porewater conditions	Illite, CO _x clay fraction and claystone	Impact of the formation of Ca-U(VI)-CO ₃ ternary complexes on the adsorption of U(VI) behaviour

The illite used for the U(VI) sorption studies is known as Illite du Puy from the Oligocene geological Formation in Le Puy-en-Velay (Haute-Loire, France). The purification and conversion into the homionic Na form was performed and provided by BRGM (Bureau de Recherches Géologiques et Minières, France).

The claystone sample was collected and provided by Andra in 2008 and corresponds to the borehole sample EST51769 of Callovo-Oxfordian claystone natural sample. The sample was stored in an inert

atmosphere of N₂(g) to avoid oxidation and carbonatation. The claystone is composed of 17 wt% of illite, 28 wt% of I/S, 2 wt% of kaolinite, 3 wt% of chlorite, 25 wt% of calcite and dolomite, 25 wt% of quartz and feldspar and 0.8 wt% of pyrite (personal communication J. C. Robinet).

The Callovo-Oxfordian clay fraction corresponds to the fraction sized below 2µm of the Callovo-Oxfordian claystone (Appendix A.6). The sample was purified and provided by BRGM and is composed by of 37.8 wt% illite and 62.2 wt% of interstratified illite/smectite.

Prior to the sorption experiments, we performed kinetic adsorption tests on COx claystone natural samples and illite to evaluate the time needed to reach steady-state equilibrium (details of the experimental procedure can be found in Appendix A.7.2). The sorption of U(VI) on COx natural sample (Figure 32a) and illite (Figure 32b) was evaluated for 14 days. As can be observed in Figure 6, the sorption of uranium in the COx claystone natural sample in synthetic COx porewater is much lower compared to the illite in ionic media (0.1 M NaCl).

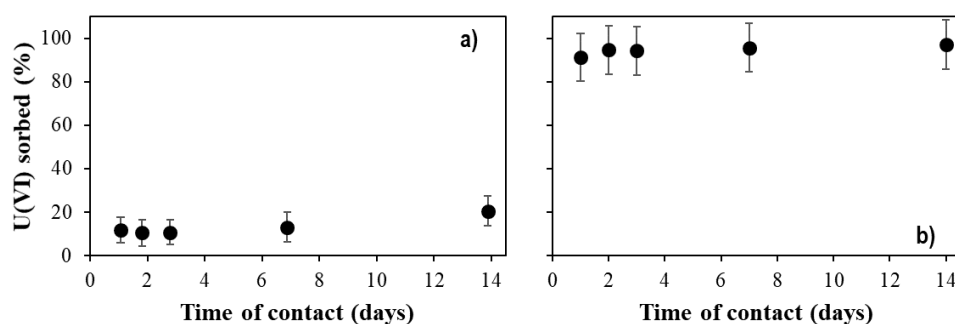


Figure 32. a) Callovo-Oxfordian claystone sample: Sorption of $6.8 (\pm 0.2) \cdot 10^{-7}$ M of U(VI) as a function of time in 1% of CO₂(g), synthetic COx porewater, pH of 7.3 (± 0.1) and S/L of 24 g/L. b) Illite: Sorption of $9.8 (\pm 0.8) \cdot 10^{-8}$ M of U(VI) as a function of time in atmospheric pCO₂, 0.1 M of NaCl, pH 6.3 (± 0.1) and S/L of 0.5 g/L.

For the experiments of sorption of U(VI) under the synthetic Callovo-Oxfordian porewater conditions, after 3 days of contact, we assumed that the steady-state was reached. In the case of illite, the equilibrium appeared to be established after one day of contact. To ensure that steady-state is always reached independently of the chemical conditions, 3 days of contact were considered for both illite and Callovo-Oxfordian claystone sample, as also proposed for other sorption studies (Bradbury et al., 2005a; Bradbury et al., 2009a; Chisholm-Brause et al., 1994; Joseph, 2013; Tournassat et al., 2018).

The experimental conditions for both sorption edge and sorption isotherms are described in Table 22.

Table 22. Summary of the experimental conditions for sorption of uranium in different components of Callovo-Oxfordian formation.

Experimental conditions	Sorption edges			Sorption isotherms			
	Illite		Illite clay fraction	Illite clay fraction	Illite clay fraction	Illite clay fraction claystone	illite
pCO ₂	0%	0.03%	0%	0.03%	1%	1%	5%
pH range	4–10	4–10	7.2	7.3	7.3	7.3	6.6
Ionic strength	0.1 (M)	0.1 (M)	0.1 (M)	0.1 (M)	0.1 (M)	0.1 (M)	0.1 (M)
Background media	NaNO ₃	NaCl	NaNO ₃	NaCl	NaNO ₃	COx pw 3	NaNO ₃
S/L (g/L)	2.0	0.5–1.0	2	2	2	2, 10 and 40	2.0

Experimental conditions	Sorption edges		Sorption isotherms				
	Illite	Illite clay fraction	Illite clay fraction	Illite clay fraction	Illite clay fraction	Illite clay fraction	
Clayey material						Illite clay fraction claystone	illite
[U(VI)] _{initial} (M)	10 ⁻⁷	10 ⁻⁷	10 ⁻⁸ -2·10 ⁻⁵				

3.2.1. Uranium sorption edge and isotherm experiments

We measured the sorption isotherms in concentration for illite, CO_x clay fraction and CO_x claystone natural samples in equilibrium with inert atmosphere-Ar(g), atmospheric pCO₂, 1% of CO₂(g) and 5% of CO₂(g). The pH of the synthetic solutions in equilibrium at the different atmospheres and alkalinity were measured at the end of the experiments. In inert atmosphere, considering the strong influence of carbonate on U(VI) speciation, alkalinity was measured even considering the *a priori* inert conditions. The samples were prepared at solid-liquid ratio of 2, 10 and 40 g/L (clay fraction, illite and claystone, respectively) in 0.1 M of NaNO₃ or synthetic CO_x porewater. For each experiment, a series of blank samples were used to control for uranium sorption/precipitation in tubes and filters, and to control for the alkalinity of the system. The details of the experimental procedure and the material used are described in Appendix A and the experimental results are detailed in Appendix C.5.1.

We carried out sorption edge measurements (initial concentration of U(VI)_{total} ≈ 10⁻⁷ M) as a function of pH in equilibrium with Ar(g) and atmospheric pCO₂ to quantify the influence of carbonates on the sorption of uranyl onto illite. In inert atmosphere, the pH of the system was controlled by adding 0.01 M of HNO₃ or free carbonated NaOH directly to each sample. For the experiments in atmospheric conditions, the pH of each stock solution was equilibrated in atmospheric conditions by overnight agitation (more details of the procedure are provided in Appendix A.7) until the pH of interest was reached. In these experiments, the carbonate content was determined by alkalinity titration measurements. The samples were prepared at solid-liquid ratio of 0.5–1 g/L (depending of the pH of the system) in 0.1 M of NaNO₃ (inert atmosphere) or NaCl (atmospheric pCO₂). For each experiment, a series of blank samples were used to control for uranium sorption/precipitation in tubes and filters and to control for the alkalinity of the system. The details of the experimental procedure and the material used are described in Appendix A and the experimental results are detailed in Appendix C.5.2.

3.3. Sorption of U(VI) on illite

3.3.1. In the absence of carbonate

The sorption of U(VI) takes place mainly on the reactive sites associated to the surface hydroxyl groups (≡SOH) located along the edges of the clay platelets, in which it can protonate and deprotonate, as a function of the pH, and form surface complexes with aqueous uranyl species (Marques Fernandes et al., 2015). In the absence of carbonates, the distribution of the aqueous speciation of the

uranyl (Figure 33a) as a function of pH in 0.1 M of NaNO₃ is controlled only by hydrolysis species, which are the most relevant for the sorption of uranyl (Figure 33b)

As expected, the sorption of uranyl is clearly dependent on the pH of the solution; the K_D increases with increasing pH, reaching a higher K_D of U(VI) at neutral pH conditions (Figure 34). As can be seen in Figure 34, the K_D obtained (open circles) is similar to the one reported by Bradbury et al., 2009b (black squares). Despite the K_D trend being the same and in the same order of magnitude, the K_D obtained in the present work is slightly lower for pH below 6, whereas slightly higher at pH range 6-8. Above pH 8, the results are similar.

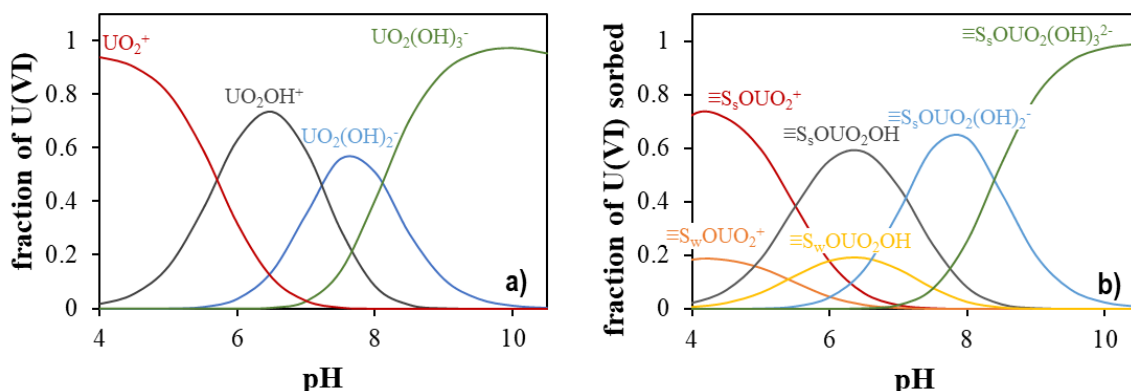


Figure 33. Speciation distribution of the aqueous uranyl species (left) and uranyl hydrolysis surface complexes (right) as function of the pH in the absence of carbonates at 0.1 M of NaNO₃ in contact with illite with S/L of 2 g/L and U(VI)_{initial} of $1.1(\pm 0.05) \cdot 10^{-7}$ M.

In the present work, using the surface complexation reactions of hydrolysis species in both strong and weak sites (Table 19), the sorption model (black solid line) reproduces relatively well the experimental curve increase.

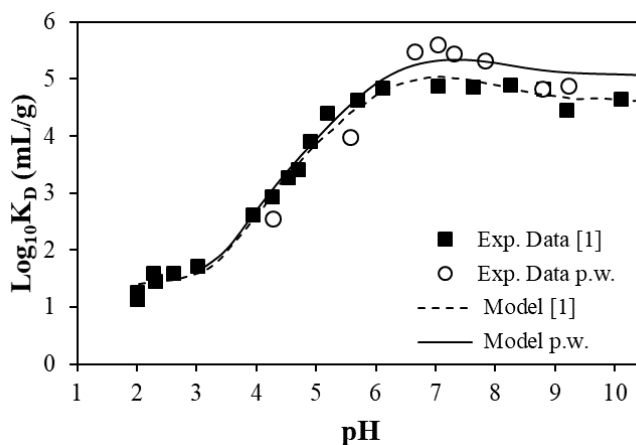


Figure 34. Comparison of the sorption edges of U(VI) on Na-illite in the absence of carbonates between present work (p.w.): present work (0.1 M of NaNO₃, S/L of 2 g/L and U(VI)_{initial} of $1.1(\pm 0.05) \cdot 10^{-7}$ M) and [1] Bradbury and Baeyens (2009) (0.1 M of NaClO₄, S/L 2.6 g/L and U(VI)_{initial} of 10^{-7} M).

The results of the sorption isotherms as a function of U(VI) concentration at constant pH are shown in Figure 35. The sorption of U(VI) onto illite in the absence of carbonates follows a linear isotherm with an increase of U(VI) sorption when U(VI) increases in solution. The measured pH of equilibrium was 6.4 and the alkalinity was $7 \cdot 10^{-5}$ eq/L (indicating negligible contamination of CO₂(g)).

When comparing the sorption isotherms of the present work (black circles, Figure 36) with the data reported by Bradbury and Baeyens (2005) (blue open squares, Figure 36), and despite the different pH at equilibrium, both experimental data (dots) and model approaches (solid lines) are in agreement. The model approach of this work (black solid line) not only reproduces the present experimental data but also the experimental data reported by Bradbury and Baeyens (2005).

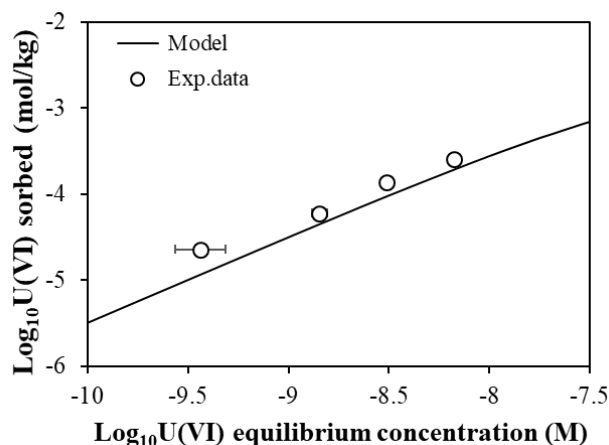


Figure 35. Sorption isotherm of U(VI) onto Na-illite in the absence of carbonates in Ar(g) atmosphere at 0.1 M of NaNO₃, S/L of 2 g/L and pH of 6.4.

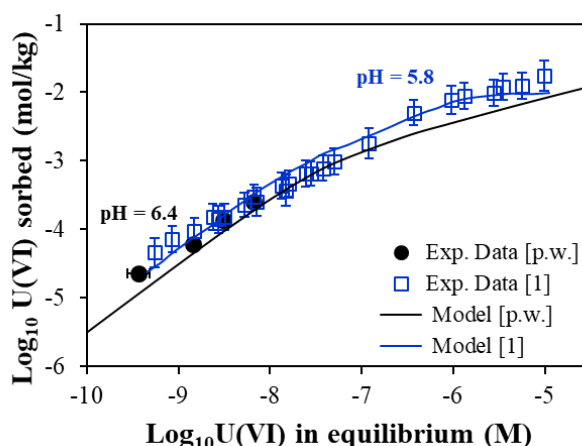


Figure 36. Sorption isotherms of U(VI) on Na-illite in the absence of carbonates between present work (0.1 M of NaNO₃ in S/L of 2 g/L and pH of 6.4) and work of Bradbury and Baeyens (2005a) (0.1 M of NaClO₄, S/L 2.6 g/L and pH of 5.8).

3.3.2. In the presence of carbonate

In the presence of carbonates, the sorption of U(VI) onto illite is clearly affected at pH > 6 in comparison with the data obtained in the absence of carbonates (Figure 37). The titration measurements of the alkalinity in the stock solutions and pH measured before and after the equilibrium with illite are shown further in Table 23.

The sorption edge experiments in the presence of carbonates in equilibrium with pCO₂ atmospheric (blue circles) indicate that the maximum K_D of U(VI) is reached at pH 6.5, one order of magnitude lower to the K_D observed in the absence of carbonates (open circles, Figure 37). Furthermore,

whereas the K_D is nearly constant at $\text{pH} > 7$ in the absence of carbonates a strong decrease is observed in the presence of carbonates.

In the present work, the model approach considers: a) the surface reactions for illite described in Table 19, where the carbonate surface complexation reactions are not considered (due to lack of data); b) the alkalinity measurements performed in the beginning of the experiments; and c) the pH measurements of the equilibrium. Here, it was assumed that alkalinity does not change significantly after the equilibrium, i.e. the alkalinity is constant.

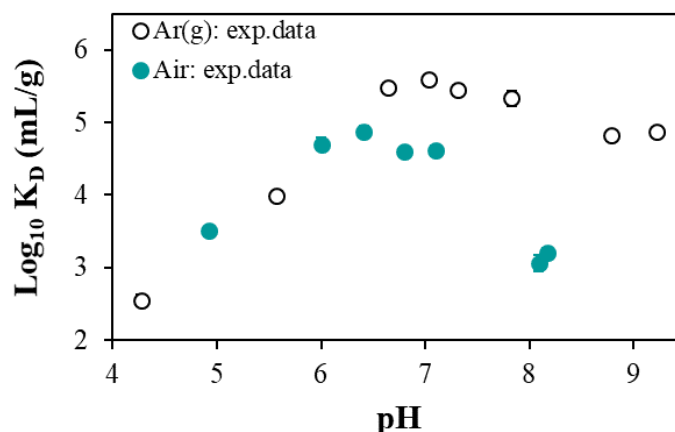


Figure 37. Sorption edges of U(VI) on illite in 0.1 M of NaNO_3 , S/L of 2 g/L and $\text{U(VI)}_{\text{initial}}$ of $1.1(\pm 0.1) \cdot 10^{-7}$ M, in the absence (open circles) and presence (blue circles) of carbonates in equilibrium with atmospheric CO_2 .

Table 23. Alkalinity and pH measurements before and after the equilibrium with illite. pCO_2 calculated from the equilibrium pH/alkalinity.

Alkalinity (meq/L)	$\text{pH}_{\text{initial}}$	pH_{final}	pCO_2 calculated ⁱ
0	3.9	4.9	
0.036 (± 0.02)	6.1	6.0	-2.58; -3.10
		6.4	-3.0; -3.53
0.1 (± 0.05)	7.2	6.8	-2.96; -3.44
		7.1	-3.26; -3.74
0.96 (± 0.5)	8.0	8.1	-3.27; -3.78
		8.2	-3.36; -3.86

As shown in Figure 38, the presence of carbonates strongly affects the speciation of uranyl in solution. This effect is more pronounced at high pH, as shown in Figure 38a while at pH 6, the speciation of U(VI) is controlled by uranium-carbonate aqueous species. In conclusion, we can assume that there is a competition for U(VI) between its complexation in surface and in solution (Figure 38b).

ⁱ Calculations in Phreeqc from the equilibrium between pH measured at the end of the experiments; maximum and minimum considering the uncertainty of the alkalinity measurements

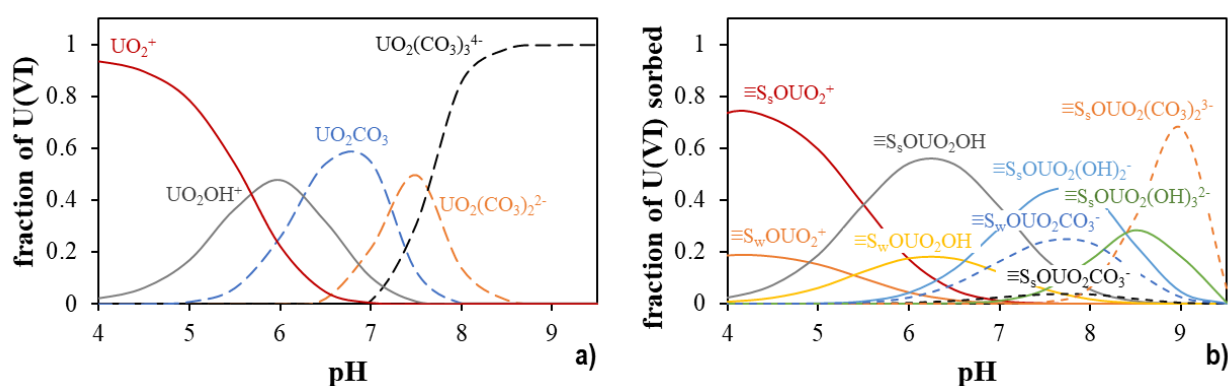


Figure 38. Speciation distribution of the aqueous uranyl species (left) and uranyl hydrolysis and carbonate surface complexes (right) as function of the pH in the absence of carbonates at 0.1 M.

The modelling results indicate that it is possible to reproduce relatively well the experimental sorption results of U(VI) at neutral pH (see further Figure 39a). In more acidic conditions (pH \approx 5), as already observed in the absence of carbonates, the model slightly overestimates the sorption of U(VI) on illite. On the other hand, in more alkaline conditions (pH \approx 8.1), the model underestimates the sorption behaviour of U(VI).

We can observe by evaluating the $p\text{CO}_2$, for these experiments (calculated based on the relation pH/alkalinity), that it is not always as expected ($p\text{CO}_2$ atmospheric = $10^{-3.5}$ atm). As shown in Table 23, the calculated $p\text{CO}_2$ is slightly higher at pH $<$ 7 than $p\text{CO}_2$ atmospheric, affecting the calculations. However, the model that considers equilibrium with atmospheric $p\text{CO}_2$ can reproduce well the data, indicating that we are not so far from the “theoretical” water/gas equilibrium.

Since it is not possible to reproduce the experimental data at pH $>$ 7, these results raise the question of whether to use or not the uranyl-carbonate surface complexation reactions. Since there is no thermodynamic data relative to the uranyl-carbonate surface complexations reaction onto illite, as a first approach, we considered the same data as for montmorillonite (see Table 19), assuming that both minerals have similar reactivity.

The results of the model approach are shown in Figure 39b. The agreement between the model and the experimental data below pH 7 is relatively good. When the pH is above 7 and the uranyl carbonate species are the major aqueous species in solution, even considering the thermodynamic constants in the U(VI)- CO_3 surface reactions as the ones for montmorillonite, the model still underestimates the sorption of U(VI) onto illite (Model I).

These results led us to question the reliability of the values of the surface reaction constants for uranyl carbonates proposed for montmorillonite on the surface edges of illite. Thus, we proposed a second approach by changing the stability constants of the uranyl carbonate surface reactions. The number of variables implicated in this approach must be restricted to avoid high uncertainty. For this reason, only one stability constant has been selected, i.e. that associated to the predominant complex in the experimental conditions of this work, $\equiv\text{S}^{\text{s}}\text{OUO}_2(\text{CO}_3)_2^{3-}$. The fitting of the stability constants was done manually, and its best fit was found to be $\log_{10} K = 17.5 \pm 0.5$ (Figure 39c). In the following calculations, the uncertainty of this constant will be considered in the prediction approach.

The $\equiv\text{S}^{\text{s,w}}\text{OUO}_2\text{CO}_3^-$ reactions were also evaluated on their ability to influence the sorption behaviour of U(VI) in the presence of carbonates. For that, $\text{Log}_{10}K$ of $\text{S}^{\text{s}}\text{OUO}_2\text{CO}_3^-$ and $\text{S}^{\text{w}}\text{OUO}_2\text{CO}_3^-$ was

defined from the montmorillonite as 9.8 and 9.3, respectively. In Figure 39d, we show the impact of considering or not these two additional reactions in the model approach. In Model 0 neither $\equiv\text{S}^{\text{s}}\text{OUO}_2(\text{CO}_3)_2^{3-}$ nor $\equiv\text{S}^{\text{s,w}}\text{OUO}_2\text{CO}_3^-$ are considered; in Model II only $\equiv\text{S}^{\text{s}}\text{OUO}_2(\text{CO}_3)_2^{3-}$ with $\log_{10} K = 17.5 (\pm 0.5)$ is considered and in Model III the $\equiv\text{S}^{\text{s}}\text{OUO}_2(\text{CO}_3)_2^{3-}$, the $\equiv\text{S}^{\text{s}}\text{OUO}_2\text{CO}_3^-$ and $\equiv\text{S}^{\text{w}}\text{OUO}_2\text{CO}_3^-$ are considered, with $\log_{10} K$ of 17.5, 9.8 and 9.3 respectively. We can observe that the presence of $\equiv\text{S}^{\text{s,w}}\text{OUO}_2\text{CO}_3^-$ does not affect the sorption of U(VI) on illite as a function of pH, indicating that $\equiv\text{S}^{\text{s}}\text{OUO}_2(\text{CO}_3)_2^{3-}$ plays the major role on the sorption of U(VI) at high pH.

Next, we evaluated the reliability of the stability constants of $\equiv\text{S}^{\text{s}}\text{OUO}_2(\text{CO}_3)_2^{3-}$ based on sorption isotherms of U(VI) at different ranges of pCO_2 . Despite the fact that $\equiv\text{S}^{\text{s,w}}\text{OUO}_2\text{CO}_3^-$ does not have a role on the sorption behaviour of U(VI) on illite, as a function of pH in equilibrium with atmospheric pCO_2 , it may have an impact on the sorption of U(VI) at higher concentrations of carbonate in solution. In this case, it will also be evaluated whether it should or not be included in the model. The model approach will follow Model III as shown in Figure 39d and Table 24.

Table 24. Uranyl carbonate surface complexation reactions proposed for illite in Model III.

Carbonato surface complexation reactions	$\log_{10} K$
$\equiv\text{S}^{\text{s}}\text{OH} + \text{UO}_2^{2+} + \text{CO}_3^{2-} \rightleftharpoons \equiv\text{S}^{\text{s}}\text{OUO}_2\text{CO}_3 + 2\text{H}^+$	9.8 ⁱ
$\equiv\text{S}^{\text{s}}\text{OH} + \text{UO}_2^{2+} + 2\text{CO}_3^{2-} \rightleftharpoons \equiv\text{S}^{\text{s}}\text{OUO}_2(\text{CO}_3)_2^{3-} + \text{H}^+$	17.5 (± 0.5)
$\equiv\text{S}^{\text{w1}}\text{OH} + \text{UO}_2^{2+} + \text{CO}_3^{2-} \rightleftharpoons \equiv\text{S}^{\text{w1}}\text{OUO}_2\text{CO}_3 + 2\text{H}^+$	9.3 ⁶

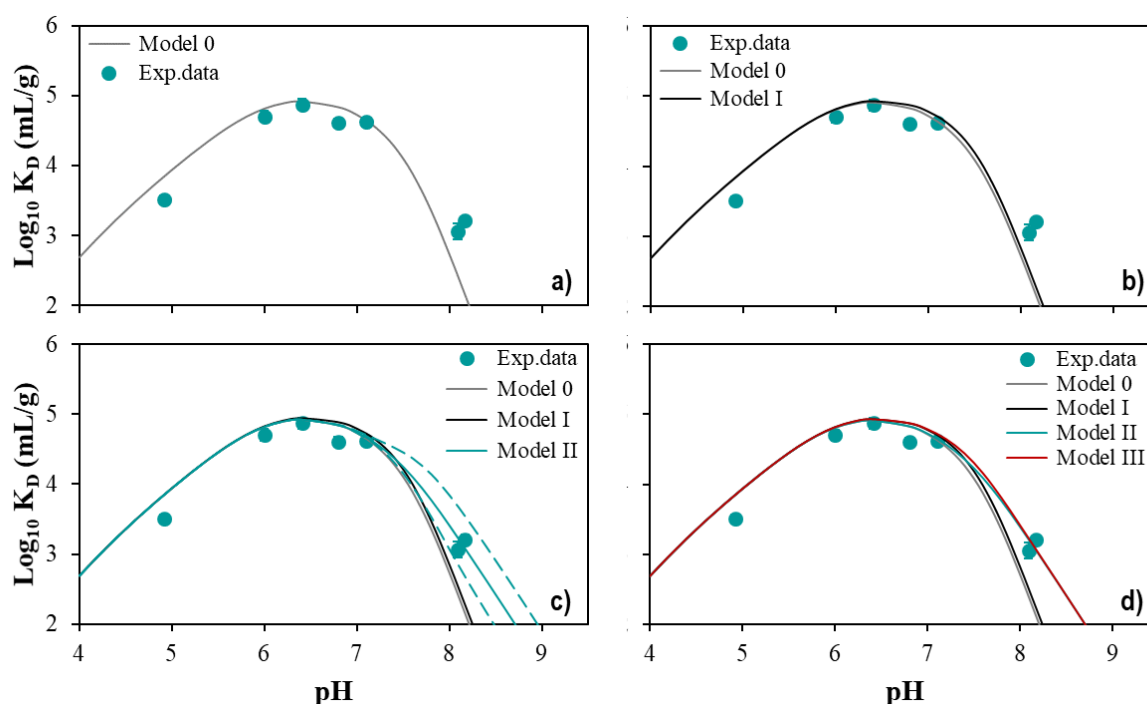


Figure 39. Model approach on sorption edge of U(VI) on illite. Model 0: neither $\equiv\text{S}^{\text{s}}\text{OUO}_2(\text{CO}_3)_2^{3-}$ or $\equiv\text{S}^{\text{s,w}}\text{OUO}_2\text{CO}_3^-$ are considered; **Model I:** considering the logK from Montmorillonite; **Model II:** only $\equiv\text{S}^{\text{s}}\text{OUO}_2(\text{CO}_3)_2^{3-}$ with $\log_{10} K = 17.5 (\pm 0.5)$ is considered; and **Model III:** the $\equiv\text{S}^{\text{s}}\text{OUO}_2(\text{CO}_3)_2^{3-}$, the $\equiv\text{S}^{\text{s}}\text{OUO}_2\text{CO}_3^-$ and $\equiv\text{S}^{\text{w}}\text{OUO}_2\text{CO}_3^-$ are considered, with $\log_{10} K$ of 17.5, 9.8 and 9.3, respectively. Error bars that are not visible are smaller than the symbol size.

ⁱ From Marques Fernandes et al. (2012)

Sorption isotherms experiments performed in presence of different concentration of carbonates (atmospheric conditions and 1% and 5% of $\text{CO}_2(\text{g})$) were used to evaluate the influence of the $\equiv\text{S}^{\text{s,w}}\text{OUO}_2\text{CO}_3^-$ complexes. The results of the sorption isotherms of U(VI) in equilibrium with pCO_2 atmospheric are shown in Figure 40. The sorption of U(VI) onto illite does not seem significantly affected when the carbonates are added to the system at $< 10^{-8}$ M of U(VI) in equilibrium in a solution with pH 7.3. However, the experiments performed in the absence of carbonates are not completely free of carbonates. Besides the low contamination observed in the latest experiments, the concentration of carbonates ($7 \cdot 10^{-5}$ eq/L) is relatively close to the one measured in atmospheric pCO_2 (alkalinity of $2 \cdot 10^{-4}$ eq/L of carbonates). The same issue was also observed on the experiments performed on montmorillonite reported by Tournassat et al., (2018).

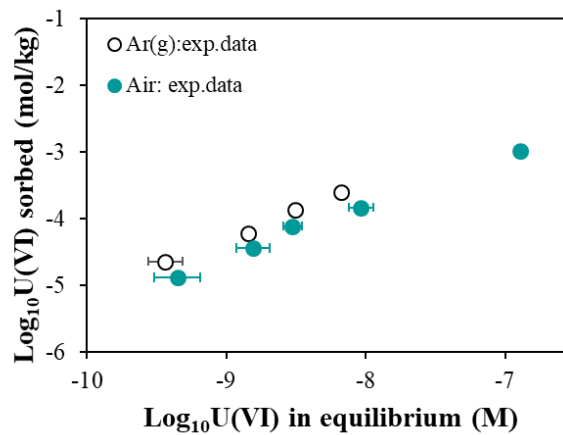


Figure 40. Sorption isotherms of U(VI) onto illite in the absence of carbonates (○) at equilibrium pH of 6.4 in 0.1 M of NaCl and presence of carbonates in equilibrium with atmospheric pCO_2 (●) at equilibrium pH of 7.3 in 0.1 M of NaNO_3 . Error bars that are not visible are smaller than the symbol size.

The model approach, using the stability constants of the carbonate surface complexation reactions proposed in this work for illite (see Table 24), reproduces well the experimental sorption of U(VI) in the presence of carbonates (atmospheric pCO_2) (Figure 41b), whereas considering only one uranyl carbonate surface complexation ($\equiv\text{S}^{\text{s}}\text{OUO}_2(\text{CO}_3)_2^{3-}$) to control the sorption of U(VI)- CO_3 complexes slightly underestimates the sorption of U(VI) (Figure 41a).

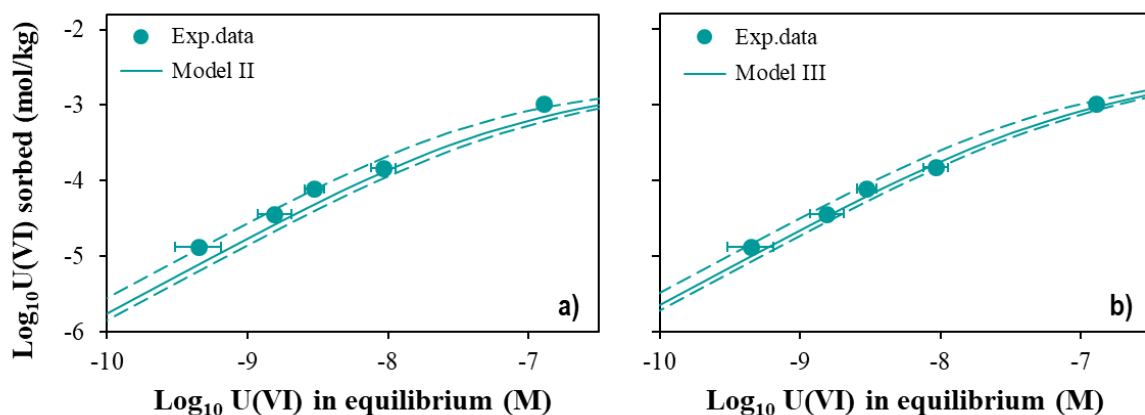


Figure 41. Prediction model of sorption of U(VI) onto illite in equilibrium with pCO_2 atmospheric in 0.1 M of NaNO_3 at pH 7.3. a) Model II: only $\equiv\text{S}^{\text{s}}\text{OUO}_2(\text{CO}_3)_2^{3-}$ is considered; b) Model III: U(VI)- CO_3 surface complexation reactions from Table 24. Error bars that are not visible are smaller than the symbol size.

Both model approaches, considering the uncertainty of the stability constants, can reproduce the behaviour of U(VI) in illite in equilibrium with pCO₂ atmospheric. However, it is difficult to define a selection criteria for the best model approach to describe the behaviour of U(VI) in the presence of low concentration of carbonates.

Finally, we performed two complementary sorption isotherms at partial pressure of 1% and 5% of CO₂(g). The final pH and alkalinity for each experiment are shown in Table 25. The results show that in the presence of higher concentrations of carbonates in solution the sorption of U(VI) on illite slightly decreases (comparison between air and 1%–5% of CO₂(g)). However, the behaviour of uranyl does not seem to be affected significantly by changing the conditions from 1 to 5% of CO₂(g), even when the pH decreases (Figure 42). The pH decrease observed does not affect the U(VI) sorption, which means that the U(VI) behaviour is not only controlled by the U(VI)-CO₃ aqueous species. These results clarify the importance of considering also the sorption mechanisms of the U-CO₃ ternary surface complexes on illite.

Table 25. pH and alkalinity measurements after equilibrium with pCO₂ atmospheric, 1% and 5% CO₂(g)

CO ₂ (g)	Measured pH	Measured Alkalinity meq/L
Air	7.3 (± 0.09)	0.24 (± 0.09)
1%	7.3 (± 0.08)	2.5 (± 0.1)
5%	6.6 (± 0.01)	2.3 (± 0.1)

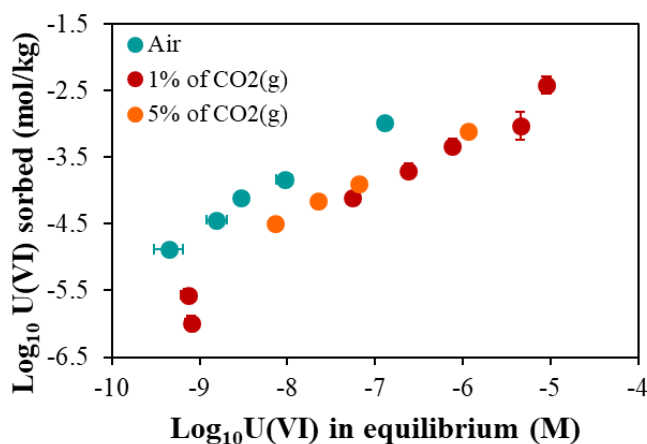


Figure 42. Sorption isotherms of U(VI) onto illite in the presence of carbonates in equilibrium with atmospheric pCO₂, 1% and 5% of CO₂(g) in 0.1 NaNO₃, pH fixed at 7.3 (● and ●), and 6.6 (●), respectively. Error bars that are not visible are smaller than the symbol size.

The prediction model was used to quantitatively describe U(VI) sorption on illite in the presence of carbonates in equilibrium with 1% and 5% of CO₂(g) (Figure 43). As shown previously, Model II considers only one carbonate surface complexation reaction (Figure 43a,b), whereas Model III considers the three reactions (as for montmorillonite) (Figure 43c,d). Both models take into account the fitted stability constant for the $\equiv S^{\circ}OUO_2(CO_3)_2^{3-}$ and its respective uncertainties.

The results from the model indicate that both approaches might be suitable to explain the sorption of U(VI) in the presence of higher concentration of carbonates in solution. Nevertheless, if we look in more detail Model II might be a better approach than Model III, in which all constants for carbonate surface complexes are considered. Model II reproduces better the sorption of U(VI) at higher

concentrations of U(VI) as shown when seeing the results in 5% of CO₂(g) (Figure 43c and d). Considering this, different experiments (*e.g.* changing the range of concentration of carbonates in the system) should be done to ensure the reliability of such surface species in the fitting of the parameters when in presence of a large experimental dataset. Alternatively, one could perform surface spectroscopic analysis to validate the existence of the U(VI)-CO₃ surface complexes. However, this is not the subject of the present work. In order to simplify and decrease the number of uncertainties, Model II will be chosen for the following work, in which only one carbonate surface complexation ($\equiv\text{S}^{\text{O}}\text{UO}_2(\text{CO}_3)_2^{3-}$) will be considered in the illite phase model.

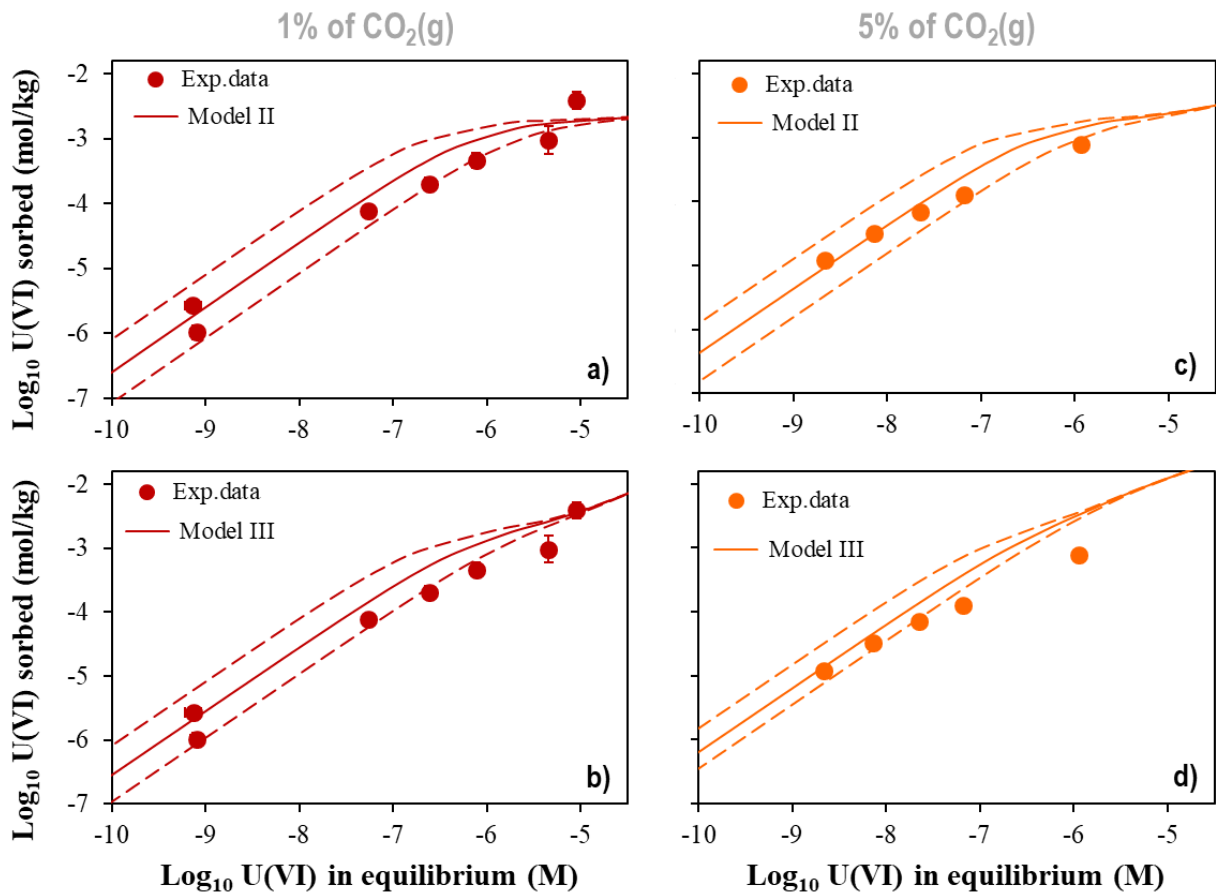


Figure 43. Model approach for the sorption isotherms of U(VI) onto illite in 0.1 M of NaNO₃, S/L of 2 g/L at pH 7.3 in equilibrium with 1% of CO₂(g) (left top and bottom) and pH 6.6 in equilibrium with 5% of CO₂(g) (right top and bottom). Model II: only $\equiv\text{S}^{\text{O}}\text{UO}_2(\text{CO}_3)_2^{3-}$ is considered; Model III: U(VI)-CO₃ surface complexation reactions from Table 24. Error bars that are not visible are smaller than the symbol size.

3.3.3. Impact of the presence of Ca-U(VI)-CO₃

We next studied the impact of the formation of calcium-uranyl-carbonate ternary complexes on the sorption of U(VI) onto illite. The experimental conditions were set as closely as possible to the ones that characterize Callovo-Oxfordian formation at 20°C in equilibrium with 1% of CO₂(g) (see synthetic CO_x porewater composition in Table C. 7). Due to the possible decrease of K_D of U(VI) onto illite, expected from the formation of stable Ca-U(VI)-CO₃ species in solution, the solid-liquid ratio was adjusted to 10 g/L to better quantify the concentration of adsorbed U(VI). The pH and

alkalinity at equilibrium were measured at $7.1 (\pm 0.02)$ and $2.5 (\pm 0.1)$ meq/L, respectively. The results of the sorption isotherm of U(VI) indeed show that the formation of Ca-U(VI)-CO₃ complexes does not favour the sorption of U(VI) (Figure 44) as compared to when we performed the experiment at 1% of CO₂ (g) in the absence of Ca.

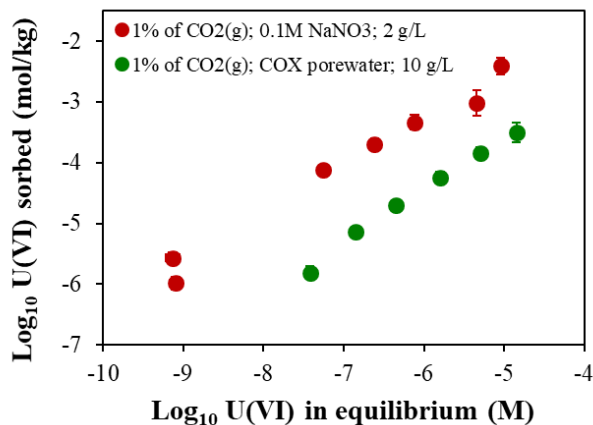


Figure 44. Sorption isotherms of U(VI) on illite in the presence of 1% of CO₂(g) under 0.1 M NaNO₃ at pH 7.3 and synthetic COx porewater at pH 7.1. Error bars that are not visible are smaller than the symbol size.

The results of the model considering the U(VI)-CO₃ surface complexation reactions given in Table 24 and the parameters of the Ca-U(VI)-CO₃ complexes proposed in the present work (Table 14 in Chapter 2) are shown in Figure 45. The model II can reproduce well the uptake of U(VI) onto illite in the presence of Ca-U(VI)-CO₃ ternary complexes.

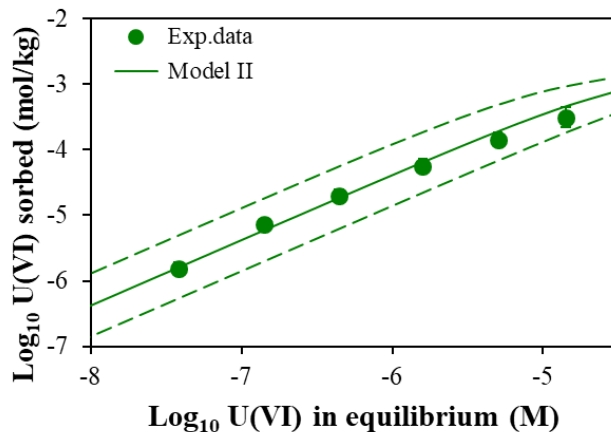


Figure 45. Sorption isotherms of U(VI) on illite as a function of the U(VI) in COx porewater in equilibrium with 1% of CO₂(g). Model II: only $\equiv S^sOUO_2(CO_3)_2^{3-}$ is considered taking also in account the thermodynamic data for Ca-U(VI)-CO₃ ternary complexes (see Chapter 2). Error bars that are not visible are smaller than the symbol size.

In summary, the presence of carbonates in solution influences the sorption of U(VI) onto illite, in which a sorption decrease is observed due to the formation of U(VI)-CO₃ aqueous species. However, the surface complexation reactions for U(VI)-CO₃ complexes must be included in the model to quantitatively explain the experimental data. The stability constants of the main surface complex ($\equiv S_sOUO_2(CO_3)_2^{3-}$) were therefore fitted from the sorption edge experimental data, in which we obtained the proposed value of $\log_{10} K = 17.5 \pm 0.5$. With this new stability constant, it was then possible to predict the behaviour of U(VI) at $pH \approx 7$ for a wide range of pCO_2 (atmospheric conditions,

1% and 5% of CO₂(g)) and in the “COx conditions” (1% of CO₂(g) in the presence of calcium in solution).

The next step is to assess whether Model II, together with the one proposed for montmorillonite (Table 3), can predict the sorption data on the COx clay fraction.

3.4. Sorption of U(VI) on Callovo-Oxfordian clay fraction

The clay fraction of Callovo-Oxfordian claystone is composed mainly by illite and interstratified I/S. Kaolinite or chlorite may be present but will be considered negligible. As a reminder, in the present study both illite and montmorillonite are considered as model phases for the modelling and I/S corresponds to a mixture of illite and smectite. In this study we evaluated the retention of U(VI) in the absence of carbonates, in the presence of carbonates in equilibrium with 1% of CO₂, and under Callovo-Oxfordian conditions, i.e. in the presence of the Ca-U(VI)-CO₃ ternary complexes in solution. We only measured the sorption isotherms in concentration at the pH values relevant to the Callovo-Oxfordian formation.

3.4.1. In the absence of carbonate

The sorption isotherm of U(VI) for COx clay fraction in the absence of carbonates is shown further in Figure 46a. The pH of equilibrium was 7.0 (± 0.2) and the alkalinity was found to be 0.2 (± 0.09) meq/L, almost 70 % higher than that measured in the illite system. From Figure 46a we can also compare the sorption of U(VI) on illite and clay fraction in the absence of carbonates. The trends are similar, although with a weaker retention for COx clay fraction than illite in the conditions studied, in concentrations of U(VI) below 10⁻⁸ M.

Independently of the possible contamination of carbonates, the model cannot completely reproduce the data as it overestimates the retention for the lowest concentrations of U(VI). However, there is a relatively good agreement between the calculation and the experimental data for the highest concentrations. The sorption experiment using clay fraction in the absence of carbonates was performed only once, and for this reason we do not have any possible explanation for such difference. Nevertheless, we decided to evaluate the model in the most realistic conditions possible, which, in this particular case, meant that the U(VI) behaviour is also governed by the presence of carbonates.

3.4.2. In the presence of carbonate

We next measured the sorption isotherms in concentration on clay fraction in the presence of carbonates in equilibrium with 1% of CO₂(g). The pH of equilibrium was 7.2 (± 0.01) and the alkalinity was 2.4 (± 0.9) meq/L. Comparing the results obtained for illite and clay fraction, no significant differences were observed between these two phases (Figure 46b).

The model approach, using the parameters given in Table 19 and Table 24, can reproduce well the U(VI) sorption on the clay fraction (Figure 46b red dash-line). The model results indicate that considering illite and montmorillonite to describe the interstratified I/S is a reliable approach.

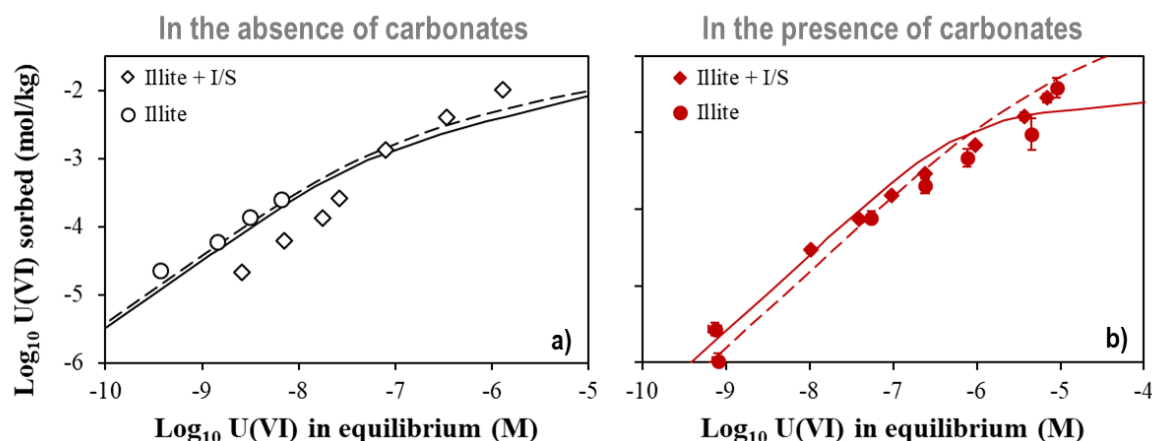


Figure 46. a) Sorption isotherm of U(VI) onto (○) illite and (◇) Callovo-Oxfordian clay fraction (illite + I/S) in the absence of carbonates in both 2 g/L under 0.1 M NaNO_3 at pH of 6.4 and 7.0 (respectively). b) Sorption isotherm of U(VI) onto (●) illite and (◆) Callovo-Oxfordian clay fraction (illite + I/S) in the presence of carbonates in equilibrium with 1% of $\text{CO}_2(\text{g})$ in both 2 g/L under 0.1 M NaNO_3 at pH of 7.3 and 7.2 (respectively). Model approach for illite (solid-line) and for COx clay fraction (dash-line). Error bars that are not visible are smaller than the symbol size.

3.4.3. Impact of the presence of Ca-U(VI)- CO_3

We performed the sorption experiments of U(VI) onto COx clay fraction in equilibrium with synthetic COx porewater that we previously prepared (see Appendix A.5 and Table C. 7.). In the presence of carbonates and calcium in the system, the sorption isotherm of U(VI) was measured at a pH of 7.1 (± 0.02) and alkalinity of 2.4 (± 0.9) meq/L. In Figure 47a, we can compare these results with those measured in the absence of Ca in equilibrium with 1% of $\text{CO}_2(\text{g})$. The formation of Ca-U(VI)- CO_3 promotes, as observed also in the illite system, a higher decrease of U(VI) sorption when comparing the experimental data where only U(VI)- CO_3 complexes are formed. As observed in the absence of calcium in the system, the sorption behaviour of U(VI) does not change comparatively either in illite or in the clay fraction (illite + I/S) (symbols in Figure 47b).

The proposed model approach, considering the surface parameters both on illite (Model II) and montmorillonite can reproduce well the behaviour of U(VI) in Callovo-Oxfordian conditions (green dashed-lines Figure 47b).

So far, we have shown that the model works in conditions relevant to the Callovo-Oxfordian conditions, *i.e.* in the presence of carbonates and Ca at $\text{pH} \approx 7$. We have also shown that using illite and montmorillonite as model phases to assume the I/S interstratified layers are useful to model the COx clay fraction. However, the agreement is not perfect since the model could not predict well the experiments performed in “inert” conditions. Considering the objectives of this work, we decided not to focus on this point and to follow the objective of understanding the U(VI) behaviour in natural systems, *i.e.* closest to real conditions, and assess the reliability of the third important assumption, which is interpolating the model used to the Callovo-Oxfordian claystone natural samples.

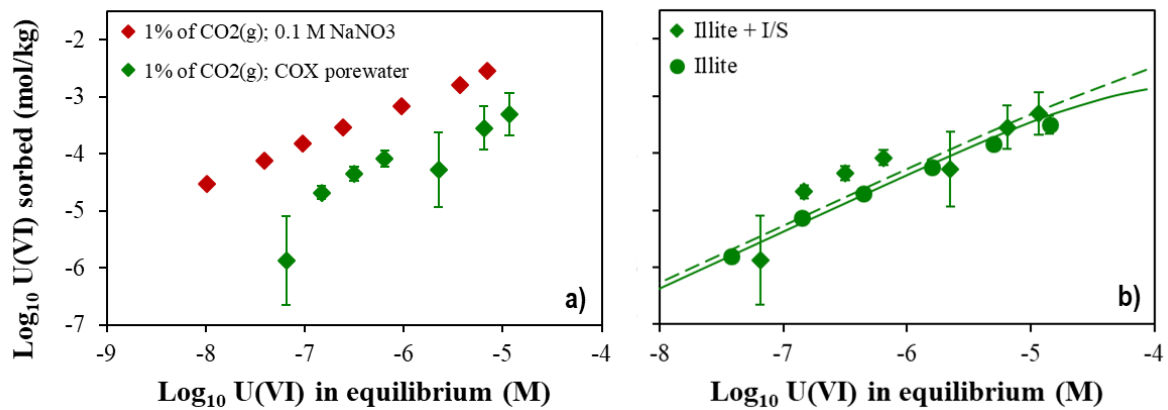


Figure 47. a) Sorption isotherms of U(VI) on 2 g/L of COx clay fraction (illite + I/S) in equilibrium with 1% of CO₂(g) in 0.1 M of NaNO₃ (♦) and synthetic COx porewater (◆). b) Sorption isotherm of U(VI) on (●) 10 g/L of illite and (◆) on 2 g/L of COx clay fraction (illite + I/S) in equilibrium with 1% of CO₂(g) in synthetic COx porewater conditions. Model approach for illite (solid-line) and for COx clay fraction (dash-line). Error bars that are not visible are smaller than the symbol size.

3.5. Sorption of U(VI) on Callovo-Oxfordian claystone

The COx claystone (as natural sample), as mentioned previously, is composed mainly of clay minerals (illite and interstratified I/S layers), carbonates (calcite) and quartz. The sorption isotherm of U(VI) on natural samples was performed in equilibrium with a synthetic COx porewater. This porewater was prepared as closely as possible to the composition of the *in situ* groundwater in the presence of 1% CO₂(g) (see Appendix A.5 and Table C. 7). Due to the possible decrease of U(VI) distribution coefficient on natural samples, expected from the formation of Ca-U(VI)-CO₃ in solution, the solid-liquid ratio was adjusted to 40 g/L to better quantify the concentration of U(VI) adsorbed. The pH of equilibrium was 7.5 ± 0.1 and the alkalinity was 3.3 ± 0.6 meq/L.

The results of the sorption isotherm of U(VI) in COx natural samples are shown in Figure 48 (white-squares). In comparison with the previous results (illite and clay fraction, see above Figure 47b), there is a significant decrease of U(VI) sorption when natural samples of COx formation are considered. This is coherent with the assumption that only the clay fraction is responsible for the retention, since it represents 45 wt% of the COx natural sample and Ca-U(VI)-CO₃ aqueous complexes are present.

The results of the model approach considering the surface reactions for illite and montmorillonite and the thermodynamic data for Ca-U(VI)-CO₃ provided in Table 14 (see Chapter 2) are shown in Figure 49. The model approach reproduces well the experimental data in Callovo-Oxfordian conditions which lie within the uncertainties of the prediction model associated to the surface complexation reaction of $\equiv S_sOUO_2(CO_3)_2^{3-}$ species.

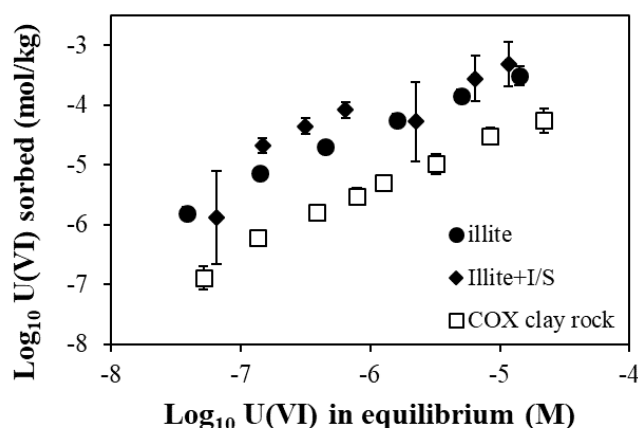


Figure 48. Sorption isotherm of U(VI) onto (●) illite and (◆) COx clay fraction (illite + I/S) and (□) Callovo-Oxfordian clays sample in equilibrium with 1% of CO₂(g) in synthetic COx porewater conditions. Error bars that are not visible are smaller than the symbol size.

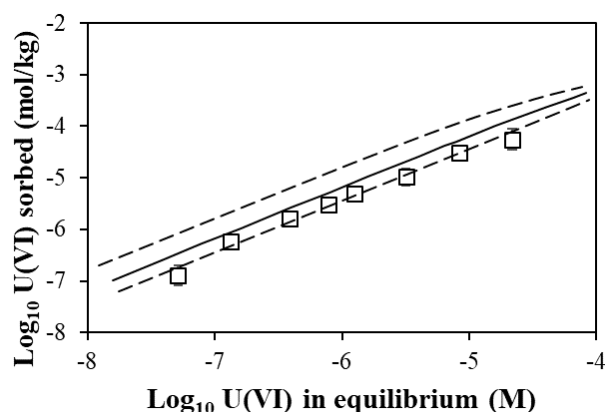


Figure 49. Model approach (solid line) for sorption isotherm of U(VI) on Callovo-Oxfordian claystone samples in equilibrium with pCO₂ of 1% of CO₂(g) in Callovo-Oxfordian synthetic porewater with pH 7.5. Error bars that are not visible are smaller than the symbol size.

According to the model calculations, the behaviour of U(VI) is controlled mainly by its aqueous speciation (Table 26). The surface complexes also play an important role on the behaviour of U(VI), in that the U(VI)-CO₃ surface complexes on the surface of illite are responsible for the sorption of U(VI) in Callovo-Oxfordian formation.

Table 26. Surface species of U(VI) distribution on illite and montmorillonite for Callovo-Oxfordian formation experimental conditions.

	Total	main species	%
Aqueous species	61 %	CaUO ₂ (CO ₃) ₃ ²⁻	81 %
		Ca ₂ UO ₂ (CO ₃) ₃ (aq)	17 %
Surface complexes	39 %	≡S _{illite} ^s OUO ₂ (CO ₃) ₂ ³⁻	33 %
		≡S _{mont} ^{w1} OUO ₂ CO ₃ ⁻	4 %

The impact of Ca-U(VI)-CO₃ ternary complexes on the sorption of U(VI) on clayey rocks was already reported by Hartmann et al. (2008) on Callovo-Oxfordian, Joseph et al. (2011) and Amayri et al. (2016) on Opalinus clay, and Marques Fernandes et al. (2015) on Opalinus and Boda clay.

For Hartmann et al. (2008), the sorption of uranyl on COx claystone was studied in 0.1 M of NaClO₄ in equilibrium with atmospheric pCO₂ as a function of pH. In the model approach proposed by Hartmann and co-workers, the U(VI)-CO₃ surface complexation reactions were not included, and this could explain why they were not able to predict the sorption of uranyl at pH between 6 and 9 (Figure 50, black line model). When those surface complexation reactions are considered, the model improves considerably (Figure 50, red lines model). Note that this improvement of the model is not only linked to the U(VI)-CO₃ surface reaction considered for illite but also to new the thermodynamic data of Ca-U(VI)-CO₃ complexes (see Table 14 in Chapter 2) (they considered the stability constants for Ca-U(VI)-CO₃ complexes reported by Bernhard et al., 2001). It should also be noted that no measurements of carbonates were done by Hartmann and co-workers, so for modelling purposes, the concentration of carbonates was controlled by pCO₂ of 10^{-3.5} and calcite.

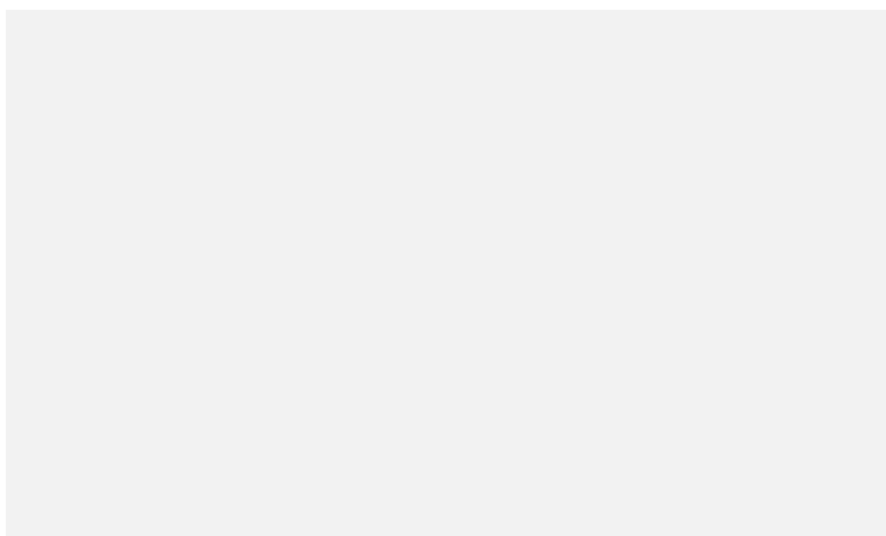


Figure 50. Experimental and model (black line) data from Hartmann et al. (2008) and the prediction model proposed in the present work (red lines) considering the new stability constant $\equiv S_sOUO_2(CO_3)_2^{3-}$ and its respective uncertainties.

When comparing the experimental results of Opalinus and Boda clay with Callovo-Oxfordian clays (present work), the sorption of U(VI) is lower for the Callovo-Oxfordian natural samples (Figure 51). Here, we can assume that the synthetic porewater composition plays a major role in the sorption mechanisms of U(VI). The main parameters that distinguish the synthetic porewaters for each study are provided in Table 27.

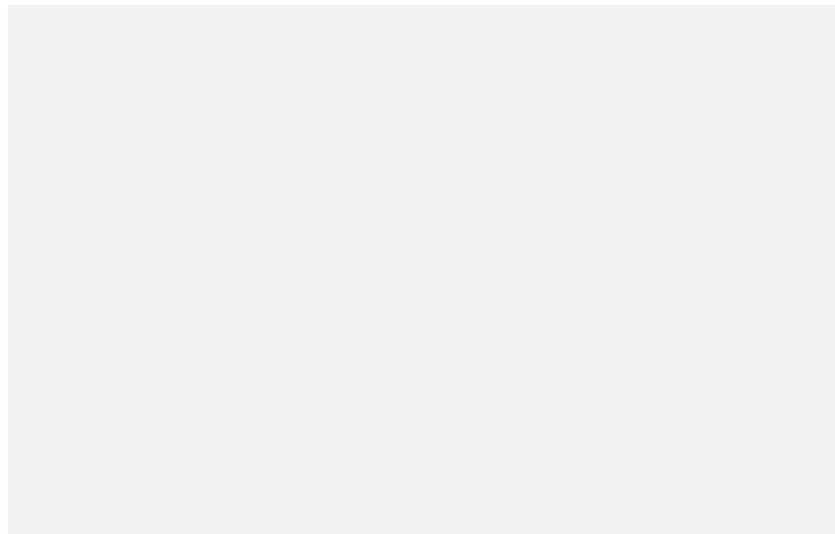


Figure 51. Comparison of sorption isotherms of U(VI) on the Opalinus clay from [1] Joseph et al. (2011) and Boda clay [2] Marques Fernandes et al. (2015) and [3] Amayri et al. (2016) with the COx clayey rock from the [p.w.] present work.

Table 27. Comparison of the main chemical parameters for OPA clay, Boda clay and COx clay. [1] Joseph et al. (2011); [2] Marques Fernandes et al. (2015); [p.w.] present work. (*) measurements of alkalinity (meq/L).

Parameters	OPA [1]	OPA [2]	Boda [2]	COx [p.w.]
Material	23 wt% illite 11 wt% I/S	17 wt% illite 30 wt% I/S	50 wt% illite	17 wt% illite 28 wt% I/S
pH	7.6	7.8	8.1	7.5
Ca mM	27	12.1	3.1	8.4
Mg mM	16.3	8.7	2.4	5.4
Carbonates mM	0.74	0.54	0.61	3.28(*)
Ionic strength M	0.37	0.23	0.03	0.1
S/L g/L	60	9.5	11.1	40
pCO ₂	atmospheric	atmospheric	atmospheric	1% of CO ₂ (g)

The model approach defined in this work was also applied to the published data. The model predictions, shown in Figure 52, can explain relatively well the sorption of U(VI) onto all clayey rocks. In Figure 52b, the model prediction slightly overestimates the experimental data reported by Marques Fernandes et al. (2015), although, for the other studies, the model predictions are within the uncertainty of the modelling parameters (Figure 52a,c).

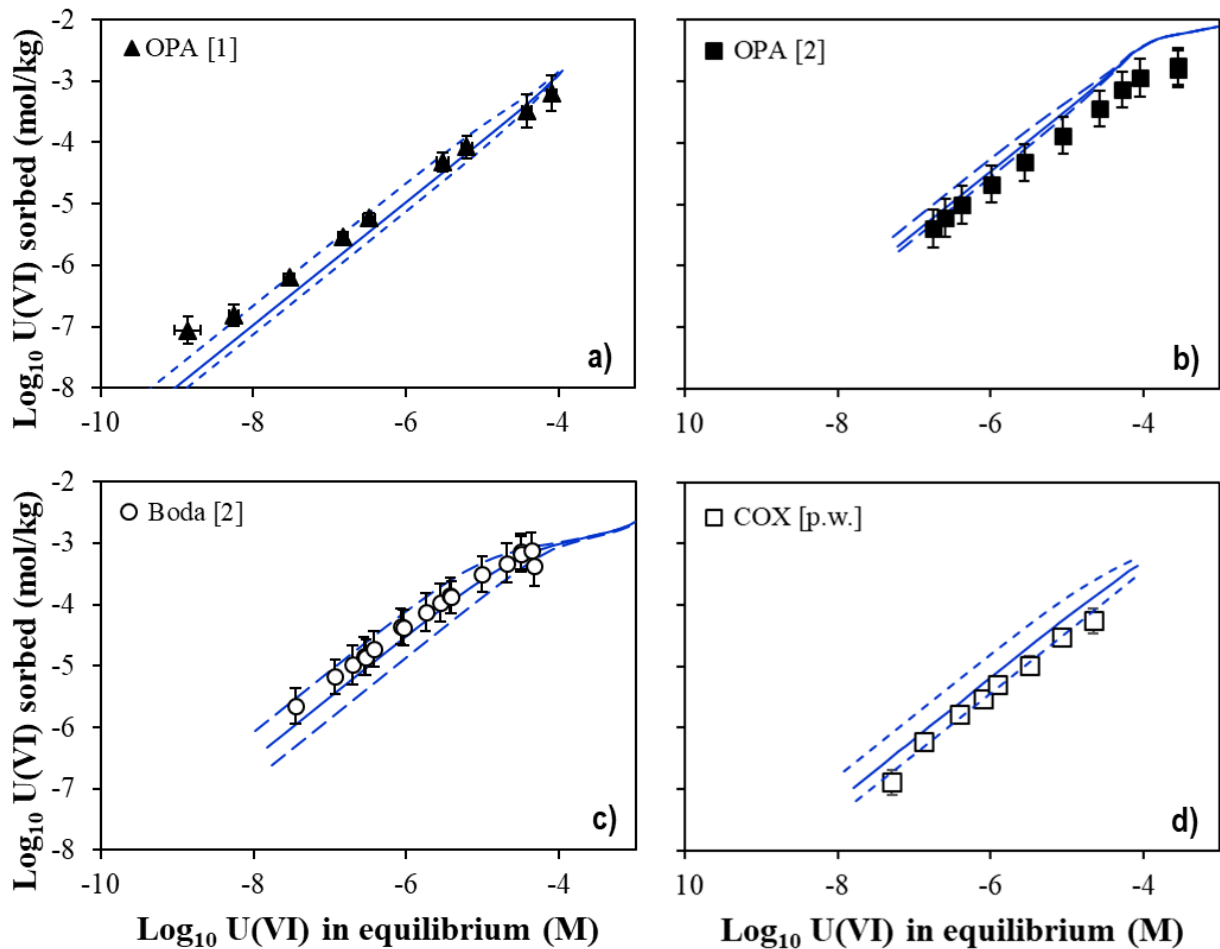


Figure 52. Model prediction for the sorption isotherms of U(VI) on a) OPA clay from [1] Joseph et al. (2011); b) OPA clay from [2] Marques Fernandes et al. (2015); and c) Boda clay from [2] Marques Fernandes et al. (2015); [p.w.] COX clay from present work. Solid-lines: model approach proposed in present work; Dash-line: model uncertainties of the $\equiv\text{S}_s\text{OUO}_2(\text{CO}_3)_2^{3-}$ ($\log_{10}K = 17.5 \pm 0.5$).

Based on this model exercise, we can validate that considering only one carbonate surface complexation ($\equiv\text{S}_s\text{OUO}_2(\text{CO}_3)_2^{3-}$) for illite, together with the surface reactions for both illite and montmorillonite (Table 19) is enough to quantify the behaviour of such complex systems as natural clay rocks.

3.6. Summary

The aim of the present work was to propose a model approach able to describe the retention of U(VI) on Callovo-Oxfordian formation as a basis for the study in temperature. The 2SPNE SC/CE model proposed by Bradbury and Baeyens (1997) was used considering the simplification already proposed in the literature (Bradbury and Baeyens, 1997, 2005c, 2011; Chen et al., 2014; Marques Fernandes et al., 2015): Callovo-Oxfordian clay fraction governs the retention of U(VI), where we consider only illite and interstratified I/S layers, I/S is a mixture of illite and smectite and montmorillonite are used as a proxy of smectite.

The sorption experimental data were performed for illite in order to better understand the impact of the formation of carbonato complexes on the retention of U(VI), taking as basis the model for montmorillonite already largely studied (Bradbury and Baeyens, 1999; Marques Fernandes et al., 2012; Tournassat et al., 2009, 2018). The results show that the model can explain relatively well the experimental data obtained with illite in a range of experimental conditions (pH = 6–7.3; pCO₂ = 10^{-3.5} and 10^{-2.1}; in 0.1 M of NaNO₃ and synthetic COx porewater) indicating that a carbonato complex is sorbed. The constant for the main complex ($\equiv S_sOUO_2(CO_3)_2^{3-}$) was fitted and shown to be higher than the one proposed for montmorillonite. The model of sorption isotherms of U(VI) also indicates that this surface complex is the main one responsible for the retention of U(VI), indicating that the impact of $\equiv S_{s,w}OUO_2(CO_3)^-$ can be considered negligible.

The proposed model explains relatively well the behaviour of U(VI) in COx clay fraction, although some divergence was observed in the absence of carbonates. Considering that the model works in Callovo-Oxfordian system, no changes of the parameters were done, and we consider at this stage that the following assumption is valid: I/S = 50% illite + 50% montmorillonite.

Finally, the proposed model was successfully applied to natural samples of Callovo-Oxfordian formation (and other clay rocks, such Opalinus clay by Amayri et al., 2016; Joseph et al., 2013; Marques Fernandes et al., 2015 and Boda clay by Marques Fernandes et al., 2015). Our results indicate that the clay fraction effectively governs the retention of U(VI). It is important to note that the model considers an important number of parameters, such as cation exchange reactions, protolysis reactions and surface complexation reactions for illite and montmorillonite. Furthermore, it is difficult to assess the uncertainty of the parameters on the model prediction. In our approach, we showed that the uncertainty of the surface carbonato complex is relatively high.

To predict the sorption behaviour of U(VI) in Callovo-Oxfordian formation system at 20°C we propose the surface parameters provided in Table 28.

We will use this proposed model approach to predict the behaviour of U(VI) in Callovo-Oxfordian formation at 20°C as a basis for the following chapter, where we will evaluate the impact of temperature on the retention of U(VI).

Table 28. Compilation of the surface reactions for both illite and montmorillonite taken in for the model prediction. (n.a. not applied)

	Illite	Montmorillonite
CATIONIC EXCHANGE REACTIONS	log₁₀ K	
$2XNa + Ca^{2+} \rightleftharpoons X_2Ca + 2Na^+$	1.04	0.61
$2XNa + UO_2^{2+} \rightleftharpoons X_2UO_2^{2+} + 2Na^+$	0.65	0.15
$2XNa + Mg^{2+} \rightleftharpoons X_2Mg + 2Na^+$	1.04	0.34
$2XNa + Fe^{2+} \rightleftharpoons X_2Fe + 2Na^+$	0.8	0.8
$2XNa + Sr^{2+} \rightleftharpoons X_2Sr + 2Na^+$	0.8	1.0
$XNa + K^+ \rightleftharpoons XK + Na^+$	1.1	0.6
PROTOLYSIS REACTIONS	log₁₀ K	
$\equiv S^sOH + H^+ \rightleftharpoons \equiv S^sOH_2^+$	4.0	4.5
$\equiv S^sOH \rightleftharpoons \equiv S^sO^- + H^+$	-6.2	-7.9
$\equiv S^{w1}OH + H^+ \rightleftharpoons \equiv S^{w1}OH_2^+$	4.0	4.5
$\equiv S^{w1}OH \rightleftharpoons \equiv S^{w1}O^- + H^+$	-6.2	-7.9

	Illite	Montmorillonite
$\equiv S^{w2}OH + H^+ \rightleftharpoons S^{w2}OH_2^+$	8.5	6.0
$\equiv S^{w2}OH \rightleftharpoons S^{w2}O^- + H^+$	-10.5	-10.5
SURFACE COMPLEXATION REACTIONS		
	log₁₀ K	
Hydrolysis reactions		
$\equiv S^sOH + UO_2^{2+} \rightleftharpoons S^sOUO_2^+ + H^+$	2.0 ^l	3.1
$\equiv S^sOH + UO_2^{2+} + H_2O \rightleftharpoons S^sOUO_2OH + 2H^+$	-3.5	-3.4
$\equiv S^sOH + UO_2^{2+} + 2H_2O \rightleftharpoons S^sOUO_2(OH)_2 + 3H^+$	-10.6	-11
$\equiv S^sOH + UO_2^{2+} + 3H_2O \rightleftharpoons S^sOUO_2(OH)_3 + 4H^+$	-19	-20.5
$\equiv S^{w1}OH + UO_2^{2+} \rightleftharpoons S^{w1}OUO_2^+ + H^+$	0.1	0.7
$\equiv S^{w1}OH + UO_2^{2+} + H_2O \rightleftharpoons S^{w1}OUO_2OH + 2H^+$	-5.3	-5.7
Carbonato reactions		
$\equiv S^sOH + UO_2^{2+} + CO_3^{2-} \rightleftharpoons S^sOUO_2CO_3^- + 2H^+$	n.a.	9.8
$\equiv S^sOH + UO_2^{2+} + 2CO_3^{2-} \rightleftharpoons S^sOUO_2(CO_3)_2^{3-} + H^+$	17.5	15
$\equiv S^{w1}OH + UO_2^{2+} + CO_3^{2-} \rightleftharpoons S^{w1}OUO_2CO_3^- + 2H^+$	n.a.	9.3

3.7. References

- Amayri, S., Fröhlich, D. R., Kaplan, U., Trautmann, N., and Reich, T.. (2016). Distribution Coefficients for the Sorption of Th, U, Np, Pu, and Am on Opalinus Clay. *Radiochimica Acta* **104** (1): 33–40.
- Baeyens, B. and Bradbury, M. H. (2004). Cation exchange capacity measurements on illite using the sodium and cesium isotope dilution technique: effects of the index cation, electrolyte concentration and competition: Modeling. *Clays and Clay Minerals* **52** (4): 421–431.
- Bergaya, F., Theng, B. K. G., and Lagaly, G. (2013). *Handbook of Clay Science*. Vol.1 1st Ed. 1246 p. Elsevier B.V.
- Bernhard, G., Geipel, G., Reich, T., Brendler, V., Amayri, S., and Nitsche, H. (2001). Uranyl (VI) Carbonate Complex Formation: Validation of the Ca₂UO₂(CO₃)₂(aq.) Species. *Radiochimica Acta* **89**: 511–518.
- Bradbury, M. H., and Baeyens, B. (1997). A Mechanistic Description of Ni and Zn Sorption on Na-Montmorillonite. Part II: modelling. *Journal of Contaminant Hydrology* **27** (3–4): 223–248.
- Bradbury, M. H. and Baeyens, B. (1999). Modelling the Sorption of Zn and Ni on Ca-Montmorillonite. *Geochimica et Cosmochimica Acta* **63** (3–4): 325–336.
- Bradbury, M. H., Baeyens, B., Geckeis, H., and Rabung, Th. (2005). Sorption of Eu(III)/Cm(III) on Ca-Montmorillonite and Na-Illite. Part 2: Surface Complexation Modelling. *Geochimica et Cosmochimica Acta* **69** (23): 5403–5412.
- Bradbury, M. H. and Baeyens, B. (2005a). Experimental and Modelling Investigations on Na-Illite: Acid-Base Behaviour and the Sorption of Strontium, Nickel, Europium and Uranyl. *NAGRA Technical Report* **04–02**. 87p. (Switzerland)
- Bradbury, M. H. and Baeyens, B. (2005b). Experimental Measurements and Modeling of Sorption Competition on Montmorillonite. *Geochimica et Cosmochimica Acta* **69** (17): 4187–4197.
- Bradbury, M. H. and Baeyens, B. (2005c). Modelling the Sorption of Mn(II), Co(II), Ni(II), Zn(II), Cd(II), Eu(III), Am(III), Sn(IV), Th(IV), Np(V) and U(VI) on Montmorillonite: Linear Free Energy Relationships and Estimates of Surface Binding Constants for Some Selected Heavy Metals and Actinide.

Geochimica et Cosmochimica Acta **69** (4): 875–892.

- Bradbury, M. H. and Baeyens, B. (2009a). Sorption Modelling on Illite. Part II: Actinide Sorption and Linear Free Energy Relationships. *Geochimica et Cosmochimica Acta* **73** (4): 1004–1013.
- Bradbury, M. H. and Baeyens, B.. (2009b). Sorption Modelling on Illite Part I: Titration Measurements and the Sorption of Ni, Co, Eu and Sn. *Geochimica et Cosmochimica Acta* **73** (4): 990–1003.
- Bradbury, M. H. and Baeyens, B. (2011). Predictive Sorption Modelling of Ni(II), Co(II), Eu(III), Th(IV) and U(VI) on MX-80 Bentonite and Opalinus Clay: A ‘Bottom-Up’ Approach. *Applied Clay Science* **52** (1–2): 27–33.
- Brigatti, M. F., Galan, E., and Theng, B. K. G. (2006). Chapter 2 Structures and Mineralogy of Clay Minerals. p 19–86. in *Developments in Clay Science*. Volume 1. Ed. Faïza Bergaya, Benny K.G. Theng, Gerhard Lagaly. Elsevier.
- Bruno, J., Duro, L., and Grivé, M.. (2002). The Applicability and Limitations of Thermodynamic Geochemical Models to Simulate Trace Element Behaviour in Natural Waters. Lessons Learned from Natural Analogue Studies. *Chemical Geology* **190** (1–4): 371–393.
- Chen, Z., Montavon, G., Ribet, S., Guo, Z., Robinet, J. C., David, K., Tournassat, C., Grambow, B., and Landesman, C. (2014). Key Factors to Understand in-Situ Behavior of Cs in Callovo-Oxfordian Clay-Rock (France). *Chemical Geology* **387** (1): 47–58.
- Chen, Z., Montavon, G., Guo, Z., Wang, X., Razafindratsima, S., Robinet, J. C., and Landesman, C.. (2014a). Approaches to Surface Complexation Modeling of Ni(II) on Callovo-Oxfordian Clayrock. *Applied Clay Science* **101**: 369–80.
- Chisholm-Brause, C., Conradson, S. D., Buscher, C. T., Eller, P. G., and Morris, D. E. (1994). Speciation of Uranyl Sorbed at Multiple Binding Sites on Montmorillonite. *Geochimica et Cosmochimica Acta* **58** (17): 3625–3631.
- Davis, J. A., and Kent, D. B. (1990). *Surface Complexation Modeling in Aqueous Geochemistry*. p. 177-260. in *Reviews of Mineralogy* Volume 23. Mineralogical Society of America
- Davis, J. A., Coston, J. A., Kent, D. B., and Fuller, C. C. (1998). Application of the Surface Complexation Concept to Complex Mineral Assemblages. *Environmental Science and Technology* **32** (19): 2820–2828.
- Davis, J. A., Meece, D. E., Kohler, M., and Curtis, G. P. (2004). Approaches to Surface Complexation Modeling of Uranium(VI) Adsorption on Aquifer Sediments. *Geochimica et Cosmochimica Acta* **68** (18): 3621–3641.
- Ferrage, E., Tournassat, C., Rinnert, E., and Lanson, B. (2005). Influence of pH on the Interlayer Cationic Composition and Hydration State of Ca-Montmorillonite: Analytical Chemistry, Chemical Modelling and XRD Profile Modelling Study. *Geochimica et Cosmochimica Acta* **69** (11): 2797–2812.
- Gaines, G. L. and Thomas, H. C. (1953). Adsorption Studies on Clay Minerals. II. A Formulation of the Thermodynamics of Exchange Adsorption. *The Journal of Chemical Physics* **21** (4): 714–718.
- Gao, Y., Shao, Z., and Xiao, Z. (2015). U(VI) Sorption on Illite: Effect of pH, Ionic Strength, Humic Acid and Temperature. *Journal of Radioanalytical and Nuclear Chemistry* **303** (1): 867–876.
- Gapon, E. N. (1933). On the Theory of Exchange Adsorption in Soils. *URRS J. Gen. Chem.* **3**: 144.
- Goldberg, S. (2013). *Surface Complexation Modeling*. p. 1–14 in *Reference Module in Earth Systems and Environmental Sciences*, Elsevier.
- Grenthe, I., Plyasunov, A., and Spahu, K. (1997). Chapter IX Estimations of Medium Effects on

- Thermodynamic Data. p. 325–426 in *Modelling in Aquatic Chemistry*.
- Hayes, K. F., Roe, A. L., Brown, G. E. Jr., Hodgson, K. O., Leckei, J. O., and Parks, G. A. (1987). In-situ X-ray absorption study of surface complexes: Selenium oxyanions on α -FeOOH. *Science* **238**: 783–786.
- Hartmann, E., Geckeis, H., Rabung, T., Lützenkirchen, J., and Fanghänel, T. (2008). Sorption of Radionuclides onto Natural Clay Rocks. *Radiochimica Acta* **96** (9–11): 699–707.
- Hochella, M. F., Jr. and White, A. F. (1990). *Mineral-Water Interface Geochemistry*. Reviews in Mineralogy Volume 23. Mineralogical Society of America
- Hohl, H. and Stumm, W. (1976). Interaction of Pb^{2+} with hydrous α - Al_2O_3 . *Journal of Colloid and Interface Science* **55**: 281–288.
- Huang, C. P. and Stumm, W. (1973). Specific adsorption of cations on hydrous α - Al_2O_3 . *Journal of Colloid and Interface Science* **22**: 231–259.
- Joseph, C., Schmeide, K., Sachs, S., Brendler, V., Geipel, G. and Bernhard, G. (2011). Sorption of uranium(VI) onto Opalinus Clay in the absence and presence of humic acid in Opalinus Clay pore water. *Chemical Geology* **284**: 240–250
- Joseph, C., Stockmann, M., Schmeide, K., Sachs, S., Brendler, V., and Bernhard, G. (2013). Sorption of U(VI) onto Opalinus Clay: Effects of pH and Humic Acid. *Applied Geochemistry* **36**: 104–117.
- Joseph, C. (2013). ‘*The Ternary System U(VI) / Humic Acid / Opalinus Clay*’. PhD thesis Helmholtz-Zentrum Dresden-Rossendorf (Germany).
- Marques Fernandes, M., Baeyens, B., Dähn, R., Scheinost, A. C., and Bradbury, M. H. (2012). U(VI) Sorption on Montmorillonite in the Absence and Presence of Carbonate: A Macroscopic and Microscopic Study. *Geochimica et Cosmochimica Acta* **93**: 262–277.
- Marques Fernandes, M., Vér, N., and Baeyens, B. (2015). Predicting the Uptake of Cs, Co, Ni, Eu, Th and U on Argillaceous Rocks Using Sorption Models for Illite. *Applied Geochemistry* **59**: 189–199.
- McBride, M. B. (1980). Interpretation of the Variability of Selectivity Coefficients for Exchange between Ions of Unequal Charge on Smectites. *Clays and Clay Minerals* **28** (4): 255–261.
- NEA. (2002). Radionuclide Retention in Geologic Media. *Radioactive Waste Management* (3061): 269.
- NEA. (2005). *NEA Sorption Project Phase II Interpretation and Prediction of Radionuclide Sorption onto Substrates Relevant for Radioactive Waste Disposal Using Thermodynamic Sorption Models*.
- Ngouana, Brice F. W. (2014). ‘*Modélisation Moléculaire de L’hydratation, de La Structure, et de La Mobilité Des Ions et de L’eau Dans L’espace Interfoliaire et À La Surface D’une Argile Smectitique*’. PhD Thesis École des Mines de Nantes (France).
- Parks, G. A. (1990). *Surface Energy and Adsorption at Mineral-Water Interfaces: An Introduction*. p. 134–175. in *Reviews of Mineralogy* Volume 23. Mineralogical Society of America
- Payne, T. E., Brendler, V., Ochs, M., Baeyens, B., Brown, P. L., Davis, J. A., Ekberg, C., Kulik, D. A., Lützenkirchen, J., Missana, T., Tachi, Y., Van Loon, L. R., and Altmann, S. (2013). Guidelines for Thermodynamic Sorption Modelling in the Context of Radioactive Waste Disposal. *Environmental Modelling and Software* **42**: 143–156.
- Poinssot, C., Baeyens, B. and Bradbury, M. H. (1999). Experimental and modelling studies of caesium sorption on illite. *Geochimica et Cosmochimica Acta* **63**: 3217–3227.
- Reinoso-Maset, E. and Ly, J. (2014). Study of Major Ions Sorption Equilibria to Characterize the Ion Exchange Properties of Kaolinite. *Journal of Chemical and Engineering Data* **59** (12): 4000–4009.

- Reinoso-Maset, E. and Ly, J. (2016). Study of uranium(VI) and radium(II) Sorption at Trace Level on Kaolinite Using a Multisite Ion Exchange Model. *Journal of Environmental Radioactivity* **157**: 136–48.
- Schindler, P. W. and Kamber, H. R. (1968). Die acidität von silanolgruppen. *Helvetica Chimica Acta* **51**: 1781–1786.
- Schindler, P. W. and Stumm, W. (1987). *The Surface Chemistry of Oxides, Hydroxides, and Oxide Minerals*. 83–110 in Aquatic Surface Chemistry. John Wiley, New York.
- Sposito, G. (1984). *The Surface Chemistry of Soils*. Oxford University Press. New York.
- Sposito, G., Skipper, N. T., Sutton, R., Park, S. H., Soper, A. K., and Greathouse, J. A. (1999). Surface Geochemistry of the Clay Minerals. *Proceedings of the National Academy of Sciences* **96** (7): 3358–3364.
- Stammose, D., Ly, J., Pitsch, H., and Dolo, J. M.. (1992). Sorption Mechanisms of Three Actinides on a Clayey Mineral. *Applied Clay Science* **7** (1–3): 225–238.
- Stumm, W., Huang, C. P. and Jenkins, S. R. (1970). Specific chemical interactions affecting the stability of dispersed systems. *Croatica Chemica Acta* **42**: 223–244.
- Tournassat, C., Gailhanou, H., Crouzet, C., Braibant, G., Gautier, A., and Gaucher, E. C. (2009). Cation Exchange Selectivity Coefficient Values on Smectite and Mixed-Layer Illite/Smectite Minerals. *Soil Science Society of American Journal* **73** (3): 928–942
- Tournassat, C., Grangeon, S., Leroy, P., and Giffaut, E. (2013). Modeling Specific pH Dependent Sorption of Divalent Metals on Montmorillonite Surfaces. a Review of Pitfalls, Recent Achievements and Current Challenges. *American Journal of Science* **313** (5): 395–451.
- Tournassat, C., Tinnacher, R. M., Grangeon, S., and Davis, J. A. (2018). Modeling uranium(VI) Adsorption onto Montmorillonite under Varying Carbonate Concentrations: A Surface Complexation Model Accounting for the Spillover Effect on Surface Potential. *Geochimica et Cosmochimica Acta* **220**: 291–308.
- Turner, G. D., Zachara, J. M., McKinley, J. P. and Smith, S. C. (1996). Surface-charge properties and UO_2^{2+} adsorption of a subsurface smectite. *Geochimica et Cosmochimica Acta* **60**: 3399–3414.
- Van Loon, L. R., Baeyens, B., and Bradbury, M. H. (2009). The Sorption Behaviour of Caesium on Opalinus Clay: A Comparison between Intact and Crushed Material. *Applied Geochemistry* **24** (5): 999–1004.
- Vanselow, A. P. (1932). The utilization of the base-exchange reaction for the determination of activity coefficients in mixed electrolytes. *Journal of the American Chemical Society* **54** (4): 1307–1311.
- Vinsot, A., Mettler, S., and Wechner, S. (2008). In Situ Characterization of the Callovo-Oxfordian Pore Water Composition. *Physics and Chemistry of the Earth* **33** (SUPPL. 1) S75–S86.
- Vinsot, A., Lundy, M., and Linard, Y. (2017). O_2 Consumption and CO_2 Production at Callovian-Oxfordian Rock Surfaces. *Procedia Earth and Planetary Science* **17**: 562–565.
- Waite, T. D., Davis, J. A., Payne, T. E., Waychunas, G. A., and Xu, N. (1994). Uranium(VI) Adsorption to Ferrihydrite: Application of a Surface Complexation Model. *Geochimica et Cosmochimica Acta* **58** (24): 5465–5478.
- Waite, T. D., David, J. A., Fenton, B. R., and Payne, T. E. (2000). Approaches to Modelling U(VI) Adsorption on Natural Mineral Assemblages. *Radiochimica Acta* **88**: 687–693.

Chapter 4

Impact of the temperature on the sorption of U(VI) in the Callovo-Oxfordian Formation

4.1. Introduction

At this stage of the work, we already know that the temperature influences the speciation of U(VI) in calcium rich solutions, specifically that temperature does not favour the formation of $\text{CaUO}_2(\text{CO}_3)_3^{2-}$ whereas it has no effect on $\text{Ca}_2\text{UO}_2(\text{CO}_3)_3(\text{aq})$ species formation. In this chapter we ask if the increase of temperature can also affect the retention of U(VI) on Callovo-Oxfordian formation.

One of the answers for this question is given in Figure 53 (see symbols). The experimental data shown in this figure corresponds to the experiments performed with the COx claystone natural sample (the experimental results are detailed in Section 4.2.4). The results indicate an increase of the sorption of U(VI) with a temperature increase. Such effect was already observed in Opalinus clay conditions for U(VI) (Joseph, 2013) and Np(V) (Fröhlich et al., 2013), or for U(VI) in granite systems (Jin et al., 2016). In conclusion, the sorption of U(VI), independently of the material, is commonly favoured by the increase of the temperature.

The increase of U(VI) sorption can be predicted by modelling the retention of U(VI)/COx system using the model proposed in Chapter 3 at 20 °C, including the thermodynamic data for the Ca-U(VI)-CO₃ ternary complexes, given in Chapter 2. The presence of Ca-U(VI)-CO₃ aqueous complexes may explain the weak retention of U(VI) at 20°C while with an increase in temperature these aqueous species are less stable in solution favouring the sorption of U(VI). However, the model does not fully predict the U(VI) sorption increase in the COx system (red solid-line in Figure 53). We must therefore consider other parameters (such as enthalpy) that will allow us to fully understand the retention mechanisms of U(VI) with the increase of temperature.

In the last years, it has been shown that the mineral assemblage of Callovo-Oxfordian formation does not change with an increase of temperature of up to 80 °C (Andra, 2005) and only the chemical

composition of the porewater changes accordingly (see Chapter 1). Therefore, the question is how the surface reactions constants are affected with a temperature increase, in the case for instance of surface protolysis reactions, ionic exchange reactions and surface complexation reactions. This question will be discussed in the following section, taking into account the published studies.

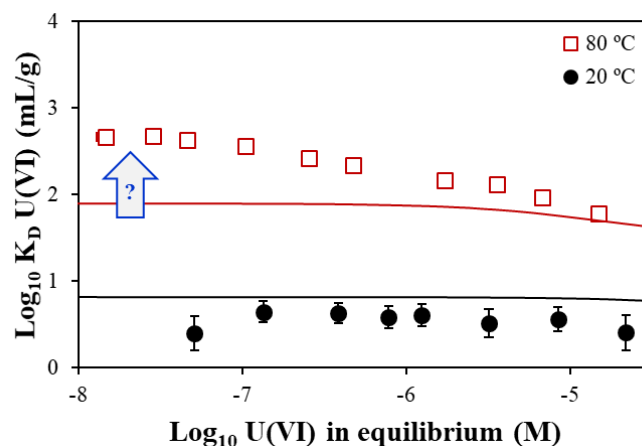


Figure 53. Impact of the temperature on the distribution coefficient of U(VI) as a function of the concentration of U(VI) in equilibrium in COx claystone samples. (●) and (□) experimental data from the present work. red-line: model approach at 80°C considering the model approach proposed in Chapter 3 and the thermodynamic parameters of U(VI) aqueous speciation (Chapter 2).

4.1.1. Thermodynamic parameters for sorption processes

The thermodynamic parameters (enthalpy and entropy) of sorption reactions have been studied for a variety of metal ions in different systems such as oxides, model phases such as silica and alumina, and even in clay minerals (kaolinite, smectite, illite) (Fokkink et al., 1989, 1990; Brady, 1992, 1994; Brady and Walther, 1992; Angove et al., 1998; Halter, 1999; Shahwan and Erten, 2004; Tertre et al., 2005, 2006; Bauer et al., 2005; Duc et al., 2008; Yang et al., 2010; Gao et al., 2015; Jin et al., 2016).

Protolysis reactions:

In some oxides, such as silica and alumina, the behaviour of the surface charge and the respective sorption of metal cations can change with temperature. Brady (1992, 1994) studied the temperature effect on SiO₂ and α-Al₂O₃ reactivity between 25 and 60°C. Both studies intended to determine the enthalpy of reactions of the most relevant sorption sites in such minerals. The authors concluded that the protonation-deprotonation surface sites in both silica and alumina could be affected by the increase of temperature, which was also observed by Halter (1999). These sites are pH-dependent which means that the pH-dependency increases with the increase of temperature. This observation was corroborated by studies on the dissolution of aluminosilicates by Brady and Walther (1992).

Duc and co-authors (2008) studied the effect of temperature on surface protolysis reactions of montmorillonite, which was considered a combination of alumina and silica layers, in more complex systems such as the clay minerals. In contrast to what was observed by Brady (1992, 1994) and Brady

and Walther (1992), the protonation-deprotonation at the edge surface sites is not temperature-dependent on montmorillonite; in particular, the PZNPC (point of zero net proton charge) did not change significantly with the increase of temperature. This effect was also observed by Tertre et al. (2006a).

Ionic exchange and surface complexation reactions:

The temperature effect on the adsorption of metal cations has also been studied for different clay minerals in a range of 20 to 150 °C (*e.g.* Brady et al., 1992; Angove et al., 1997, 1998; Bauer et al., 2005; Shahwan et al., 2004; Tertre et al., 2005, 2006; Chang et al., 2007; Donat, 2009; Sun et al., 2014; Yang et al., 2010). In general, all studies indicate temperature-dependency of the adsorption of metal cations in clay mineral systems. The adsorption of the metal cations increases with temperature, indicating an endothermic process. This however depends on the mechanism of retention considered, for example Tertre et al. (2005, 2006) showed that the temperature effect depends on the surface complexation mechanisms, which slightly increase when the temperature increases, whereas the influence of the cation exchange is negligible.

Even if a general trend, indicating the endothermic character of the metal cations sorption, can be perceived from most studies it cannot be generalised. For example, Bauer et al. (2005) show that the effect of temperature on the adsorption of Eu(III) on smectite was negligible.

4.1.2. Conceptual approach

The literature review allowed us to conclude that a temperature effect and the surface reactivity cannot be excluded. However, to the best of our knowledge, there are no enthalpy values which can be directly applied to the surface parameters describing U(VI)/Callovo-Oxfordian formation at 20 °C (see Table 28 in Chapter 3).

Simplifications of the model in temperature must be done in order to decrease the number of parameters to study. Based on the literature review we can carefully assume that:

- Since the protolysis reactions are not temperature-dependent for montmorillonite (Tertre et al., 2006a; Duc et al., 2008;) we can apply the same assumption for illite;
- The temperature effect is also negligible for the cationic exchange reactions (Tertre et al., 2005, 2006);

Despite these simplifications, there are still an important number of surface complexation constants to consider in the model and this remains a challenge, in which a large number of experimental data should be acquired in order to allow all the species to be formed with different ranges of existence.

The complexity of such experimental and modelling approach was also raised in the work of Jin and co-workers (2016) while evaluating the main mechanisms involved in the sorption of U(VI) on granites under different conditions (pH, ionic strength, initial concentration of U(VI) and temperature). The authors also observed an increase in U(VI) sorption in temperature, proposing enthalpy values for the different surface complexation reactions involved. The determination of the thermodynamic data was based on the model fit constraining the system to three surface complexation reactions at constant pH (4.5, 5.2 and 6.3). Considering the complexity of the granite composition, the generalised

model approach described the U(VI) adsorption at high concentrations of U(VI) ($> 10^{-5}$ M) in equilibrium. These authors also aimed to understand the influence of carbonates on U(VI)/granite systems, but their model was not able to interpret the experimental data.

The determination of enthalpy values for surface species could be helped by analysing the thermodynamic data known for the aqueous system. A good correlation between surface complexation constants and the corresponding species in aqueous phase at 25°C was already shown for the parameters of the 2SPNE SC/CE model (Bradbury and Baeyens, 2009). We could therefore expect such good correlation in temperature. Brady (1992, 1994) showed that the adsorption of Cd(II) and Pb(II) is favoured with an increase of temperature for silica or alumina and there was a good correlation between the aqueous complexation and the respective surface complexation reactions. Their results indicated that the enthalpy of hydrolysis of metal cations is positively correlated with the enthalpy of silica surface, but weakly correlated with the enthalpy of alumina surface.

Thus, the model approach proposed in this study will take into account the correlation between the aqueous complexation and surface complexation thermodynamic data, in addition to the two other assumptions mentioned above (temperature effect negligible for the protolysis reactions and cation exchange reactions).

4.2. Effect of the temperature on the adsorption processes of uranium on clays and clay minerals

The temperature changes of the system affect not only the chemical composition and properties of the solution but also the surface reactivity of the solids. The overall system changes will have implications on the uranium's behaviour on Callovo-Oxfordian formation. We evaluated the effect of the temperature on its behaviour through the analysis of sorption experiments carried out in different mineral assemblages at different conditions and different temperatures, together with modelling exercises.

4.2.1. Experimental approach

As in Chapter 3, we started first with the analysis of a single mineral, illite, followed by an increase of the complexity of the system, through the analysis of the clay fraction (illite and interstratified I/S layers) and the natural samples (clay minerals, carbonates and silicates) of the Callovo-Oxfordian formation, measuring and assessing the effect of pH and carbonate contents of the solution at different temperatures. The experimental cases are described in Table 29.

The experimental set-up for both the sorption edge and isotherm experiments follows the same procedure as described in Chapter 2 (see Figure 6) using the chemical conditions as described in Table 30. It should be noted that all solutions were prepared at room temperature (approx. 20°C) and heated during the period of equilibration using the incubator adjusted to the temperature of interest. The

material and methods used for the sorption experiments are described in Appendix A, and the details of the experimental results are provided in Appendix C.5.

Table 29. Description of the U(VI) sorption experiments carried out on illite, Callovo-Oxfordian clay fraction and clays samples as a function of temperature.

Case	Methods	Observations
Illite	Sorption edges and isotherms of U(VI) in the absence of carbonates at different temperatures	Evaluate the correlation between aqueous and surface hydrolysis reactions on the surface of illite
	Sorption edges and isotherms of U(VI) in the presence of carbonates at different temperatures	Evaluate the correlation between aqueous and surface carbonate complexation reactions on the surface of illite
	Sorption isotherms of U(VI) in synthetic COx porewater composition at 80 °C	Evaluate the influence of ternary complexes on the retention of U(VI) with the increase of temperature
COx clay fraction	Sorption isotherms of U(VI) in the absence or presence of carbonates at 80 °C	Can we apply the results obtained for illite directly to smectite?
	Sorption isotherms of U(VI) in synthetic COx porewater composition at 80 °C	Evaluate the influence of ternary complexes on the retention with the increase of temperature
COx claystone	Sorption isotherms of U(VI) in synthetic COx porewater composition at 80 °C	Blind prediction in temperature

Table 30. Experimental conditions of the sorption experimental cases for the different phases of Callovo-Oxfordian formation at different temperatures. (pw = porewater).

Experimental conditions	Sorption edges			Sorption isotherms			
	illite		Illite clay fraction	Illite	Illite clay fraction		Illite clay fraction claystone
Atmosphere	Ar(g)	air	Ar(g)	Air	1%	5%	5%
Temperature	80 °C	80 °C	80 °C	60–80 °C	60–80 °C	60–80 °C	80 °C
pH range	4–10	4–10	Equilibrium	7	7.2	6.6	6.6
Ionic strength (M)	0.1	0.1	0.1	0.1	0.1	0.1	0.1
Background media	NaNO ₃	NaCl	NaNO ₃	NaCl	NaNO ₃	NaNO ₃	COx pw
S/L (g/L)	2.0	0.5–1.0	2	2	2	2	2–10
[U(VI)] _{initial} (M)	10 ⁻⁷	10 ⁻⁷	10 ⁻⁸ –2·10 ⁻⁵				
Equilibration (days)	3	3	3	3	3	3	3

4.2.2. Model Approach

The model approach that we propose for studying the temperature effect on the retention of U(VI) considers that the ionic exchange reactions (Tertre et al., 2005, 2006) and the protonation/deprotonation reactions (Tertre et al., 2006a; Duc et al., 2008) are not influenced by the temperature. The thermodynamic data describing the surface complexation reaction with U(VI) are unknown and will be derived from the experimental data. Note that the two surface carbonato for illite, which do not

play a major role at 20°C for the studied experimental conditions (see Section 3.4.2), will not be considered in this study.

Table 31. Aqueous speciation of U(VI) (Guillaumont et al., 2003) and surface complexation reactions and respective stability constants (Bradbury and Baeyens, 2009; Marques Fernandes et al., 2015) and enthalpy values (unknown: to be determined) used on the predictive model. (n.a.: not applied).

AQUEOUS COMPLEXATION	$\log_{10} K^\circ$		$\Delta_r H^\circ$ kJ/mol	
$UO_2^{2+} + H_2O \rightleftharpoons UO_2(OH)^+ + H^+$	-5.25 (± 0.24)		43.46 (± 14.99)	
$UO_2^{2+} + 2H_2O \rightleftharpoons UO_2(OH)_2 + 2H^+$	-12.15 (± 0.07)		111.16 (± 1.51)	
$UO_2^{2+} + 3H_2O \rightleftharpoons UO_2(OH)_3^- + 3H^+$	-20.25 (± 0.42)		148.06 ⁱ	
$UO_2^{2+} + 4H_2O \rightleftharpoons UO_2(OH)_4^{2-} + 4H^+$	-32.4 (± 0.68)		156.14 ¹	
$UO_2^{2+} + CO_3^{2-} \rightleftharpoons UO_2CO_3$	9.94 (± 0.03)		5 (± 2)	
$UO_2^{2+} + 2CO_3^{2-} \rightleftharpoons UO_2(CO_3)_2^{2-}$	16.61 (± 0.09)		18.5 (± 4)	
$UO_2^{2+} + 3CO_3^{2-} \rightleftharpoons UO_2(CO_3)_3^{4-}$	21.84 (± 0.04)		-39.2 (± 4.1)	
	Illite		Montmorillonite	
SURFACE COMPLEXATION REACTIONS	$\log_{10} K_x$	$\Delta_r H$ kJ/mol	$\log_{10} K_x$	$\Delta_r H$ kJ/mol
$\equiv S^s OH + UO_2^{2+} \rightleftharpoons \equiv S^s OUO_2^+ + H^+$	2.0	unknown	3.1	unknown
$\equiv S^{w1} OH + UO_2^{2+} \rightleftharpoons \equiv S^{w1} OUO_2^+ + H^+$	0.1	unknown	0.7	unknown
$\equiv S^s OH + UO_2^{2+} + H_2O \rightleftharpoons \equiv S^s OUO_2 OH + 2H^+$	-3.5	unknown	-3.4	unknown
$\equiv S^{w1} OH + UO_2^{2+} + H_2O \rightleftharpoons \equiv S^{w1} OUO_2 OH + 2H^+$	-5.3	unknown	-5.7	unknown
$\equiv S^s OH + UO_2^{2+} + 2H_2O \rightleftharpoons \equiv S^s OUO_2(OH)_2^- + 3H^+$	-10.6	unknown	-11	unknown
$\equiv S^s OH + UO_2^{2+} + 3H_2O \rightleftharpoons \equiv S^s OUO_2(OH)_3^{2-} + 4H^+$	-19	unknown	-20.5	unknown
$\equiv S^s OH + UO_2^{2+} + CO_3^{2-} \rightleftharpoons \equiv S^s OUO_2 CO_3^- + H^+$	n.a.	n.a.	9.8	unknown
$\equiv S^{w1} OH + UO_2^{2+} + CO_3^{2-} \rightleftharpoons \equiv S^{w1} OUO_2 CO_3^- + H^+$	n.a.	n.a.	9.3	unknown
$\equiv S^s OH + UO_2^{2+} + 2CO_3^{2-} \rightleftharpoons \equiv S^s OUO_2(CO_3)_2^{3-} + H^+$	17.5	unknown	15	unknown

The model will be developed firstly using the U(VI)/illite system in order to propose a modelling strategy which will be further used, in a predictive way, to the COx clay fraction and claystone natural sample.

We will use the model approach 2SPNE SC/CE proposed in Chapter 3 at 20 °C (Model II) using the thermodynamic data of the aqueous species (Appendix E), *i.e.* no enthalpy values are considered for the surface species. This way we will be able to evaluate from the beginning if the surface species on illite (and after on montmorillonite) are, or not, controlled by enthalpy.

As mentioned previously, there is a correlation between complexation in solution and complexation at the surface (Figure 54). Considering the important number of surface reactions to be considered, we decided to assume in a second approach a correlation factor of 1 for the known enthalpies, from the aqueous species complexation reactions to the corresponding surface complexation reaction. Depending on the results, the enthalpy values will be fitted in order to obtain a good agreement between the experiment and the model, aiming to obtain a correlation between complexation and surface complexation constants.

ⁱ Uncertainty not available

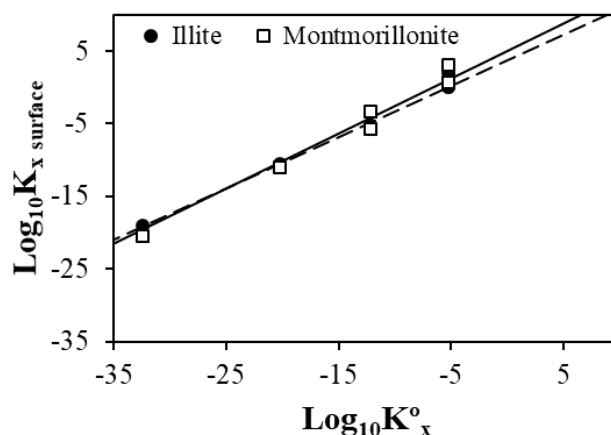


Figure 54. Linear relationship between $\text{Log}_{10}K_x^o$ of aqueous species and $\text{Log}_{10}{}^S K_x$ of surface complexes for illite and montmorillonite, considering both hydrolysis complexes. Solid-line: correlation of illite surface complexation data; dashed-line: correlation of montmorillonite surface complexation data.

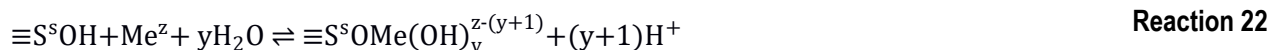
We will describe next the conceptual approach used to link the hydrolysis and carbonate surface complexation, using the corresponding aqueous species, as described in Bradbury and Baeyens (2009).

The hydrolysis constants (${}^{\text{OH}}K_x$ values) for the metal Me^z are given in the literature for aqueous hydrolysis reactions. The general form can be written as follows:



In Reaction 21, x is an integer > 1 , and $\text{Me}(\text{OH})_x^{(z-x)}$ is a general form corresponding to the hydrolysed species.

The reaction between aqueous hydrolysed species and amphoteric surface hydroxyl sorption sites can be written in a generalised form as:



In Reaction 22, y is an integer, and, when $y = 0$ the surface complex is $\equiv\text{S}^{\text{S}}\text{OMe}^{z-1}$. The corresponding surface stability constant is expressed as ${}^{\text{S}}K_y$, through the standard mass action relationship, and the general form of the surface species is $\equiv\text{S}^{\text{S}}\text{OMe}(\text{OH})_y^{z-(y+1)}$. In the approach proposed by Bradbury and Baeyens (2009), ${}^{\text{OH}}K_x$ is correlated to ${}^{\text{S}}K_y - 1$.

In the case of the carbonation constants (${}^{\text{CO}_3}K_x$ values) for Me^z the action mass law can be expressed in a general form as:



In Reaction 23, x is also an integer > 1 . Taking the Reaction 22 and assuming $y = 0$, and that the reaction between aqueous carbonate species and amphoteric surface hydroxyl sorption sites exists, the mass action reaction of the carbonation of surface can follow the same principle described above and it can then be written as:



The corresponding surface stability constant is expressed as ${}^S K_x$, via a standard mass action relationship, and the surface species is $\equiv S^s OMe(CO_3)_y^{(z-2y)}$. If we follow the approach of Bradbury and Baeuens (2009), the surface species $\equiv S^s OMe(CO_3)_y^{(z-2y)}$ must correspond to the aqueous mixed complex $HOme(CO_3)_y^{(z-2y-1)}$. However, such species are not proposed in the thermodynamic database, and as such the surface enthalpy values will be directly evaluated by fitting, if necessary.

In our study, Me^z is UO_2^{2+} and the main hydrolysis and carbonate aqueous and surface complexes and their respective complexation reactions are described in Table 31. The ionic exchange reactions and protonation/deprotonation reactions are also included in the model while enthalpy values are not included (see Table 28).

4.2.3. U(VI)/illite system in temperature up to 80 °C

We performed sorption edges and isotherms experiments to study the effect of temperature on U(VI) sorption onto illite at 60 and 80 °C, in the absence or in the presence of carbonates in equilibrium with different $pCO_2(g)$ atmospheres. The experimental data will be considered in order to propose a modelling strategy which will be further used to predict the U(VI) sorption on the COx clay fraction (in order to assess whether it can be used also with smectite, i.e. montmorillonite) and COx natural samples (to evaluate its applicability to a natural complex mixture with additional mineral phases).

4.2.3.1. In the absence of carbonate

Experimental data:

In Figure 55, we show the distribution coefficient values of U(VI) obtained as a function of the pH at 80 °C in the absence of carbonates (in inert atmosphere). In comparison with the results obtained at 20 °C, the experimental behaviour of U(VI) does not change at neutral conditions, however it is slightly higher at low pH. At pH below 5, the K_D increases about 1 order of magnitude with the increase of temperature to 80 °C.

The sorption isotherms of U(VI) at 60 and 80 °C are compared with the sorption isotherms performed at 20 °C (Figure 56). At the end of the experiments the pH measured reached a value of 6.4 (± 0.5). Note that the alkalinity titration measurements indicate that in these experiments there is a possible contamination of carbonates in the glove-box. This issue was already observed when we performed the experiments at 20 °C. The corresponding pCO_2 values were calculated and are indicated in Table 32. The uncertainties of the alkalinity measurements are relatively high considering the low content of carbonates measured. The contamination was taken into account in the model without considering at this point an enthalpy value for the carbonate surface species.

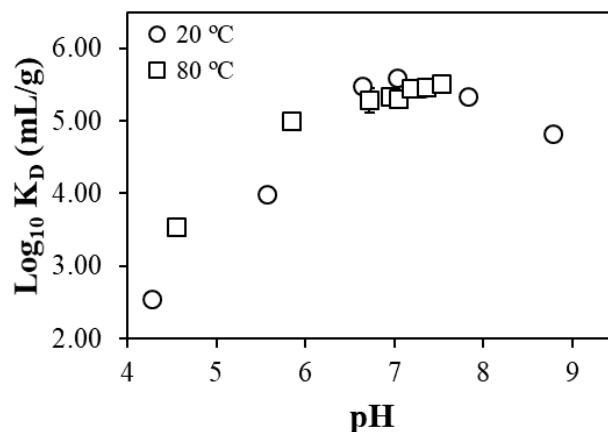


Figure 55. Distribution coefficient for the sorption of U(VI) at $1 \cdot 10^{-7}$ M of U(VI) onto illite as a function of pH in 0.1 M of NaNO_3 in the absence of carbonates. Error bars that are not visible are smaller than the symbol size.

Table 32. pH and alkalinity measured in equilibrium for the sorption isotherms on illite in inert atmosphere at different temperatures.

Temperature	pH _{final}	Alkalinity (meq/L)	pCO ₂ calculated ⁱ
20 °C	6.4 (± 0.2)	0.08 (± 0.03)	-2.7/-3.0
60 °C	6.4 (± 0.5)	0.08 (± 0.03)	-2.5/-2.8
80 °C	6.5 (± 0.1)	0.08 (± 0.03)	-2.5/-2.9

As it was observed for the sorption edge experiments, the experimental results show no significant change in sorption when the temperature increases; a slight increase is nonetheless observed at concentrations below $10^{-8.5}$ M for temperatures up to 80 °C.

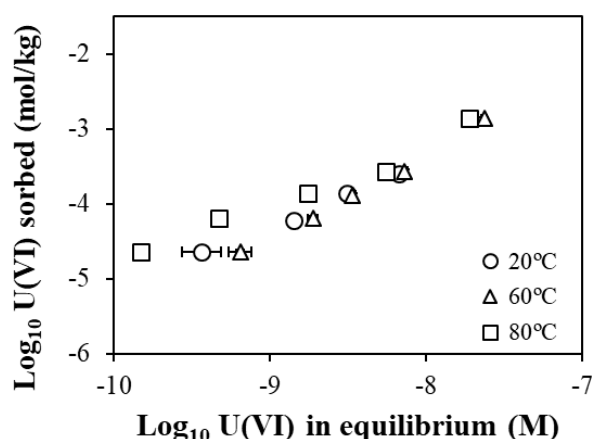


Figure 56. Temperature effect on the sorption isotherm of U(VI) onto illite in the absence of carbonates at pH of equilibrium of 6.4–6.5 in 0.1 M of NaNO_3 . Error bars that are not visible are smaller than the symbol size.

Modelling results:

Firstly, we performed blind predictions to assess the influence of temperature on aqueous speciation (Figure 57). These results show that the increase of temperature “shifts” the aqueous species

ⁱ Calculated considering the uncertainty of the alkalinity measurements. Maximum and minimum values of pCO₂ calculated.

distribution to a lower pH. For example, at neutral pH the predominant aqueous species at 80 °C is $\text{UO}_2(\text{OH})_2$ instead of UO_2OH^+ at 20 °C. We reason that this must affect the surface complexation reaction.

As mentioned previously, in a first approach, we did not consider any enthalpy values in the geochemical model for the surface species (Model II). In a second approach, the enthalpy values for the aqueous species were directly applied to the corresponding surface complexation species (i.e. considering a correlation factor of 1) (Model IV, Table 33).

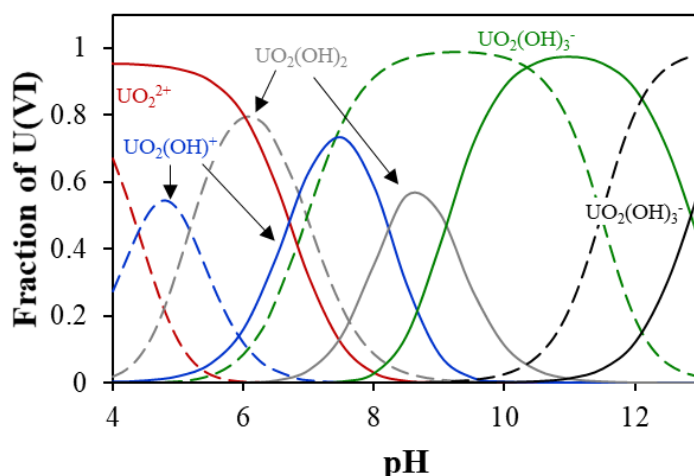


Figure 57. Distribution of U(VI) aqueous species as a function of the pH at 20°C (solid lines) and 80°C (dashed lines) in the absence of the carbonates.

Table 33. Surface complexation constants on strong sites together with the corresponding hydrolysis constants and enthalpy values for illite considered in Model IV.

Surface species	$\log_{10} \text{OH}K_x$	$\Delta_r H^\circ$ kJ/mol	Aqueous species	$\log_{10} \text{OH}K$	$\Delta_r H^\circ$ kJ/mol
$\equiv\text{S}^\circ\text{OUO}_2^+$	2.0	43.46	$\text{UO}_2(\text{OH})^+$	-5.25	43.46
$\equiv\text{S}^\circ\text{OUO}_2\text{OH}$	-3.5	111.16	$\text{UO}_2(\text{OH})_2^0$	-12.15	111.16
$\equiv\text{S}^\circ\text{OUO}_2(\text{OH})_2$	-10.6	148.06	$\text{UO}_2(\text{OH})_3^-$	-20.25	148.06
$\equiv\text{S}^\circ\text{OUO}_2(\text{OH})_3^{2-}$	-19	156.14	$\text{UO}_2(\text{OH})_4^{2-}$	-32.4	156.14

The results are shown in Figure 58. The model approach that does not consider a temperature effect on the surface reaction (Model II) cannot explain the experimental data at 80 °C: the model predicts a strong decrease of the retention as a function of temperature, whereas a slight effect is observed experimentally at lower pH. This can be explained by the strong influence of the temperature on the formation of the hydrolysis species (as it was shown in Figure 57), which increases the competition between the formation of aqueous species and the surface complexation.

When the enthalpy values for the hydrolysis surface complexation reactions are considered (Model IV), the model approach can effectively reproduce an increase of the sorption of U(VI) as a function of pH at 80 °C (Figure 58b), indicating that the hydrolysis surface complexation is also favoured in temperature. However, this approach highly overestimates the sorption of U(VI) at pH below 7.5 at 80 °C. Furthermore, the model can no longer reproduce the experimental data at 20 °C for pH values between 6 and 8 (Figure 58a). The same effect is observed for the sorption isotherms of U(VI) at different temperatures (20, 60 and 80 °C) (Figure 59a, b and c, respectively).

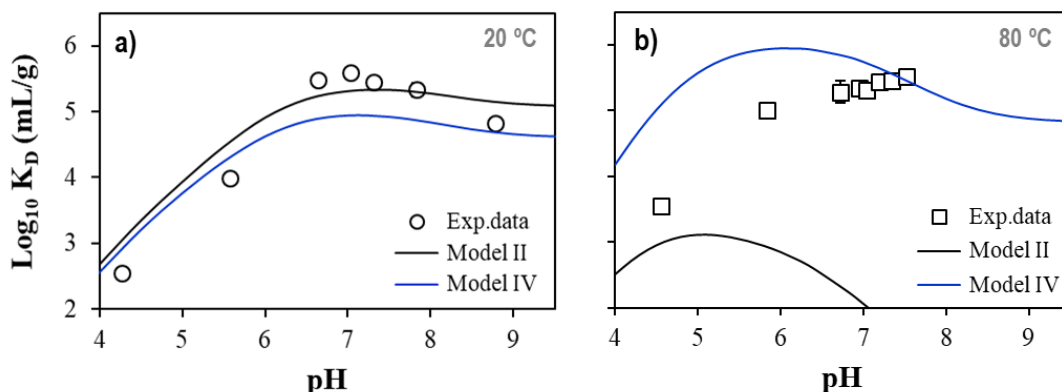


Figure 58. Model approach for the distribution coefficient of U(VI) as a function of the pH at a) 20 °C and b) 80 °C in the absence of carbonates. Model II: base model without enthalpy data (see Chapter 3); Model IV: model considering the correlation factor 1 with aqueous and surface complexes for enthalpy values (Table 33). Error bars that are not visible are smaller than the symbol size.

From these results, we conclude that the slight increase of U(VI) sorption with the increase of temperature can be quantitatively explained by considering a positive effect of temperature on the surface complexation reactions, which can “compensate” the same result predicted in solution thus resulting in a “null” effect. This positive effect cannot be explained by applying correlation factor of 1 for the enthalpy values (following the correlation of the stability constants for the surface and aqueous species proposed by Bradbury and Baeyens (2009)) and they must be fitted.

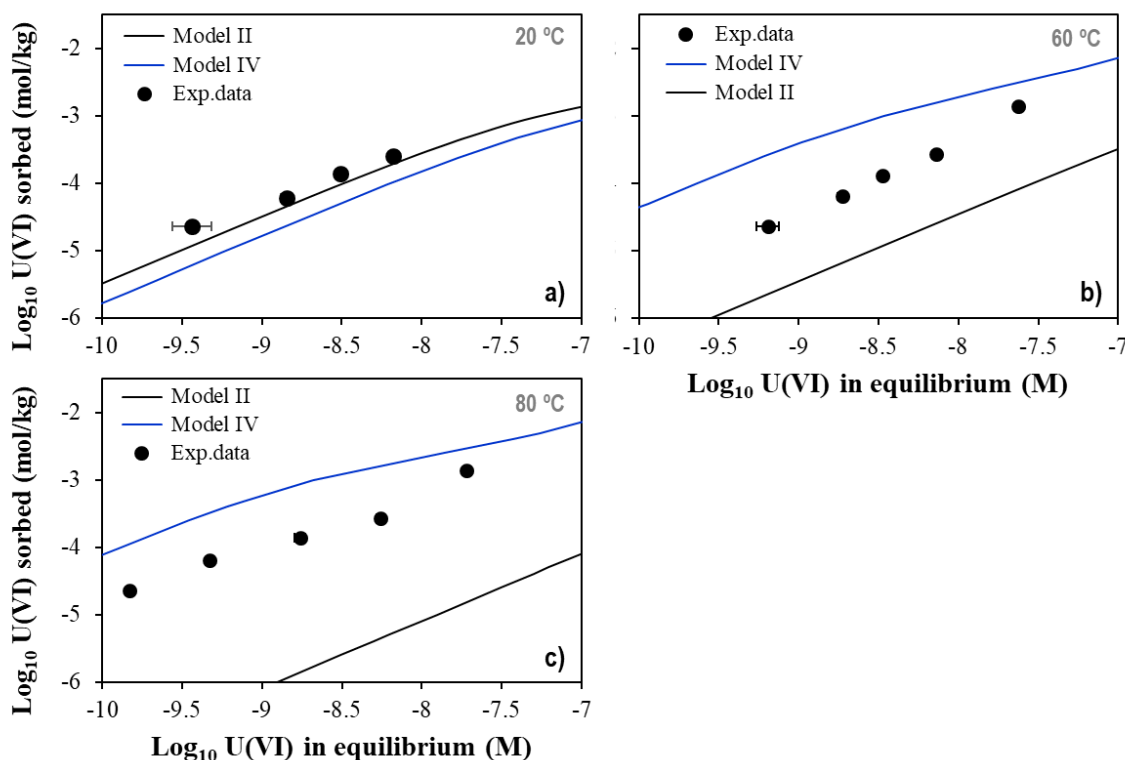


Figure 59. Model approach on sorption of isotherms of U(VI) in the absence of carbonates at a) 20 °C; b) 60 °C; and c) 80 °C. Model II: model approach without enthalpy values (see Chapter 3); Model IV: model approach considering the enthalpy values (see Table 33). Error bars that are not visible are smaller than the symbol size.

This fitting approach was done manually since PEST is not the most suitable tool, as it does not provide reliable fitting parameters as a consequence of the high number of equilibria reactions and

the limited number of experimental points. The procedure to determine the enthalpy values for the surface complexation reactions relies on five criteria:

- I. The surface speciation shown in Figure 60 was used as a guide for finding the best fit for: 1) $\equiv\text{S}^{\text{s}}\text{OUO}_2^+$ in $\text{pH} < 5$; 2) $\equiv\text{S}^{\text{s}}\text{OUO}_2\text{OH}$ between $\text{pH} 5$ and 6 ; and 3) $\equiv\text{S}^{\text{s}}\text{OUO}_2\text{O}(\text{OH})_2^-$ at $\text{pH} > 6$ together with the $\equiv\text{S}^{\text{s}}\text{OUO}_2(\text{OH})_2^-$. The iterative procedure was performed considering both the sorption edge and isotherm data. Note that since we only have the sorption isotherm of U(VI) at pH of $6.4\text{--}6.5$, the constants of $\equiv\text{S}^{\text{s}}\text{OUO}_2(\text{OH})_2^-$ and $\equiv\text{S}^{\text{s}}\text{OUO}_2(\text{OH})_3^{2-}$ will be relatively more reliable;
- II. The surface constants obtained in temperature must be correlated with those describing the formation of the corresponding aqueous species;
- III. The same enthalpy values are fixed for strong and weak sites when the surface species are similar (i.e. $\equiv\text{S}^{\text{s,w1}}\text{OUO}_2^+$ and $\equiv\text{S}^{\text{s,w1}}\text{OUO}_2\text{OH}$);
- IV. According to the van't Hoff equation, the complexation constants at different temperatures can be expressed as Equation 3ⁱ;

Since the surface standard constants for illite are known ($\log_{10} {}^{\text{OH}}K_x^\circ(25\text{ }^\circ\text{C})$, see Table 31), the Equation 3 can be readjusted to determine the enthalpy values for each surface species (Equation 10).

$$\log_{10} K_s^\circ(T) - \log_{10} K_s^\circ(T_0) = -\frac{\Delta_r H^\circ(T_0)}{R \ln 10} \left(\frac{1}{T} - \frac{1}{T_0} \right) \quad \text{Equation 10}$$

- V. Applying the enthalpy values should not significantly modify the modelling at 20°C with respect to that presented in Chapter 3.

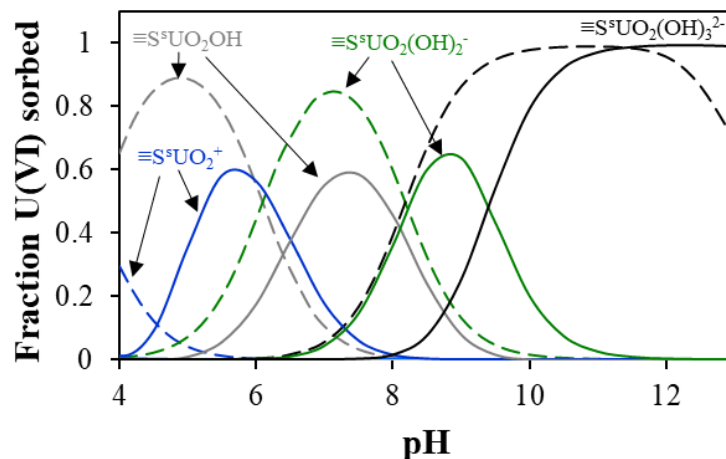


Figure 60. Distribution of U(VI) hydrolysis surface complexes of illite at 20°C (solid-lines) and 80°C (dashed-lines) as a function of the pH . Calculations taking the parameters given in Table 33.

The results of the fitting process considering the five previous criteria are presented in Table 34 and shown in Figure 61. The agreement between the model and the experimental data is good for both the sorption edge and isotherms data. For the sorption edges at 20 and 80°C and the sorption isotherms at 20°C the uncertainty of the surface constants was estimated to be ± 0.2 log units, whereas for the

ⁱ As reminder of Equation 2: $\log_{10} K_s^\circ(T) = \log_{10} K_s^\circ(T_0) - \frac{\Delta_r H^\circ(T_0)}{R \ln 10} \left(\frac{1}{T} - \frac{1}{T_0} \right)$

sorption isotherms at 60 and 80 °C the uncertainty was found to be ± 0.5 log units (in order to cover maximum number of experimental data).

Table 34. $\text{Log}_{10}^{\text{OH}K_x^{\circ}}$ fitted based on sorption edges and isotherms experiments performed at different temperatures for illite.

$\text{Log}_{10}K_x^{\circ}$	Sorption edges		Sorption Isotherms		
	20 °C	80 °C	20 °C	60 °C	80 °C
$\equiv\text{S}^{\circ}\text{OUO}_2^+$	1.3	1.7	1.3	1.9	1.7
$\equiv\text{S}^{\circ}\text{OUO}_2\text{OH}$	-3.3	-2.1	-3.3	-3.0	-2.1
$\equiv\text{S}^{\circ}\text{OUO}_2(\text{OH})_2$	-10.4	-7.2	-10.1	-8.6	-7.3
$\equiv\text{S}^{\circ}\text{OUO}_2(\text{OH})_3^{2-}$	-19.7	-14.3	-19.7	-16.5	-15.0

The correlation between the surface and the aqueous complexation constants obtained at different temperatures in the log-log scale is shown in Figure 62. This correlation is similar to the one shown in Figure 54 (compare solid-line for both Figure 54 and Figure 62), indicating that the second criterion is respected.

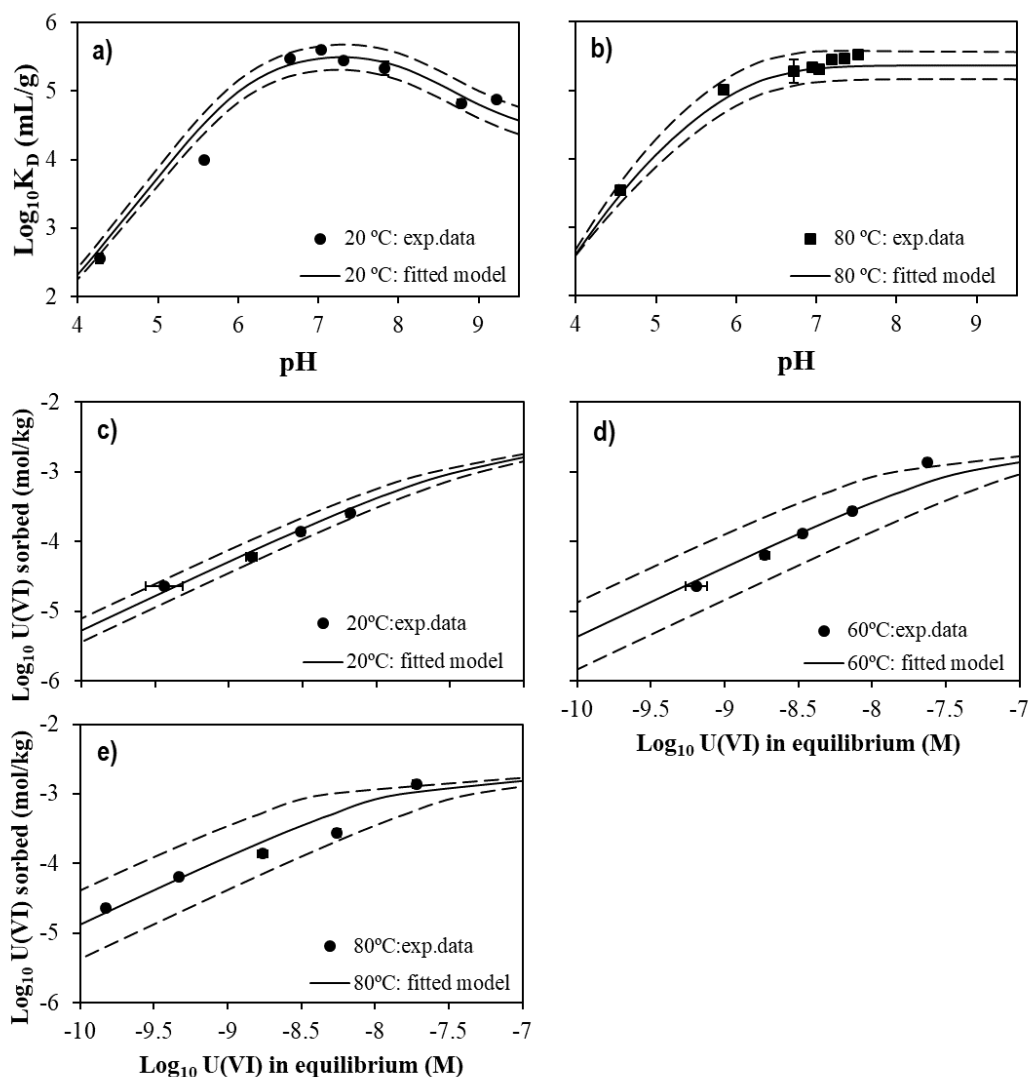


Figure 61. Fitting model for sorption edge experiments (a) at 20 °C and (b) at 80 °C (with ± 0.2 log units of uncertainty for the stability constants); for sorption isotherm experiments (c) at 20 °C (with ± 0.2 log units of uncertainty

for the stability constants); (d) at 60 °C and (e) at 80 °C (with ± 0.5 log units of uncertainty for the stability constants). Error bars that are not visible are smaller than the symbol size.

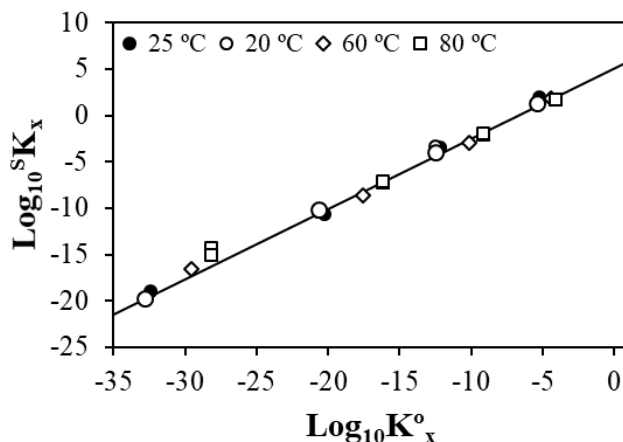


Figure 62. Relationship between $\text{Log}_{10}K_x^o$ of aqueous species and $\text{Log}_{10}^S K_x^o$ of surface complexes for illite determined at 20, 60 and 80°C in comparison with the respective standard stability constants at 25°C (solid-line) for illite reported by Bradbury and Baeyens (2009).

The dependency of constants with the temperature using the formalism described in Equation 10 is given in Figure 63. Despite the fact that the uncertainties for the constants are significantly high, especially for the surface species $\equiv S^S\text{OUO}_2^+$ and $\equiv S^S\text{OUO}_2\text{OH}$, globally the expected linear tendency is observed. The enthalpy values determined by the fitting are shown in Table 35.

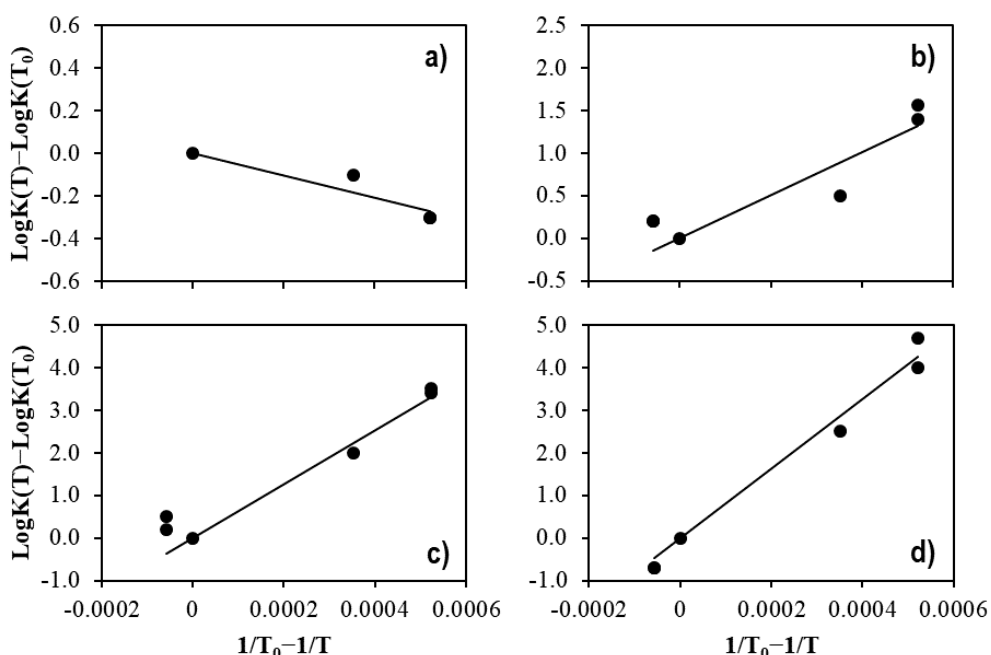


Figure 63. Relation of constant of hydrolysis surface complexation (T) and standard constant of hydrolysis surface complexation (T_0) as a function of the $1/T_0 - 1/T$ for the surface species a) $\equiv S^S\text{OUO}_2^+$, b) $\equiv S^S\text{OUO}_2\text{OH}$, c) $\equiv S^S\text{OUO}_2(\text{OH})_2^-$, and d) $\equiv S^S\text{OUO}_2(\text{OH})_3^{2-}$. Symbols: experimental data; Dashed-lines: regression line calculated for the enthalpy values.

The final results are given in Figure 64 using the enthalpy values for the hydrolysis surface complexes given Table 35. The agreement between the calculated and measured concentration of U(VI) is good if we consider the sorption isotherm data. For the sorption edge data, the model approach (Model V)

is not able to fully reproduce the behaviour of U(VI) as a function of pH, although an improvement is observed comparatively to when using Model IV, which considers the enthalpy values with a correlation factor of 1 (see Figure 58).

Table 35. Enthalpy values calculated from fitting of the stability constants of hydrolysis surface site species at different temperatures. The uncertainty was determined considering only the propagation error of the standard deviation of the stability constants.

Strong surface sites	$\Delta_r^{\text{OH}}H_x$ (kJ/mol)
$\equiv\text{S}^{\text{s}}\text{OUO}_2^+$	-10 (± 20)
$\equiv\text{S}^{\text{w1}}\text{OUO}_2^+$	-10 (± 20)
$\equiv\text{S}^{\text{s}}\text{OUO}_2\text{OH}$	48 (± 19)
$\equiv\text{S}^{\text{w1}}\text{OUO}_2\text{OH}$	48 (± 19)
$\equiv\text{S}^{\text{s}}\text{OUO}_2(\text{OH})_2$	121 (± 19)
$\equiv\text{S}^{\text{s}}\text{OUO}_2\text{O}(\text{OH})_3^{2-}$	156 (± 19)

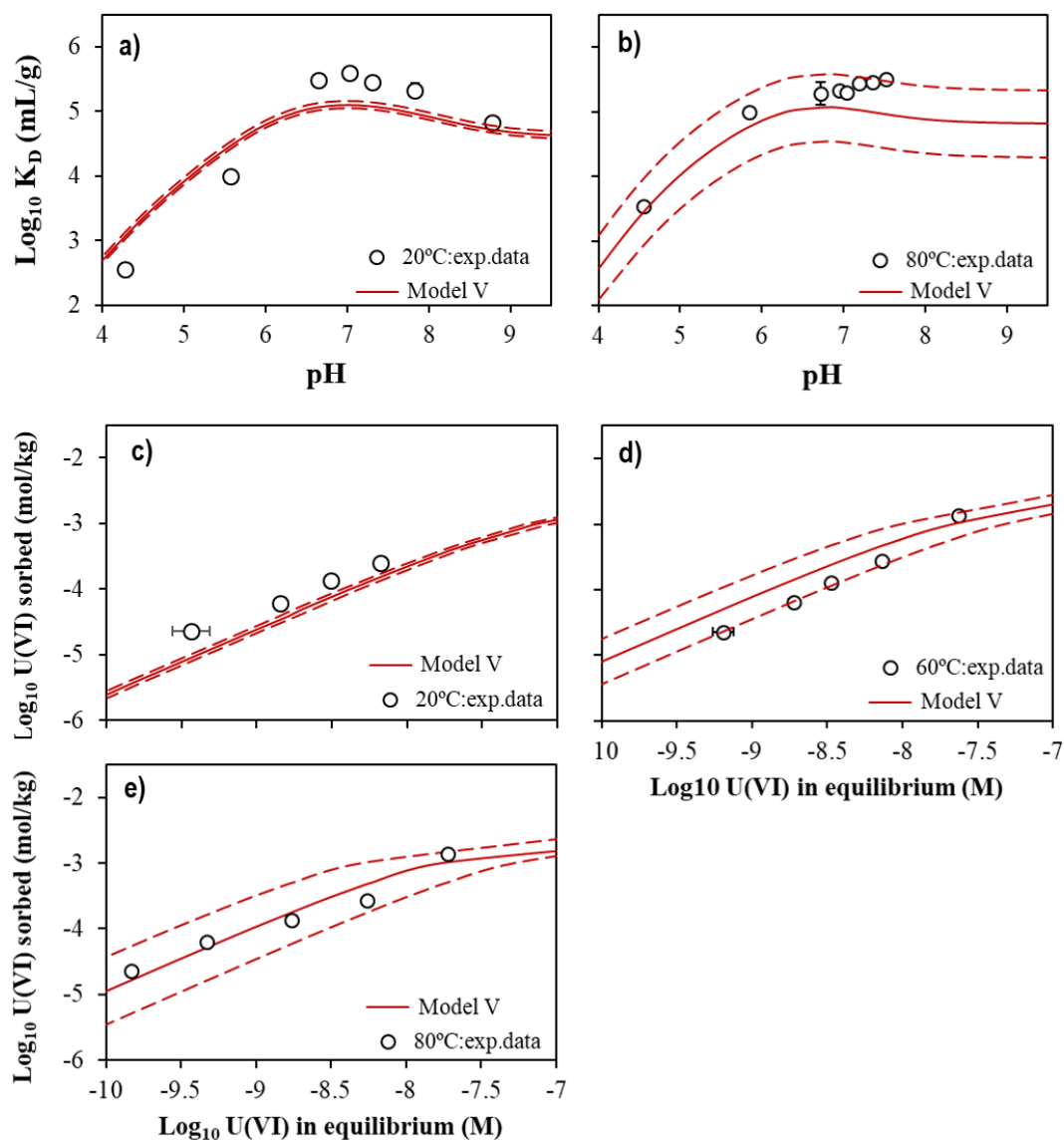


Figure 64. Symbols: measured experimental data from sorption edge and isotherm of U(VI) at different temperatures. Solid-lines: calculated U(VI) concentration using enthalpy values calculated from Table 35. Dashed-lines

correspond to the uncertainty of the enthalpy values. Error bars that are not visible are smaller than the symbol size.

In summary, the temperature effect on the retention of U(VI) on illite in the absence of carbonates can be explained by considering an endothermic effect to describe the surface complexation reactions between U(VI) and U(VI) hydrolysis species with the strong and weak sites present at the illite surface. The next step is to apply Model V to conditions where carbonate complexes are formed to study their behaviour in temperature. These data will also allow us to assess the potential impact of the contamination of carbonates, found in the experiments performed under inert atmosphere, on the parameters proposed in Table 35.

4.2.3.2. In the presence of carbonate

Experimental data:

We performed the sorption edge experiments in atmospheric $p\text{CO}_2$ at 80 °C in 0.1 M of NaCl and the initial concentration of U(VI) was set at $3.3 \cdot 10^{-8}$ M (Figure 65). The alkalinity titration and pH measurements were done before and after the equilibrium and the results are provided in Table 36. The results indicate that the alkalinity does not change significantly with the increase of temperature, whereas the pH slightly decreases with the increase of temperature. The corresponding calculated $p\text{CO}_2$ shows that the equilibrium is not completely reached for most pH values.

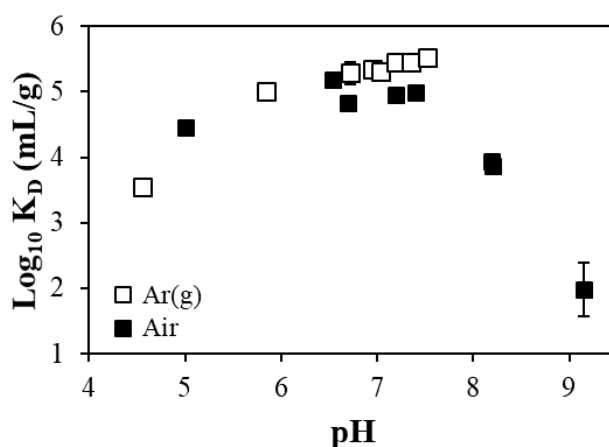


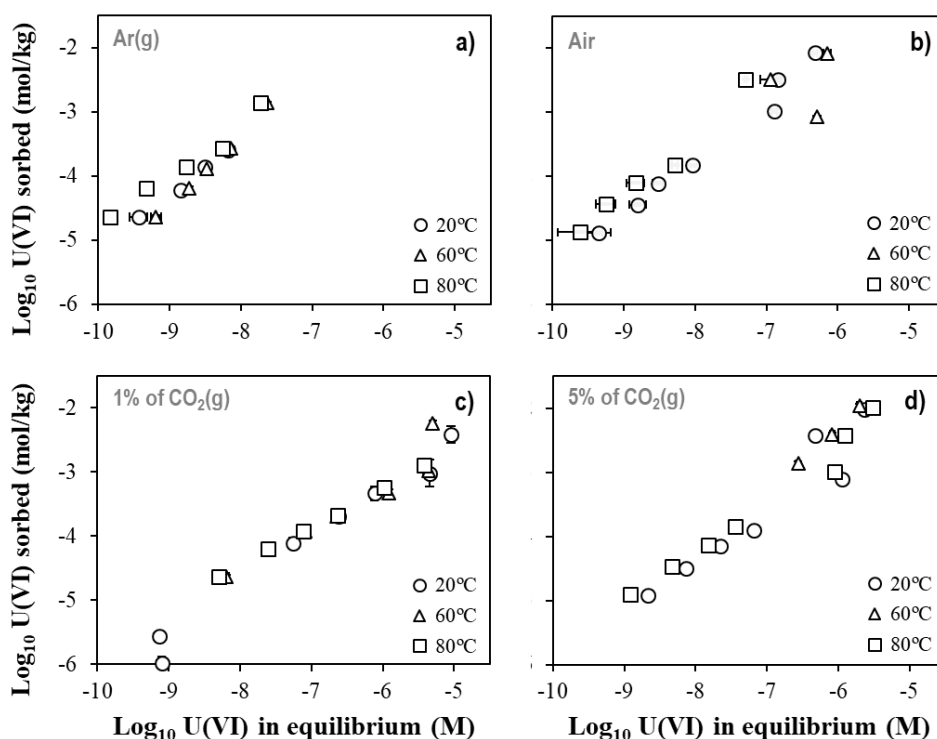
Figure 65. Distribution coefficient of U(VI) as a function of the pH in 0.1 NaCl a) in the absence or presence of carbonates in equilibrium with $p\text{CO}_2$ atmospheric at 80 °C. Error bars that are not visible are smaller than the symbol size.

The sorption of U(VI) appears similar at 80 °C for the experiments performed in the presence or absence of carbonates when the pH is below 7.5 (Figure 65). For $\text{pH} > 7.5$, a decrease of the sorption is observed resulting from the formation of strong complexes that stabilise U(VI) in solution. This indicates a weak influence from surface speciation on the retention at 80°C. In comparison, at 20 °C and above pH 6 we observed a significant difference on the retention of U(VI) between the experiments performed in inert atmosphere and those performed in atmospheric $p\text{CO}_2$ (see Figure 37 in Chapter 3).

Table 36. Alkalinity and pH measurements before and after the equilibrium with illite at 80 °C. pCO₂ calculated from the equilibrium pH/alkalinity.

pH _{initial} 20 °C	Alkalinity _{initial} meq/L	pH _{final} 80 °C	Alkalinity _{final} meq/L	pH _{final} 20 °C	pCO ₂ calculated ⁱ
3.9	0	5.0	0		
6.1	0.036 (± 0.02)	6.5	0.036 ⁱⁱ (± 0.02)		-2.82/-3.39
		6.8			-2.18/-2.55
7.4	0.17 (± 0.07)	7.2	0.25 (± 0.1)	7.7	-2.69/-3.07
		7.4			-2.92/-3.31
		8.2			-2.87/3.25
8.5	2.5 (± 0.5)	8.2	2.5 (± 1.0)	8.8	-2.89/-3.27
9.31	18.1 (± 7.3)	9.2	18.5 (± 7.4)	9.3	-3.54/-3.94

The sorption isotherms of U(VI) in equilibrium with different pCO₂ at different temperatures are shown in Figure 66. The alkalinity of the solution is the same at pCO₂ of 1 or 5% of CO₂(g) but the pH of equilibrium is lower at 5% of CO₂(g). The calculations indicate a water/gas system close to equilibrium (taking into account the uncertainty of the alkalinity titration measurements, see Table 37). A qualitative analysis indicates that temperature changes do not have a strong effect, and when observed this effect is slightly positive (i.e. there is a increase on the retention of U(VI) with the increase of temperature).


Figure 66. Sorption isotherms of U(VI) on illite at different temperatures in equilibrium with a) Ar(g); b) pCO₂ at atmospheric; c) pCO₂ of 1% of CO₂(g); and d) pCO₂ of 5% of CO₂(g). Error bars that are not visible are smaller than the symbol size.

ⁱ Calculations in Phreeqc from the equilibrium between pH and alkalinity measured after the equilibrium with illite; maximum and minimum pCO₂ considering the uncertainty of alkalinity measurements

ⁱⁱ Alkalinity measured before the beginning of the experiment

Table 37. pH of equilibrium and alkalinity measurements in the presence of carbonates at 60 and 80°C.

Atmosphere	Temperature °C	pH	Alkalinity (meq/L)	pCO ₂ calculated ⁱ
Ar(g)	60	6.4 (±0.1)	0.08 (±0.03)	-2.5/-2.8
	80	6.5 (±0.2)	0.08 (±0.03)	-2.5/-2.9
Air	60	7.5 (±0.1)	0.84(±0.3)	-2.6/-2.9
	80	7.5 (±0.1)	0.2(±0.1)	-3.1/-3.5
1% CO ₂ (g)	60	7.5 (±0.03)	2.5(±1.0)	-2.0/-2.4
	80	7.6 (±0.03)	2.4(±0.9)	-2.2/-2.6
5% CO ₂ (g)	60	6.8 (±0.01)	2.5(±1)	-1.4/-1.7
	80	7.0 (±0.02)	2.4(±0.9)	-1.5/-1.9

Modelling Results:

The behaviour of U(VI) in solution was first studied by blind modelling prediction for atmospheric pCO₂. The results are presented in Figure 67 at 20 °C (solid-lines) and 80 °C (dashed-lines). An important observation is that the presence of uranyl-carbonate aqueous complexes is much less relevant for pH < 7 at 80 °C as compared to 20 °C. The temperature increasing favours the formation of hydrolysis species in detriment of carbonate ones. For example, at pH 7 the proportion of carbonate complexes changes from 60% to 10% for 20 and 80 °C, respectively. Above pH 7 the U(VI) speciation is governed by the UO₂(CO₃)₃⁴⁻ at 20 °C and UO₂(OH)₃⁻ at 80 °C.

The distribution of the U(VI) speciation can explain qualitatively the sorption experiments, indicating that at pH >7 the retention decreases (as at 20 °C) due to the formation of U(VI)-CO₃ complexes, even if that retention is small (compare orange and blue dashed-lines in Figure 67 with symbols in Figure 68). Below pH 7, the presence of carbonates does not influence the retention since U(VI) speciation is dominated by the hydrolysis species (see green dashed-line in Figure 67 and symbols in Figure 68).

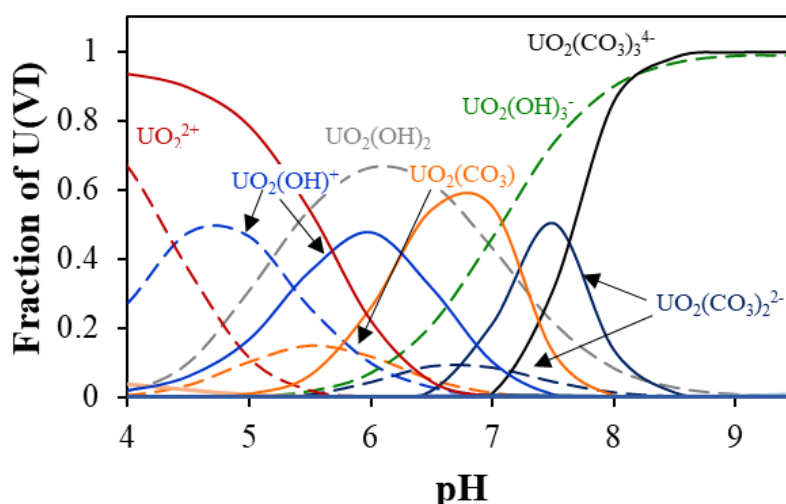


Figure 67. Distribution of the speciation U(VI) in solution as a function of the pH at 20 (solid-lines) and 80 °C (dashed-lined) in equilibrium with pCO₂ atmospheric.

ⁱ Calculations in Phreeqc from the equilibrium between pH and alkalinity measured after the equilibrium with illite; maximum and minimum pCO₂ considering the uncertainty of alkalinity measurements

Based on these results, we propose to model firstly the data considering only a temperature effect on the surface hydrolysis complexes, i.e. Model V (see above Table 35). These modelling results correspond to the red solid-lines in Figure 68 and Figure 69.

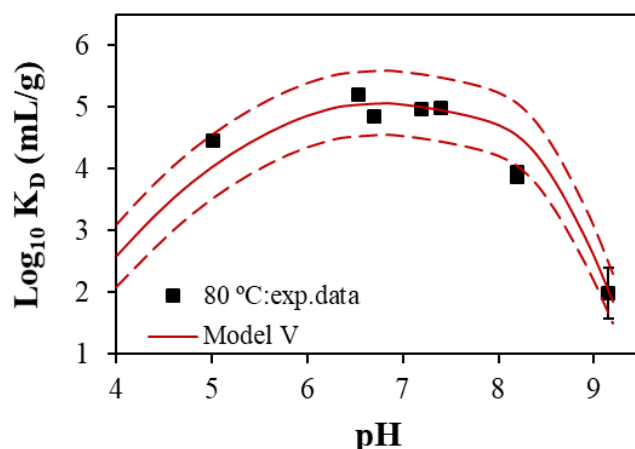


Figure 68. Sorption edge of U(VI) in equilibrium with $p\text{CO}_2$ atmospheric. Model V: enthalpy values considered only for hydrolysis surface complexation reactions (Table 35).

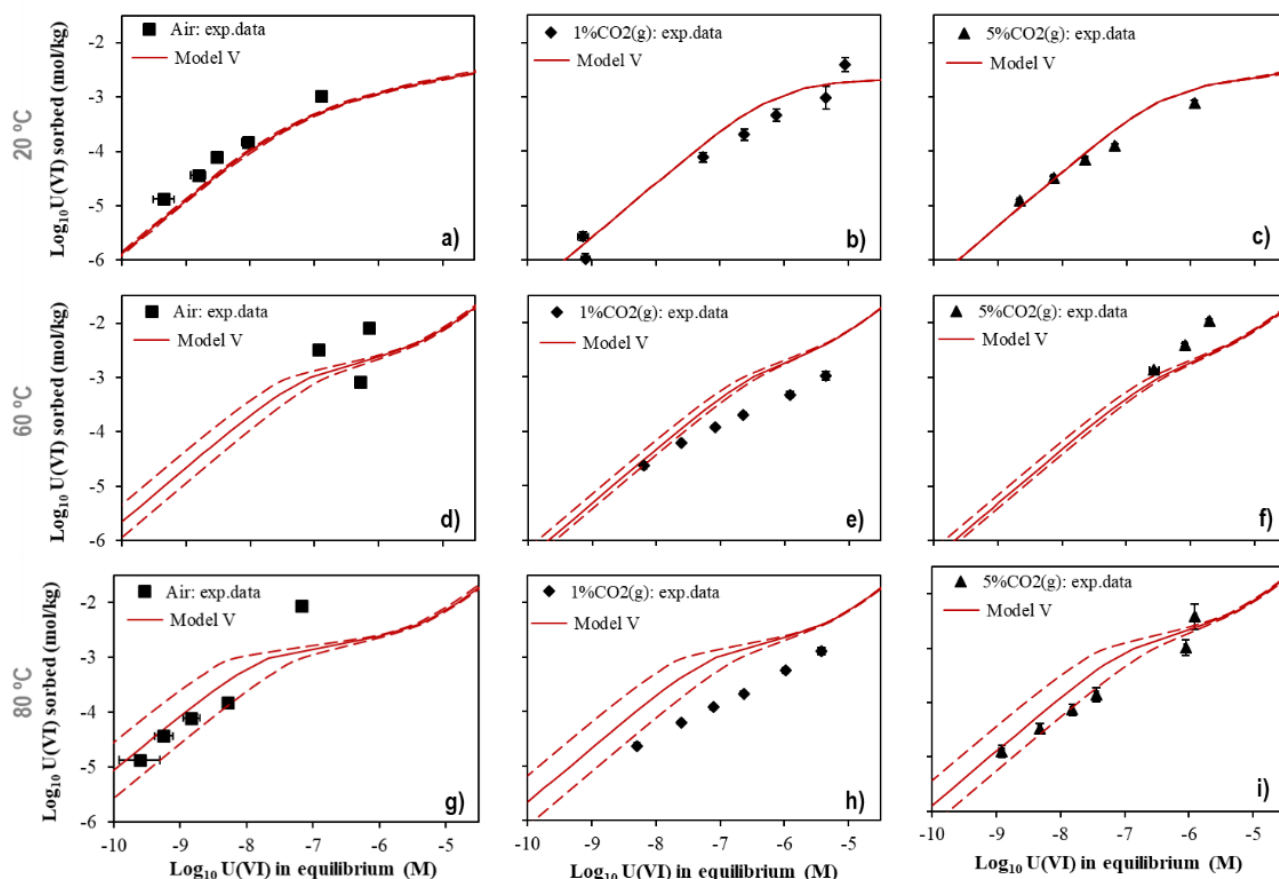


Figure 69. Model approach considering only the enthalpy of the hydrolysis of surface complexes at different temperatures in the presence of carbonates (see Table 35). Dashed-lines correspond to the uncertainty of the enthalpy values of the hydrolysis surface complexes.

Overall, the agreement between the calculation (modelling) and the experimental data is acceptable. The presence of trace amounts of carbonates for the experiments performed in inert atmosphere does not affect the modelling results. The model can reproduce well the pH-edge for atmospheric $p\text{CO}_2$

but it overestimates the retention for the isotherms obtained in temperature in the presence of CO₂, particularly at 80 °C. The analysis of the surface speciation below pH 7 (thus including the isotherm in concentration) indicates that the retention is governed by the surface hydrolysis species. At this point and in agreement with the qualitative analysis of the data presented in Figure 66, we can conclude that the surface carbonate complexes do not play any role on the sorption of U(VI) at 60 and 80°C and there is consequently no reason to consider a temperature effect on the formation of such surface complexes.

In conclusion, we propose from here to use Model V and to assess its ability to explain sorption data in temperature in the context of the Callovo-Oxfordian clay fraction and claystone natural samples.

4.2.4. U(VI)/ Callovo-Oxfordian clay fraction system at 80°C

In the present work we have also studied the increase in complexity of the mineral assemblage in temperature. As mentioned in the previous chapter, at 20 °C the sorption of U(VI) slightly changes in the presence of the different clay minerals. In this section, we study the behaviour of U(VI) on clay fraction of Callovo-Oxfordian formation at 80°C for different solution compositions (see Table 30), focusing on the measure of sorption isotherms in concentration of U(VI) only.

The experimental results on the sorption isotherms of U(VI) at 80 °C in the absence or presence of carbonates (in equilibrium with 5% of CO₂(g)) are shown in Figure 70a and b. The pH and alkalinity measurements performed at the end of the experiments are provided in Table 38. The results indicate that there is a contamination of carbonates in the “inert” system. As compared to the previous experiments (U(VI)/illite system, Table 32) where the alkalinity was relatively small with high uncertainties, the alkalinity here appears relevant, and as such it was considered in the modelling analysis.

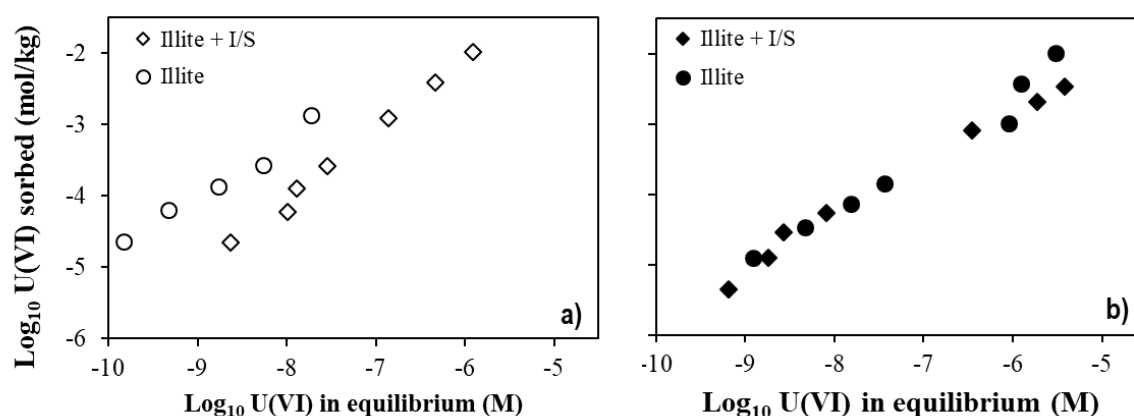


Figure 70. Sorption isotherms of U(VI) on illite and Callovo-Oxfordian clay fraction (illite + I/S) system at 80 °C a) in the absence of carbonates and b) in the presence of carbonates in equilibrium with pCO₂ of 5% of CO₂(g).

As already observed at 20 °C, in the absence of carbonates the sorption of U(VI) decreases for the clay fraction (Figure 70a) as compared to illite, whereas in the presence of carbonates, no significant differences are observed between the illite system or the clay fraction system (Figure 70b).

Table 38. pH and alkalinity measurements in equilibrium for the sorption isotherms on clay fraction at 80 °C in different atmospheres.

Atmosphere	pH _{final}	Alkalinity (meq/L)	pCO ₂ calculated ⁱ
Ar(g)	7.2 (± 0.1)	0.22 (± 0.1)	-2.8/-3.2
5 % of CO ₂ (g)	7.2 (± 0.02)	2.2 (± 0.9)	-1.8/-2.2

By comparing the experimental data at 20 and 80°C in the presence or absence of carbonates we can conclude that the temperature effect is not significant, as it was previously observed for illite (Figure 71a, b).

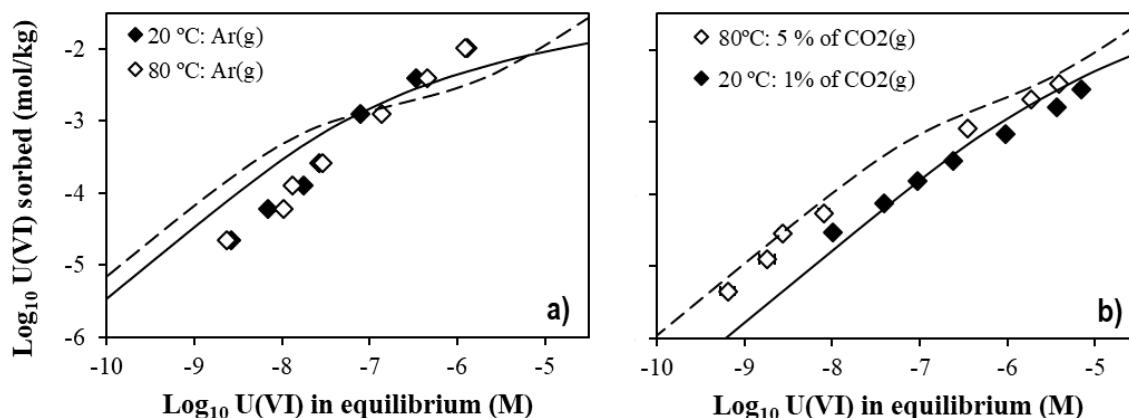


Figure 71. Model approach for describing the sorption isotherms of U(VI) on Callovo-Oxfordian clay fraction (illite + I/S) at 20 and 80 °C a) in the absence and b) in the presence of carbonates in equilibrium with 1% and 5% of CO₂(g), respectively. Taking the thermodynamic parameters for illite and montmorillonite (see Table 39) the solid-lines correspond to the model prediction at 20°C; and the dashed-lines correspond to the model prediction at 80 °C.

As reported by Bradbury and Baeyens (2009), illite and montmorillonite are reactively similar. Thus, the same thermodynamic considerations were considered for both clay minerals. The thermodynamic parameters that we considered to describe the retention of U(VI) on the Callovo-Oxfordian clay fraction are given in Table 39.

Table 39. Enthalpy values for the hydrolysis surface complexation reactions for illite and montmorillonite considered in the present study.

SURFACE COMPLEXATION REACTIONS	Illite		Montmorillonite	
	log ₁₀ K	Δ _r H kJ/mol	log ₁₀ K	Δ _r H kJ/mol
≡S ^s OH+UO ₂ ²⁺ ⇌ ≡S ^s OUO ₂ ⁺ +H ⁺	2.0	-10		-10
≡S ^{w1} OH+UO ₂ ²⁺ ⇌ ≡S ^{w1} OUO ₂ ⁺ +H ⁺	0.1	-10		-10
≡S ^s OH+UO ₂ ²⁺ +H ₂ O ⇌ ≡S ^s OUO ₂ OH+2H ⁺	-3.5	48		48
≡S ^{w1} OH+UO ₂ ²⁺ +H ₂ O ⇌ ≡S ^{w1} OUO ₂ OH+2H ⁺	-5.3	48		48
≡S ^s OH+UO ₂ ²⁺ +2H ₂ O ⇌ ≡S ^s OUO ₂ (OH) ₂ +3H ⁺	-10.6	121		121
≡S ^s OH+UO ₂ ²⁺ +3H ₂ O ⇌ ≡S ^s OUO ₂ (OH) ₃ ²⁻ +4H ⁺	-19	156		156
≡S ^s OH+UO ₂ ²⁺ +CO ₃ ²⁻ ⇌ ≡S ^s OUO ₂ CO ₃ ⁻ +H ⁺	n.a.	n.a.	9.8	0
≡S ^{w1} OH+UO ₂ ²⁺ +CO ₃ ²⁻ ⇌ ≡S ^{w1} OUO ₂ CO ₃ ⁻ +H ⁺	n.a.	n.a.	9.3	0
≡S ^s OH+UO ₂ ²⁺ +2CO ₃ ²⁻ ⇌ ≡S ^s OUO ₂ (CO ₃) ₂ ²⁻ +H ⁺	17.5	0	15	0

ⁱ Calculations in Phreeqc from the equilibrium between pH and alkalinity measured after the equilibrium with illite; maximum and minimum pCO₂ considering the uncertainty of alkalinity measurements

Overall, the model can explain relatively well the experimental results, especially in the presence of carbonates at 20 and 80°C. In the absence of carbonates, the model approach overestimates the sorption for tracer concentrations of U(VI) ($< 10^{-7}$ M).

In conclusion, the use of the enthalpy values for illite appears applicable to montmorillonite. In the conditions of interest for the Callovo-Oxfordian formation regarding pH and alkalinity, the temperature increase will favour the predominance of hydrolysis species with respect to carbonato complexes, both in solution and at the surface. In the following section we will assess and discuss the impact of the presence of ternary complexes on retention in temperature.

4.2.5. Impact of Ca-U(VI)-CO₃ on the retention of U(VI) at 80 °C

We performed the sorption isotherms experiments in concentration on illite, CO_x clay fraction and natural samples at 80 °C in equilibrium with synthetic CO_x porewater. The sorption experiments were performed in closed atmosphere with 1% of CO₂(g) for experiments at 20 °C and 5% of CO₂(g) for experiments at 80 °C and the synthetic porewater was prepared following the composition given in Table A. 2. The pH of equilibrium and alkalinity measurements for each case are provided in the Table 40.

Table 40. Experimental pH and alkalinity measurements at 20 and 80 °C for illite, Callovo-Oxfordian clay fraction and claystone samples in synthetic Callovo-Oxfordian porewater in equilibrium with 1% and 5% of CO₂(g), respectively.

	Temperature	Atmosphere	pH	Alkalinity (meq/L)	pCO ₂ calculated ⁱ
Illite	20 °C	1% CO ₂ (g)	7.1 (± 0.02)	2.5 (± 0.1)	-2.06/-2.09
	80 °C	5% CO ₂ (g)	6.8 (± 0.01)	2.2 (± 0.8)	-1.4/-1.8
Clay fraction	20 °C	1% CO ₂ (g)	7.1 (± 0.02)	2.4 (± 0.9)	-2.3/-1.9
	80 °C	5% CO ₂ (g)	7.1 (± 0.04)	3.4 (± 1.3)	-1.8/-1.5
Claystone	20 °C	1% CO ₂ (g)	7.5 (± 0.01)	3.3 (± 1.3)	-2.7/-2.2
	80 °C	5% CO ₂ (g)	7.0 (± 0.01)	1.4 (± 0.8)	-2.3/-1.7

The experimental results show that the temperature increase leads to an increase in the sorption capacity of U(VI) in all cases. The K_D of illite increases from 37 (± 9) to 153 (± 47) mL/g; for CO_x clay fraction it increases from 78 (± 39) to 157 (± 50) mL/g and for CO_x natural samples, the K_D increases from 0.5 (± 1) to 263 (± 31) mL/g (see symbols in Figure 72). The temperature effect is more pronounced for CO_x natural samples, where the sorption capacity increases more than two orders of magnitude. We found that the difference in pH/alkalinity between the two temperatures is the highest for the Callovo-Oxfordian system.

We applied the model approach proposed in this work to the different solid phases (illite, clay fraction and claystone natural samples), and the results are shown in Figure 72 (solid- and dashed-lines). This model approach can explain the tendency for the presence of an endothermic character of U(VI)

ⁱ Calculations in Phreeqc from the equilibrium between pH and alkalinity measured after the equilibrium with illite; maximum and minimum pCO₂ considering the uncertainty of alkalinity measurements

sorption when the temperature increases, although with a slight overestimation for U(VI)/illite system and U(VI)/clay fraction at 80°C.

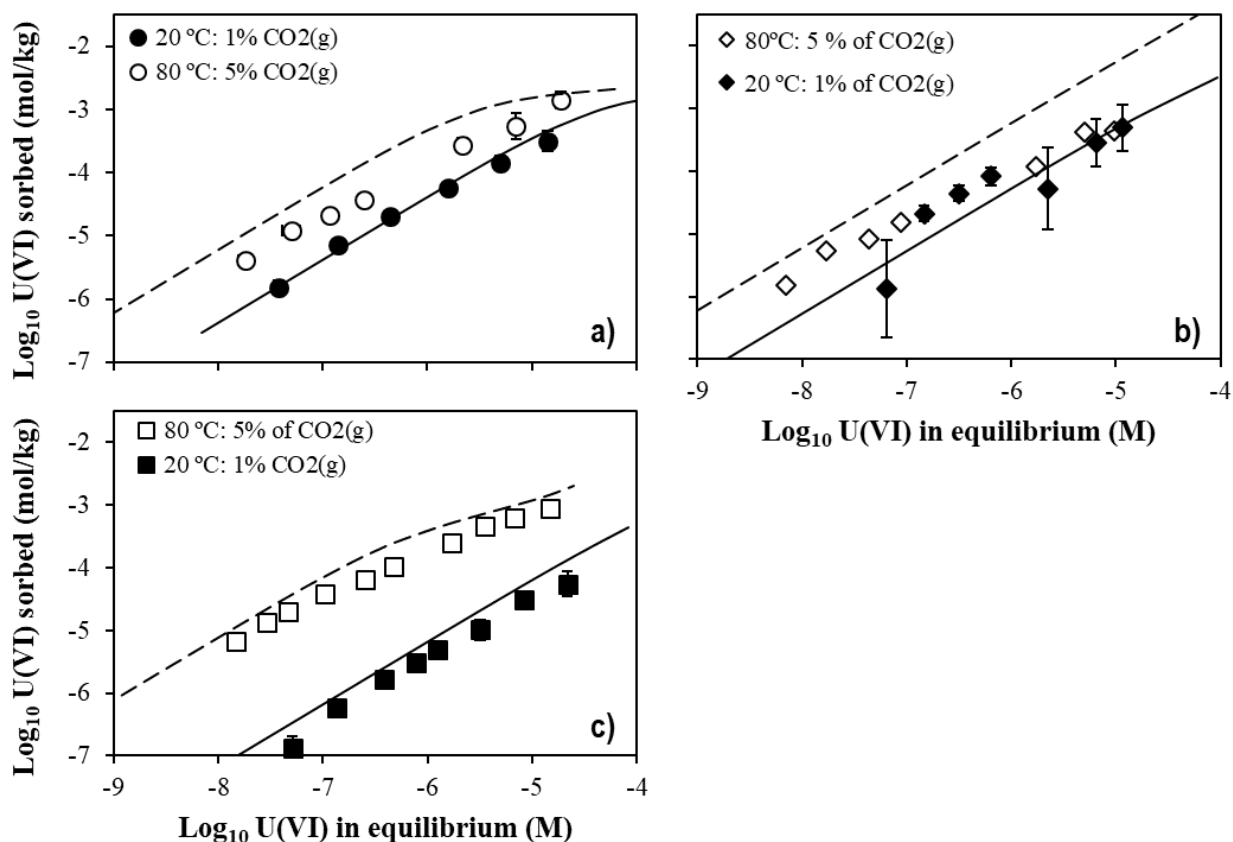


Figure 72. Sorption isotherms of the U(VI) in synthetic porewater performed at 20 and 80 °C for a) U(VI)/illite system; b) U(VI)/ Callovo-Oxfordian clay fraction system; and c) U(VI)/ Callovo-Oxfordian claystone system. Model approach considering thermodynamic data for surface reactions from Table 39 and using the thermodynamic data for Ca-U(VI)-CO₃ aqueous complexes (see Table 14). Solid-line: model at 20 °C; dashed-line: model at 80°C.

In conclusion, the model that we propose, which considers the enthalpy values for the surface complexation reactions for both illite and montmorillonite, can predict relatively well the behaviour of U(VI) in different systems in the presence of Ca-U(VI)-CO₃ ternary complexes (Figure 73).

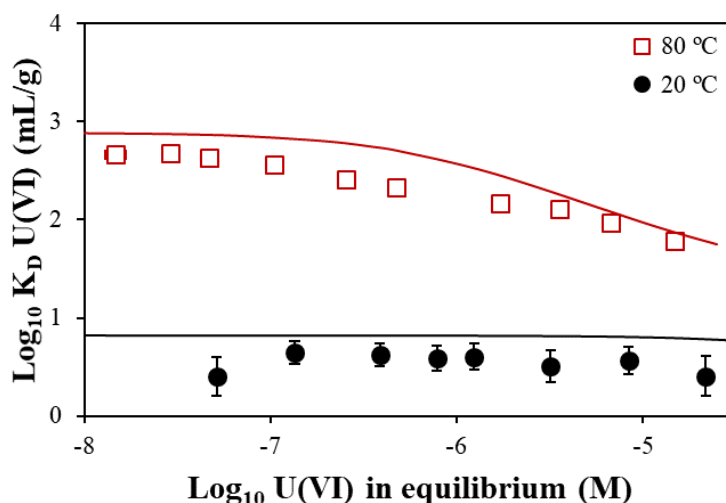


Figure 73. Impact of the temperature on the distribution coefficient of U(VI) as a function of the concentration of U(VI) in equilibrium in Callovo-Oxfordian claystone system. (●) and (□) experimental data from the present work.

red-line: model approach at 80 °C considering the model approach proposed in the present study and the thermodynamic parameters of U(VI) aqueous speciation (Table 14).

A summary of the most relevant aqueous and surface complexation reactions is given in Table 41 for the U(VI)/Callovo-Oxfordian system. Although the formation of ternary complexes is not favoured in temperature these are still the dominant species at 80 °C in solution. In contrast, at the surface at 20 °C the sorption is dominated by the carbonate surface complex species whereas at 80°C the surface hydrolysis species are dominant. Moreover, the clay fraction, including both illite and illite from I/S interstratified clay, represents the main reactive surface at both temperatures.

It is interesting to note that Joseph and co-workers (2013) suggested that this increase in retention with temperature was due to the formation of U(VI) colloids which are formed when the temperature increases. In the present study, we did not evaluate the possible formation of colloids; although, based on ICP-MS analysis of the blank solutions we do not have evidences of their occurrence. However, we can expect a possible precipitation of U(VI) phases based on the evaluation of the geochemical calculations using the thermodynamic database available.

Table 41. Aqueous and surface speciation at 20 and 80°C for the Callovo-Oxfordian formation system in equilibrium with synthetic porewater for [U(VI)] = 10⁻⁷M.

	20 °C		80 °C	
	Total	main species	Total	main species
Aqueous species	61 %	CaUO ₂ (CO ₃) ₃ ²⁻	81%	5 %
		Ca ₂ UO ₂ (CO ₃) ₃ (aq)	17%	Ca ₂ UO ₂ (CO ₃) ₃ (aq)
Surface complexes	39 %	≡S _{illite} ^s OUO ₂ (CO ₃) ₂ ³⁻	33%	95 %
		≡S _{mont} ^{w1} OUO ₂ CO ₃ ⁻	4%	Hydrolysis surface complexes of illite

4.3. Summary

The behaviour of U(VI) sorption in temperature was studied from the simplest clay system (illite) to the most complex (with Callovo-Oxfordian claystone mineralogical assemblage), where the pH, the pCO₂ and solution composition were changed.

As already observed for the different conditions presented in Chapter 2, the control of the pH/alkalinity at a given pCO₂ is not straightforward, affecting more the experiments performed as a function of the pH. For modelling purposes, in the experiments at constant pH, the pCO₂ was never fixed, it was instead freely controlled by the pH and alkalinity measurements, even though we are aware that the uncertainty of the alkalinity analysis is usually high and small changes of the alkalinity values can lead to different results. Although, we recommend that the pCO₂ should be fixed at pH > 7.5.

A main conclusion of this study is that the effect of temperature on the sorption of U(VI) is almost negligible for ionic strength of 0.1 M, using NaNO₃ or NaCl as electrolyte background, for both edge- and planar-surfaces of illite. This is in contradiction with the strong effect of the temperature expected in solution, based on the thermodynamic data available (ThermoChimie database, Giffaut et al.,

2014). Indeed, the formation of the aqueous complexes (specially the hydrolysis complexes) are favoured in temperature and this would then lead to a decrease of the retention.

To allow a quantitative explanation of the data, it is therefore necessary to consider also an endothermic effect of surface complexes in order to counterbalance the aqueous chemistry effect. We cannot explain the data by applying directly the enthalpy values of aqueous species to the corresponding surface species as the model always overestimates the experimental data. We therefore fitted the enthalpy values from the experimental data following a stepwise approach with constraints (taking the van't Hoff equation and the linear correlation between the aqueous and surface speciation).

We can obtain a relatively good agreement between the model and the experimental data when considering the fitted enthalpy values associated to the hydrolysis species. We do not need to consider an endothermic effect for surface carbonate species, which are not favoured with an increase in temperature, provided that the pH remains below 7. We provide a summary of the final surface parameters used for the model approach in Table 42.

Thus, the model developed for illite can apply satisfactorily to COx clay fraction and COx claystone natural samples, in both the case of absence or presence of the Ca-U(VI)-CO₃ ternary complexes.

It is clear that the uncertainties associated to the enthalpy values are high and, in the present work, they were estimated using “manual” fitting, as more robust data can be obtained by increasing the number of experimental data. Nevertheless, the model reproduces the Callovo-Oxfordian conditions and can be applied to predict *in situ* conditions.

Table 42. Proposed thermodynamic parameters for the surface complexation reactions considered in the model approach.

	Illite		Montmorillonite	
	log ₁₀ K	Δ _r H kJ/mol	log ₁₀ K	Δ _r H kJ/mol
CATIONIC EXCHANGE REACTIONS				
2XNa + Ca ²⁺ ⇌ X ₂ Ca + 2Na ⁺	1.04	n.a.	0.61	n.a.
2XNa + UO ₂ ²⁺ ⇌ X ₂ UO ₂ ²⁺ + 2Na ⁺	0.65	n.a.	0.15 ^{b)}	n.a.
2XNa + Mg ²⁺ ⇌ X ₂ Mg + 2Na ⁺	1.04	n.a.	0.34	n.a.
2XNa + Fe ²⁺ ⇌ X ₂ Fe + 2Na ⁺	0.8	n.a.	0.8	n.a.
2XNa + Sr ²⁺ ⇌ X ₂ Sr + 2Na ⁺	0.8	n.a.	1.0	n.a.
XNa + K ⁺ ⇌ XK + Na ⁺	1.1	n.a.	0.6	n.a.
PROTOLYSIS REACTIONS				
≡ S ^s OH + H ⁺ ⇌ ≡ S ^s OH ₂ ⁺	4.0 ^{a)}	n.a.	4.5 ^{b)}	n.a.
≡ S ^s OH ⇌ ≡ S ^s O ⁻ + H ⁺	-6.2 ^{a)}	n.a.	-7.9 ^{b)}	n.a.
≡ S ^{w1} OH + H ⁺ ⇌ ≡ S ^{w1} OH ₂ ⁺	4.0 ^{a)}	n.a.	4.5 ^{b)}	n.a.
≡ S ^{w1} OH ⇌ ≡ S ^{w1} O ⁻ + H ⁺	-6.2 ^{a)}	n.a.	-7.9 ^{b)}	n.a.
≡ S ^{w2} OH + H ⁺ ⇌ ≡ S ^{w2} OH ₂ ⁺	8.5 ^{a)}	n.a.	6.0 ^{b)}	n.a.
≡ S ^{w2} OH ⇌ ≡ S ^{w2} O ⁻ + H ⁺	-10.5 ^{a)}	n.a.	-10.5 ^{b)}	n.a.
SURFACE COMPLEXATION REACTIONS				
≡ S ^s OH + UO ₂ ²⁺ ⇌ ≡ S ^s OUO ₂ ⁺ + H ⁺	2.0 ^{a)}	-10 (±20)*	3.1 ^{e)}	0 (±20)*
≡ S ^s OH + UO ₂ ²⁺ + H ₂ O ⇌ ≡ S ^s OUO ₂ OH + 2H ⁺	-3.5 ^{a)}	48 (±19)*	-3.4 ^{e)}	48 (±19)*
≡ S ^s OH + UO ₂ ²⁺ + 2H ₂ O ⇌ ≡ S ^s OUO ₂ (OH) ₂ + 3H ⁺	-10.6 ^{a)}	121 (±19)*	-11 ^{e)}	121 (±19)*
≡ S ^s OH + UO ₂ ²⁺ + 3H ₂ O ⇌ ≡ S ^s OUO ₂ (OH) ₃ ²⁻ + 4H ⁺	-19 ^{a)}	156 (±19)*	-20.5 ^{e)}	156 (±19)*
≡ S ^{w1} OH + UO ₂ ²⁺ ⇌ ≡ S ^{w1} OUO ₂ ⁺ + H ⁺	0.1 ^{d)}	0*	0.7 ^{e)}	0*

	Illite		Montmorillonite	
	$\log_{10} K$	$\Delta_r H$ kJ/mol	$\log_{10} K$	$\Delta_r H$ kJ/mol
$\equiv S^{w1}OH + UO_2^{2+} + H_2O \rightleftharpoons \equiv S^{w1}OUO_2OH + 2H^+$	-5.3 ^{d)}	0*	-5.7 ^{e)}	0*
$\equiv S^sOH + UO_2^{2+} + CO_3^{2-} \rightleftharpoons \equiv S^sOUO_2CO_3 + 2H^+$	n.a.*	n.a.*	9.8 ^{d)}	0*
$\equiv S^sOH + UO_2^{2+} + 2CO_3^{2-} \rightleftharpoons \equiv S^sOUO_2(CO_3)_2 + H^+$	17.5 (± 0.5)*	0*	15 ^{d)}	0*
$\equiv S^{w1}OH + UO_2^{2+} + CO_3^{2-} \rightleftharpoons \equiv S^{w1}OUO_2CO_3 + 2H^+$	n.a.*	n.a.*	9.3 ^{d)}	0*

a) Bradbury and Baeyens, 2009

b) Bradbury and Baeyens, 2005

c) Bradbury and Baeyens, 2005

d) Marques Fernandes et al., 2012

e) Bradbury and Baeyens, 2011

*proposed in the present work

4.4. References

- Andra. (2005). *Dossier 2005 Argile - Synthèse Evaluation de La Faisabilité Du Stockage Géologique En Formation Argileuse*. 240p. Andra, Châtenay-Malabry (France).
- Angove, M. J., Johnson, B. B., Wells, J. D., and Box, P. O. (1997). Adsorption of Cadmium (II) on Kaolinite. *Colloids and Surfaces A: Physicochemical and Engineering Aspects* **126**: 137–147.
- Angove, M. J., Johnson, B. B., and Wells, J. D. (1998). The Influence of Temperature on the Adsorption of Cadmium (II) and Cobalt (II) on Kaolinite. **103** (204): 93–103.
- Bauer, A., Rabung, T., Claret, F., Schäfer, T., Buckau, G., and Fanghänel, T. (2005). Influence of Temperature on Sorption of Europium onto Smectite: The Role of Organic Contaminants. *Applied Clay Science* **30** (1): 1–10.
- Bradbury, M. H. and Baeyens, B. (2005). Experimental Measurements and Modeling of Sorption Competition on Montmorillonite. *Geochimica et Cosmochimica Acta* **69** (17): 4187–4197.
- Bradbury, M. H. and Baeyens, B. (2009). Sorption Modelling on Illite. Part II: Actinide Sorption and Linear Free Energy Relationships. *Geochimica et Cosmochimica Acta* **73** (4): 1004–1013.
- Bradbury, M. H. and Baeyens, B. (2011). Predictive Sorption Modelling of Ni(II), Co(II), Eu(III), Th(IV) and U(VI) on MX-80 Bentonite and Opalinus Clay: A ‘Bottom-Up’ Approach. *Applied Clay Science* **52** (1–2): 27–33.
- Brady, P. V. (1992). Silica Surface Chemistry at Elevated Temperatures. *Geochimica et Cosmochimica Acta* **56** (7): 2941–2946.
- Brady, P. V. and Walther, J. V. (1992). Surface Chemistry and Silicate Dissolution at Elevated Temperatures. *American Journal of Science* **292** (9): 639–658.
- Brady, P. V. (1994). Alumina Surface Chemistry at 25, 40, and 60 °C. *Geochimica et Cosmochimica Acta* **58** (3): 1213–1217.
- Chang, P., Wang, X., Yu, S., and Wu, W. (2007). Sorption of Ni(II) on Na-Rectorite from Aqueous Solution: Effect of pH, Ionic Strength and Temperature. *Colloids and Surfaces A: Physicochemical and Engineering Aspects* **302** (1–3): 75–81.
- Donat, R. (2009). The Removal of Uranium (VI) from Aqueous Solutions onto Natural Sepiolite. *Journal of Chemical Thermodynamics* **41** (7): 829–835.
- Duc, Myriam, Carteret, Cédric, Thomas, Fabien and Gaboriaud, Fabien. (2008). Temperature Effect on the

- Acid-Base Behaviour of Na-Montmorillonite. *Journal of Colloid and Interface Science* **327** (2): 472–76.
- Fokkink, L. G. J., De Keizer, A. and Lyklema, J. (1989). Temperature Dependence of the Electrical Double Layer on Oxides: Rutile and Hematite. *Journal of Colloid and Interface Science* **127** (1): 116–131.
- Fokkink, L. G. J., De Keizer, A., and Lyklema, J. (1990). Temperature Dependence of Cadmium Adsorption on Oxides. I. Experimental Observations and Model Analysis. *Journal of Colloid and Interface Science* **135** (1): 118–131.
- Fröhlich, D. R., Amayri, S., Drebert, J., Reich, T. (2013). Influence of Humic Acid on neptunium(V) Sorption and Diffusion in Opalinus Clay. *Radiochimica Acta* **101** (9): 553–560.
- Gao, Y., Shao, Z., and Xiao, Z.. (2015). U(VI) Sorption on Illite: Effect of pH, Ionic Strength, Humic Acid and Temperature. *Journal of Radioanalytical and Nuclear Chemistry* **303** (1): 867–876.
- Halter, W. E. (1999). Surface Acidity Constants of α -Al₂O₃ between 25 and 70 °C. *Geochimica et Cosmochimica Acta* **63** (19): 3077–3085.
- Jin, Q., Su, L., Montavon, G., Sun, Y., Chen, Z., Guo, Z., and Wu, W. (2016). *Surface Complexation Modeling of U(VI) Adsorption on Granite at Ambient/elevated Temperature: Experimental and XPS Study*. *Chemical Geology* **433** : 81-91.
- Joseph, C. (2013). ‘*The Ternary System U(VI) / Humic Acid / Opalinus Clay*’. PhD thesis Helmholtz-Zentrum Dresden-Rossendorf (Germany).
- Marques Fernandes, M., Baeyens, B., Dähn, R., Scheinost, A. C., and Bradbury, M. H. (2012). U(VI) Sorption on Montmorillonite in the Absence and Presence of Carbonate: A Macroscopic and Microscopic Study. *Geochimica et Cosmochimica Acta* **93**: 262–277.
- Shahwan, T. and Erten, H. N. (2004). Temperature Effects in Barium Sorption on Natural Kaolinite and Chlorite-Illite Clays. *Journal of Radioanalytical and Nuclear Chemistry* **260** (1): 43–48.
- Sun, Y., Li, J., and Wang, X. (2014). The Retention of Uranium and Europium onto Sepiolite Investigated by Macroscopic, Spectroscopic and Modeling Techniques. *Geochimica et Cosmochimica Acta* **140**: 621–643.
- Tertre, E., Berger, G., Castet, S., Loubet, M., and Giffaut, E. (2005). Experimental Sorption of Ni²⁺, Cs⁺ and Ln³⁺ onto a Montmorillonite up to 150°C. *Geochimica et Cosmochimica Acta* **69** (21): 4937–4948.
- Tertre, E., Berger, G., Simoni, E., Castet, S., Giffaut, E., Loubet, M., and Catalette, H. (2006). Europium Retention onto Clay Minerals from 25 to 150 ° C: Experimental Measurements, Spectroscopic Features and Sorption Modelling. *Geochimica et Cosmochimica Acta* **70** (18): 4563–4578.
- Tertre, E., Castet, S., Berger, G., Loubet, M., and Giffaut, E.. (2006a). Surface Chemistry of Kaolinite and Na-Montmorillonite in Aqueous Electrolyte Solutions at 25 and 60 °C: Experimental and Modeling Study. *Geochimica et Cosmochimica Acta* **70** (18): 4579–4599.
- Yang, Z., Huang, L., Lu, Y., Guo, Z., Montavon, G., and Wu, W. (2010). Temperature Effect on U(VI) Sorption onto Na-Bentonite. *Radiochimica Acta* **98** (12): 785–791.

Chapter 5

Conclusions

The aim of this study was to have a better understanding and a better quantification of the behaviour of U(VI) on Callovo-Oxfordian (COx) formation, which will host high-level radioactive waste in France. We have focused our study on the effect of an increase in temperature of up to 80 °C on U(VI) behaviour in solution and onto mineral surfaces.

The first part of the work focused on determining the thermodynamic properties of the calcium uranyl carbonate aqueous complexes, which govern the speciation of U(VI) in the clay porewater's surroundings of the repository. For that, an experimental method was developed in controlled atmospheres to determine the stability constants of the Ca-U(VI)-CO₃ ternary complexes at different temperatures: 20, 40, 60 and 80 °C.

The main experimental challenge of this work was to control the pH/carbonates equilibrium with temperature during the batch experiments. In initial experiments we guaranteed the correct performance of the experimental set-up and evaluated the equilibrium between CO₂(g) and the solutions.

We determined the stability constants of Ca-U(VI)-CO₃ complexes at different temperatures by fitting a geochemical model to the experimental data. The results showed that the two aqueous complexes studied have different behaviours in temperature. The formation of the anionic complex (CaUO₂(CO₃)₃²⁻) is not favoured with an increase in temperature, while the neutral complex (Ca₂UO₂(CO₃)₃(aq)) forms independently of temperature changes.

We obtained, from these data, the thermodynamic data for the CaUO₂(CO₃)₃²⁻ and Ca₂UO₂(CO₃)₃(aq). The log₁₀ β^o₁₁₃ and log₁₀ β^o₂₁₃ are consistent with those previously published, which provided confidence on the methodology used and the conceptual model proposed. Thus, we determined the Δ_rH^o of Ca-U(VI)-CO₃ ternary complexes, proposing new enthalpy data for CaUO₂(CO₃)₃²⁻ (27.4 ± 8.2 kJ/mol) and Ca₂UO₂(CO₃)₃(aq) (0 ± 1.8 kJ/mol). In comparison with Endrizzi and Rao (2014) enthalpy data, the anionic complex is also exothermic, although the Δ_rH^o is two times lower; on other hand, the neutral complex is not affected by the temperature which contradicts the value published (-47 kJ/mol). Despite the high uncertainty of Δ_rH^o of the Ca₂UO₂(CO₃)₃(aq), we consider that its Δ_rH^o is zero.

In the second part of this work we proposed a model approach to describe the retention of U(VI) on Callovo-Oxfordian formation at 20 °C, that was further used for the study in temperature. We used the well-know 2SPNE SC/CE model to quantify the retention mechanisms of the U(VI) firstly on

illite and then on Callovo-Oxfordian clay fraction system (illite and montmorillonite). Here, montmorillonite was used as proxy for smectite from the interstratified I/S minerals present in the Callovo-Oxfordian clay fraction.

Due to a lack of available data for surface-carbonato complexation reactions for illite, we performed sorption experiments at different concentrations of carbonates. As a first approach, we used the model proposed in the literature for montmorillonite and we found that it could explain the experimental data, indicating that together with U(VI)-OH surface complexes, the U(VI)-CO₃ complex was also sorbed. The results also indicated that the ($\equiv S_5OUO_2(CO_3)_2^{3-}$) surface species is responsible for the sorption of U(VI) in the presence of carbonates at pH > 7. The constant of this surface species was manually fitted and the constant value was determined as 17.5 (± 0.5).

Considering the new surface data for illite and the surface data published for montmorillonite, the model considering both minerals also explained the behaviour of U(VI) in Callovo-Oxfordian clay fraction systems (illite and I/S = 50% illite and 50% montmorillonite). No other parameters were needed to change in order to explain the sorption behaviour.

We have also successfully applied our model to natural samples of Callovo-Oxfordian formation and other clay rocks, such as Opalinus and Boda clay. Our results indicated that the retention of U(VI) is essentially governed by the clay fraction. Nevertheless, it was difficult to assess the uncertainty of the different parameters on the model prediction.

In the last part of the work, we discussed the temperature effect on the U(VI)/ Callovo-Oxfordian system. The retention of U(VI) in CO_x conditions is favoured with the increase of the temperature as already observed in the literature. However, our modelling predictions indicated that thermodynamic parameters (enthalpy data) for the aqueous speciation (including the new $\Delta_r H^\circ$ for Ca-U(VI)-CO₃ aqueous complexes) and the surface data used in the model at 20 °C were not enough to completely explain the sorption of U(VI) on the U(VI)/ Callovo-Oxfordian system at 80°C. For this reason, we considered that enthalpy data for the surface complexation reactions was needed.

The effect of the temperature on the retention of U(VI) was negligible for illite in the absence of calcium. The formation of U(VI) hydrolysis complexes is favoured in solution with the increase of the temperature either in the absence or presence of carbonates in solution. This would lead to a general decrease of the retention due to the competition between the complexation processes occurring in solution and at the surface. To explain quantitatively the retention of U(VI), it was therefore necessary to consider an endothermic effect of surface complexes, in order to counterbalance the solution effect. Since the hydrolysis surface complexes are responsible for the retention of U(VI), their enthalpy values were determined by fitting. The new thermodynamic parameters for the hydrolysis surface complexation reactions explained the behaviour of U(VI) on illite.

On the other hand, in the presence of calcium in the system, the Ca-(VI)-CO₃ aqueous species are formed, which are not favoured (or not affected) with the increase of the temperature. Considering the endothermic effect considered for the surface reactions, the retention of the U(VI) is thus favoured with the increase of the temperature.

In conclusion, the model developed for illite in temperature was applied satisfactorily to CO_x clay fraction and natural samples considering the presence or absence of Ca-U(VI)-CO₃ ternary complexes. It was clear that the uncertainties associated to the enthalpy values are high, nevertheless, the

model could reproduce the Callovo-Oxfordian conditions and can be applied to predict *in situ* conditions.

5.1. Perspectives

The question of the existence of the carbonato-surface complexes on either illite or montmorillonite is still unanswered. The interpretation of the sorption data for illite indicates that such complexes must be considered in the model predictions. To increase the accuracy of the proposed stability constants of carbonato-surface complexes, sorption edge experiments at 20–25 °C should be performed in the presence of a wide range of carbonates concentration. Additionally, the interpretation of the sorption data at different temperatures revealed also a lack of knowledge concerning the enthalpy of reaction for the surface complexes for both illite and montmorillonite. As such, future experimental work, complemented by modelling, should be focused on the determination of their specific contributions for the retention of U(VI) in dependence of pH at different temperatures and different concentrations of carbonates in solution. The formed U(VI) surface complexes should be then characterised by suitable spectroscopic techniques (e.g. ATR FT-IR spectroscopy, EXAFS spectroscopy) at different temperatures.

The robustness of the model here developed for uranium's behaviour should be tested in more realistic conditions. Sorption experiments performed with Callovo-Oxfordian claystone intact samples are on progress with U(VI). Furthermore, data are being generated in order to assess the behaviour on naturally-occurring U, *i.e.* U distribution between the different phases and its exchangeable character. These data will derive in K_D value knowing the concentration of U naturally found in the COx porewater.

Finally, although U(VI) is expected to control uranium speciation in the porewater, it is important to point out that Callovo-Oxfordian conditions are characterized by reducing conditions, where the U(IV) may also occur. U(IV) may then be an important species to consider for surface complexation reactions. To understand the mechanism of retention of U(IV) in Callovo-Oxfordian formation, we suggest that batch-type sorption experiments using U(IV) at different temperatures should be performed as a function of key parameters such as pH, pCO_2 , [U(IV)] and [Ca]. The nature and structure of the surface complexation for U(VI) and U(IV) should also be investigated. For example, one could use EXAFS spectroscopy to verify which are the surface species that control the sorption of U(VI) and U(IV) and clarify if there are or not uranyl carbonato surface complexes. In this way we would achieve a full understanding of the uranium's behaviour in Callovo-Oxfordian conditions and thus define a reliable K_D of uranium in *in situ* conditions.

Appendices

Appendix A: Material and Methods

A.1. ICP-MS analysis:

The ThermoScientific XSERIES 2 ICP-MS (Thermo Fisher Scientific) has been used in the present study. The ICP-MS (Inductively Coupled Plasma Mass Spectroscopy) is an analytical technique used for elemental determinations. This technique has good detection capacities, especially for the rare-earth elements. It has also many advantages over other elemental analytical techniques which include: low detection limits for most of the elements; high throughput with protocol compliance; ability of handle both simple and complex matrices with low interferences due to the high-temperature of the ICP source; superior detection capability; and ability to obtain isotopic information.

A.1.1. Optimisation method

The ignition of the plasma and the optimisation of the device are controlled by the software PlasmaLab's.

After switching on the device, the number of cps of the selected elements (Li, Co, In and U) are displayed continuously, which will be useful for the optimisation of the device. The ^{59}Co is used to optimise the low mass ions, the ^{115}In for the medium mass ions, and the ^{238}U is used for the heavy mass ions.

The procedure of signal optimisation starts by controlling the position of the ICP torch (depth, vertical and horizontal position). Then after, the flux of gas that is expressed by L/min is set by controlling the cooling gas (> 13 L/min), the flow rate of the nebuliser, and the auxiliary gas (Ar). Once the gas flux is set, the lens system is adjusted to focus the ion beam created in the plasma. After, the amplitude of the signal is adjusted simultaneously to the bias which corresponds to tension over the entrance to the quadrupole. Here, the adjustment of the sensitivity of the signal is set. These adjustments must be done to obtain a large number of cps and a good stability of the signal of the selected elements ($< 2\%$), and the oxide levels ($< 5\%$), which are controlled by the Ce^{++}/Ce and CeO/Ce ratios.

Internal standard solution:

The internal standard solution is normally prepared to verify the signal of the measurements and to correct the drift of the analysis. Here, ^{205}Tl was used as internal standard. A solution of 2% ultrapure HNO_3 and 2.5 ppb of ^{205}Tl was prior prepared for each dilution, such for the calibration curve.

The solution was firstly prepared by dilute 62.4 μL of 1002 $\mu\text{g}/\text{mL}$ ICP-MS standard solution in 25 mL of 2% ultrapure HNO_3 to obtain a solution of 25 ppm of ^{205}Tl . A second dilution was prepared by diluting 2 mL of 25 ppm ^{205}Tl solution in 2000 mL of 2% ultrapure HNO_3 .

Internal standard correction:

The internal standard signal was used to correct of drift from the matrix effect. The calculations were as follow:

$$\text{coups}_{238\text{U}}(\text{corrected}) = \frac{\text{coups}_{238\text{U}}}{\text{signal}_{238\text{U}}} \times \bar{x}_{\text{signal}_{205\text{Tl}}}$$

Calibration curve:

The calibration curve was determined previously to each ICP-MS analysis. The ^{238}U standard solution of 999 $\mu\text{g}/\text{mL}$ was used to prepare the standard solutions. Firstly, a mother solution of 500 ppb was prepared by diluting 25 μL of ^{238}U standard solution in 50 mL of 2% $\text{HNO}_3 + ^{205}\text{Tl}$ solution. 6 standard solutions were prepared as followed:

Table A. 1. Concentration and dilution calculations of the standard solutions for determination of the calibration curve of ICP-MS analysis

Standard	Concentration	Dilution
1	500 ppt	$\frac{25 \mu\text{L mother solution}}{25 \text{ mL HNO}_3 + ^{205}\text{Tl}}$
2	100 ppt	$\frac{1 \text{ mL standard 1}}{4 \text{ mL HNO}_3 + ^{205}\text{Tl}}$
3	50 ppt	$\frac{0.5 \text{ mL standard 1}}{4.5 \text{ mL HNO}_3 + ^{205}\text{Tl}}$
4	10 ppt	$\frac{0.2 \text{ mL standard 1}}{9.8 \text{ mL HNO}_3 + ^{205}\text{Tl}}$
5	5 ppt	$\frac{500 \mu\text{L standard 1}}{4.95 \text{ mL HNO}_3 + ^{205}\text{Tl}}$
6	2 ppt	$\frac{20 \mu\text{L standard 1}}{4.98 \text{ mL HNO}_3 + ^{205}\text{Tl}}$

The calculation of the calibration curve was determined based on the linear regression between the standard concentration and the coups determined by ICP-MS for each standard solution:

$$y_{\text{calc}} = bx + c$$

y_{calc} is the y -values calculated (coups), x is the x -values (concentration of the standard solutions), b is the slope of the line and c the intersection on the y -axis. The mean of all x -values is \hat{x} and the mean of all y -values is \hat{y} . The position (\hat{x}, \hat{y}) is the centroid of all points.

The slope of the line was calculated as:

$$b = \frac{\sum(x_i - \hat{x})^2}{\sum(y_i - \hat{y})^2}$$

And, the intersection as:

$$c = \hat{y} - b\hat{x}$$

The random errors of the slope and the intersection values were respectively calculated as follows:

$$sb \text{ (standard deviation of slope)} = \frac{s_{yx}}{\sqrt{\sum(x_i - \hat{x})^2}}$$

$$sc \text{ (standard deviation of intersection)} = s_{yx} \times \sqrt{\frac{1}{n} + \frac{\sum \hat{x}^2}{\sum(x_i - \hat{x})^2}}$$

$$s_{yx} = \sqrt{\frac{\sum(y_i - y_{calc})^2}{n-2}}$$
 is the random errors in the y -direction.

The correlation coefficient, so-called r^2 , should be included in the interval $0 \leq r^2 \leq 1$, following:

$$r^2 = 1 - \frac{\sum(y_i - y_{calc})^2}{\sum(y_i - \hat{y})^2}$$

The uncertainty of the calculated y_{calc} was obtained by the application of the standard deviation of the calculated values and the statistical significance of the r^2 of the calibration curve assuming a t -test and $n - 2$ degrees of freedom.

The error of y_{calc} was calculated based on its standard deviation and the probability of its occurrence. The inferior and superior error of the y_{calc} follows, respectively:

$$y_{calc_{inf}} = y_{calc} - s_{y_{calc}} \times P|X| > t; P|X| \sim 2 \text{ at } 95 \% \text{ of significance}$$

$$y_{calc_{sup}} = y_{calc} + s_{y_{calc}} \times P|X| > t$$

$s_{y_{calc}} = s_{yx} \times \sqrt{\frac{1}{m} + \frac{1}{n} + \frac{(x_{calc} - \hat{x})^2}{\sum(x_i - \hat{x})^2}}$ corresponds to the standard deviation of the y_{calc} , m to the number of measurements unknown, and n the number of calibration points.

The limite of detection was calculated as:

$$LD = \frac{3sc}{b}$$

The concentration of the unknown solution was calculated as:

$$x = (coups - c)/b$$

And,

$$sx = \frac{syx}{b} \sqrt{\frac{1}{m} + \frac{1}{n} + \frac{(x_{calc} - \hat{x})^2}{\sum_n (x_i - \hat{x})^2}}$$

Then, $u = k \cdot sx$, where $k = 2$ for 95% of significance.

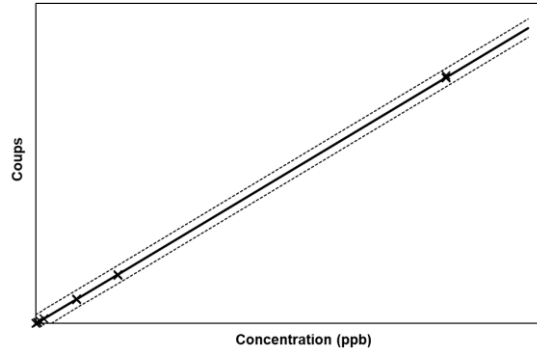


Figure A. 1. Schematic representation of the calibration plot of ICP-MS measurements. Black-cross correspond to the measurement of each standard solution; solid-line corresponds to the regression line ($y_{calc} = bx + c$); dash-lines corresponds to the inferior and superior error of y_{calc} .

A.2. TOC Analyser:

The total organic carbon of the samples was measured by a Total Organic Carbon Analyser TOC V-CSH series Shimadzu (Standalone high-sensitivity model). The TOC analyser is an analytical technique to measure the total inorganic and total carbon in liquid (or solid) sample by combustion catalytic oxidation/NDIR (non-dispersive infrared detector) method.

Method of measurement

The total organic carbon is determined indirectly by the difference of the total carbon (TC) and the total inorganic carbon (TIC) measured by the analyser.

$$TOC = TC - TIC$$

The TC is measured when a volume of sample is injected through a carrier gas and catalyst-filled TC combustion tube heated to 680°C. The TC in the sample is then oxidized or decomposes to create CO₂. After, the combustion product is cooled and dehumidified by a halogen scrubber into the sample cell of the NDIR, where the carbon dioxide is detected.

The TIC is measured by acidifying the sample through a reactor containing 25 % of H₃PO₄ and transform inorganic carbon in carbon dioxide which is further transported by gas carrier. This carbon dioxide is detected by the NDIR and the TIC is measured in the same way as TC. The TIC is a combination of carbonate and bicarbonate.

Uncertainty of measurement:

The uncertainty of the TOC analysis was calculated considering the measurements of the TC and IC from the ultra-pure water, and their respective standard solutions.

$$Uncertainty (\%) = \left| \frac{[theoretical] - [measure\ standard] - [ultrapure\ water]}{[Theoretical]} \right|$$

The TOC measurements are rather sensitive to the atmospheric conditions, such as humidity and atmospheric pressure. For this reason, the TC and TIC was measured in ultra-pure water and used to correct the TC and TIC measurements of the sample.

A.3. Determination of the alkalinity:

The alkalinity was determined by colorimetric analysis using Bromocresol Green-Methyl Red Indicator Powder Pillow as colour indicator and a Digital Titrator (Hach method 8203) with a digital titrator cartridges containing 0.16 N (or 0.02 N for low concentration of carbonates in the system) of H₂SO₄.

The measurements of alkalinity were performed in the blank samples in the absence of uranium in solution. The procedure included the following steps:

- Cooling of the sample at room temperature (for all samples carried out at temperature above 20 °C)
- An aliquot of 10 mL was sampled, filtrated using 0.2 µm cellulose acetate membrane and added to a flask
- The colour indicator was added and swirled to mix until all powder was dissolved
- The cartridges containing the titrant were hold in a digital titration and turning the digital titrator's knob the titrant is added to the solution. The flask is swirled every time the titrant was added until the colour changed from green to pink.
- The number of digits was recorded from digital titrator counter.
- The alkalinity was determined as following:

$$alkalinity_{total} = N_{acid} \left(\frac{eq}{L} \right) \cdot \frac{number\ of\ digits}{800} (mL) \cdot \frac{1}{volume_{sample}} (mL)$$

A.4. pH measurements

The pH was measured by a pH-meter combined with a pH electrode and thermometer detector (pHC2085, Hach Lange) as hydrogen ion activity. The pH electrode was composed by glass combined with a red rod reference electrode composed by silver/silver chloride (Ag/AgCl). The

calibration of the pHmeter was automatically performed by PHM220 Lab pHmeter (Radiometer Analytical) at the beginning of each experiment using 2 standard buffer solutions of pH 4.005 and 7.000 manufactured according to Radiometer Analytical specifications. All standard solutions were stable in a temperature range of 0 to 95°C. The calibration of the pHmeter were carried out under the temperature of interest using a duo dry-bath device previously heated (Fisher Scientific).

A.5. Stock solutions

All solutions were prepared with ultra-pure deionized water (18.2 MΩ/cm) and with commercially available chemical products of analytical grade or superior.

Calcium, Sodium and carbonate:

The stock solutions of calcium, sodium and carbonate were prepared by dissolving Ca(NO₃)₂, NaNO₃ (or NaClO₄, NaCl) and NaHCO₃ (Sigma Aldrich, St. Louis MO), respectively, in ultrapure deionised water.

Uranium:

Stock solutions of uranium were prepared for all different batch experiments performed with U(VI). ²³⁸U(VI)-impoverished solution is prepared from ICP-MS standard solution (1000 µg/mL in 4% of HNO₃ matrix) (SCP Science, France) or ICP-MS standard solution (10000 µg/mL in 0.4% of HNO₃ matrix) (SCP Science, France).

The U(VI) samples, previously acidified to pH 2 with HNO₃ ultrapure (70%) were measured by ICP-MS (ThermoScientific XSERIES 2 ICP-MS).

Synthetic Callovo-Oxfordian porewater:

The synthetic Callovo-Oxfordian porewater was prepared according to the reported data from BRGM (2008). The chemical composition of the synthetic porewater follows the reduced mineralogical system at 20 and 80°C. The chemical composition was corrected by previous calculations using PhreeqC by equilibrating the solution in pCO₂ of 10^{-2.1} and 10^{-1.3} at 20 and 80 °C, respectively (Table A. 2). Therefore, stock solutions were prepared in controlled atmosphere of 1% or 5% of CO₂(g) (accordingly to the pH/pCO₂/T) at room temperature by dissolving in 1L of degassed ultrapure deionised water the salts described in Table A. 3. The final chemical composition of the synthetic porewaters are provided in Table C. 7.

Table A. 2. Theoretical chemical composition of the Callovo-Oxfordian porewater at 20 °C and 80°C.

mM	Ca	Mg	Na	K	Cl	SO ₄ ²⁻	Sr	CO ₃ ²⁻
20 °C	8.55	5.42	43.35	1.04	40.8	14.75	0.21	2.5
80 °C	9.35	2.65	36.59	0.95	40.8	10.77	0.17	2.4

Table A. 3. Salt content in g/L used in preparation of synthetic CO_x porewater at 20 and 80°C

Salt product	Purity (%)	Provided	20 °C (g/L)	80 °C (g/L)
SrCl ₂ · 6H ₂ O	100%	Aldrich	0.0562	0.0453
KCl	99%	Fisher	0.0786	0.0715
MgCl ₂ · 6H ₂ O	99%	Merck	1.1127	0.5442
CaCl ₂ · 2H ₂ O	99%	Aldrich	1.2697	1.3885
NaCl	99.5%	Sigma Aldrich	0.6666	0.8839
Na ₂ SO ₄	99%	Panréac	2.1163	3.5051
NaHCO ₃	99.5%	Sigma Aldrich	0.2111	0.2025

A.6. Solid phases:

Anion Exchange resin:

The gel-type Dowex 1x2 strong base anion exchange resin was purchased from Sigma-Aldrich (France) in chloride form. This resin is characterised by a total exchange capacity of 0.7 meq/mL by wetted bed volume; 70 % wt water retention capacity; and density of 44 lbs/ft³ ≈ 0.705 g/cm³. Primarily, the resin is converted to nitrate form by equilibrating with 250 mL of 1 M NaNO₃ (or NaClO₄) during 1 day on a magnetic shaker. The supernatant is filtrated and replaced by 250 mL of NaNO₃ (or NaClO₄) (1 M) and the process was repeated for 3 times. After 3 equilibration cycles, the resin is filtrated and rinsed with deionised water after overnight equilibration. After rising overnight, the resin is once again filtrated and air dried.

Callovo-Oxfordian claystone:

Callovo-Oxfordian claystone samples were extracted from the borehole EST51779 drilled in the Callovo-Oxfordian formation. The sample was selected and provided by Andra in July 2015. It has always been storage in closed and clean atmosphere to avoid any oxidation and carbonatation of the mineral surface. The composition is provided in Table A. 4.

Table A. 4. Mineral composition of Callovo-Oxfordian claystone

Mineral	Wt%
Illite	17
IS R0	28
ISR1	0
Calcite+dolomite	25
Quartz+feldspath	25
Celestite	0
Dolomite	0
Siderite	0
Pyrite	0.8
kaolinite	2

Mineral	Wt%
chlorite	3

Callovo-Oxfordian clay fraction:

The Callovo-Oxfordian claystone was purified, and the clay fraction was separated. The separation and purification of the clay fraction was performed and provided by BRGM. The clay fraction samples were storage in open atmosphere.

The procedure is divided in 4 stages: Stage 1: separation of the < 2 μm fraction; Stage 2: acidification of the carbonates; Stage 3: Oxidation of iron and manganese oxides; and Stage 4: reduction of organic matter. The procedure of separation and purification is described below:

Stage 1: < 2 μm Clay Fraction Separation

1. 20 g/L clay dispersed in Milli-Q Water.
2. The fine fraction (<2 μm) separated by sedimentation or centrifugation
3. The depth of fine fraction (<2 μm) is calculated by using Stoke's Law.
4. Fine fraction is taken into vacuum flask
5. Centrifuge suspension at high speed to get 0.1-2 μm clay fraction

Stage 2: Carbonate Removal with Acetic Acid (treated with 0.1 M acetic acid in 0.5 M NaCl (pH ~5))

1. Prepare 2 L 0.2 M Acetic acid stock solution at pH 5
2. 20 g clay fraction (dry equivalent) dispersed in 0.5 L Milli-Q water.
3. 0.5 L clay suspension mixed with 0.5 L 0.2 M Acetic acid (pH ~5) in a pot
4. Add 29.22 g NaCl into pot and close the pot, shake by hand few seconds and open the pot in order to release excess CO₂ pressure under a vapor extractor
5. Close the pot and shake it on horizontal shaker for 1 h
6. High speed centrifugation to settle particles above 0.1 μm
7. Waste the supernatant (!! Not in the sink; organic acid)
8. Repeat acid attack one more time
9. After last centrifugation, disperse the clay with 0.5 M NaCl solution, shake and centrifuged
10. Repeat washing 2 times

Stage 3: Oxidation to remove Fe and Mn oxides with DCB (dithionite–citrate–bicarbonate) (treated with 0.2 M Citrate, NaCl 0.5 M, NaHCO₃ 0.1 M (pH ~6))

1. Prepare 2 L stock solution having 0.4 M Citrate, 1 M NaCl, 0.2 NaHCO₃ M (pH ~6) First solve citrate and buffered with NaOH, then add NaCl and NaHCO₃ then final pH become ~6
2. In order to get fine dispersed clay suspension, 20 g (dry equivalent) clay fraction obtained from stage 2 dispersed in 0.5 L water.
3. 0.5 L clay suspension mixed with 0.5 L buffered Citrate stock solution in 1 L pot
4. Add one spatula (teaspoon) of sodium dithionite into pot and closed it.
5. Shake and put the pots at 40°C for 5 minutes and then open the pot under the vapor extractor
6. Close the pot and shake it on horizontal shaking table for 1 h
7. Centrifuge the suspension
8. Repeat DCB attack 1 more time
9. After last centrifugation, wash the clay by dispersing with 0.5 M NaCl solution, shake and centrifuge
10. Repeat washing 2 times

Stage 4: Reduction to remove organic matter (treated with 3% H₂O₂, 0.5 M NaCl at 60 °C)

1. Prepare 2 L stock solution H₂O₂ 6% + NaCl 1 M
2. 20 g (dry equivalent) clay dispersed clay in 0.5 L water
3. Rinse a **big glass beaker** with the H₂O₂ solution
4. Add 0.5 L clay dispersion and 0.5 L H₂O₂ 6% + NaCl 1 M Solution
5. Pour the clay dispersion in the beaker and heat the beaker at 55°C–60°C (STAY IN FRONT OF THE BEAKER AND WATCH FOR THE TEMPERATURE), 1 h
6. Wait for cooling, put in centrifuge pot and centrifuge the clay (use old but not cracked pots)
7. Wash clay by dispersing with 0.5 M NaCl solution, shake and centrifuged
8. Repeat washing 2 more times

Illite:

Illite is originated from Oligocene geological formation from Le Puy-en-Valey (Haute-Loire, France). The so-called illite du Puy was purified and provided by BRGM. The purification procedure was also performed by BRGM.

A.7. Batch experiments procedures

Batch experiments are performed to: 1) determine the stability constants of Ca-U(VI)-CO₃ at different temperatures; 2) to study the main mechanisms of retention of uranium onto Callovo-Oxfordian formation; and 3) the respective effect of the temperature on these retention mechanisms. The batch experiments are performed in both open and closed atmosphere. The experimental procedure in open or closed system was applied in the same way for all batch. The details of the experimental conditions for each batch experiment are described in Table A. 5.

Table A. 5. Experimental conditions for the batch experiments. Temp.= temperature; COx = Callovo-Oxfordian; I = Ionic strength.

Exp.	Temp.		pCO ₂		Time		pH	Range of S/L		Background	I		[Ca]	[U(VI)]	
	°C		atm		days			g/L	M		mM	mM			μM
Anionic-exchange resin															
ΔS/L	20	atmospheric	1, 3 and 5%	5	8.1	1-25	NaNO ₃	0.24	0	0.5	0.1	0	0	0.5	
	20, 40, 60 and 80	7.2-6.6			2.0										
ΔCa	20	atmospheric	1, 3 and 5%	5	8.1	2.5	NaNO ₃ or NaClO ₄	0.24	0-5	0.05	0.1	0	0	0.05	
	20, 40, 60 and 80	7.2-6.6			2.0										
Kinetics															
illite	20	atmospheric	1, 2, 3, 7 and 14	equilibrium	0.5	NaCl	0.1	0	0	0.5	0.1	0	0	0.5	
															COx claystone
Sorption edge															
illite	20 and 80	inert	3	4-10	2.0	NaNO ₃	0.1	0	0	0.1	0	0	0	0.1	
															atmospheric
Sorption isotherms															
illite	20, 60 and 80	inert	3	equilibrium	2	NaNO ₃	0.1	0	0	0.05-20	0.1	0	0	0.05-20	
															atmospheric, 1% and 5%
	20	1%	7.2	10	NaNO ₃	2.0	8.5	2.0	8.5						
	80	5%	6.6	2	NaNO ₃	2.0	8.5	2.0	8.5						
COx clay fraction	20	Inert and 1%	3	7.2	2	NaNO ₃	0.1	0-2.0	0	0.01-10	0.1	2.0	8.5	0.01-10	
															1%
	80	Inert and 5%	3	6.6	2	NaNO ₃	COx porewater	2.0	8.5	2.0	8.5	2.0	8.5	2.0	8.5
COx claystone	20	1%	3	7.2	40	COx porewater	0.1	2.01	8.5	0.05-20	0.1	2.01	8.5	0.05-20	
	80	5%	3	6.6	5	COx porewater	0.1	2.01	8.5	0.05-20	0.1	2.01	8.5	0.05-20	

A.7.1. Open system (atmospheric conditions) procedure:

The procedure at open system consisted in firstly weighting the solid phase in 35 mL PPCO tubes at room temperature and prepare the stock solutions with ultrapure water.

Anionic-exchange batch experiments were performed in atmospheric conditions to test the efficiency of using NaClO_4 instead of NaNO_3 . In this case, the initial pH controlled by adding 0.1 M of NaHCO_3 and was adjusted for each tube by adding 0.01 M of HNO_3 or NaOH until the pH 8.1 was reached.

Concerning the sorption edge batch experiments, the pH of the stock solution of 0.1 NaCl was controlled by bubbling with $\text{Na}_2(\text{g})/\text{CO}_2(\text{g})$ (99/1 ratio) the solution until reach pH of interest. Afterwards, the solutions were agitated over night to favour the equilibrium with atmospheric pCO_2 . In each tube, the pH of the solution was measured and adjusted by adding 0.01 M of HCl or NaOH . The results of the pH of each stock solution are shown in Table C. 8.

Each tube was sealed with Teflon-film to avoid any leaking. The samples were transferred to the incubator coupled with a reciprocating shaker (Thermotron InforsHT) and let in equilibrium for 24 h by agitation at temperature of interest. After 24 h, each sample was introduced in the thermo-Teflon-aluminium box, specially prepared to maintain the temperature of the samples, and an aliquot of a solution of uranium was added. Each tube was closed and transferred once more to the incubator at the temperature of interested. After 3 days of equilibration, the samples were introduced again in the thermo-Teflon-aluminium box, and an aliquot of 5 mL was sampled by 5 mL syringe PP and filtrated by 0.22 μm filters of cellulose acetate (20 °C) or Millex IC (higher temperatures), discarding the first 1-2 mL, acidified to pH 2 with HNO_3 ultrapure (70%) and saved for further analysis of uranium. The final pH was measured in the remaining solution just after the sampling to avoid the loss of heat.

Two blanks were prepared with and without solid or uranium in solution. The alkalinity was measured at end of the experiments when the temperature of the sample was cooled down using blank sample without U in solution.

A.7.2. Closed system (controlled atmosphere) procedure:

In the experiments performed in closed system, the samples were weight in room conditions in 35 mL PPCO tubes and transferred into the glove-box $\text{Ar}(\text{g})$ or $\text{Ar}(\text{g})/\text{CO}_2(\text{g})$ (with $\text{CO}_2(\text{g})$ percentage according to temperature of interest). Simultaneously, 1 L of ultrapure water was degassed by agitating and heating at approx. 50 °C using a vacuum pumping system and transferred into the glove-box. The stock solutions were prepared individually using degassed ultrapure water in the glove-box and added to each tube.

In case of the sorption edge, the pH of the solutions was adjusted for each tube by adding different aliquots of 0.01 M of HNO_3 or NaOH (Table C. 38 and Table C. 39).

For the anionic-exchange experiments and sorption isotherms, the pH was controlled by adding 0.1M of NaHCO_3 .

Each tube was sealed with Teflon-film to avoid any leaking, closed and removed from the glove-box. The samples were quickly packed in vacuum by wrapping with an aluminium-envelope using a Vacupac system. After, the packed samples were transferred into an incubator coupled with reciprocating shaker (Thermotron InforsHT) heated previously to the temperature of interested and left in equilibrium for 1 day.

After 24 h of equilibration, the aluminium-envelopes were opened, and each sample was introduced inside of a thermo-Teflon-aluminium box, specially prepared to maintain the temperature of the samples, and transfer into the glove-box as quick as possible. In the glove-box an aliquot of a solution of U(VI). Each tube was closed and removed from the glove-box, and quickly packed in an aluminium-envelope once more in vacuum. The packed samples were transferred into the incubator coupled with reciprocating shaker and left in equilibration.

After equilibration, the aluminium-envelope was opened, and each sample was introduced inside of a thermo-Teflon-aluminium box and transferred into the glove-box, and 5 mL were sampled by 5 mL syringe PP and filtrated by 0.22 µm filters of cellulose acetate (20 °C) or Millex IC (higher temperatures), discarding the first 1-2 mL, acidified to pH 2 with HNO₃ ultrapure (70%) and saved for further analysis of uranium. The final pH was measured in the remaining solution just after the sampling to avoid the loss of heat. Two blanks were prepared with and without solid or uranium in solution. The alkalinity was measured at end of the experiments when the temperature of the sample was cool down to room temperature using blank sample without U in solution (see Table C. 9, Table C. 23, Table C. 44 and Table C. 51).

Appendix B: Auxiliary calculations

B.1. Calculation of the amount of exchanger considered in the resin

The amount of exchange sites of the resin Dowex 1x2 can be calculated based on:

- Assuming 70 % wt is water retention capacity of the resin, 30 % is the dry fraction of the resin;
- The density of the resin (ρ_{resin}) is 0.705 g/cm³;
- The capacity of exchanging (CE) of 0.7 meq/mL by wetted bed volume;

$$\text{amount}_{\text{XNO}_3}(\text{eq/L}) = \frac{\frac{0.3 g_{resin}}{0.705 g_{resin}/\text{cm}^3_{resin}} + 0.7 \text{ cm}^3_{water}}{0.3 g_{resin}} \cdot \frac{0.7 \text{ eq/L}}{\chi \text{ g/L}} \cdot \frac{1 \text{ L}}{1000 \text{ cm}^3}$$

Table B. 1. Amount of exchanger-NO₃ (mol/L) for the different solid-liquid ratio (χ) considered in the closed system experiments.

χ (g/L)	Amount of XNO ₃ (mol/L)
1	$2.62 \cdot 10^{-3}$
2.5	$6.55 \cdot 10^{-3}$
5	$1.31 \cdot 10^{-2}$
10	$2.62 \cdot 10^{-2}$
15	$3.93 \cdot 10^{-2}$
20	$5.24 \cdot 10^{-2}$
25	$6.55 \cdot 10^{-2}$

B.2. Calculation of the sorption parameters of clay minerals

The main sorption parameters of the clay minerals taken into account in this study are: the grams of mass of each clay mineral, the respective number of surface and exchange sites and their specific surface. The specific surface was provided from the literature. The mass of clay mineral and number of sites were calculated as follow:

$$\text{gram of clay}(g) = \frac{w_{clay}\%}{100} \cdot \text{mass of sample}(g)$$

$$\text{number of surface sites (mol)} = \text{site capacities (mol/kg)} \cdot \text{gram of clay}(kg)$$

Assuming that the fraction of illite and smectite in the interstratified illite/smectite corresponds each to 50%, then:

$$\text{number of exchange sites (mol)} = \frac{\text{wt}_{\text{clay}}\%}{100} \cdot 0.5 \cdot \text{CEC} \left(\frac{\text{eq}}{\text{kg}} \right) \cdot \text{mass of sample (kg)}$$

Where, CEC corresponds to the cationic exchange capacity.

B.3. Calculation of the concentration of U(VI) sorbed on the solid:

The concentration of U(VI) sorbed on the solid was calculated based on ICP-MS measurements and follows:

$$[U(VI)]_{\text{sorbed}} = \frac{([U(VI)]_{\text{initial}}(\text{mol/L}) \times \text{dilution factor}) - [U(VI)]_{\text{solution}}(\text{mol/L})}{S/L(\text{g/L})}$$

where,

$$S/L = \frac{\text{mass of solid}}{\text{volume of solution}} (\text{g/L})$$

B.4. Calculation of distribution coefficient of U(VI):

The distribution coefficient of U(VI) is calculated as follow:

$$K_D(\text{mL/g}) = \frac{[U(VI)]_{\text{sorbed}}(\text{mol/g})}{[U(VI)]_{\text{solution}} \left(\frac{\text{mol}}{\text{L}} \right)} \times 1000$$

Appendix C: Experimental results

C.1. Complementary tests

C.1.1. Temperature control test:

The control of the temperature was performed: a) during the transport of the sample from the incubator (Thermotron InforsHT) to the glove-box where the sampling was carried out; and, b) during the sampling. To maintain the temperature constant, or at least minimising the loss of the temperature, an isolation box was manufactured in Subatech by the mechanical services (Figure C. 1). The isolation box is comprised by two isolation layers, intern layer of aluminium and an external layer of Teflon.

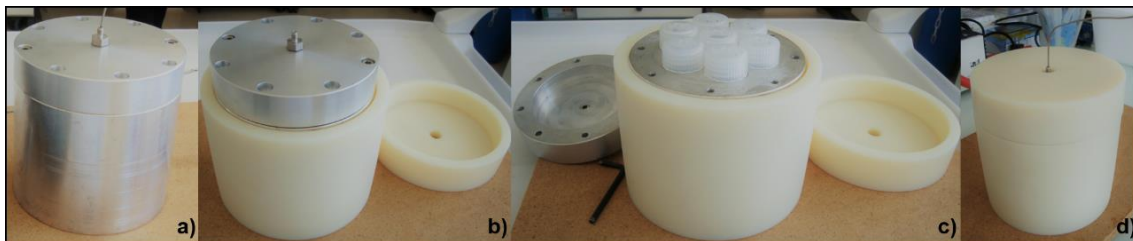


Figure C. 1. Temperature isolation box. a) internal layer aluminium; b) external layer of Teflon; c) tubes inside isolation box; d) closure of the isolation box.

The experimental test to monitor the temperature of the isolation box consisted in measuring the temperature of the 25 mL of the deionised water added in 35 mL PPCO tubes previously heated at 80°C. Different tests were performed: a) transferring the pre-heated tubes from the incubator into the glove-box using only the internal isolation box of aluminium; and b) transferring the pre-heated tubes from the incubator into the glove-box using pre-heated the isolation box (internal and external isolation layers) with different closing lid systems

The results are detailed in Table C. 1 and Table C. 2 and show that the most suitable procedure for transfer the samples from the incubator into the glove-box is using a pre-heated isolation box (internal and external layers) at 90 °C using a faster closing lid system (Figure C. 2 and Figure C. 3). The system was validated in real conditions, where the increase of + 4°C in the beginning of the transfer and loss 1 °C after 20 minutes. The temperature is maintained ± 5 °C for more than 20 minutes outside of the incubator. This time is enough to transport the samples and for the sampling.

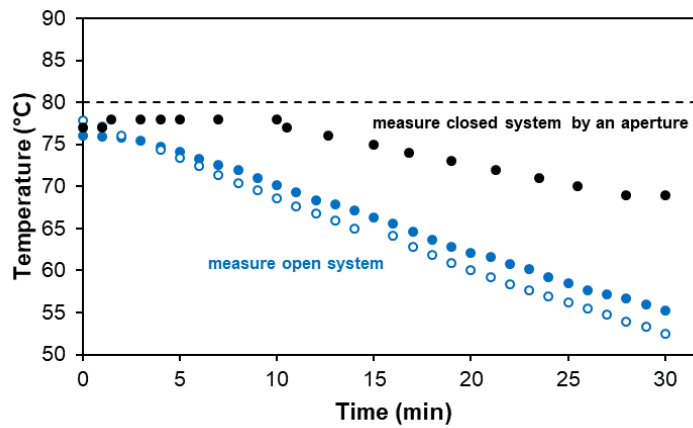


Figure C. 2. Temperature measurements as a function of time at open lid and closed lid with small aperture.

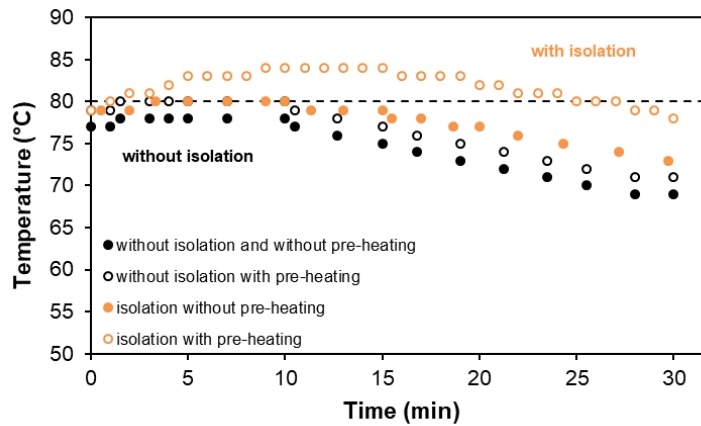


Figure C. 3. Temperature measurements as a function of time in presence or absence of the isolation Teflon layer.

Table C. 1. Experimental test of the control of the temperature using an isolation-aluminium box without external layer of Teflon.

Open-box				closed box measure by a small aperture			closed box pre-heated at 90°C		
1 st test		duplicated		2 nd test			3 rd test		
Time	Temp	Time	Temp	Time	Temp	corrected Temp	time	Temp	corrected Temp
min	°C	min	°C	min	°C	°C	min	°C	°C
0	76	0	77.8	0	74	77	0	74	79
1	75.9	1	77.1	1	74	77	1	74	79
2	75.8	2	76.1	1.5	75	78	1.5	75	80
3	75.4	3		3	75	78	3	75	80
4	74.7	4	74.3	4	75	78	4	75	80
5	74.1	5	73.4	5	75	78	5	75	80
6	73.3	6	72.4	7	75	78	7	75	80
7	72.5	7	71.4	10	75	78	10	75	80
8	71.9	8	70.4	10.5	74	77	10.5	74	79
9	71	9	69.5	12.66	73	76	12.66	73	78
10	70.1	10	68.6	15	72	75	15	72	77
11	69.3	11	67.6	16.8	71	74	16.8	71	76

Open-box				closed box measure by a small aperture			closed box pre-heated at 90°C		
1 st test		duplicated		2 nd test			3 rd test		
Time	Temp	Time	Temp	Time	Temp	corrected Temp	time	Temp	corrected Temp
min	°C	min	°C	min	°C	°C	min	°C	°C
12	68.4	12	66.8	19	70	73	19	70	75
13	67.9	13	65.9	21.25	69	72	21.25	69	74
14	67.1	14	65	23.5	68	71	23.5	68	73
15	66.3	15		25.5	67	70	25.5	67	72
16	65.6	16	64.1	28	66	69	28	66	71
17	64.6	17	62.8	30	66	69	30	66	71
18	63.6	18	61.8	/	/	/	/	/	/
19	62.8	19	60.9	/	/	/	/	/	/
20	62.1	20	60.1	/	/	/	/	/	/
21	61.6	21	59.2	/	/	/	/	/	/
22	60.8	22	58.4	/	/	/	/	/	/
23	60.2	23	57.6	/	/	/	/	/	/
24	59.2	24	56.9	/	/	/	/	/	/
25	58.5	25	56.2	/	/	/	/	/	/
26	57.6	26	55.5	/	/	/	/	/	/
27	57.1	27	54.7	/	/	/	/	/	/
28	56.7	28	53.9	/	/	/	/	/	/
29	55.9	29	53.3	/	/	/	/	/	/
30	55.2	30	52.5	/	/	/	/	/	/

Table C. 2. Experimental test of the control of the temperature using an isolation-aluminium box with external layer of Teflon.

pre-heating at 90 °C			special closing system (pre-heated 90 °C)		
4 th test			5 th test		
time	Temp	corrected Temp	time	Temp	corrected Temp
min	°C	°C	min	°C	°C
0.5	77	79	0	76	79
2	77	79	1	77	80
3.33	78	80	2	78	81
5	78	80	3	78	81
7	78	80	4	79	82
9	78	80	5	80	83
10	78	80	6	80	83
11.33	77	79	7	80	83
13	77	79	8	80	83
15	77	79	9	81	84
15.5	76	78	10	81	84
17	76	78	11	81	84
18.66	75	77	12	81	84

pre-heating at 90 °C			special closing system (pre-heated 90 °C)		
4 th test			5 th test		
time	Temp	corrected Temp	time	Temp	corrected Temp
min	°C	°C	min	°C	°C
20	75	77	13	81	84
22	74	76	14	81	84
24.33	73	75	15	81	84
27.2	72	74	16	80	83
29.75	71	73	17	80	83
/	/	/	18	80	83
/	/	/	19	80	83
/	/	/	20	79	82
/	/	/	21	79	82
/	/	/	22	78	81
/	/	/	23	78	81
/	/	/	24	78	81
/	/	/	25	77	80
/	/	/	26	77	80
/	/	/	27	77	80
/	/	/	28	76	79
/	/	/	29	76	79
/	/	/	30	75	78

C.1.2. Sealing control test:

The sealing test was monitored by a) following a possible oxidation of Fe(II) to Fe (III) and b) the measure of the pH at approx. 20°C (CO₂ of equilibrium). The experimental tests are described below:

- a) Tubes PPCO containing 25 mL of 0.01 M of FeCl₂ were prepared in different conditions, where the stability of Fe(II) was check by possible precipitation of Fe(III)-oxides by verifying the changes of colour of the solution.
- b) Tubes PPCO containing 25 mL of Callovo-Oxfordian synthetic porewater (prepared at 20°C in 1% of CO₂(g)) were prepared in different condition and the pH was monitored.

All solutions were prepared previously in the glove-box with 1% CO₂(g). The experimental conditions of sealing of the samples are detailed in Table C. 3.

In case of the Fe(II)/Fe(III), the results show that only the test where the tube was agitated at open atmosphere exhibit changes of the colour of the solution (Figure C. 4). The experimental tests performed in closed systems, such the ones left in agitation inside of the glove-box or the ones left in agitation outside of the glove-box but conditioned using aluminised envelops under vacuum, do not show any changes of the colour of solution for the time of the experiment.

Table C. 3. Experimental test for sealing control.

Test	Control	Observations
0	Fe(II)/Fe(III) pH	Closed tubes and agitated in open atmosphere
1	Fe(II)/Fe(III) pH	Closed tubes and agitated inside of the glove-box for 7 days
2	pH	Tubes sealed with an aluminised envelop in vacuum (50 mbar) and agitated for 7 days outside glove-box
3	Fe(II)/Fe(III) pH	Tubes sealed with an aluminised envelop in vacuum (50 mbar) and agitated for 3 days outside glove-box
4	pH	Tubes sealed with an aluminised envelop in 1% CO ₂ (g) (750 mbar), left in vacuum (50 mbar) and agitated for 7 days outside glove-box
5	pH	Tubes sealed with an aluminised envelop in 1% CO ₂ (g) (750 mbar), left in vacuum (50 mbar) and agitated for 3 days outside glove-box

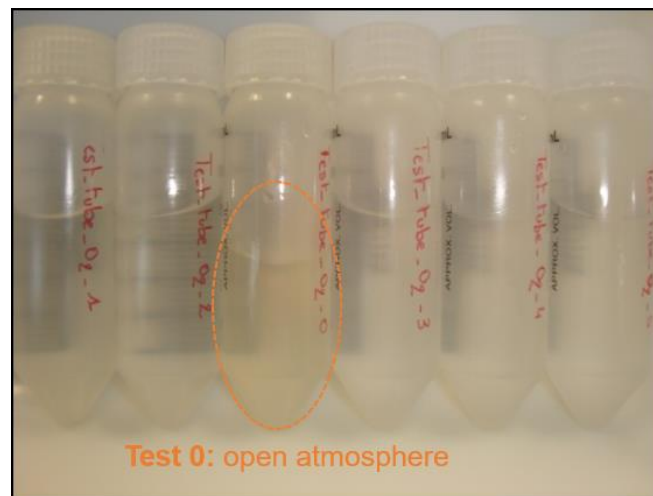


Figure C. 4. Experimental test of the oxidation of Fe(II) to Fe(III) as gas sealing control.

The pH measurements were performed in the glove-box, except for the test 0, which was measured in atmospheric conditions. The results show that for the pH measured in controlled atmosphere no changes were observed, which is constant at pH 7.3 (± 0.03). However, for the pH measured in atmospheric conditions the pH change with time (Figure C. 5).

As conclusion, the packing of the tubes using aluminised envelops (under vacuum or CO₂(g) atmosphere) is necessary and is effective as the glove-box, and the pH must be measured under a controlled atmosphere to avoid any changes of chemical equilibrium.

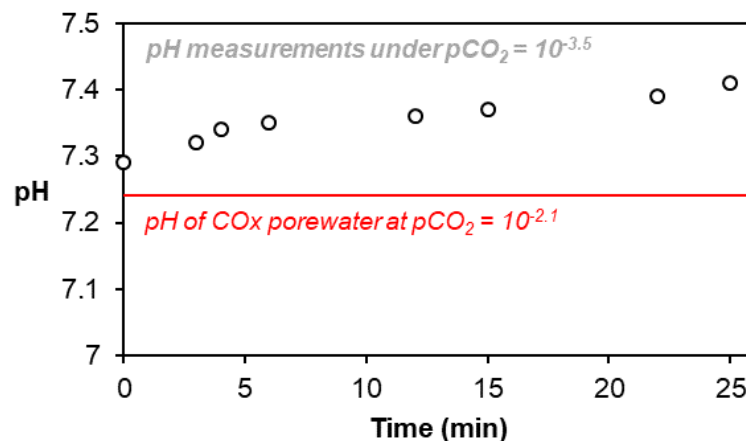


Figure C. 5. pH measured in atmospheric conditions of the COx porewater as a function of time.

C.1.3. Tightness control test:

The possible leak of the tubes PPCO in temperature was tested by measure the volume of water before and after the agitation of the tubes along the time. Different sealing tapes were used: a) tubes closed with no sealing tape; b) tubes closed and sealed with parafilm; and c) tubes closed and sealed with Teflon tape. All experimental tests were performed at 80°C.

The results detailed in Table C. 4 show that the absence of any sealing tape, after 6 days of the agitation, there is a loss of approximately 1% of the volume of the sample (Figure C. 6). For the test using the parafilm, the results show that the parafilm is melted, although using Teflon tape no significant losses of the solution were observed.

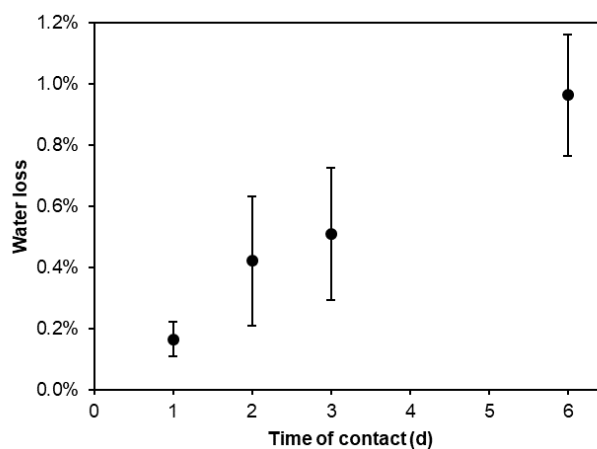


Figure C. 6. Volume of water loss (%) at 80 °C during agitation with tubes with no sealing tape as a function of time.

Table C. 4. Experimental results of the tightness of the tubes without sealing tape.

	Tare	Vol. water	Total vol. in- initial	Contact	Total vol.	Vol. water	Loss	Contact	Total vol.	Vol. water	Loss
Tube	(g)	(g)	(g)	days	(g)	(g)	%	days	(g)	(g)	%
1	13.662	24.665	38.327	1	38.292	24.630	0.14	2	38.254	24.592	0.30
2	13.627	24.060	37.687	1	37.646	24.019	0.17	2	37.611	23.984	0.32
3	13.641	23.668	37.309	1	37.276	23.635	0.14	2	37.233	23.592	0.32
4	13.663	24.428	38.091	1	38.046	24.383	0.18	2	37.995	24.332	0.39
5	13.664	24.856	38.520	1	38.455	24.791	0.26	2	38.411	24.747	0.44
6	13.652	24.437	38.089	1	38.060	24.408	0.12	2	37.977	24.325	0.46
7	13.652	25.057	38.709	1	38.679	25.027	0.12	2	38.633	24.981	0.30
8	13.665	24.269	37.934	1	37.908	24.243	0.11	2	37.861	24.196	0.30
9	13.554	24.705	38.259	1	38.194	24.640	0.26	2	38.013	24.459	1.00
10	13.585	24.662	38.247	1	38.211	24.626	0.15	2	38.152	24.567	0.39
\bar{u}		24.48					0.17				0.42
σ^2		0.41					0.06				0.21
RDS%		1.65%					34.02%				50.04%
	Con- tact	Total vol.	Vol. water	Loss	Con- tact	Total vol.	Vol. water	Loss			
Tube	days	(g)	(g)	%	days	(g)	(g)	%			
1	3	38.233	24.571	0.38	6	38.088	24.426	1.00			
2	3	37.590	23.963	0.40	6	37.470	23.843	0.90			
3	3	37.216	23.575	0.39	6	37.103	23.462	0.87			
4	3	37.976	24.313	0.47	6	37.870	24.207	0.90			
5	3	38.389	24.725	0.53	6	38.286	24.622	0.94			

6	3	37.956	24.304	0.54	6	37.847	24.195	0.99			
7	3	38.613	24.961	0.38	6	38.507	24.855	0.81			
8	3	37.838	24.173	0.40	6	37.733	24.068	0.83			
9	3	37.988	24.434	1.10	6	37.887	24.333	1.51			
10	3	38.124	24.539	0.50	6	38.025	24.440	0.90			
$\bar{\mu}$				0.51				0.96			
σ^2				0.22				0.20			
RDS%				42.34%				20.74%			

C.1.4. PPCO tubes control tests:

Total Organic Carbon:

The tubes of PPCO may release organic carbon due to deterioration by increasing the temperature. This organic carbon might influence the speciation of U(VI) in the chemical system. For this reason, some tests were performed to ensure the minor impact of the organic carbon released by the degradation of the tubes.

The experimental tests were prepared according the time of washing and the number of washes need to release the maximum of organic carbon from the tubes. An additional test was performed using 5% of HNO₃ to rinse the tubes before starting the washes process.

In the beginning of each analysis, the uncertainty of the signal is calculated considering the TC and IC from ultra-pure water and the respective standard solutions. The uncertainty of the signal of the TC and IC are expressed in the Table C. 5. All analytical results are summarised in Table C. 6.

The number of washes was limited to TOC < 1 ppm. At 20 °C, this limit is reached after one wash, however, in temperature, it was only after 3 washes (Figure C. 7a). For all temperatures, the three washes procedure can be done in 1 day, no significant difference is observed increasing the timing between washes (Figure C. 7).

The results also show that use the acidic rinse before the washes does not affect the release of the organic carbon from the PPCO tubes in comparison with rinsing with ultra-pure water before washing process (Figure C. 8b).

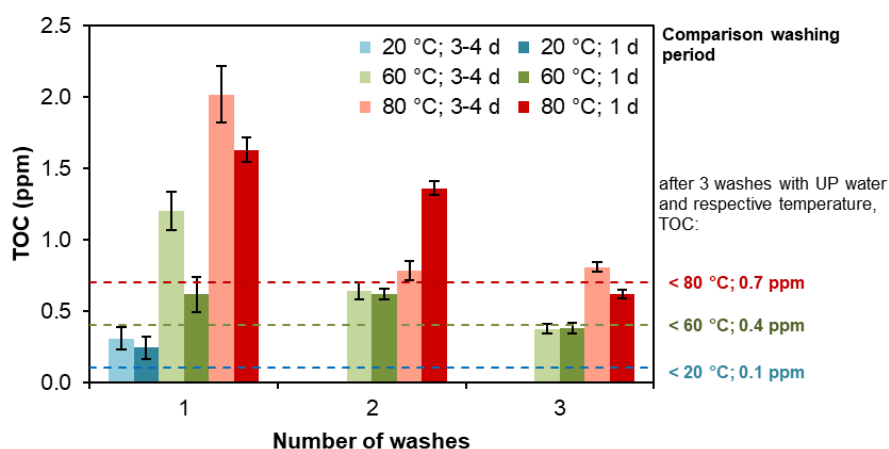


Figure C. 7. Comparison results of the number of washes with ultra-pure water between 3-4 days or 1 days.

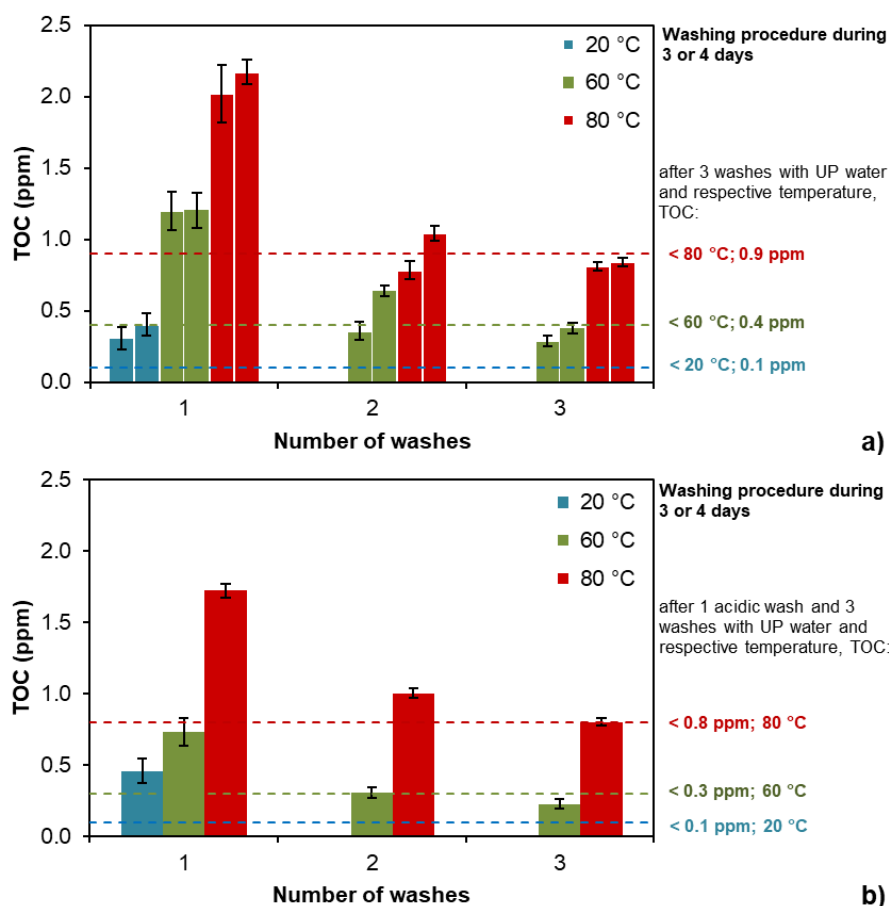


Figure C. 8. Total organic carbon as function of the number of washing and time of contact. a) washing with ultra-pure water and rinsed with ultra-pure water between each wash; b) first rinsed with 5% of HNO₃ at 100 °C before washed with ultra-pure water and rinsed with ultra-pure water between washes.

As a conclusion of these experimental tests, a cycle of 3 washes with ultrapure water was carried out at the temperature of interest before using the PPCO tubes in the batch experiments.

Table C. 5. Uncertainty of the signal of the TOC Analyser determined using standard solution of IC, TC and ultra-pure water.

Date	Ultra-pure water		Standard TC			Standard IC			Uncertainty	
	TC	IC	theoretical	measured	±	theoretical	measured	±	TC	IC
	ppm	ppm	ppm	ppm	ppm	ppm	ppm	ppm	%	%
11/06/15	-0.035	-0.004	5	5.09		5	5.18		2.4	3.7
25/06/15	-0.097	-0.019	2	1.837		2	1.838		3.3	7.2
08/09/15	0.015	-0.022	2	1.958	0.13	2	1.977	0.050	2.9	0.05
08/09/15	/	/	2	2.155	0.07	/	/	/	7.0	/
10/09/15	-0.058	-0.004	2	1.949	0.09	2	1.862	0.008	0.4	6.7
10/09/15	/	/	2	1.992	0.03	2	2.073	0.07	2.5	3.9
25/09/15	0.010	-0.017	2	1.959	0.12	2	1.921	0.02	2.6	3.1
25/09/15	0.144	0.024	2	2.089	0.05	2	2.146	0.02	4.0	8.2

Table C. 6. TOC measurements of the experimental tests.

ID	TC (ppm)		IC(ppm)		TOC éch. (ppm)	
	valeur	± (k=2)	valeur	± (k=2)	valeur	± (k=2)
Test_blanc_eau UP 25/06	0.13	0.01	0.0420	0.0031	0.084	0.007
Test_tube_1_80°C_COT_t1	2.42	0.12	0.0040	0.0003	2.413	0.116
Test_tube_1_80°C_COT_t2	0.94	/	0.4880	/	0.449	/
Test_tube_1_80°C_COT_t3	1.33	/	0.4630	/	0.862	/
Test_tube_1_80°C_COT_t4	1.15	/	0.7440	/	0.409	/
Test_tube_1_80°C_COT_t5	0.75	/	0.2540	/	0.500	/
Test_tube_1_80°C_COT_t6	1.39	/	0.9290	/	0.464	/
Test_tube_1_80°C_COT_t7	1.29	/	0.5030	/	0.788	/
Test_tube_2_80°C_COT_t1	1.60	/	0.6580	/	0.939	/
Test_tube_2_80°C_COT_t2	1.27	/	0.3260	/	0.944	/
Test_tube_2_80°C_COT_t3	1.35	/	0.8510	/	0.498	/
Test_tube_2_80°C_COT_t4	1.48	/	0.7110	/	0.764	/
Test_tube_2_80°C_COT_t5	1.19	/	0.2470	/	0.945	/
Test_tube_1_20°C_COT_t1	0.74	/	0.6230	/	0.120	/
Test_tube_1_20°C_COT_t2	1.17	/	0.9080	/	0.260	/
Test_tube_1_20°C_COT_t3	0.64	/	0.5750	/	0.064	/
Test_tube_blanc 10/09	0.40	0.01	0.4760	0.0319	-0.08	0.03
Test_tube_COT_20°C_A0	1.15	0.08	0.8410	0.0004	0.31	0.08
Test_tube_COT_20°C_A1	0.20	0.01	0.2400	0.0001	<lq	
Test_tube_COT_20°C_B0	1.12	0.08	0.7130	0.0004	0.40	0.08
Test_tube_COT_20°C_B1	0.26	0.02	0.2040	0.0001	0.05	0.02
Test_tube_COT_20°C_B2	0.17	0.01	0.1490	0.0001	0.022	0.012
Test_tube_COT_20°C_C1	1.22	0.09	0.7650	0.0004	0.46	0.09
Test_tube_COT_20°C_C2	0.17	0.01	0.1680	0.0001	<lq	
Test_tube_COT_20°C_D0	0.77	0.05	0.7270	0.0004	0.04	0.05
Test_tube_COT_60°C_A0	1.91	0.13	0.7060	0.0004	1.20	0.13
Test_tube_COT_60°C_A1	0.88	0.06	0.2410	0.0001	0.64	0.06
Test_tube_COT_60°C_A2	0.52	0.04	0.1390	0.0001	0.38	0.04
Test_tube_COT_60°C_B0	1.78	0.12	0.5770	0.0003	1.20	0.12
Test_tube_COT_60°C_B1	0.52	0.04	0.1660	0.0001	0.36	0.04
Test_tube_COT_60°C_B2	0.53	0.04	0.2450	0.0001	0.29	0.04
Test_tube_COT_60°C_C1	1.40	0.10	0.6700	0.0003	0.73	0.10
Test_tube_COT_60°C_C2	0.54	0.04	0.2370	0.0001	0.31	0.04
Test_tube_COT_60°C_C3	0.46	0.03	0.2320	0.0001	0.23	0.03
Test_tube_COT_60°C_D0	1.04	0.07	0.6710	0.0003	0.37	0.07
Test_tube_COT_60°C_D1	0.46	0.03	0.2050	0.0001	0.26	0.03
Test_tube_COT_60°C_D2	0.38	0.03	0.2090	0.0001	0.17	0.03
Test_tube_COT_80°C_A0	2.84	0.20	0.8260	0.0004	2.0	0.2
Test_tube_COT_80°C_A1	0.94	0.07	0.1590	0.0001	0.78	0.07
Test_tube_COT_80°C_A2	1.05	0.03	0.2440	0.0163	0.81	0.03
Test_tube_COT_80°C_B0	2.87	0.07	0.7010	0.0470	2.17	0.09
Test_tube_COT_80°C_B1	1.51	0.04	0.4690	0.0314	1.04	0.05
Test_tube_COT_80°C_B2	1.03	0.03	0.1850	0.0124	0.84	0.03
Test_tube_COT_80°C_C1	1.91	0.05	0.1840	0.0123	1.72	0.05
Test_tube_COT_80°C_C2	1.25	0.03	0.2420	0.0162	1.00	0.04
Test_tube_COT_80°C_C3	0.99	0.02	0.1830	0.0123	0.80	0.03
Test_tube_COT_80°C_D0	1.24	0.03	0.0720	0.0048	1.17	0.03
Test_tube_COT_80°C_D1	0.72	0.02	0.2280	0.0153	0.49	0.02
Test_tube_COT_80°C_D2	0.61	0.02	0.1970	0.0132	0.41	0.02
Test_tube_blanc 22/09	0.58	0.02	0.6160	0.0502	<lq	0.06
Test_tube_COT_20°C_E1	0.89	0.03	0.6430	0.0524	0.24	0.06
Test_tube_COT_20°C_E2	0.29	0.01	0.3140	0.0256	<lq	0.03
Test_tube_COT_60°C_E1	1.18	0.05	0.5640	0.0460	0.62	0.07

ID	TC (ppm)		IC(ppm)		TOC éch. (ppm)	
	valeur	± (k=2)	valeur	± (k=2)	valeur	± (k=2)
Test_tube_COT_60°C_E2	0.81	0.03	0.1930	0.0157	0.62	0.04
Test_tube_COT_60°C_E3	0.45	0.02	0.0690	0.0056	0.38	0.02
Test_tube_COT_60°C_E1	2.20	0.09	0.5710	0.0465	1.63	0.10
Test_tube_COT_80°C_E2	1.70	0.07	0.3420	0.0279	1.36	0.07
Test_tube_COT_80°C_E3	0.71	0.03	0.0870	0.0071	0.62	0.03
Test_tube_blanc_22/09	17.32	0.68	3.5300	0.2877	13.79	0.74
Test_tube_COT_20°C_E1	-0.01	0.00	0.0170	0.0014	-0.03	0.00

C.2. Chemical composition of stock solutions:

Table C. 7. Chemical composition of the synthetic Callovo-Oxfordian porewater. Uncertainty of k=2

Porewater	Na	Ca	K	Mg	Cl	SO42+
1% CO ₂ (g)	42.8(±1.3)	8.3(±0.3)	1.06(±0.16)	5.4(±0.2)	40.2(±1.4)	13.9(±0.6)
5% CO ₂ (g)	42.9(±1.3)	8.4(±0.3)	0.91(±0.17)	5.4(±0.2)		

Table C. 8. Measurements of the pH for the sorption edge experiments in atmospheric pCO₂. ⁽¹⁾ used only in the experiments at 80°C; ⁽²⁾ this solution was not taken for the experiments performed at 20°C.

	bubbling Ar/CO ₂ (g)	After overnight agitation in pCO ₂ atmospheric
pH Theoretical	time	pH final
3.8	-	3.9
6	-	6.1
7	1h	7.2
7.5	30 min	7.4 ⁽¹⁾
8	1h	8.0
8.5	50 min	8.5 ⁽¹⁾
9.3	3h	9.8 ⁽²⁾

C.3. Speciation of Ca-U(VI)-CO₃ species experimental results:

Table C. 9. Alkalinity measurements using H₂SO₄ (0.16 N) in the blank samples of the batch experiments using anionic-exchange resin. *measured

Experiment	T	NaHCO ₃ (0.01M)	pH	digits acid	vol. sample	Alkalinity meq/L
E1A	20°C	600 µL	7.43	105	10	2.10 (±0.1)
E1B			7.18	124	10	2.48 (±0.12)
E2A	40°C	595 µL	7.25*	115.5	10	2.16 (±0.11)
E2B			7.17	124	10	2.48 (±0.12)
E3A	60°C	580 µL	6.88	114	10	1.90 (±0.1)
E3B			6.93	100	10	2.23 (±0.1)
E4A	80°C	568 µL	6.91	109	10	2.18 (±0.1)

Experiment	T	NaHCO ₃ (0.01M)	pH	digits acid	vol. sample	Alkalinity meq/L
E4B			6.89	110	10	2.20 (±0.1)

Table C. 10. Experimental results of the ionic exchange method at 20 °C in atmospheric conditions in the presence of calcium, 0.1 M of NaClO₄ at fixed solid-liquid ratio adding initially [U(VI)] = 5·10⁻⁷M.

ID	Ca	resin		pH	U-238 in solution		U-238 in sorbed		K _D	
	mM	g	±	final	mol/L	±	mol/g	±	mL/g	±
Mother sol.	/	/	/	/	4.74E-05	3.32E-06	/	/	/	/
E0-0	0	0.06345	0.002	7.6	4.64E-07	2.90E-08	4.14E-09	1.74E-08	8.9	37.4
E0-0_0	/	0	0	7.82	4.03E-07	4.62E-08	/	/	/	/
E0-1	0.1	0.06306	0.002	7.6	4.60E-07	2.77E-08	5.66E-09	1.71E-08	12.3	37.3
E0-1_0	/	0	0	7.81	4.16E-07	4.20E-08	/	/	/	/
E0-2	0.2	0.06336	0.002	7.62	4.28E-07	3.15E-08	1.82E-08	1.81E-08	42.6	42.3
E0-2_0	/	0	0	7.89	4.16E-07	5.04E-08	/	/	/	/
E0-3	0.3	0.06256	0.002	7.65	4.48E-07	3.40E-08	1.06E-08	1.90E-08	23.6	42.5
E0-3_0	/	0	0	7.84	4.08E-07	4.62E-08	/	/	/	/
E0-4	0.4	0.06237	0.002	7.68	4.20E-07	3.95E-08	2.19E-08	2.07E-08	52.2	49.5
E0-4_0	/	0	0	7.89	4.50E-07	4.20E-08	/	/	/	/
E0-5	0.5	0.06341	0.002	7.71	4.42E-07	3.91E-08	1.28E-08	2.02E-08	28.9	45.8
E0-5_0	/	0	0	7.94	4.21E-07	3.36E-08	/	/	/	/
E0-6	1.0	0.06372	0.002	7.72	4.26E-07	4.03E-08	1.91E-08	2.05E-08	44.9	48.4
E0-6_0	/	0	0	7.95	4.08E-07	2.65E-08	/	/	/	/
E0-7	2.0	0.06292	0.002	7.73	4.33E-07	4.62E-08	1.65E-08	2.26E-08	38.2	52.4
E0-7_0	/	0	0	7.98	4.16E-07	2.82E-08	/	/	/	/
E0-8	3.0	0.06249	0.002	7.65	4.29E-07	5.04E-08	1.83E-08	2.42E-08	42.8	56.6
E0-8_0	/	0	0	7.86	4.12E-07	2.27E-08	/	/	/	/
E0-9	4.0	0.0622	0.002	7.64	4.24E-07	5.88E-08	2.01E-08	2.72E-08	47.4	64.3
E0-9_0	/	0	0	7.89	4.43E-07	2.23E-08	/	/	/	/
E0-10	5.0	0.06282	0.002	7.67	4.54E-07	5.88E-08	8.19E-09	2.69E-08	18.1	59.3
E0-10_0	/	0	0	7.81	4.17E-07	2.02E-08	/	/	/	/

Table C. 11. Experimental results of the ionic exchange method at 20 °C in closed system at 1% of CO₂(g) in the absence of calcium and varying the solid-liquid ration, in 0.1M of NaNO₃ adding initially [U(VI)] = 5·10⁻⁷M. (Ba: blank sample without U(VI); Bb: blank sample without resin with U)

ID	resin		S/L	pH		T	U-238 in solution		U sorbed		K _D	
	g	±	g/L	±	final	°C	mol/L	±	mol/g	±	mL/g	±
	Mother sol.	/	/	/	/	/	/	5.21E-05	2.61E-06	/	/	/
E1A-1	0.03119	0.001	1.25	0.06	7.44	21.2	8.74E-08	7.98E-09	3.48E-07	2.79E-08	3981	484
E1A-2	0.06649	0.002	2.66	0.13	7.41	21.2	4.92E-08	7.98E-09	1.78E-07	1.36E-08	3612	648
E1A-3	0.07609	0.002	5.07	0.37	7.35	21.1	2.65E-08	8.82E-09	9.76E-08	8.96E-09	3686	1274
E1A-4	0.1592	0.005	10.61	0.78	7.24	21.2	1.39E-08	7.14E-09	4.78E-08	4.32E-09	3449	1804
E1A-5	0.22736	0.007	15.16	1.11	7.2	21.1	1.13E-08	7.14E-09	3.37E-08	3.04E-09	2966	1887
E1A-6	0.20939	0.006	20.94	2.19	7.18	20.6	9.24E-09	7.14E-09	2.45E-08	2.86E-09	2646	2068
E1A-7	0.25824	0.008	25.82	2.70	7.14	20.8	6.43E-09	2.73E-09	1.99E-08	2.32E-09	3102	1366
E1A-Ba	0.06287	0.002	2.51	0.13	7.43	20.9	/	/	/	/	/	/
E1A-Bb	/	/	/	/	7.5	21.2	1.01E-06	2.10E-06	/	/	/	/

Table C. 12. Experimental results of the ionic exchange method at 20 °C in closed system at 1% of CO₂(g) in the presence of calcium, 0.1 M of NaNO₃ at fixed solid-liquid ratio adding initially [U(VI)] = 5·10⁻⁷M. (blank samples in the absence of calcium or presence of calcium for Ba: without U(VI); and Bb: without resin with U)

ID	Ca	resin		pH Final	U-238 in solution		U-sorbed		K _D	
		mM	g		±	mol/L	±	mol/g	±	mL/g
Mother sol.	/	/	/	/	5.42E-05	3.32E-06	/	/	/	/
E1B-0	0	0.06247	0.0019	7.32	4.45E-08	1.68E-08	1.99E-07	1.60E-08	4470	1725
E1B-1	0.1	0.06242	0.0019	7.18	8.15E-08	1.60E-08	1.84E-07	1.58E-08	2263	484
E1B-2	0.2	0.06319	0.0019	7.16	9.41E-08	1.60E-08	1.77E-07	1.55E-08	1883	359
E1B-3	0.2	0.06225	0.0019	7.17	1.07E-07	1.55E-08	1.75E-07	1.56E-08	1630	278
E1B-4	0.2	0.06236	0.0019	7.18	1.28E-07	1.55E-08	1.66E-07	1.55E-08	1295	198
E1B-5	0.2	0.06302	0.0019	7.15	1.34E-07	1.60E-08	1.62E-07	1.54E-08	1213	185
E1B-6	1	0.06288	0.0019	7.16	1.94E-07	1.81E-08	1.38E-07	1.56E-08	715	105
E1B-7	2	0.06231	0.0019	7.16	2.50E-07	1.81E-08	1.17E-07	1.56E-08	470	71
E1B-8	3	0.06235	0.0019	7.14	3.17E-07	2.61E-08	9.03E-08	1.71E-08	285	59
E1B-9	4	0.06228	0.0019	7.16	3.69E-07	3.61E-08	6.93E-08	1.98E-08	188	57
E1B-10	5	0.06271	0.0019	7.22	4.02E-07	3.78E-08	5.59E-08	2.01E-08	139	52
E1B-Ba_0	0	0.06261	0.0019	7.23	2.52E-09	1.55E-08	/	/	/	/
E1B-Ba_10	5	0.06287	0.0019	7.2	2.52E-09	1.55E-08	/	/	/	/
E1B-Bb_0	0	/	/	7.12	3.46E-07	2.18E-08	/	/	/	/
E1B-Bb_10	5	/	/	7.12	5.00E-07	3.66E-08	/	/	/	/

Table C. 13. Experimental results of the ionic exchange method at 40 °C in closed system at 1% of CO₂(g) in the absence of calcium and varying the solid-liquid ration, in 0.1M of NaNO₃ adding initially [U(VI)] = 5·10⁻⁷M. (Ba: blank sample without U(VI); Bb: blank sample without resin with U)

ID	resin		S/L	pH final	T °C	U-238 in solution		U sorbed		K _D	
	g	±				g/L	±	mol/L	±	mol/g	±
	Mother sol.	/	/	/	/	/	5.21E-05	2.61E-06	/	/	/
E2A-1	0.02577	0.001	1.03	0.05	/	1.03E-07	7.56E-09	4.06E-07	3.32E-08	3944	434
E2A-2	0.06331	0.002	2.53	0.13	/	5.34E-08	9.66E-09	1.85E-07	1.43E-08	3464	682
E2A-3	0.07602	0.002	5.07	0.37	/	3.03E-08	5.88E-09	9.69E-08	8.83E-09	3204	688
E2A-4	0.15057	0.005	10.04	0.73	/	1.51E-08	5.46E-09	5.04E-08	4.54E-09	3335	1241
E2A-5	/	/	/	/	/	/	/	/	/	/	/
E2A-6	/	/	/	/	/	/	/	/	/	/	/
E2A-7	0.25065	0.008	25.32	2.67	/	1.09E-08	5.88E-09	2.02E-08	2.37E-09	1846	1017
E2A-Ba	0.0624	0.002	2.50	0.12	/	/	/	/	/	/	/
E2A-Bb	0	0.000	0	/	/	7.14E-07	1.76E-06	/	/	/	/

Table C. 14. Experimental results of the ionic exchange method at 40 °C in closed system at 1% of CO₂(g) in the presence of calcium, 0.1 M of NaNO₃ at fixed solid-liquid ratio adding initially [U(VI)] = 5·10⁻⁷M. (blank samples in the absence of calcium or presence of calcium for Ba: without U(VI); and Bb: without resin with U)

ID	Ca	resin		pH Final	T °C	U-238 in solution		U-sorbed		K _D	
		mM	g			±	mol/L	±	mol/g	±	mL/g
Mother sol.	/	/	/	/	/	5.21E-05	1.26E-05	/	/	/	/
E2B-0	0	0.0637	0.002	7.16	38.8	5.17E-08	1.13E-08	1.84E-07	5.00E-08	3564	1244
E2B-1	0.1	0.0621	0.002	7.18	35	6.09E-08	1.30E-08	1.85E-07	5.13E-08	3040	1064
E2B-2	0.2	0.0627	0.002	7.19	38	7.61E-08	1.43E-08	1.77E-07	5.09E-08	2333	800
E2B-3	0.2	0.0622	0.002	7.18	39	8.70E-08	1.51E-08	1.74E-07	5.13E-08	2006	685
E2B-4	0.2	0.0633	0.002	7.16	38.3	9.79E-08	1.60E-08	1.67E-07	5.04E-08	1707	586
E2B-5	0.2	0.0622	0.002	7.15	37.9	1.08E-07	1.72E-08	1.66E-07	5.14E-08	1530	533
E2B-6	1	0.0627	0.002	7.17	38	1.59E-07	2.02E-08	1.44E-07	5.11E-08	906	341

ID	Ca	resin		pH	T	U-238 in solution		U-sorbed		K _D	
						Final	°C				
		mM	g	±			mol/L	±	mol/g	±	mL/g
E2B-7	2	0.0628	0.002	7.17	37.9	2.45E-07	3.36E-08	1.10E-07	5.20E-08	450	222
E2B-8	3	0.0633	0.002	7.13	37.8	2.94E-07	4.20E-08	8.96E-08	5.25E-08	305	184
E2B-9	4	0.0631	0.002	7.16	37.6	3.26E-07	3.99E-08	7.72E-08	5.24E-08	237	163
E2B-10	5	0.0622	0.002	7.16	37.9	3.61E-07	4.62E-08	6.42E-08	5.40E-08	178	151
E2B-Ba_0	0	/	/	7.12	38.6	4.50E-07	5.88E-08	/	/	/	/
E2B-Ba_10	5	/	/	7.16	38	4.58E-07	5.88E-08	/	/	/	/
E2B-Bb_0	0	0.0622	0.002	7.23	38	8.40E-10	9.66E-09	/	/	/	/
E2B-Bb_10	5	0.0632	0.002	7.2	37.2	8.40E-10	9.66E-09	/	/	/	/

Table C. 15. Experimental results of the ionic exchange method at 60 °C in closed system at 3% of CO₂(g) in the absence of calcium and varying the solid-liquid ration, in 0.1M of NaNO₃ adding initially [U(VI)] = 5·10⁻⁷M. (Ba: blank sample without U(VI); Bb: blank sample without resin with U)

ID	resin		S/L		pH	T	U-238 in solution		U sorbed		K _D	
							final	°C				
	g	±	g/L	±			mol/L	±	mol/g	±	mL/g	±
Mother sol.	/	/	/	/	/	/	4.83E-05	2.31E-06	/	/	/	/
E3A-1	0.02561	0.001	1.02	0.05	/	/	1.10E-07	6.72E-09	3.64E-07	2.97E-08	3305	337
E3A-2	0.06252	0.002	2.50	0.13	/	/	6.29E-08	3.99E-09	1.68E-07	1.26E-08	2667	262
E3A-3	0.07438	0.002	4.96	0.36	/	/	3.56E-08	3.07E-09	9.02E-08	8.10E-09	2534	315
E3A-4	0.14737	0.004	9.82	0.72	/	/	2.49E-08	2.94E-09	4.66E-08	4.15E-09	1870	277
E3A-5	/	/	/	/	/	/	/	/	/	/	/	/
E3A-6	/	/	/	/	/	/	/	/	/	/	/	/
E3A-7	0.2551	0.008	25.51	2.66	/	/	1.71E-08	2.82E-09	1.83E-08	2.11E-09	1070	216
E3A-Ba	0.06321	0.002	2.53	0.13	/	/	/	/	/	/	/	/
E3A-Bb	/	/	/	/	/	/	1.51E-09	2.73E-09	/	/	/	/

Table C. 16. Experimental results of the ionic exchange method at 60 °C in closed system at 3% of CO₂(g) in the presence of calcium, 0.1 M of NaNO₃ at fixed solid-liquid ratio adding initially [U(VI)] = 5·10⁻⁷M. (blank samples in the absence of calcium or presence of calcium for Ba: without U(VI); and Bb: without resin with U)

ID	Ca	resin		pH	T	U-238 in solution		U-sorbed		K _D	
						Final	°C				
		mM	g	±			mol/L	±	mol/g	±	mL/g
Mother sol.	/	/	/	/	/	5.47E-05	3.40E-06	/	/	/	/
E3B-0	0	0.06529	0.002	6.89	57.9	4.03E-08	8.40E-09	1.94E-07	1.46E-08	4810	1066
E3B-1	0.1	0.06224	0.002	6.89	58.1	5.55E-08	8.82E-09	1.97E-07	1.53E-08	3560	630
E3B-2	0.2	0.0624	0.002	6.89	54	4.71E-08	7.98E-09	2.00E-07	1.52E-08	4257	791
E3B-3	0.2	0.06223	0.002	6.89	57.6	5.59E-08	7.56E-09	1.97E-07	1.52E-08	3531	550
E3B-4	0.2	0.06478	0.002	6.89	56.4	6.34E-08	9.66E-09	1.87E-07	1.48E-08	2942	505
E3B-5	0.2	0.06222	0.002	6.89	59.4	7.02E-08	9.66E-09	1.92E-07	1.53E-08	2731	435
E3B-6	1	0.06264	0.002	6.88	58.9	1.01E-07	1.22E-08	1.78E-07	1.54E-08	1766	262
E3B-7	2	0.06215	0.002	6.9	58.7	1.59E-07	1.55E-08	1.56E-07	1.58E-08	983	138
E3B-8	3	0.0626	0.002	6.88	58.3	2.17E-07	1.51E-08	1.32E-07	1.54E-08	606	82
E3B-9	4	0.06236	0.002	6.86	58.1	2.66E-07	1.60E-08	1.13E-07	1.54E-08	425	64
E3B-10	5	0.0622	0.002	6.86	56.2	3.09E-07	1.97E-08	9.56E-08	1.61E-08	309	56
E3B-Ba_0	0	/	/	6.98	57.7	6.72E-07	1.81E-06	/	/	/	/
E3B-Ba_10	5	/	/	6.96	57.3	7.56E-07	1.76E-06	/	/	/	/
E3B-Bb_0	0	0.06295	0.002	6.95	56.8	/	/	/	/	/	/
E3B-Bb_10	5	0.06445	0.002	6.91	56.3	/	/	/	/	/	/

Table C. 17. Experimental results of the ionic exchange method at 80 °C in closed system at 5% of CO₂(g) in the absence of calcium and varying the solid-liquid ration, in 0.1M of NaNO₃ adding initially [U(VI)] = 5·10⁻⁷M. (Ba: blank sample without U(VI); Bb: blank sample without resin with U)

ID	resin		S/L		pH	T	U-238 in solution		U sorbed		K _D	
					final							
	g	±	g/L	±		°C	mol/L	±	mol/g	±	mL/g	±
Mother sol.	/	/	/	/	/	/	4.93E-05	2.77E-06	/	/	/	/
E4A-1	0.0254	0.001	1.02	0.05	6.9	62.2	1.48E-07	7.56E-09	3.40E-07	1.85E-08	2296	172
E4A-2	0.06324	0.002	2.50	0.12	6.89	62.2	9.08E-08	5.04E-09	1.61E-07	8.24E-09	1775	134
E4A-3	0.07611	0.002	5.07	0.37	6.77	59.6	4.81E-08	3.32E-09	8.77E-08	6.44E-09	1822	184
E4A-4	0.14902	0.004	9.93	0.73	6.73	72.2	5.50E-08	3.49E-09	4.41E-08	3.24E-09	801	78
E4A-5	0.22179	0.007	14.79	1.08	6.72	73.7	5.58E-08	3.32E-09	2.96E-08	2.17E-09	530	50
E4A-6	0.19618	0.006	19.62	2.05	6.67	72.8	4.52E-08	2.98E-09	2.28E-08	2.39E-09	505	63
E4A-7	0.24639	0.007	24.64	2.57	6.6	69	3.53E-08	2.82E-09	1.86E-08	1.94E-09	526	69
E4A-Ba	0.06221	0.002	2.49	0.12	6.87	58.7	-3.36E-10	1.51E-09	/	/	/	/
E4A-Bb	/	/	/	/	6.88	57.3	2.10E-12	4.62E-12	/	/	/	/

Table C. 18. Experimental results of the ionic exchange method at 80 °C in closed system at 5% of CO₂(g) in the presence of calcium, 0.1 M of NaNO₃ at fixed solid-liquid ratio adding initially [U(VI)] = 5·10⁻⁷M. (blank samples in the absence of calcium or presence of calcium for Ba: without U(VI); and Bb: without resin with U)

ID	Ca	resin		pH	T	U-238 in solution		U-sorbed		K _D	
				Final	°C						
	mM	g	±			mol/L	±	mol/g	±	mL/g	±
Mother sol.	/	/	/	/	/	6.22E-08	4.62E-09	/	/	/	/
E4B-0	0	0.06278	0.002	6.87	78.1	6.85E-08	5.04E-09	1.92E-07	1.53E-08	3081	336
E4B-1	0.1	0.06229	0.002	6.87	79.1	7.18E-08	4.62E-09	1.91E-07	1.54E-08	2782	304
E4B-2	0.2	0.06234	0.002	6.86	77.7	7.39E-08	5.04E-09	1.89E-07	1.54E-08	2631	273
E4B-3	0.2	0.06357	0.002	6.85	76.7	7.90E-08	5.04E-09	1.85E-07	1.51E-08	2496	266
E4B-4	0.2	0.06284	0.002	6.9	77.7	8.36E-08	5.04E-09	1.85E-07	1.52E-08	2338	244
E4B-5	0.2	0.0623	0.002	6.89	78.1	1.09E-07	5.88E-09	1.84E-07	1.53E-08	2206	227
E4B-6	1	0.06255	0.002	6.89	77	1.72E-07	8.40E-09	1.73E-07	1.52E-08	1588	163
E4B-7	2	0.06357	0.002	6.87	76	2.24E-07	1.01E-08	1.46E-07	1.49E-08	847	96
E4B-8	3	0.06266	0.002	6.85	75	2.87E-07	1.51E-08	1.27E-07	1.51E-08	567	72
E4B-9	4	0.06244	0.002	6.82	73	3.20E-07	1.60E-08	1.03E-07	1.57E-08	358	58
E4B-10	5	0.06302	0.002	6.81	75.4	1.92E-07	1.05E-08	8.85E-08	1.56E-08	276	51
E4B-Ba_0	0	/	/	6.93	75.4	5.50E-07	2.31E-08	/	/	/	/
E4B-Ba_10	5	/	/	6.91	73	/	/	/	/	/	/
E4B-Bb_0	0	0.06229	0.002	6.89	73.3	/	/	/	/	/	/
E4B-Bb_10	5	0.06327	0.002	6.86	56.3	6.22E-08	4.62E-09	/	/	/	/

C.4. Kinetic experiments

C.4.1. Callovo-Oxfordian claystone:

Table C. 19. Kinetic results of sorption of U(VI) onto Callovo-Oxfordian claystone at 20 °C in 1% CO₂(g), using synthetic Callovo-Oxfordian porewater and initial U(VI) = 6.8(±0.2)·10⁻⁷M.

ID	Time	S/L		pH	Temp	U(VI) in solution		U(VI) sorbed		K _D	
		g/L	±			°C	mol/L	±	mol/g	±	mL/g
1	1	24.3	0.3	7.38	19.6	6.1E-7	2E-8	2.9E-9	6E-9	4.8	2.5

ID	Time days	S/L		pH	Temp °C	U(VI) in solution		U(VI) sorbed		K _D	
		g/L	±			mol/L	±	mol/g	±	mL/g	±
2	2	24.3	0.3	7.35	18.8	6.2E-7	3E-8	2.7E-9	5E-9	4.3	2.5
3	3	24.3	0.3	7.07	20	6.2E-7	2E-8	2.7E-9	5E-9	4.4	2.3
4	7	24.4	0.3	7.30	19.7	6.1E-7	3E-8	3.2E-9	6E-9	5.4	2.8
5	14	24.3	0.3	7.25	19.7	5.7E-7	3E-8	4.8E-9	1E-8	8.4	2.8

Table C. 20. Kinetic results of sorption of U(VI) onto Callovo-Oxfordian claystone at 80 °C in 5% CO₂(g), using synthetic Callovo-Oxfordian porewater and initial U(VI) = 6.8(±0.2)·10⁻⁷M.

ID	Time days	S/L		pH	Temp °C	U(VI) in solution		U(VI) sorbed		K _D	
		g/L	±			mol/L	±	mol/g	±	mL/g	±
1	1	24.3	0.3	6.85	80.0	8.7E-8	5E-9	2.9E-9	6E-9	284	25
2	2	24.3	0.3	6.88	80.2	7.6E-8	7E-9	2.7E-9	5E-9	329	37
3	3	24.3	0.3	6.88	75.6	6.8E-8	4E-9	2.7E-9	5E-9	370	32
4	7	24.4	0.3	6.85	81.2	4.9E-8	5E-9	3.2E-9	6E-9	537	68
5	14	24.3	0.3	6.87	80.2	3.4E-8	4E-9	4.8E-9	1E-8	793	109

C.4.2. Illite:

Table C. 21. Kinetic results of sorption of U(VI) onto Illite at 20 °C in 1% CO₂(g), using synthetic Callovo-Oxfordian porewater and initial U(VI) = 9.6(±0.8)·10⁻⁸M.

ID	Time days	S/L		pH	Temp °C	U(VI) in solution		U(VI) sorbed		K _D	
		g/L	±			mol/L	±	mol/g	±	mL/g	±
1	1	0.50	0.03	6.27	21.8	8.5E-9	5E-10	1.03E-8	2.63E-8	20694	2626
2	2	0.50	0.03	6.31	22.0	5.2E-9	5E-10	1.00E-8	2.63E-8	35269	4910
3	3	0.50	0.03	6.23	20.4	5.5E-9	5E-10	1.01E-8	2.63E-8	32993	4486
4	7	0.50	0.03	6.33	20.5	4.1E-9	4E-10	1.06E-8	2.62E-8	45259	6654
5	14	0.50	0.03	6.41	22.2	2.6E-9	4E-10	1.21E-8	2.63E-8	72416	13404

Table C. 22. Kinetic results of sorption of U(VI) onto illite at 80 °C in 5% CO₂(g), using synthetic Callovo-Oxfordian porewater and initial U(VI) = 6.8(±0.2)·10⁻⁷M.

ID	Time days	S/L		pH	Temp °C	U(VI) in solution		U(VI) sorbed		K _D	
		g/L	±			mol/L	±	mol/g	±	mL/g	±
1	1	0.50	0.03	6.63	79.8	2.8E-9	4E-10	1.87E-07	1.96E-08	67037	11811
2	2	0.50	0.03	6.63	78.8	2.4E-9	5E-10	1.88E-07	1.97E-08	77035	17863
3	3	0.50	0.03	6.16	80.3	1.7E-9	4E-10	1.89E-07	1.97E-08	110630	28773
4	7	0.50	0.03	6.54	79.9	1.8E-9	4E-10	1.89E-07	1.97E-08	106626	26449
5	14	0.50	0.03	6.28	81.6	8.5E-10	4E-10	1.91E-07	1.98E-08	223814	101897

C.5. Illite: sorption experiments

C.5.1. Sorption isotherms:

Table C. 23. Alkalinity measurements in sorption isotherms experiments of U(VI)/illite system (2 g/L) at different temperatures. *synthetic Callovo-Oxfordian porewater.

atmosphere	T	pH	Acid H ₂ SO ₄	Vol. acid	±	Alkalinity	±
	°C		N	digits		meq/L	
Ar(g)	20	6.57	0.02	31	13.0	0.08	0.03
Atmospheric	20	7.3	0.02	94	37.6	0.24	0.09
1% CO ₂ (g)	20	7.26	0.2	127	50.8	2.54	1.02
5% CO ₂ (g)	20	6.62	0.2	114	45.6	2.28	0.91
1% CO ₂ (g)*	20	7.18	0.2	127	50.8	2.54	1.02
Ar(g)	60	6.48	0.02	33	13.2	0.08	0.03
Atmospheric	60	7.57	0.02	96	134	0.24	0.34
1% CO ₂ (g)	60	7.45	0.2	127	50.8	2.54	1.02
5% CO ₂ (g)	60	6.89	0.2	127	50.8	2.54	1.02
Ar(g)	80	6.53	0.02	31	12.4	0.08	0.03
Atmospheric	80	7.11	0.02	91	36.4	0.23	0.09
1% CO ₂ (g)	80	7.67	0.2	118	47.2	2.36	0.94
5% CO ₂ (g)	80	7.08	0.2	118	47.2	2.36	0.94
5% CO ₂ (g)*	80	6.85	0.2	108	43.2	2.16	0.86

Table C. 24. Experimental results of the sorption isotherms of U(VI) onto illite at 20 °C in Ar(g) in 0.1 M of NaNO₃ at fixed solid-liquid ratio. (BF: blank sample filtrated; BNF: blank sample no filtrated)

ID		1	2	3	4	5	6	7
illite	(g)	0.05	0.053	0.05	0.054	0.049	0.051	0.052
	g/L	2	2.12	2	2.16	1.96	2.04	2.08
	±	0.05	0.05	0.05	0.05	0.05	0.05	0.05
U(VI) ini	mol/L	4.61E-08	1.29E-07	2.77E-07	5.54E-07	2.76E-06	8.29E-06	2.21E-05
	±	2.70E-09	7.06E-09	1.57E-08	3.17E-08	1.43E-07	4.45E-07	1.20E-06
pH	/	6.46	6.52	6.52	6.52	6.44	6.28	6.01
	°C	22.1	22.3	22.3	22.2	22.1	22.1	22.1
U(VI) eq.	mol/L	3.66E-10	1.43E-09	3.09E-09	6.64E-09	7.10E-09	1.32E-08	3.11E-08
	±	1.05E-10	1.22E-10	1.72E-10	3.53E-10	3.36E-10	1.26E-09	2.06E-09
U(VI) sorb.	mol/g	2.29E-08	6.03E-08	1.37E-07	2.53E-07	1.41E-06	4.06E-06	1.06E-05
	±	1.47E-09	3.65E-09	8.59E-09	1.59E-08	8.17E-08	2.41E-07	6.35E-07
K _d	mL/g	62603	42181	44316	38120	198137	306699	341978
	±	18436	4412	3720	3138	14844	34423	30541

Table C. 25. Experimental results of the sorption isotherms of U(VI) onto illite at 20 °C in atmospheric conditions in 0.1 M of NaCl at fixed solid-liquid ratio. (BF: blank sample filtrated; BNF: blank sample no filtrated)

ID		8-BF	8-BNF	9-BF	9-BNF	1	2	3	4	5	6	7
illite	(g)	/	/	/	/	0.049	0.05	0.05	0.052	0.049	0.049	0.05
	g/L					1.96	2	2	2.08	1.96	1.96	2
	±					0.05	0.05	0.05	0.05	0.05	0.05	0.05
U(VI) ini	mol/L	2.64E-08	2.64E-08	1.73E-05	1.73E-05	2.64E-08	7.39E-08	1.58E-07	3.17E-07	2.16E-06	6.48E-06	1.73E-05
	±	1.45E-09	1.45E-09	9.74E-07	9.74E-07	1.49E-09	3.86E-09	8.60E-09	1.74E-08	1.08E-07	3.36E-07	9.08E-07
pH	/	7.3	7.3	6.76	6.76	7.31	7.35	7.36	7.34	7.33	7.27	7.11
T	°C	20.6	20.6	20.3	20.3	20.7	20.7	20.3	20.6	20.7	20.5	20.7
U(VI) eq.	mol/L	2.67E-08	1.78E-05	1.80E-05	4.45E-10	1.55E-09	2.98E-09	9.24E-09	1.29E-07	1.47E-07	4.78E-07	2.56E-08
	±	1.26E-09	7.98E-07	8.82E-07	1.68E-10	4.20E-10	4.62E-10	1.85E-09	1.05E-08	7.14E-09	2.82E-08	1.51E-09
U(VI) sorb.	mol/g	/	/	/	/	1.32E-08	3.61E-08	7.77E-08	1.48E-07	1.04E-06	3.23E-06	8.40E-06
	±	/	/	/	/	8.37E-10	2.15E-09	4.74E-09	9.19E-09	6.15E-08	1.91E-07	5.02E-07
K _D	mL/g	/	/	/	/	29717	23262	26035	15988	8060	22032	17583
	±	/	/	/	/	11370	6438	4336	3348	814	1687	1476

Table C. 26. Experimental results of the sorption isotherms of U(VI) onto illite at 20 °C in 1% of CO₂(g) in 0.1 M of NaNO₃ at fixed solid-liquid ratio. (BF: blank sample filtrated; BNF: blank sample no filtrated)

ID		10-BF	10-BNF	11-BF	11-BNF	12-BF	12-BNF	1	2	3	4	5	6	7	8	9
illite	(g)	/	/	/	/	/	/	0.051	0.05	0.05	0.05	0.051	0.049	0.05	0.051	0.053
S/L	g/L	/	/	/	/	/	/	2.04	2	2	2	2.04	1.96	2	2.04	2.12
	±	/	/	/	/	/	/	0.05	0.05	0.05	0.05	0.05	0.05	0.05	0.05	0.05
U(VI) ini	mol/L	1.03E-09	1.03E-09	1.69E-06	1.69E-06	1.69E-06	1.69E-06	1.03E-09	2.87E-09	6.15E-09	1.23E-08	2.12E-07	6.35E-07	1.69E-06	6.48E-06	1.73E-05
	±	1.49E-10	1.49E-10	2.47E-07	2.47E-07	2.47E-07	2.47E-07	1.50E-10	4.15E-10	8.93E-10	1.79E-09	2.97E-08	8.94E-08	2.39E-07	9.13E-07	2.44E-06
pH	/	7.31	7.31	7.09	7.09	7.28	7.28	7.33	7.32	7.32	7.33	7.28	7.21	7.09	7.28	7.29
T	°C	21.5	21.5	21.7	21.7	21.2	21.2	20.6	21	20.9	21.1	21.2	20.8	22	21.1	21.1
U(VI) eq.	mol/L	1.18E-09	1.15E-09	1.67E-06	1.67E-06	1.76E-05	1.75E-05	3.66E-10	7.98E-10	7.35E-10	1.56E-09	5.46E-08	2.41E-07	7.66E-07	4.53E-06	9.03E-06
	±	1.30E-10	1.39E-10	7.98E-08	7.56E-08	7.98E-07	8.40E-07	1.18E-10	1.26E-10	1.39E-10	1.39E-10	2.98E-09	1.13E-08	3.95E-08	2.14E-07	4.16E-07
U(VI) sorb.	mol/g	/	/	/	/	/	/	3.98E-10	1.25E-09	3.16E-09	6.28E-09	7.71E-08	2.01E-07	4.64E-07	9.54E-07	3.89E-06
	±	/	/	/	/	/	/	1.03E-10	2.48E-10	5.23E-10	1.04E-09	1.47E-08	4.63E-08	1.22E-07	4.60E-07	1.17E-06
K _d	mL/g	/	/	/	/	/	/	1087.4	1563.2	4300	4016.1	1411.7	833.7	606.5	210.3	430.5
	±	/	/	/	/	/	/	448.5	397	1079.1	755.6	280.9	195.8	161.9	102.1	131

Table C. 27. Experimental results of the sorption isotherms of U(VI) onto illite at 20 °C in 5% of CO₂(g) in 0.1 M of NaNO₃ at fixed solid-liquid ratio. (BF: blank sample filtrated; BNF: blank sample no filtrated)

ID		1	2	3	4	5	6	7
Illite	(g)	0.05	0.052	0.049	0.05	0.05	0.05	0.05
	g/L	2	2.08	1.96	2	2	2	2
	±	0.05	0.05	0.05	0.05	0.05	0.05	0.05
U(VI) ini	mol/L	2.66E-08	7.44E-08	1.59E-07	3.19E-07	2.71E-06	8.12E-06	2.16E-05
	±	1.38E-09	3.64E-09	8.15E-09	1.65E-08	1.43E-07	4.43E-07	1.20E-06
pH	/	6.6	6.61	6.63	6.61	6.61	6.62	6.6
T	°C	21.2	21.3	21	21.1	21	20.9	21.8
U(VI) eq.	mol/L	2.15E-09	7.27E-09	2.25E-08	6.59E-08	1.14E-06	4.79E-07	2.29E-06
	±	1.68E-10	5.88E-10	2.18E-09	3.24E-09	5.46E-08	3.66E-08	1.22E-07
U(VI) sorb.	mol/g	1.25E-08	3.30E-08	7.15E-08	1.30E-07	7.82E-07	3.82E-06	9.68E-06
	±	7.95E-10	1.99E-09	4.76E-09	9.20E-09	7.91E-08	2.43E-07	6.50E-07
K _d	mL/g	5798.8	4538.1	3180.4	1966.5	683.8	7981.1	4235.3
	±	584.6	457.9	374.8	169.7	76.5	793.3	363.1

Table C. 28. Experimental results of the sorption isotherms of U(VI) onto illite at 20 °C in 1% of CO₂(g) in synthetic Callovo-Oxfordian porewater at fixed solid-liquid ratio. (BF: blank sample filtrated; BNF: blank sample no filtrated)

ID		8-BF	8-BNF	9-BF	9-BNF	1	2	3	4	5	6	7
Illite	(g)	/	/	/	/	0.25	0.251	0.249	0.249	0.249	0.249	0.25
	g/L	/	/	/	/	9.994	10.028	9.964	9.956	13.33	9.96	9.994
	±	/	/	/	/	0.165	0.165	0.164	0.164	0.22	0.164	0.165
U(VI) ini.	mol/L	5.35E-08	5.35E-08	1.73E-05	1.73E-05	5.35E-08	2.14E-07	6.42E-07	2.16E-06	6.94E-06	1.73E-05	5.35E-08
	±	2.87E-09	2.87E-09	9.52E-07	9.52E-07	2.95E-09	1.09E-08	3.44E-08	1.08E-07	3.73E-07	9.08E-07	2.87E-09
pH	/	7.18	7.18	7.1	7.1	7.12	7.14	7.14	7.13	7.11	7.08	7.18
	°C	21.6	21.6	21.6	21.6	20.3	20.6	20.7	20.9	20.9	20.9	
U(VI) eq.	mol/L	5.42E-08	5.31E-08	1.75E-05	1.71E-05	3.80E-08	1.41E-07	4.44E-07	1.59E-06	5.01E-06	1.42E-05	5.42E-08
	±	3.61E-09	3.82E-09	8.40E-07	8.40E-07	1.89E-09	6.30E-09	2.02E-08	7.14E-08	2.31E-07	6.72E-07	3.61E-09
U(VI) sorb.	mol/g	/	/	/	/	1.54E-09	7.27E-09	1.99E-08	5.69E-08	1.44E-07	3.13E-07	1.54E-09
	±	/	/	/	/	3.54E-10	1.27E-09	4.06E-09	1.30E-08	3.30E-08	1.14E-07	3.54E-10
K _d	mL/g	/	/	/	/	40.6	51.7	44.7	35.7	28.8	22.1	40.6
	±	/	/	/	/	9.5	9.3	9.4	8.3	6.7	8.1	9.5

Table C. 29. Experimental results of the sorption isotherms of U(VI) onto illite at 60 °C in Ar(g) in 0.1 M of NaNO₃ at fixed solid-liquid ratio. (BF: blank sample filtrated; BNF: blank sample no filtrated)

ID		8-BF	8-BNF	9-BF	9-BNF	1	2	3	4	5	6	7
Illite	(g)	/	/	/	/	0.05	0.05	0.053	0.05	0.05	0.049	0.05
	g/L					2	2	2.12	2	2	1.96	2
	±					0.05	0.05	0.05	0.05	0.05	0.05	0.05
U(VI) ini	mol/L	4.61E-08	4.61E-08	2.21E-05	2.21E-05	4.61E-08	1.29E-07	2.77E-07	5.54E-07	2.76E-06	8.29E-06	2.21E-05
	±	2.64E-09	2.64E-09	1.30E-06	1.30E-06	2.70E-09	7.06E-09	1.57E-08	3.17E-08	1.43E-07	4.45E-07	1.20E-06
	/	5.67	5.67	4.68	4.68	5.39	6.55	6.63	6.65	6.64	6.56	6.38
pH												
	°C	61.5	61.5	61	61	60.4	60.5	61.9	62.3	62	61.4	61.4
	mol/L	/	1.06E-08	2.28E-05	2.29E-05	6.43E-10	1.88E-09	3.36E-09	7.30E-09	2.35E-08	4.47E-08	3.63E-08
U(VI) eq.	±	/	6.30E-10	1.09E-06	1.05E-06	1.05E-10	1.34E-10	1.76E-10	3.57E-10	1.05E-09	2.02E-09	1.64E-09
	mol/g	/	/	/	/	2.27E-08	6.36E-08	1.29E-07	2.73E-07	1.37E-06	4.21E-06	1.10E-05
	±	/	/	/	/	1.47E-09	3.89E-09	8.05E-09	1.73E-08	7.98E-08	2.52E-07	6.63E-07
K _D	mL/g	/	/	/	/	35382.4	33889.3	38421.3	37427.5	58250	94057.2	304129.6
	±	/	/	/	/	6219	3189.5	3135.9	2997.5	4272.8	7046.3	22856.9

Table C. 30. Experimental results of the sorption isotherms of U(VI) onto illite at 60 °C in atmospheric pCO₂ in 0.1 M of NaCl at fixed solid-liquid ratio. (BF: blank sample filtrated; BNF: blank sample no filtrated)

ID		8-BF	8-BNF	9-BF	9-BNF	1	2	3	4	5	6	7
Illite	(g)	/	/	/	/	0.049	0.05	0.05	0.052	0.049	0.049	0.05
	g/L	/	/	/	/	1.96	2	2	2.08	1.96	1.96	2
	±	/	/	/	/	0.05	0.05	0.05	0.05	0.05	0.05	0.05
U(VI) ini.	mol/L	2.64E-08	2.64E-08	1.73E-05	1.73E-05	2.64E-08	7.39E-08	1.58E-07	3.17E-07	2.16E-06	6.48E-06	1.73E-05
	±	1.45E-09	1.45E-09	9.74E-07	9.74E-07	1.49E-09	3.86E-09	8.60E-09	1.74E-08	1.08E-07	3.36E-07	9.08E-07
pH	/	7.49	7.49	7.42	7.42	7.59	7.67	7.66	7.64	7.65	7.57	7.41
	°C	56.7	56.7	56.3	56.3	57.9	58.3	58.3	58.2	57.7	57	57.7
U(VI) eq.	mol/L	2.17E-08	2.20E-08	7.90E-07	7.48E-07	/	/	/	/	5.11E-07	1.16E-07	7.06E-07
	±	1.13E-09	1.09E-09	8.82E-08	9.24E-08	/	/	/	/	2.98E-08	3.87E-08	8.40E-08
U(VI) sorb.	mol/g	/	/	/	/	/	/	/	/	8.41E-07	3.25E-06	8.29E-06
	±	/	/	/	/	/	/	/	/	2.67E-08	8.68E-08	2.17E-07
K _d	mL/g	/	/	/	/	/	/	/	/	1644.6	28098.3	11738.1
	±	/	/	/	/	/	/	/	/	109.2	9430.2	1430.9

Table C. 32. Experimental results of the sorption isotherms of U(VI) onto illite at 60 °C in 5% of CO₂(g) in 0.1 M of NaNO₃ at fixed solid-liquid ratio. (BF: blank sample filtrated; BNF: blank sample no filtrated)

ID		8-BF	8-BNF	9-BF	9-BNF	1	2	3	4	5	6	7
Illite	(g)	/	/	/	/	0.05	0.049	0.05	0.049	0.049	0.051	0.049
	g/L	/	/	/	/	2	1.96	2	1.96	1.96	2.04	1.96
	±	/	/	/	/	0.05	0.05	0.05	0.05	0.05	0.05	0.05
U(VI) ini.	mol/L	2.66E-08	2.66E-08	2.36E-05	2.36E-05	2.66E-08	7.44E-08	1.59E-07	3.19E-07	2.95E-06	8.85E-06	2.36E-05
	±	1.38E-09	1.38E-09	1.26E-06	1.26E-06	1.42E-09	3.64E-09	8.15E-09	1.65E-08	1.68E-07	5.19E-07	1.40E-06
pH	/	6.85	6.85	6.8	6.8	6.84	6.84	6.84	6.84	6.83	6.83	6.82
	°C	59.4	59.4	59.2	59.2	58.8	60.2	59.8	59.5	59.8	59.9	59.7
U(VI) eq.	mol/L	2.45E-08	2.48E-08	2.03E-05	2.07E-05	/	/	/	/	2.72E-07	8.19E-07	1.97E-06
	±	1.30E-09	1.26E-09	1.01E-06	9.24E-07	/	/	/	/	2.27E-08	6.30E-08	1.51E-07
U(VI) sorb.	mol/g	/	/	/	/	/	/	/	/	1.37E-06	3.94E-06	1.10E-05
	±	/	/	/	/	/	/	/	/	9.35E-08	2.75E-07	7.72E-07
K _d	mL/g	/	/	/	/	/	/	/	/	541.1	499.2	581.7
	±	/	/	/	/	/	/	/	/	3.7	3.7	3.7

Table C. 33. Experimental results of the sorption isotherms of U(VI) onto illite at 80 °C in Ar(g) in 0.1 M of NaNO₃ at fixed solid-liquid ratio. (BF: blank sample filtrated; BNF: blank sample no filtrated)

ID		1	2	3	4	5	6	7
Illite	(g)	0.05	0.05	0.05	0.05	0.05	0.051	0.049
	g/L	2	2	2	2	2	2.04	1.96
	±	0.05	0.05	0.05	0.05	0.05	0.05	0.05
U(VI) ini.	mol/L	4.61E-08	1.29E-07	2.77E-07	5.54E-07	2.76E-06	8.29E-06	2.21E-05
	±	2.70E-09	7.06E-09	1.57E-08	3.17E-08	1.43E-07	4.45E-07	1.20E-06
pH	/	6.49	6.61	6.5	6.58	6.71	6.59	6.33
	°C	80	80.3	78.7	79.3	78.8	78.8	79.7
U(VI) eq.	mol/L	1.48E-10	4.69E-10	1.73E-09	5.51E-09	1.90E-08	2.99E-08	3.99E-08
	±	6.72E-12	1.93E-11	1.39E-10	2.77E-10	8.82E-10	1.34E-09	1.68E-09
U(VI) sorb.	mol/g	2.30E-08	6.44E-08	1.38E-07	2.74E-07	1.37E-06	4.05E-06	1.13E-05
	±	1.47E-09	3.90E-09	8.59E-09	1.73E-08	7.98E-08	2.41E-07	6.78E-07
K _d	mL/g	155024.1	137118.6	79451.5	49713.4	72287.6	135606.4	282196.6
	±	12174.6	10039.4	8071	4016.6	5379	10115.2	20739.2

Table C. 34. Experimental results of the sorption isotherms of U(VI) onto illite at 80 °C in atmospheric pCO₂ in 0.1 M of NaCl at fixed solid-liquid ratio. (BF: blank sample filtrated; BNF: blank sample no filtrated)

ID		1	2	3	4	5	6	7
Illite	(g)	0.049	0.05	0.05	0.052	0.049	0.049	0.05
	g/L	1.96	2	2	2.08	1.96	1.96	2
	±	0.05	0.05	0.05	0.05	0.05	0.05	0.05
U(VI) ini.	mol/L	2.64E-08	7.39E-08	1.58E-07	3.17E-07	2.16E-06	6.48E-06	1.73E-05
	±	1.45E-09	3.86E-09	8.60E-09	1.74E-08	1.08E-07	3.36E-07	9.08E-07
pH	/	7.58	7.63	7.55	7.63	7.54	7.45	7.46
	°C	76.5	73.1	73.4	72.9	76.5	71.9	76.6
U(VI) eq.	mol/L	2.44E-10	5.59E-10	1.47E-09	5.17E-09	/	5.11E-08	6.74E-08
	±	1.72E-10	1.76E-10	4.20E-10	5.04E-10	/	2.65E-09	3.15E-09
U(VI) sorb.	mol/g	4.96E-09	1.37E-08	2.91E-08	5.50E-08	/	6.50E-08	2.04E-07
	±	3.26E-10	8.13E-10	1.80E-09	3.45E-09	/	5.19E-09	1.36E-08
K _D	mL/g	20337.8	24447.4	19814.3	10635.6	/	1272.4	3026.5
	±	14438.8	7856	5791.7	1233.9	/	121.2	246.7

Table C. 35. Experimental results of the sorption isotherms of U(VI) onto illite at 80 °C in 1% of CO₂(g) in 0.1 M of NaNO₃ at fixed solid-liquid ratio. (BF: blank sample filtrated; BNF: blank sample no filtrated)

ID		8-BF	8-BNF	9-BF	9-BNF	1	2	3	4	5	6	7
Illite	(g)	/	/	/	/	0.052	0.05	0.051	0.048	0.049	0.053	0.052
	g/L	/	/	/	/	2.08	2	2.04	1.92	1.96	2.12	2.08
	±	/	/	/	/	0.05	0.05	0.05	0.05	0.05	0.05	0.05
U(VI) ini.	mol/L	5.35E-08	5.35E-08	1.73E-05	1.73E-05	5.35E-08	1.50E-07	3.21E-07	6.42E-07	2.16E-06	6.48E-06	1.73E-05
	±	2.87E-09	2.87E-09	9.52E-07	9.52E-07	2.95E-09	7.62E-09	1.70E-08	3.44E-08	1.08E-07	3.36E-07	9.08E-07
pH	/	7.7	7.7	7.64	7.64	7.64	7.66	7.66	7.67	7.6	7.59	7.63
T	°C	77	77	73.6	73.6	77.7	79.1	79.5	78.7	75.2	78.3	73.6
U(VI) eq.	mol/L	4.10E-08	4.20E-08	1.16E-05	1.17E-05	5.04E-09	2.46E-08	7.77E-08	2.32E-07	1.05E-06	3.77E-06	2.51E-06
	±	2.18E-09	2.06E-09	5.46E-07	5.46E-07	5.04E-10	1.39E-09	4.62E-09	1.09E-08	5.04E-08	2.14E-07	1.47E-07
U(VI) sorb.	mol/g	/	/	/	/	1.73E-08	4.51E-08	8.25E-08	1.36E-07	5.68E-07	1.28E-06	7.10E-06
	±	/	/	/	/	1.19E-09	3.22E-09	7.10E-09	1.53E-08	6.26E-08	1.91E-07	4.76E-07
K _D	mL/g	/	/	/	/	3429.5	1831.7	1061.5	586.2	543	338.3	2830.7
	±	/	/	/	/	416.8	166.5	111	71.6	65.3	54.1	252.2

Table C. 36. Experimental results of the sorption isotherms of U(VI) onto illite at 80 °C in 5% of CO₂(g) in 0.1 M of NaNO₃ at fixed solid-liquid ratio. (BF: blank sample filtrated; BNF: blank sample no filtrated)

ID		1	2	3	4	5	6	7
Illite	(g)	0.05	0.052	0.049	0.05	0.05	0.05	0.05
	g/L	2	2.08	1.96	2	2	2	2
	±	0.05	0.05	0.05	0.05	0.05	0.05	0.05
U(VI) ini.	mol/L	2.66E-08	7.44E-08	1.59E-07	3.19E-07	2.95E-06	8.85E-06	2.36E-05
	±	1.38E-09	3.64E-09	8.15E-09	1.65E-08	1.68E-07	5.19E-07	1.40E-06
pH	/	7.05	7.05	7.05	7.06	7.02	7.03	7.02
	°C	77.6	80.1	79.3	79.5	79.3	79.8	79.7
U(VI) eq.	mol/L	1.22E-09	4.73E-09	1.53E-08	3.63E-08	8.91E-07	1.24E-06	3.04E-06
	±	1.30E-10	2.69E-10	8.40E-10	2.14E-09	4.62E-08	6.30E-08	1.68E-07
	mol/g	5.29E-09	1.36E-08	2.84E-08	5.27E-08	1.03E-06	3.80E-06	1.03E-05
U(VI) sorb.	±	3.49E-10	8.59E-10	2.04E-09	4.06E-09	9.11E-08	2.79E-07	7.52E-07
	mL/g	4344.8	2881.6	1859.5	1451.4	1155.7	3069.5	3383.8
K _D	±	545.7	244.8	168.3	140.8	118.6	273.9	310.3
	/	/	/	/	/	/	/	/
8-BF	/	/	/	/	/	/	/	/
8-BNF	/	/	/	/	/	/	/	/
9-BF	/	/	/	/	/	/	/	/
9-BNF	/	/	/	/	/	/	/	/

Table C. 37. Experimental results of the sorption isotherms of U(VI) onto illite at 80 °C in 5% of CO₂(g) in synthetic Callovo-Oxfordian porewater at fixed solid-liquid ratio. (BF: blank sample filtrated; BNF: blank sample no filtrated)

ID		1	2	3	4	5	6	7
Illite	(g)	0.051	0.05	0.051	0.049	0.05	0.05	0.051
	g/L	2.04	2	2.04	1.96	2	2	2.04
	±	0.05	0.05	0.05	0.05	0.05	0.05	0.05
U(VI) ini.	mol/L	2.66E-08	7.44E-08	1.59E-07	3.19E-07	2.71E-06	8.12E-06	2.16E-05
	±	1.42E-09	3.64E-09	8.15E-09	1.65E-08	1.43E-07	4.43E-07	1.20E-06
pH	/	6.84	6.84	6.84	6.86	6.86	6.85	6.84
	°C	81.3	81.6	81.2	76.7	80.2	81.3	81.8
U(VI) eq.	mol/L	1.82E-08	5.02E-08	1.16E-07	2.47E-07	2.16E-06	7.05E-06	1.88E-05
	±	1.68E-09	3.36E-09	6.72E-09	1.26E-08	1.18E-07	3.49E-07	9.24E-07
	mol/g	4.08E-09	1.21E-08	2.13E-08	3.65E-08	2.71E-07	5.36E-07	1.38E-06
U(VI) sorb.	±	1.08E-09	2.50E-09	5.21E-09	1.06E-08	9.28E-08	2.82E-07	7.42E-07
	mL/g	223.64	241.04	183.29	147.86	125.24	76.03	73.53
K _D	±	62.83	52.32	46.14	43.73	43.43	40.24	39.56

C.5.2. Sorption edges:

Table C. 38. pH results of each tube measured before the batch equilibrium at 20 °C in atmospheric pCO₂.

Tubes	S/L	pH of NaCl equilibrated	HCl/NaOH (0.01M)	pH final
	g/L		μL	
edge 1	1	3.89	-	3.9
edge 2	1	5.6+HCl	60μL	4.5
edge3	0.5	5.6	-	5.6
edge4	0.5	7+HCl	60μL	6.5
edge5	0.5	7	-	7
edge6	0.5	7.7	-	7.7
edge7	1	7.7+NaOH	60μL	8.5
edge8	1	9.8	-	9.8
Blanc 9	0	3.89	-	
Blanc 10	0	7	-	
Blanc 11	0	9.8	-	

Table C. 39. pH results of each tube measured before the batch equilibrium at 80 °C in atmospheric pCO₂.

Tubes	S/L	pH of NaCl equilibrated	HCl/NaOH (0.01M)	pH final
	g/L		μL	
edge 1	1	/	/	3.89
edge 2	1	HCl 0,01 mol/L	0.0600	6.05
edge3	0.5	/	/	6.05
edge4	0.5	HCl 0,01 mol/L	0.0600	7.22
edge5	0.5	/	/	7.22
edge6	0.5	/	/	7.99
edge7	1	NaOH 0,01 mol/L	0.0600	7.99
edge8	1	/	/	9.84
Blanc 9	0	/	/	3.89
Blanc 10	0	/	/	7.22
Blanc 11	0	/	/	9.84

Table C. 40. Experimental results of the sorption edges of U(VI) onto illite at 20 °C in Ar(g) in 0.1 M of NaNO₃ at fixed solid-liquid ratio of 2 g/L with [U(VI)]_{initial} = 1.02(±0.06)·10⁻⁷M. (BF: blank sample filtrated; BNF: blank sample no filtrated)

ID	Illite (g)	S/L		pH /	Temp °C	U(VI) eq.		U(VI) sorb.		K _D	
		g/L	±			mol/L	±	mol/g	±	mL/g	±
8-BF	/	/	/	7.03	19.9	7.08E-08	3.45E-09	/	/	/	/
8-BNF	/	/	/	7.03	19.9	1.15E-07	5.46E-09	/	/	/	/
9-BF	/	/	/	8.66	20.1	1.12E-07	5.04E-09	/	/	/	/
9-BNF	/	/	/	8.66	20.1	1.16E-07	5.46E-09	/	/	/	/
10-BF	/	/	/	9.6	20.1	1.16E-07	5.04E-09	/	/	/	/
10-BNF	/	/	/	9.6	20.1	1.18E-07	5.04E-09	/	/	/	/
11-BF	/	/	/	9.85	20.1	1.15E-07	5.46E-09	/	/	/	/
10-BNF	/	/	/	9.85	20.1	1.09E-09	5.46E-10	/	/	/	/
1	0.051	2.04	0.05	4.27	20.5	5.86E-08	2.61E-09	2.10E-08	3.06E-09	359	55
2	0.052	2.08	0.05	5.57	20.7	4.76E-09	2.35E-10	4.65E-08	2.92E-09	9760	780
3	0.052	2.08	0.05	6.64	20.9	1.62E-10	6.30E-12	4.87E-08	2.94E-09	301168	21651
4	0.055	2.2	0.05	7.03	20.9	1.15E-10	4.62E-12	4.61E-08	2.77E-09	400275	28920
5	0.054	2.16	0.05	7.31	20.9	1.66E-10	5.88E-12	4.69E-08	2.82E-09	281944	19683
6	0.051	2.04	0.05	7.83	20.9	2.31E-10	5.04E-11	4.96E-08	3.01E-09	214804	48639
7	0.05	2	0.05	8.78	20.9	7.52E-10	8.40E-11	5.04E-08	3.07E-09	66975	8524

Table C. 41. Experimental results of the sorption edges of U(VI) onto illite at 20°C in atmospheric pCO₂ in 0.1 M of NaCl at fixed solid-liquid ratio of 0.5-1 g/L with [U(VI)]_{initial} = 1.02(±0.06)·10⁻⁷M. (BF: blank sample filtrated; BNF: blank sample no filtrated)

ID	Illite (g)	S/L		pH /	Temp °C	U(VI) eq.		U(VI) sorb.		K _D	
		g/L	±			mol/L	±	mol/g	±	mL/g	±
8-BF	/	/	/	3.92	19.9	1.14E-07	5.88E-09	/	/	/	/
8-BNF	/	/	/	3.92	19.9	1.13E-07	5.46E-09	/	/	/	/
9-BF	/	/	/	6.94	20.1	9.66E-08	4.62E-09	/	/	/	/
9-BNF	/	/	/	6.94	20.1	1.01E-07	4.62E-09	/	/	/	/
10-BF	/	/	/	9.88	20.1	1.10E-07	5.04E-09	/	/	/	/
10-BNF	/	/	/	9.88	20.1	1.09E-07	5.46E-09	/	/	/	/
1	0.025	1	0.04	6.41	20.9	2.66E-09	3.53E-10	8.05E-08	9.21E-09	3221.8	424.6
2	0.025	1	0.04	6.8	20.6	5.00E-09	4.62E-10	1.03E-07	9.49E-09	50370.1	9627.4
3	0.01298	0.52	0.04	7.1	20.7	4.82E-09	3.91E-10	1.98E-07	2.24E-08	74386.5	12965.5
4	0.01247	0.5	0.04	8.09	20.7	6.74E-08	3.87E-09	2.02E-07	2.35E-08	40315.2	6005

ID	Illite (g)	S/L		pH /	Temp °C	U(VI) eq.		U(VI) sorb.		K _D	
		g/L	±			mol/L	±	mol/g	±	mL/g	±
5	0.01256	0.5	0.04	8.17	20.8	4.04E-08	2.18E-09	2.00E-07	2.33E-08	41601.5	5897.1
6	0.01235	0.49	0.04	9.87	20.9	1.11E-07	5.04E-09	7.71E-08	1.97E-08	1143.9	299.7
7	0.025	1	0.04	3.92	19.9	1.14E-07	5.88E-09	6.52E-08	9.10E-09	1613.9	241.6

Table C. 42. Experimental results of the sorption edges of U(VI) onto illite at 80 °C in Ar(g) in 0.1 M of NaNO₃ at fixed solid-liquid ratio of 2 g/L with [U(VI)]_{initial} = 1.02(±0.06)·10⁻⁷M. (BF: blank sample filtrated; BNF: blank sample no filtrated)

ID	Illite (g)	S/L		pH /	Temp °C	U(VI) eq.		U(VI) sorb.		K _D	
		g/L	±			mol/L	±	mol/g	±	mL/g	±
8-BF	/	/	/	7.06	78	1.43E-09	5.46E-10	/	/	/	/
8-BNF	/	/	/	7.06	78	1.34E-09	5.46E-10	/	/	/	/
9-BF	/	/	/	7.35	77.2	1.81E-09	5.46E-10	/	/	/	/
9-BNF	/	/	/	7.35	77.2	2.90E-09	5.88E-10	/	/	/	/
10-BF	/	/	/	7.76	76.7	4.58E-09	6.30E-10	/	/	/	/
10-BNF	/	/	/	7.76	76.7	5.92E-09	7.14E-10	/	/	/	/
11-BF	/	/	/	7.99	74.5	7.44E-09	7.14E-10	/	/	/	/
11-BNF	/	/	/	7.99	74.5	3.36E-08	5.88E-08	/	/	/	/
1	0.05	2	0.04	4.55	78.2	1.27E-08	5.04E-10	4.44E-08	3.02E-09	3499.3	275.7
2	0.05	2	0.04	5.84	80.5	5.00E-10	6.72E-11	5.05E-08	3.07E-09	100995.8	14904.7
3	0.049	1.96	0.04	6.72	80.2	2.69E-10	1.05E-10	5.16E-08	3.14E-09	192059.9	75928.7
4	0.048	1.92	0.04	6.95	78.9	2.40E-10	9.24E-12	5.27E-08	3.22E-09	219431.1	15821.2
5	0.054	2.16	0.04	7.04	78	2.33E-10	1.51E-11	4.69E-08	2.82E-09	201402.3	17844.7
6	0.054	2.16	0.04	7.19	75.9	1.68E-10	6.30E-12	4.69E-08	2.82E-09	279120.4	19796.1
7	0.048	1.92	0.04	7.35	78.9	1.83E-10	8.82E-12	5.28E-08	3.22E-09	288703.3	22449.2

Table C. 43. Experimental results of the sorption edges of U(VI) onto illite at 80 °C in atmospheric pCO₂ in 0.1 M of NaCl at fixed solid-liquid ratio of 0.5-1 g/L with [U(VI)]_{initial} = 3.07(±0.01)·10⁻⁸M. (BF: blank sample filtrated; BNF: blank sample no filtrated)

ID	Illite (g)	S/L		pH /	Temp °C	U(VI) eq.		U(VI) sorb.		K _D	
		g/L	±			mol/L	±	mol/g	±	mL/g	±
8-BF	/	/	/	3.89	77	3.58E-08	1.64E-09				
8-BNF	/	/	/	3.89	77	3.59E-08	1.60E-09				
9-BF	/	/	/	7.04	79.8	2.04E-08	9.66E-10				
9-BNF	/	/	/	7.04	79.8	2.39E-08	1.18E-09				

ID	Illite	S/L		pH	Temp	U(VI) eq.		U(VI) sorb.		K _D	
	(g)	g/L	±	/	°C	mol/L	±	mol/g	±	mL/g	±
10-BF	/	/	/	9.16	76.2	3.66E-08	1.76E-09				
10-BNF	/	/	/	9.16	76.2	3.50E-08	1.55E-09				
1	0.025	1	0.04	5.01	79.7	1.17E-09	1.13E-10	2.95E-08	1.99E-09	25150.5	2966.7
2	0.025	1	0.04	6.54	80.7	1.18E-10	2.35E-11	3.05E-08	2.01E-09	257723.4	53929.7
3	0.013	0.52	0.04	6.7	80.5	5.46E-10	9.24E-11	5.79E-08	5.42E-09	106005.9	20497.6
4	0.014	0.56	0.04	7.19	79.2	3.91E-13	5.88E-14	5.47E-08	4.85E-09	1.4E+08	24464341
5	0.015	0.6	0.04	7.4	77.5	3.40E-13	5.46E-14	5.11E-08	4.33E-09	1.5E+08	27244360
6	0.013	0.52	0.04	8.19	76.3	6.37E-12	3.32E-13	5.89E-08	5.48E-09	9247101	985716.4
7	0.013	0.52	0.04	8.2	78.7	7.34E-12	4.03E-13	5.89E-08	5.48E-09	8024833	866807.8

C.6. Callovo-Oxfordian clay fraction: sorption isotherm experiments

Table C. 44. Alkalinity measurements in sorption isotherms experiments of U(VI)/clay fraction system at different temperatures. *synthetic Callovo-Oxfordian porewater.

atmosphere	T	Illite	pH	Acid H ₂ SO ₄	Vol. acid	±	[CO ₃ ²⁻ /HCO ₃ ⁻]	±
	°C	g		N	digits		meq/L	
Ar(g)	20.5	0.049	7.06	0.1	89	35.6	2.23E-04	8.90E-05
1% CO ₂ (g)	21.5	0.059	7.24	0.16	118	47.2	2.36E-03	9.44E-04
1% CO ₂ (g)*	21.5	0.05	7.24	0.16	118	47.2	2.36E-03	9.44E-04
Ar(g)	77.5	0.05	7.08	0.16	89	35.6	2.23E-04	8.90E-05
5% CO ₂ (g)	67.	0.05	7.15	0.16	115	46	2.30E-03	9.20E-04
5% CO ₂ (g)*	68	0.049	7.08	0.16	168	67.2	3.36E-03	1.34E-03

Table C. 45. Experimental results of the sorption isotherms of U(VI) onto Callovo-Oxfordian clay fraction at 20 °C in Ar(g) in 0.1 M of NaNO₃ at fixed solid-liquid ratio.

7	0.051	2.04	0.05	2.21E-05	1.20E-06	6.69	21.2	1.30E-06	9.66E-08	1.02E-05	6.44E-07	7860.6	767.2
6	0.049	1.96	0.05	8.29E-06	4.45E-07	6.98	21.2	3.41E-07	1.68E-08	4.06E-06	2.50E-07	11908.3	940.6
5	0.05	2	0.05	2.76E-06	1.43E-07	7.13	21.2	7.90E-08	5.04E-09	1.34E-06	7.95E-08	17000	1480
4	0.05	2	0.05	5.54E-07	3.17E-08	7.11	21.2	2.63E-08	1.55E-09	2.64E-07	1.72E-08	10040.8	885.6
3	0.049	1.96	0.05	2.77E-07	1.57E-08	7.08	21.3	1.78E-08	1.01E-09	1.32E-07	8.72E-09	7436	646.9

ID		8-BF	8-BNF	9-BF	9-BNF	1	2
Clay fraction	(g)	/	/	/	/	0.052	0.05
S/L	g/L	/	/	/	/	2.08	2
	±	/	/	/	/	0.05	0.05
U(VI) ini	mol/L	2.21E-05	2.21E-05	4.61E-08	4.61E-08	4.61E-08	1.29E-07
	±	1.20E-06	1.20E-06	2.70E-09	2.70E-09	2.70E-09	7.06E-09
pH	/	4.75	4.75	5.46	5.46	7.09	7.08
T	°C	21	21	21	21	21.4	21.4
U(VI) eq.	mol/L	2.23E-05	2.22E-05	4.25E-08	3.54E-08	2.60E-09	7.02E-09
	±	1.09E-06	1.01E-06	1.93E-09	1.68E-09	1.55E-10	4.62E-10
U(VI) sorb.	mol/g	/	/	/	/	2.09E-08	6.11E-08
	±	/	/	/	/	1.40E-09	3.87E-09
K _b	ml/g	/	/	/	/	8047.3	8704.8
	±	/	/	/	/	722.9	795.4

Table C. 46. Experimental results of the sorption isotherms of U(VI) onto Callovo-Oxfordian clay fraction at 20 °C in 1% of CO₂(g) in 0.1 M of NaNO₃ at fixed solid-liquid ratio. (BF: blank sample filtrated; BNF: blank sample no filtrated)

1	2	3	4	5	6	7
0.0487	0.05004	0.05085	0.04943	0.05085	0.05167	0.05048
1.95	2	2.03	1.98	2.03	2.07	2.02
0.05	0.05	0.05	0.05	0.05	0.05	0.05
5.35E-08	1.50E-07	3.21E-07	6.42E-07	2.16E-06	6.48E-06	1.17E-05
2.95E-09	7.62E-09	1.70E-08	3.44E-08	1.10E-07	3.36E-07	6.13E-07
7.23	7.23	7.23	7.23	7.23	7.22	7.21
20.7	20.8	20.7	20.9	20.9	20.9	21
1.02E-08	3.91E-08	9.45E-08	2.42E-07	9.50E-07	3.67E-06	6.95E-06
9.66E-10	2.44E-09	5.88E-09	1.34E-08	4.62E-08	1.85E-07	4.12E-07
2.94E-08	7.49E-08	1.53E-07	2.87E-07	6.85E-07	1.62E-06	2.82E-06
2.03E-09	5.10E-09	1.12E-08	2.35E-08	6.41E-08	2.00E-07	3.90E-07
2880	1916.6	1614.3	1189.7	721.1	442	405.6
337.3	177	155.4	117.5	76.1	58.7	61

ID			8-BF	9-BF
Clay fraction	(g)	/	/	/
S/L	g/L	/	/	/
	±	/	/	/
U(VI) ini.	mol/L	1.73E-05	5.35E-08	5.35E-08
	±	9.08E-07	2.95E-09	2.95E-09
pH	/	7.17	7.22	7.22
T	°C	21	20.8	20.8
U(VI) eq.	mol/L	1.87E-05	6.75E-08	6.75E-08
	±	1.05E-06	2.98E-09	2.98E-09
U(VI) sorb.	mol/g	/	/	/
	±	/	/	/
K _D	mL/g	/	/	/
	±	/	/	/

Table C. 47. Experimental results of the sorption isotherms of U(VI) onto Callovo-Oxfordian clay fraction at 20 °C in 1% of CO₂(g) in synthetic Callovo-Oxfordian porewater at fixed solid-liquid ratio. (BF: blank sample filtrated; BNF: blank sample no filtrated)

9-BF	1	2	3	4	5	6	7
/	0.05002	0.04989	0.04996	0.05006	0.05065	0.05053	0.05109
/	2	1.996	1.998	2.002	2.026	2.021	2.044
/	0.05	0.05	0.05	0.05	0.05	0.05	0.05
5.35E-08	5.35E-08	1.50E-07	3.21E-07	6.42E-07	2.16E-06	6.48E-06	1.17E-05
2.95E-09	2.95E-09	7.62E-09	1.70E-08	3.44E-08	1.10E-07	3.36E-07	6.13E-07
7.22	7.11	7.13	7.13	7.12	7.12	7.1	7.08
20.8	21.1	21.2	21.3	21.3	21.2	21.1	21.2
6.75E-08	6.48E-08	1.47E-07	3.16E-07	6.44E-07	2.24E-06	6.46E-06	1.16E-05
2.98E-09	2.98E-09	6.72E-09	1.60E-08	2.90E-08	1.09E-07	3.40E-07	5.46E-07
/	1.32E-09	2.10E-08	4.45E-08	8.30E-08	5.29E-08	2.82E-07	4.94E-07
/	2.38E-09	5.89E-09	1.34E-08	2.61E-08	8.00E-08	2.47E-07	4.21E-07
/	20.4	142.8	140.9	129	23.7	43.6	42.5
/	36.8	40.6	43	41	35.8	38.3	36.2

ID			8-BF
Clay fraction	(g)	/	
S/L	g/L	/	
	±	/	
U(VI) ini.	mol/L	1.73E-05	
	±	9.08E-07	
pH	/	7.17	
T	°C	21	
U(VI) eq.	mol/L	1.87E-05	
	±	1.05E-06	
U(VI) sorb.	mol/g	/	
	±	/	
K_D	mL/g	/	
	±	/	

Table C. 48. Experimental results of the sorption isotherms of U(VI) onto Callovo-Oxfordian clay fraction at 80 °C in Ar(g) in 0.1 M of NaNO₃ at fixed solid-liquid ratio of 2 g/L. (BF: blank sample filtrated; BNF: blank sample no filtrated)

9-BF	9-BNF	1	2	3	4	5	6	7
/	/	0.05	0.05	0.052	0.05	0.053	0.05	0.05
/	/	2	2	2.08	2	2.12	2	2
/	/	0.05	0.05	0.05	0.05	0.05	0.05	0.05
4.61E-08	4.61E-08	4.61E-08	1.29E-07	2.77E-07	5.54E-07	2.76E-06	8.29E-06	2.21E-05
2.57E-09	2.57E-09	2.57E-09	6.66E-09	1.48E-08	3.00E-08	1.43E-07	4.45E-07	1.20E-06
5.82	5.82	7.14	7.23	7.25	7.25	7.2	7.17	7.08
78.6	78.6	78.3	78.5	78.8	77.9	78.5	77.9	77.1
4.54E-10	8.99E-10	2.34E-09	1.04E-08	1.31E-08	2.88E-08	1.38E-07	4.59E-07	1.22E-06
3.61E-10	3.70E-10	1.43E-10	7.56E-10	7.98E-10	1.68E-09	9.66E-09	2.14E-08	5.46E-08
/	/	2.19E-08	5.94E-08	1.27E-07	2.62E-07	1.24E-06	3.92E-06	1.04E-05
/	/	1.40E-09	3.68E-09	7.82E-09	1.65E-08	7.43E-08	2.44E-07	6.58E-07
/	/	9338.7	5723.5	9670.9	9117.5	8962.3	8530.2	8575.9
/	/	826.1	547.4	838.3	781.8	825.7	664.3	662.7

ID			8-BF	8-BNF
Clay fraction	(g)	/	/	/
S/L	g/L	/	/	/
	±	/	/	/
U(VI) ini.	mol/L	2.21E-05	2.21E-05	2.21E-05
	±	1.20E-06	1.20E-06	1.20E-06
pH	/	4.06	4.06	4.06
T	°C	77.6	77.6	77.6
U(VI) eq.	mol/L	1.84E-05	1.81E-05	1.81E-05
	±	8.82E-07	8.82E-07	8.82E-07
U(VI) sorb.	mol/g	/	/	/
	±	/	/	/
K _D	mL/g	/	/	/
	±	/	/	/

Table C. 49. Experimental results of the sorption isotherms of U(VI) onto Callovo-Oxfordian clay fraction at 80 °C in 5% of CO₂(g) in 0.1 M of NaNO₃ at fixed solid-liquid ratio. (BF: blank sample filtrated; BNF: blank sample no filtrated)

9-BNF	1	2	3	4	5	6	7
/	0.052	0.052	0.05	0.051	0.05	0.049	0.049
/	2.08	2.08	2	2.04	2	1.96	1.96
/	0.05	0.05	0.05	0.05	0.05	0.05	0.05
9.96E-09	9.96E-09	2.79E-08	5.97E-08	1.19E-07	1.97E-06	5.90E-06	1.06E-05
6.10E-10	6.10E-10	1.60E-09	3.55E-09	7.16E-09	9.89E-08	3.08E-07	5.61E-07
7.1	7.25	7.22	7.21	7.23	7.19	7.22	7.21
76.8	78.6	78.5	77.7	76	76.7	75.3	74.5
5.50E-09	6.43E-10	1.82E-09	2.70E-09	8.03E-09	3.47E-07	1.86E-06	3.87E-06
4.62E-10	1.26E-10	3.74E-10	3.07E-10	1.09E-09	2.44E-08	1.13E-07	1.89E-07
/	4.48E-09	1.25E-08	2.85E-08	5.46E-08	8.10E-07	2.06E-06	3.44E-06
/	3.20E-10	8.51E-10	1.92E-09	3.81E-09	5.50E-08	1.76E-07	3.15E-07
/	6966.4	6904.4	10557.5	6808.8	2336.4	1110.4	889.8
/	1453.6	1497.7	1394.1	1041.3	228.4	116.4	92.3

ID			8-BF	8-BNF	9-BF
Clay fraction	(g)	/	/	/	/
S/L	g/L	/	/	/	/
	±	/	/	/	/
U(VI) ini.	mol/L	1.57E-05	1.57E-05	1.57E-05	9.96E-09
	±	8.31E-07	8.31E-07	8.31E-07	6.10E-10
pH	/	7.18	7.18	7.18	7.1
T	°C	75.7	75.7	75.7	76.8
U(VI) eq.	mol/L	1.48E-05	1.48E-05	1.53E-05	5.16E-09
	±	7.14E-07	7.14E-07	7.14E-07	3.78E-10
U(VI) sorb.	mol/g	/	/	/	/
	±	/	/	/	/
K _D	mL/g	/	/	/	/
	±	/	/	/	/

Table C. 50. Experimental results of the sorption isotherms of U(VI) onto Callovo-Oxfordian clay fraction at 80 °C in 5% of CO₂(g) in Callovo-Oxfordian porewater at fixed solid-liquid ratio. (BF: blank sample filtrated; BNF: blank sample no filtrated)

9-BNF	1	2	3	4	5	6	7
	0.05	0.05	0.049	0.051	0.051	0.049	0.052
	2	2	1.96	2.04	2.04	1.96	2.08
	0.05	0.05	0.05	0.05	0.05	0.05	0.05
9.96E-09	9.96E-09	2.79E-08	5.97E-08	1.19E-07	1.97E-06	5.90E-06	1.06E-05
6.10E-10	6.10E-10	1.60E-09	3.55E-09	7.16E-09	9.89E-08	3.08E-07	5.61E-07
6.9	7.16	7.17	7.16	7.09	7.07	7.07	7.1
73.6	77.6	77.2	77.2	76.4	77.4	76.5	74
8.74E-09	6.97E-09	1.69E-08	4.35E-08	8.82E-08	1.72E-06	5.08E-06	9.71E-06
6.72E-10	4.20E-10	1.51E-09	2.73E-09	5.46E-09	7.98E-08	2.31E-07	4.62E-07
/	1.49E-09	5.50E-09	8.30E-09	1.53E-08	1.19E-07	4.18E-07	4.39E-07
/	3.72E-10	1.11E-09	2.29E-09	4.43E-09	6.24E-08	1.97E-07	3.50E-07
/	213.9	325.4	190.8	173.7	69.3	82.3	45.2
/	54.9	71.9	54.1	51.4	36.4	38.9	36.1

ID									
Clay fraction	(g)								
S/L	g/L								
	±								
U(VI) ini.	mol/L	1.57E-05	1.57E-05	8.31E-07	8.31E-07	6.93	6.93	74.3	73.6
	±								
pH	/								
T	°C								
U(VI) eq.	mol/L	1.53E-05	1.53E-05	6.72E-07	6.72E-07	6.30E-10	6.30E-10		
	±								
U(VI) sorb.	mol/g	/	/	/	/	/	/	/	/
	±								
K _D	mL/g	/	/	/	/	/	/	/	/
	±								

C.7. Callovo-Oxfordian claystone samples: isotherm experiments

Table C. 51. Alkalinity measurements in sorption isotherms experiments of U(VI)/claystone system at 20 and 80°C in synthetic Callovo-Oxfordian porewater.

atmosphere	T	pH	Acid H ₂ SO ₄	Vol. acid	±	Alkalinity	±
	°C		N	digits		meq/L	
1% CO ₂ (g)	20	7.42	0.16	164	65.6	3.28	1.31
5% CO ₂ (g)	80	6.85	0.16	108	43.2	2.16	0.84

Table C. 52. Experimental results of the sorption isotherms of U(VI) onto Callovo-Oxfordian claystone at 20 °C in 1% of CO₂(g) in Cox porewater at fixed solid-liquid ratio.

4	5	6	7	8
0.2	0.4	0.03	0.075	0.2
39.4	39.4	39.5	39.4	39.4
0.6	0.6	0.6	0.6	0.6
4.51E-07	9.02E-07	1.44E-06	3.61E-06	9.61E-06
2.26E-08	4.58E-08	6.94E-08	1.83E-07	4.95E-07
7.5	7.5	7.5	7.5	7.51
18.1	18.1	18.4	18.2	18.2
3.87E-07	7.83E-07	1.24E-06	3.20E-06	8.41E-06
1.72E-08	3.53E-08	5.88E-08	1.51E-07	3.78E-07
1.64E-09	3.02E-09	5.02E-09	1.04E-08	3.06E-08
4.38E-10	8.96E-10	1.49E-09	3.85E-09	9.61E-09
4.24	3.85	4.03	3.24	3.64
1.15	1.16	1.21	1.21	1.15

ID		9-BF	9-BNF	10-BF	10-BNF	1	2
CO _x	(g)	/	/	/	/	0.025	0.07
S/L	g/L	/	/	/	/	39.4	39.4
	±	/	/	/	/	0.6	0.6
U(VI) initial	mol/L	2.40E-05		5.63E-08		5.64E-08	1.58E-07
	±	1.24E-06		2.95E-09		2.95E-09	7.56E-09
pH	/	7.27	7.27	7.34	7.34	7.49	7.5
Temp	°C	18.9	18.9	18.9	18.9	18.2	18.2
U(VI) eq.	mol/L	2.40E-05	2.41E-05	5.68E-08	5.73E-08	5.13E-08	1.34E-07
	±	1.09E-06	1.13E-06	2.52E-09	2.52E-09	2.31E-09	6.30E-09
U(VI) sorb.	mol/g	/	/	/	/	1.29E-10	5.95E-10
	±	/	/	/	/	5.87E-11	1.60E-10
K _b	mL/g	/	/	/	/	2.52	4.42
	±	/	/	/	/	1.15	1.21

Table C. 53. Experimental results of the sorption isotherms of U(VI) onto Callovo-Oxfordian claystone samples at 80 °C in 5% of CO₂(g) in Callovo-Oxfordian porewater at fixed solid-liquid ratio.

1	2	3	4	5	6	7
0.051	0.05	0.051	0.049	0.05	0.05	0.051
2.04	2	2.04	1.96	2	2	2.04
0.05	0.05	0.05	0.05	0.05	0.05	0.05
2.66E-08	7.44E-08	1.59E-07	3.19E-07	2.71E-06	8.12E-06	2.16E-05
1.42E-09	3.64E-09	8.15E-09	1.65E-08	1.43E-07	4.43E-07	1.20E-06
6.84	6.84	6.84	6.86	6.86	6.85	6.84
81.3	81.6	81.2	76.7	80.2	81.3	81.8
1.82E-08	5.02E-08	1.16E-07	2.47E-07	2.16E-06	7.05E-06	1.88E-05
1.68E-09	3.36E-09	6.72E-09	1.26E-08	1.18E-07	3.49E-07	9.24E-07
4.08E-09	1.21E-08	2.13E-08	3.65E-08	2.71E-07	5.36E-07	1.38E-06
1.08E-09	2.50E-09	5.21E-09	1.06E-08	9.28E-08	2.82E-07	7.42E-07
223.6	241	183.3	147.9	125.2	76	73.5
62.8	52.3	46.1	43.7	43.4	40.2	39.6

Impact of Increasing the Temperature up to 80 °C on the Behaviour of Radionuclides in Callovo-Oxfordian Formation:
Application to Uranium

ID		8-BF	8-BNF	9-BF	9-BNF
Claystone	(g)	/	/	/	/
S/L	g/L	/	/	/	/
	±	/	/	/	/
U(VI) ini.	mol/L	2.66E-08	2.66E-08	2.16E-05	2.16E-05
	±	1.38E-09	1.38E-09	1.15E-06	1.15E-06
pH	/	6.79	6.79	6.8	6.8
Temp	°C	79.1	79.1	80	80
U(VI) eq.	mol/L	2.49E-08	2.45E-08	2.13E-05	2.12E-05
	±	1.85E-09	1.81E-09	1.01E-06	1.01E-06
U(VI) sorb.	mol/g	/	/	/	/
	±	/	/	/	/
K _b	ml/g	/	/	/	/
	±	/	/	/	/

Appendix D: Modelling results

D.1. Geochemical modelling literature data for the Ca-U(VI)-CO₃ ternary species

The Ca-U(VI)-CO₃ complexes have been studied in different experimental conditions (Bernhard et al., 2001; Dong and Brooks, 2006; Endrizzi and Rao, 2014; Kalmykov and Choppin, 2000; Lee and Yun, 2013). In Table D. 1, a summary of the experimental conditions considered for each work and the thermodynamic data for the Reaction 1 and Reaction 2 (see Chapter 2) are presented.

Calculations of the experimental conditions from the literature data were performed using Phreeqc with ThermoChimie database taking in account the ionic strength corrections (Davies or SIT conventions) (Giffaut et al., 2014). The results of the speciation of U(VI) as a function of Ca in solution and the saturation indexes of the most relevant minerals for each work are indicated in the following Figures (D. 1 to D. 4). These geochemical calculations are useful for evaluate the geochemical conditions of each work and evaluate the possible precipitation of solid phases. They are also useful for the comparison with the present Ph.D-work.

It should be noted Dong and Brooks (2006) data was already shown and discussed in Chapter 2, therefore we will not be shown here.

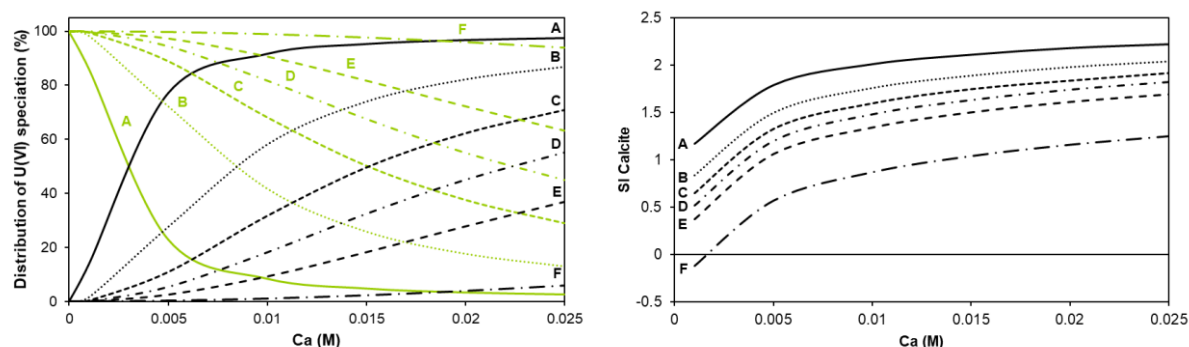


Figure D. 1. Left: distribution of the U(VI) (black-lines: $\text{Ca}_2\text{UO}_2(\text{CO}_3)_3(\text{aq})$; green-lines: $\text{UO}_2(\text{CO}_3)_3^{4-}$); Right: saturation index of Calcite as a function of calcium for: A) $I = 0.1 \text{ m}$; B) $I = 0.3 \text{ m}$; C) $I = 0.5 \text{ m}$; D) $I = 0.7 \text{ m}$; E) $I = 1 \text{ m}$; and F) $I = 3 \text{ m}$ from Kalmykov and Choppin (2000) using ThermoChimie database SIT (2009).

Table D. 1. Summary of the main parameters used for determination of stability constants of Ca-U(VI)-CO₃ complexes using different experimental methods (n.d.: not determined).

IS	pH	pCO ₂	Experimental method	Observations	References
0.1	2 – 10 and 8.1	10 ^{-3.5}	Anion exchange resin	Seepage solution at pH between 2 and 10	(a)
			TRLFS	Synthetic solution of: [UO ₂ ²⁺] = 1.1·10 ⁻⁵ M; [CO ₃ ²⁻] = 1·10 ⁻³ M; [Ca ²⁺] = 2·10 ⁻² M at pH 8; 0.1 M NaClO ₄	
				Temperature of 25 °C and pCO ₂ atmospheric	
				All samples were filtrated using 15 nm and 1 nm cellulose acetate filters; more than 98 %wt of U _{initial} was adsorbed;	
0.1 – 3	8.1	10 ^{-3.5}	TRLFS	Synthetic solution: [U(VI)] = 3.35·10 ⁻⁵ M; [CO ₃ ²⁻] = 7·10 ⁻³ M; [Ca ²⁺] = 1·10 ⁻³ – 2.5·10 ⁻² M at pH 8.1; Δ[NaClO ₄]	(b)
				Temperature of 25 °C and pCO ₂ atmospheric	
				All samples were filtrated with 0.2 μm cellulose acetate membrane filters	
0.1	8	10 ^{-3.5}	TRLFS	Synthetic solution: [U(VI)] = 2·10 ⁻⁵ – 1·10 ⁻⁴ M; [Ca ²⁺] = 1·10 ⁻⁴ – 1·10 ⁻² M; [HCO ₃ ⁻ /CO ₃ ²⁻] = 8·10 ⁻³ M; 0.1 M NaClO ₄	(c)
			Competition of Ca ²⁺ with EDTA ⁴⁻	EDTA ⁴⁻ was adjusted to pH 8 to titrate the [Ca ²⁺]	
				Temperature of 25 °C and pCO ₂ atmospheric	
				Comparison with chemical composition of natural and synthetic Liebigite by EXAFS analysis	
0.1	8.1	10 ^{-3.5}	Anion exchange resin	Synthetic solution: [U(VI)] = 1–50 μM; [Ca ²⁺] = 0.1–5 mM; at pH 8.1; 0.1 M NaNO ₃	(d)
				All samples were maintained in equilibrium with atmospheric CO ₂ (g) by bubbling with air at 25 °C	
				All samples were filtrated using 2 μm polysulfone filters and acidified	
				Experiments conducted in duplicate with resin-free controls	
				Desorption experiments were performed to correct the U distribution coefficients	
0.1	7.4 – 9	10 ^{-3.5}	TRLFS	Synthetic solution: [U(VI)] = 1·10 ⁻⁴ M; [CO ₃ ²⁻] = 5·10 ⁻² M; [Ca ²⁺] = 1·10 ⁻⁵ – 1·10 ⁻¹ M; [EDTA] = 0.1 M at pH 7 and 9; ionic strength controlled by Na/HClO ₄ .	(e)
			Competition of Ca ²⁺ with EDTA ⁴⁻	Samples equilibrated with CO ₂ (g) atmospheric	
0.1 and 0.5	10	10 ^{-3.5}	Ca ²⁺ ion selective electrode potentiometry	Synthetic solution: [U(VI)] = 0.2 – 1 mM; [CO ₃ ²⁻] = 0.8 – 4 mM; [Ca ²⁺] = 10 mM at pH 10; 0.1 and 0.5 M NaCl	(f)
				Temperature of 25 °C and atmospheric conditions	
			Microcalometry	Microcalometry experiments performed at low temperature with a solution of [U(VI)] = 0.2 – 0.5 mM; [CO ₃ ²⁻] = 0.8 – 2 mM; [Ca ²⁺] = 10 mM in 0.1 M of NaCl.	
0.1	8	10 ^{-3.5}	TRLFS	Synthetic solution: [U(VI)] = 4 – 44 mM; [Ca ²⁺] = 0 – 3.3 mM; [CO ₃ ²⁻] = 15 mM; Na/HClO ₄ control the ionic strength of the media	(g)
				The concentration of U(VI) changes according to the temperature of the system	
			Competition of Ca ²⁺ with EDTA ⁴⁻	Temperature 10 – 70 °C and pCO ₂ atmospheric	

(a) Bernhard et al. (1996); (b) Kalmykov and Choppin (2000); (c) Bernhard et al. (2001); (d) Dong and Brooks (2006); (e) Lee and Yun (2013); (f) Endrizzi and Rao (2014); (g) Jo and Yun (2017)

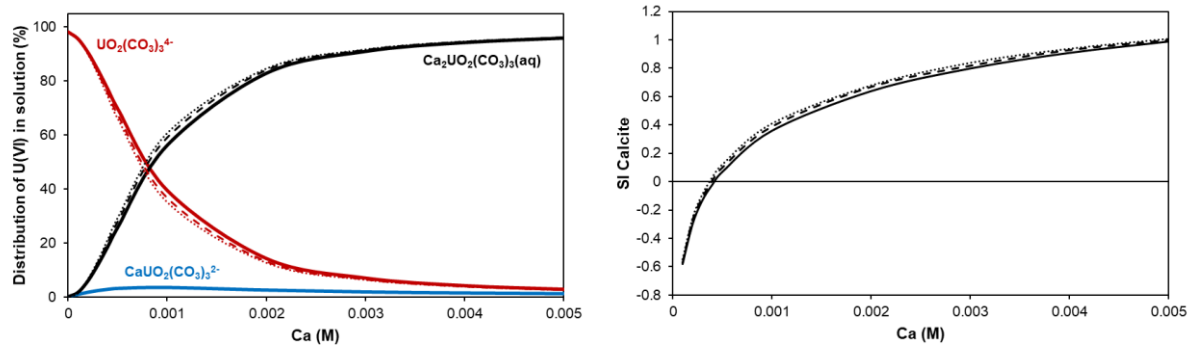


Figure D. 2. (left) distribution of U(VI) speciation and (right) saturation index of Calcite as a function of the calcium concentration considering the experimental conditions of Bernhard et al. (2001) using Thermochemie database Davies (2014). Solid-line: $\text{U(VI)} = 1 \cdot 10^{-4}$ M; dash-line: $\text{U(VI)} = 5 \cdot 10^{-5}$ M; dot-line: $\text{U(VI)} = 2 \cdot 10^{-5}$ M.

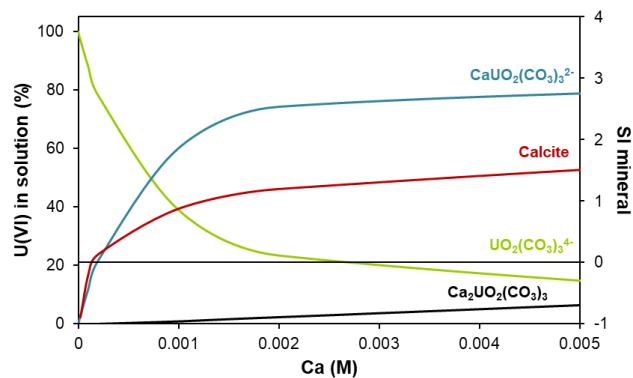


Figure D. 3. Distribution of U(VI) speciation and the saturation index of calcite as a function of the calcium concentration considering the experimental conditions of Lee and Yun (2013) using Thermochemie database Davies (2014).

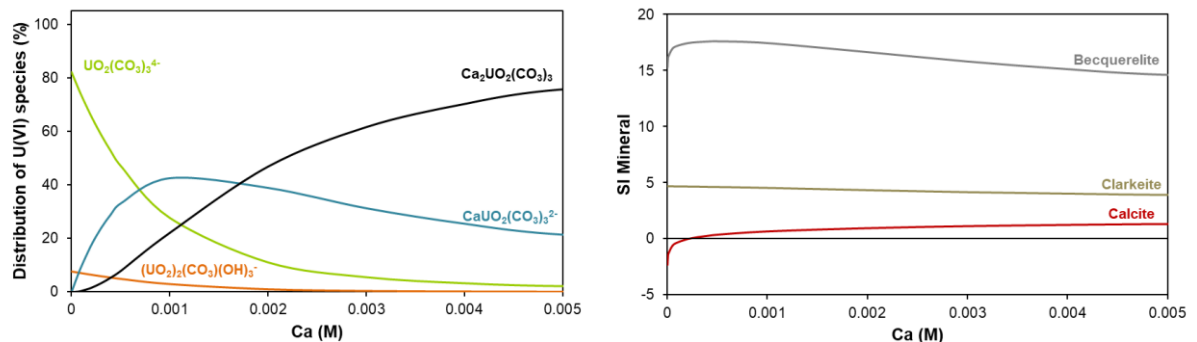


Figure D. 4. (left) distribution of U(VI) speciation and (right) mineral saturation index as a function of the calcium concentration considering the experimental conditions of Endrizzi and Rao (2006) using Thermochemie database Davies (2014).

D.2. Ionic exchange method

D.2.1. Type I experiments ($\Delta S/L$):

Table D. 2. Modelling results using PEST coupled to Phreeqc for experiments as a function of S/L in the absence of Ca at 20 °C and 1% of CO₂(g)

Experimental				Modelled
S/L		U(VI) sol		
mL/g	±	µmol/L	±	µM
1.2476	0.06238	0.087395	0.007983	0.093707
2.6596	0.13298	0.04916	0.007983	0.042252
5.072667	0.370841	0.026471	0.008824	0.022362
10.61333	0.775895	0.013866	0.007143	0.011844
15.15733	1.108088	0.011345	0.007143	0.008081
20.939	2.186096	0.009244	0.007143	0.006135
25.824	2.696105	0.006429	0.002731	0.005009

Table D. 3. Modelling results using PEST coupled to Phreeqc for experiments as a function of S/L in the absence of Ca at 40 °C and 1% of CO₂(g)

Experimental				Modelled
S/L		U(VI) sol		
mL/g	±	µmol/L	±	µM
1.0308	0.05154	0.115126	0.008403	0.035137
2.5324	0.12662	0.059664	0.010504	0.092077
5.068	0.3705	0.034034	0.006303	0.225963
10.038	0.733835	0.017227	0.005882	0.45691
25.31818	2.667801	0.012185	0.006303	1.518603

Table D. 4. Modelling results using PEST coupled to Phreeqc for experiments as a function of S/L in the absence of Ca at 60 °C and 3% of CO₂(g)

Experimental				Modelled
S/L		U(VI) sol		U(VI) sol
mL/g	±	µmol/L	±	µM
1.0244	0.05122	0.110084	0.006723	0.031181
2.5008	0.12504	0.062941	0.003992	0.07871
4.958667	0.362507	0.035588	0.003067	0.199101
9.824667	0.718239	0.024916	0.002941	0.400656
25.51	2.663322	0.017059	0.002815	1.37519

Table D. 5. Modelling results using PEST coupled to Phreeqc for experiments as a function of S/L in the absence of Ca at 80 °C and 5% of CO₂(g)

Experimental				Modelled
S/L		U(VI) sol		U(VI) sol
mL/g	±	µmol/L	±	µM
1.016	0.0508	0.147899	0.007563	0.017524
2.496644	0.123794	0.090756	0.005042	0.049778
5.074	0.370938	0.048109	0.003319	0.164974
9.934667	0.726281	0.055	0.003487	0.318007
14.786	1.080941	0.055798	0.003319	0.472435
19.618	2.048179	0.045168	0.002983	0.916948
24.639	2.572387	0.035294	0.002983	

D.2.2. Type II experiments (ΔCa):

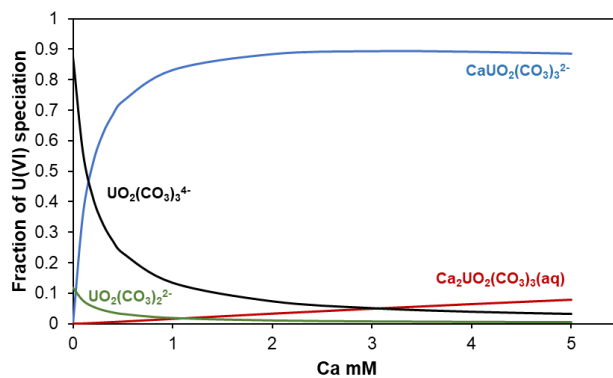


Figure D. 5. Distribution of U(VI) speciation at 20°C and 1% of CO₂(g) taking the $\log_{10}\beta_{113} = 27.4 \pm 0.1$ and $\log_{10}\beta_{213} = 29.8 \pm 1.1$ (calculated from PEST-Phreeqc).

Table D. 6. Modelling results using PEST coupled to Phreeqc for experiments as a function of Ca at fixed S/L, 20 °C and 1% of CO₂(g)

Ca	Experimental		Modelled
	U(VI) sol		U(VI) sol
mM	µM	±	µM
0	0.044538	0.016807	0.016043
0.1	0.081513	0.015966	0.015756
0.2	0.094118	0.015966	0.015512
0.3	0.107143	0.015546	0.015625
0.4	0.128151	0.015546	0.015514
0.5	0.133613	0.015966	0.015399
1	0.193697	0.018067	0.015589
2	0.24958	0.018067	0.015566
3	0.316807	0.02605	0.017134
4	0.369328	0.036134	0.019805
5	0.401681	0.037815	0.020129

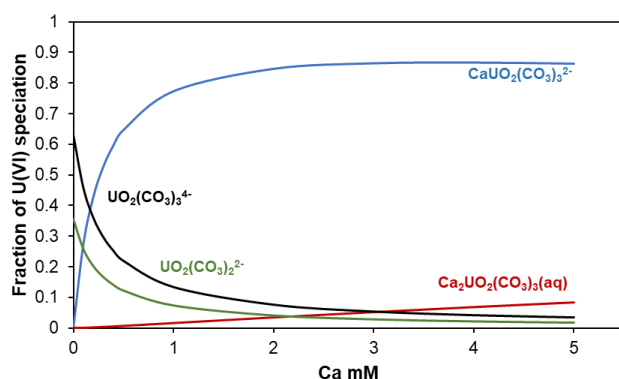


Figure D. 6. Distribution of U(VI) speciation at 40°C and 1% of CO₂(g) taking the $\log_{10}\beta_{113} = 27.2 \pm 0.1$ and $\log_{10}\beta_{213} = 29.9 \pm 0.7$ (calculated from PEST-Phreeqc).

Table D. 7. Modelling results using PEST coupled to Phreeqc for experiments as a function of Ca at fixed S/L, 40 °C and 1% of CO₂(g)

Ca mM	Experimental U(VI) sol		Modelled U(VI) sol
	μM	±	μM
0	0.051681	0.011345	0.030333
0.1	0.060924	0.013025	0.031205
0.2	0.07605	0.014286	0.03097
0.3	0.086975	0.015126	0.031266
0.4	0.097899	0.015966	0.030772
0.5	0.108403	0.017227	0.031409
1	0.159244	0.020168	0.03137
2	0.244538	0.033613	0.033017
3	0.294118	0.042017	0.034205
4	0.32605	0.039916	0.033902
5	0.361345	0.046218	0.035633

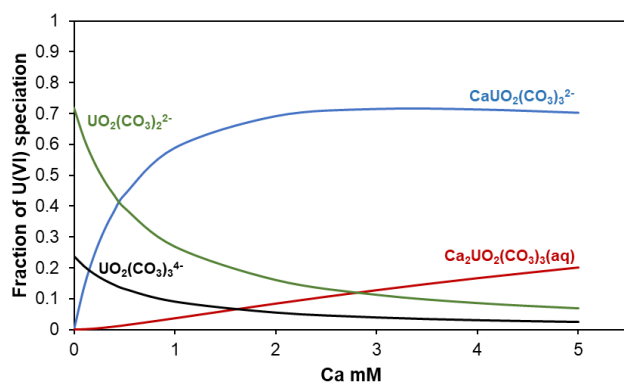


Figure D. 7. Distribution of U(VI) speciation at 60°C and 3% of CO₂(g) taking the $\log_{10}\beta_{113} = 26.7 \pm 0.03$ and $\log_{10}\beta_{213} = 29.6 \pm 0.1$ (calculated from PEST-Phreeqc).

Table D. 8. Modelling results using PEST coupled to Phreeqc for experiments as a function of Ca at fixed S/L, 60 °C and 3% of CO₂(g)

Ca mM	Experimental U(VI) sol		Modelled U(VI) sol
	μM	±	μM
0	0.040756	0.008403	0.014631
0.1	0.055462	0.008824	0.015316

0.2	0.047479	0.007983	0.01524
0.3	0.055882	0.007563	0.015208
0.4	0.063866	0.009664	0.014757
0.5	0.070588	0.009664	0.015334
1	0.101261	0.012185	0.015385
2	0.159244	0.015546	0.015763
3	0.217647	0.015126	0.01539
4	0.266387	0.015966	0.015445
5	0.310084	0.019748	0.016072

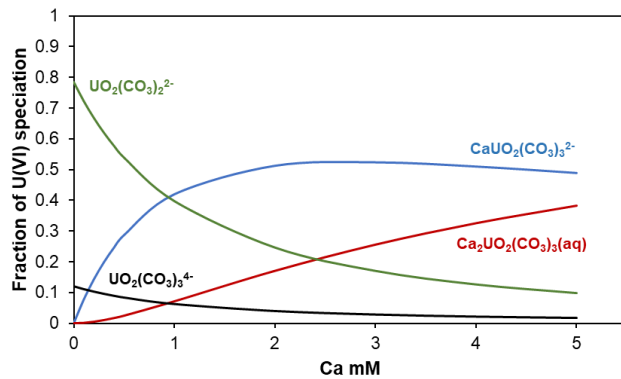


Figure D. 8. Distribution of U(VI) speciation at 80°C and 5% of CO₂(g) taking the $\log_{10}\beta_{113} = 26.5 \pm 0.1$ and $\log_{10}\beta_{213} = 29.7 \pm 0.1$ (calculated from PEST-Phreeqc).

Table D. 9. Modelling results using PEST coupled to Phreeqc for experiments as a function of Ca at fixed S/L, 80 °C and 5% of CO₂(g)

Ca mM	Experimental U(VI) sol		Modelled U(VI) sol
	μM	\pm	μM
0	0.062185	0.004622	0.015296
0.1	0.068487	0.005042	0.015409
0.2	0.071849	0.004622	0.01536
0.3	0.07395	0.005042	0.015075
0.4	0.078992	0.005042	0.015228
0.5	0.083613	0.005042	0.01534
1	0.109244	0.005882	0.015218
2	0.172269	0.008403	0.014924
3	0.22437	0.010084	0.015134
4	0.286975	0.015126	0.01568
5	0.320168	0.015966	0.015595

Appendix E: Thermodynamic data

In this appendix the thermodynamic data included in ThermoChimie database (Giffaut et al., 2014) for Ca-UO₂²⁺-CO₃²⁻-Na⁺-NO₃⁻-H₂O systems are shown in Table E. 10 and E. 11. This thermodynamic data is useful for the experiments of the ionic exchange and sorption of U(VI) on Illite, Callovo-Oxfordian clay fraction and claystone samples. All the geochemical model calculations were performed taking in account these thermodynamic data.

Table E. 1. Thermodynamic data for the aqueous species considered for the calculation of stability constants of Ca-U(VI)-CO₃ complexes. Note that log₁₀ β° values and enthalpies of reaction are in agreement with the chemical reactions that are included in ThermoChimie database v.9

Component	log ₁₀ β°	Δ _r H°
CO ₂ (g)	-18.15	4.11
H ₂ O(g)	1.50	-44.004
OH ⁻	-14.0	55.815
Ca(OH) ⁺	-12.78	77.206
CO ₂ (aq)	16.68	-23.860
HCO ₃ ⁻	10.33	-14.70
Ca(HCO ₃) ⁺	11.43	-23.597
CaCO ₃ (aq)	3.22	14.830
Na(CO ₃) ⁻	1.27	37.279
Na(HCO ₃)(aq)	10.08	-26.127
(UO ₂) ₁₁ (CO ₃) ₆ (OH) ₁₂ ²⁻	36.43	No data available
(UO ₂) ₂ (CO ₃)(OH) ₃ ⁻	-0.86	No data available
(UO ₂) ₂ (OH) ³⁺	-2.70	14.354
(UO ₂) ₂ (OH) ₂ ²⁺	-5.62	37.595
(UO ₂) ₃ (CO ₃)(OH) ₃ ⁺	0.66	81.159
(UO ₂) ₃ (CO ₃) ₆ ⁶⁻	54.0	-62.7
(UO ₂) ₃ (OH) ₄ ²⁺	-11.9	84.264
(UO ₂) ₃ (OH) ₅ ⁺	-15.55	97.063
(UO ₂) ₃ (OH) ₇ ⁻	-32.20	229.868
(UO ₂) ₄ (OH) ₇ ⁺	-21.90	No data available
UO ₂ (OH) ⁺	-5.25	43.458
UO ₂ (OH) ₂ (aq)	-12.15	111.16
UO ₂ (OH) ₃ ⁻	-20.25	148.06
UO ₂ (OH) ₄ ²⁻	-32.40	156.138
UO ₂ (NO ₃) ⁺	0.1	3.90
UO ₂ (CO ₃) (aq)	9.94	5.0
UO ₂ (CO ₃) ₂ ²⁻	16.61	18.50
UO ₂ (CO ₃) ₃ ⁴⁻	21.84	-39.20
UO ₂ (CO ₃) ₃ ⁵⁻	6.95	No data available
CaUO ₂ (CO ₃) ₃ ²⁻	in study	in study
Ca ₂ UO ₂ (CO ₃) ₃	in study	in study

Table E. 2. Thermodynamic data for the solid phases considered for the calculation of stability constants of Ca-U(VI)-CO₃ complexes. Note that log₁₀K and enthalpies of reaction are in agreement with the chemical reactions that are included in ThermoChimie database v.9.

Component	log ₁₀ K°	Δ _r H°
Aragonite	-8.31	-10.454
Becquerelite(nat)	29.0	-378.31
Becquerelite(syn)	40.5	No data available
C(cr)	53.83	-377.266
Ca(NO ₃) ₂ (s)	5.89	No data available
Ca(s)	139.84	-822.763
CaCO ₃ :H ₂ O(s)	-7.6	-5.77
Calcite	-8.48	-10.62
CaO(cr)	32.7	-193.91
CaU ₂ O ₇ :3H ₂ O(cr)	23.4	No data available
Clarkeite	9.4	-106.3
Gaylussite	-9.43	31.099
Na(cr)	67.385	-380.222
Na(NO ₃)(s)	1.09	No data available
Na ₂ (CO ₃)(cr)	1.12	-26.71
Na ₂ CO ₃ :7H ₂ O(s)	-0.46	42.682
Na ₂ O(cr)	67.46	-351.71
Nahcolite	-10.74	33.43
Natron	-0.83	64.87
Pirssonite	-8.91	9.58
Portlandite	22.81	-130.078
Rutherfordine	-14.76	-2.929
Schoepite	5.96	No data available
Schoepite(des)	5.0	-55.777
Sodium-compreignacite	39.4	-517.390
Thermonatrite	0.48	-12.04
Trona	-11.38	38.96
U(cr)	178.81	-1150.726
U ₂ O ₇ Na ₂ (s)	22.6	-172.37
UO ₂ (CO ₃) ₃ Na ₄ (cr)	-27.18	No data available
UO ₂ (OH) ₂ (beta)	4.93	-56.86
Vaterite	-7.9	-14.93

Appendix F: PEST and PhreeqC files

In this appendix, the input and output files from both PEST and PhreeqC are given as an example for all type of modelling calculations.

PEST input files:

20 °C and 1% of CO₂(g) as a function of S/L ratio

Template file:

```
ptf @

EXCHANGE_MASTER_SPECIES
  X          X+

EXCHANGE_SPECIES
X+ = X+
  log_k      0

X+ + NO3- = XNO3
  log_k 0.0

4X+ + UO2 (CO3) 3-4 = X4UO2 (CO3) 3
  log_k      @kx1          @ #unknown

PHASES
fix_pH
H+ = H+
log_k 0.0

CALCULATE_VALUES
ratio
-start
30 A = MOL("X4UO2 (CO3) 3")
40 D = TOT("U(6)")
50 ratio = A/D
60 SAVE ratio
-end

U_ads
-start
  10 U_sorbed = SYS("U(6)") - TOT("U(6)")
  20 SAVE U_sorbed
-end

SELECTED_OUTPUT 1
  -file          fittingE1A.prn
  -totals        C U
  -calculate_values  ratio U_ads
```

Impact of Increasing the Temperature up to 80 °C on the Behaviour of Radionuclides in Callovo-Oxfordian Formation: Application to Uranium

#pH measured after equilibrium and alkalinity measured in the blank sample

```
SOLUTION 1
  temp      20
  pH        7.44
  units     mol/kgw
  Alkalinity 2.25e-3
  U         5.21e-7
  Na 0.1
  N(5) 0.1 charge
  -water   1 # kg
```

```
EXCHANGE 1
XNO3 2.62e-3
EQUILIBRIUM_PHASES 1
fix_pH -7.44 NaOH 10
Clarkeite 0 0
END
```

```
SOLUTION 2
  temp      20
  pH        7.41
  units     mol/kgw
  Alkalinity 2.25e-3
  U         5.21e-7
  Na 0.1
  N(5) 0.1 charge
  -water   1 # kg
```

```
EXCHANGE 2
XNO3 6.55e-3
EQUILIBRIUM_PHASES 2
fix_pH -7.41 NaOH 10
Clarkeite 0 0
END
```

```
SOLUTION 3
  temp      20
  pH        7.35
  units     mol/kgw
  Alkalinity 2.25e-3
  U         5.21e-7
  Na 0.1
  N(5) 0.1 charge
  -water   1 # kg
```

```
EXCHANGE 3
XNO3 1.31e-2
EQUILIBRIUM_PHASES 3
fix_pH -7.35 NaOH 10
Clarkeite 0 0
END
```

```
SOLUTION 4
  temp      20
  pH        7.24
  units     mol/kgw
  Alkalinity 2.25e-3
  U         5.21e-7
  Na 0.1
  N(5) 0.1 charge
  -water   1 # kg
```

```
EXCHANGE 4
XNO3 2.62e-2
EQUILIBRIUM_PHASES 4
fix_pH -7.24 NaOH 10
Clarkeite 0 0
END
```

```

SOLUTION 5
  temp      20
  pH        7.2
  units     mol/kgw
  Alkalinity 2.25e-3
  U         5.21e-7
  Na 0.1
  N(5) 0.1 charge
  -water   1 # kg
EXCHANGE 5
XNO3 3.93e-2
EQUILIBRIUM_PHASES 5
fix_pH -7.2 NaOH 10
Clarkeite 0 0
END

```

```

SOLUTION 6
  temp      20
  pH        7.18
  units     mol/kgw
  Alkalinity 2.25e-3
  U         5.21e-7
  Na 0.1
  N(5) 0.1 charge
  -water   1 # kg
EXCHANGE 6
XNO3 5.24e-2
EQUILIBRIUM_PHASES 5
fix_pH -7.18 NaOH 10
Clarkeite 0 0
END

```

```

SOLUTION 7
  temp      20
  pH        7.14
  units     mol/kgw
  Alkalinity 2.25e-3
  U         5.21e-7
  Na 0.1
  N(5) 0.1 charge
  -water   1 # kg
EXCHANGE 7
XNO3 6.55e-2
EQUILIBRIUM_PHASES 7
fix_pH -7.14 NaOH 10
Clarkeite 0 0
END

```

Control File:

```

pcf
* control data
restart estimation
1 7 1 0 1
1 1 single point 1 0 0
5.0 2.0 0.3 0.01 10
5.0 5.0 1.0e-3
0.1
50 5e-3 4 3 0.01 3
1 1 1
* parameter groups
kx   relative 0.01 0.0   switch 2.0 parabolic
* parameter data
kx1  none      factor 1.0      -5.0      5.0      kx      1.0
      0.0      1

```

Impact of Increasing the Temperature up to 80 °C on the Behaviour of Radionuclides in Callovo-Oxfordian Formation: Application to Uranium

```
* observation groups
U_data
* observation data
U_1      8.73950E-08 1   U_data
U_2      4.91597E-08 1   U_data
U_3      2.64706E-08 1   U_data
U_4      1.38655E-08 1   U_data
U_5      1.13445E-08 1   U_data
U_6      9.24370E-09 1   U_data
U_7      6.42857E-09 1   U_data
* model command line
phreeqc fittingE1A.pqi fittingE1A.pqi ThermoChimie_PHREEQC_Davies_v9b0.dat
* model input/output
fittingE1A.tpl fittingE1A.pqi
fittingE1A.ins fittingE1A.prn
```

80 °C and 5% of CO₂(g) [U(VI)] as a function of calcium

Template file:

```
ptf @

EXCHANGE_MASTER_SPECIES
  X          X+

EXCHANGE_SPECIES
X+ = X+
  log_k      0

X+ + NO3- = XNO3
  log_k 0.0

4X+ + UO2(CO3)3-4 = X4UO2(CO3)3
  log_k      @kx2          @ #0.70068 #unknown

PHASES
fix_pH
H+ = H+
log_k 0.0

CALCULATE_VALUES
ratio
-start
20 B = MOL("X4UO2(CO3)3")
#30 B = MOL("X2UO2(CO3)2")
40 D = TOT("U(6)")
50 ratio = (B)/D
60 SAVE ratio
-end

U_ads
-start
  10 U_sorbed = SYS("U(6)") - TOT("U(6)")
  20 SAVE U_sorbed
-end

SELECTED_OUTPUT 1
  -file          fittingE5B.prn
  -totals        C U
  -calculate_values  ratio U_ads
```

```

SOLUTION 1
  temp      80
  pH        6.9
  units     mol/kgw
  Alkalinity 2.2e-3
  U         4.93E-07
  Na        0.1
  N(5)     0.1 charge
  -water    1 # kg
EXCHANGE 1
XNO3 2.62e-3 #1 g/L
EQUILIBRIUM_PHASES 1
fix_pH -6.9 HNO3 10
Clarkeite 0 0
END

```

```

SOLUTION 2
  temp      80
  pH        6.89
  units     mol/kgw
  Alkalinity 2.2e-3
  U         4.93E-07
  Na        0.1
  N(5)     0.1 charge
  -water    1 # kg
EXCHANGE 2
XNO3 6.55e-3 #2.5 g/L
EQUILIBRIUM_PHASES 2
fix_pH -6.89 HNO3 10
Clarkeite 0 0
END

```

```

SOLUTION 3
  temp      80
  pH        6.77
  units     mol/kgw
  Alkalinity 2.2e-3
  U         4.93E-07
  Na        0.1
  N(5)     0.1 charge
  -water    1 # kg
EXCHANGE 3
XNO3 1.31e-2 # 5g/L
EQUILIBRIUM_PHASES 3
fix_pH -6.77 HNO3 10
Clarkeite 0 0
END

```

```

SOLUTION 4
  temp      80
  pH        6.73
  units     mol/kgw
  Alkalinity 2.2e-3
  U         4.93E-07
  Na        0.1
  N(5)     0.1 charge
  -water    1 # kg
EXCHANGE 4
XNO3 2.62e-2 #10 g/L
EQUILIBRIUM_PHASES 4
fix_pH -6.73 HNO3 10
Clarkeite 0 0
END

```

```

SOLUTION 5 rep
  temp      80
  pH        6.72

```

Impact of Increasing the Temperature up to 80 °C on the Behaviour of Radionuclides in Callovo-Oxfordian Formation: Application to Uranium

```
units      mol/kgw
Alkalinity 2.2e-3
U          4.93E-07
Na         0.1
N(5)      0.1 charge
-water    1 # kg
EXCHANGE 5
XNO3 3.93e-2 #15 g/L
EQUILIBRIUM_PHASES 5
fix_pH -6.72 HNO3 10
Clarkeite 0 0
END
```

```
SOLUTION 6 rep
temp      80
pH        6.67
units     mol/kgw
Alkalinity 2.2e-3
U         4.93E-07
Na        0.1
N(5)     0.1 charge
-water    1 # kg
EXCHANGE 6
XNO3 5.24e-2 #20 g/L
EQUILIBRIUM_PHASES 5
fix_pH -6.67 HNO3 10
Clarkeite 0 0
END
```

```
SOLUTION 7
temp      80
pH        6.6
units     mol/kgw
Alkalinity 2.2e-3
U         4.93E-07
Na        0.1
N(5)     0.1 charge
-water    1 # kg
EXCHANGE 7
XNO3 6.55e-2 #25 g/L
EQUILIBRIUM_PHASES 5
fix_pH -6.6 HNO3 10
Clarkeite 0 0
END
```

Control file:

```
Pcf
* control data
restart estimation
1 7 1 0 1
1 1 single point 1 0 0
5.0 2.0 0.3 0.01 10
5.0 5.0 1.0e-3
0.1
25 5e-3 4 3 0.01 3
1 1 1
* parameter groups
kx      relative 0.01 0.0  switch 2.0 parabolic
* parameter data
kx2     none      factor 1.0      -10      10      kx      1.0
        0.0      1
* observation groups
U_data
* observation data
```

```

U_1    1.4790E-07 1 U_data
U_2    9.0756E-08 1 U_data
U_3    4.8109E-08 1 U_data
U_4    5.5000E-08 1 U_data
U_5    5.5798E-08 1 U_data
U_6    4.5168E-08 1 U_data
U_7    3.5294E-08 1 U_data
* model command line
phreeqc fittingE17R.pqi fittingE17R.pqo ThermoChimie_PHREEQC_Davies_v9b0.dat
* model input/output
fittingE5B.tpl fittingE5B.pqi
fittingE5B.ins fittingE5B.prn

```

Phreeqc input files:

```

DATABASE C:\Program Files (x86)\USGS\Phreeqc Interactive 3.1.4-8929\database\Thermo-
Chimie_PHREEQC_v9.dat

```

```

TITLE Model of U(VI) coefficient distribution in COX claystone using COX porewater at 80
°C

```

```

#NO redox is consider in the experiment#

```

SOLUTION_SPECIES

```

2.000Ca+2      + 3.000CO3-2      + 1.000UO2+2      = Ca2UO2 (CO3) 3
      log_k    29.7 #    p.w.
      delta_h  0
1.000Ca+2      + 1.000UO2+2      + 3.000CO3-2      = CaUO2 (CO3) 3-2
      log_k    27.3 #    p.w.
      delta_h -27.4
2.000Mg+2      + 3.000CO3-2      + 1.000UO2+2      = Mg2UO2 (CO3) 3
      log_k    27.1 #    #17LEE/VES
      delta_h  0
1.000Mg+2      + 1.000UO2+2      + 3.000CO3-2      = MgUO2 (CO3) 3-2
      log_k    25.8 #    #17LEE/VES
      delta_h -27.4

```

PHASES

```

fix_pH
H+ = H+
log_k 0

```

EXCHANGE_MASTER_SPECIES

```

X      X-
Z      Z-

```

EXCHANGE_SPECIES

```

#illite
X- = X-
log_k    0
Na+ + X- = XNa
log_k    0
Ca+2 + 2X- = X2Ca
log_k    1.04
UO2+2 + 2X- = X2UO2
log_k    0.65
K+ + X- = XK
log_k    1.1
Mg+2 + 2X- = X2Mg
log_k    1.04
Fe+2 + 2X- = X2Fe
log_k    0.8
Sr+2 + 2X- = X2Sr
log_k    0.8

```

Impact of Increasing the Temperature up to 80 °C on the Behaviour of Radionuclides in Callovo-Oxfordian Formation: Application to Uranium

```
#smectite/illite
Z- = Z-
log_k      0
Na+ + Z- = ZNa
log_k      0
Ca+2 + 2Z- = Z2Ca
log_k      0.613
UO2+2 + 2Z- = Z2UO2
log_k      0.146
K+ + Z- = ZK
log_k      0.6
Mg+2 + 2Z- = Z2Mg
log_k      0.34
Fe+2 + 2Z- = Z2Fe
log_k      0.8
Sr+2 + 2Z- = Z2Sr
log_k      1.0

SURFACE_MASTER_SPECIES
  Surfill_s      Surfill_sOH
  Surfill_w      Surfill_wOH
  Surfill_z      Surfill_zOH
  Surfsm_s      Surfsm_sOH
  Surfsm_w      Surfsm_wOH
  Surfsm_z      Surfsm_zOH

SURFACE_SPECIES

#Illite
Surfill_sOH = Surfill_sOH
  log_k      0
Surfill_wOH = Surfill_wOH
  log_k      0
Surfill_zOH = Surfill_zOH
  log_k      0

#Acid-base reactions (protolysis)
H+ + Surfill_sOH = Surfill_sOH2+
  log_k      4.0 #Marques Fernandes 2015 from BB2009
Surfill_sOH = Surfill_sO- + H+
  log_k      -6.2
H+ + Surfill_wOH = Surfill_wOH2+
  log_k      4.0
Surfill_wOH = Surfill_wO- + H+
  log_k      -6.2
H+ + Surfill_zOH = Surfill_zOH2+
  log_k      8.5
Surfill_zOH = Surfill_zO- + H+
  log_k      -10.5

#Surface complexation reactions #marques 2015
#hydrolysis
Surfill_sOH + UO2+2 = Surfill_sOUO2+ + H+
  log_k      2.0
  delta_h    -10
H2O + Surfill_sOH + UO2+2 = Surfill_sOUO2OH + 2H+
  log_k      -3.5
  delta_h    48
2H2O + Surfill_sOH + UO2+2 = Surfill_sOUO2(OH)2- + 3H+
  log_k      -10.6
  delta_h    121
3H2O + Surfill_sOH + UO2+2 = Surfill_sOUO2(OH)3-2 + 4H+
  log_k      -19
  delta_h    156
Surfill_wOH + UO2+2 = Surfill_wOUO2+ + H+
  log_k      0.1
```

```

delta_h -10
H2O + Surfll_wOH + UO2+2 = Surfll_wOUO2OH + 2H+
log_k -5.3
delta_h 48

#carbonates
2CO3-2 + Surfll_sOH + UO2+2 = Surfll_sOUO2(CO3)2-3 + H+
log_k 17.5
delta_h 0

#Smectite
Surfsm_sOH = Surfsm_sOH
log_k 0
Surfsm_wOH = Surfsm_wOH
log_k 0
Surfsm_zOH = Surfsm_zOH
log_k 0

#Acid-base reactions (protolysis)
H+ + Surfsm_sOH = Surfsm_sOH2+
log_k 4.5
Surfsm_sOH = Surfsm_sO- + H+
log_k -7.9
H+ + Surfsm_wOH = Surfsm_wOH2+
log_k 4.5
Surfsm_wOH = Surfsm_wO- + H+
log_k -7.9
H+ + Surfsm_zOH = Surfsm_zOH2+
log_k 6.0
Surfsm_zOH = Surfsm_zO- + H+
log_k -10.5

#Surface complexation reactions
Surfsm_sOH + UO2+2 = Surfsm_sOUO2+ + H+
log_k 3.1
delta_h -10
H2O + Surfsm_sOH + UO2+2 = Surfsm_sOUO2OH + 2H+
log_k -4.6
delta_h 48
2H2O + Surfsm_sOH + UO2+2 = Surfsm_sOUO2(OH)2- + 3H+
log_k -12.6
delta_h 121
3H2O + Surfsm_sOH + UO2+2 = Surfsm_sOUO2(OH)3-2 + 4H+
log_k -20.9
delta_h 156
Surfsm_wOH + UO2+2 = Surfsm_wOUO2+ + H+
log_k 0.5
delta_h -10
H2O + Surfsm_wOH + UO2+2 = Surfsm_wOUO2OH + 2H+
log_k -5.7
delta_h 48

#Carbonates
CO3-2 + Surfsm_sOH + UO2+2 = Surfsm_sOUO2CO3- + H+
log_k 9.8
delta_h 0
2CO3-2 + Surfsm_sOH + UO2+2 = Surfsm_sOUO2(CO3)2-3 + H+
log_k 15.5
delta_h 0
CO3-2 + Surfsm_wOH + UO2+2 = Surfsm_wOUO2CO3- + H+
log_k 9.3
delta_h 0

SELECTED_OUTPUT 1
-file Kd_U_COX_80_newdeltaH_dH.sel
-high_precision true

```

Impact of Increasing the Temperature up to 80 °C on the Behaviour of Radionuclides in Callovo-Oxfordian Formation: Application to Uranium

```
-reset                false
-state                true
-calculate_values     TOT_U R(D)  U_sorbed

CALCULATE_VALUES

SYS_U
-start
10 SAVE SYS("U")
-end

TOT_U
-start
10 SAVE log10(TOT("U"))
-end

R(D)
-start
#5 if TOT("U") =0 then Kd = 1e-10 else Kd = (SYS("U") - TOT("U"))/TOT("U")/wt
10 U_ads = SYS("U")
20 U_sol = TOT("U")
30 wt = 3.94e-2
40 KD = (U_ads - U_sol)/U_sol/wt
#50 ratio = LOG10(KD)
100 SAVE log10(KD)
-end

U_sorbed
-start
05 wt = 3.94e-2
10 Total_U_sorbed = SYS("U")/(TOT("water") - TOT("U"))/wt
100 SAVE log10(Total_U_sorbed)
-end

U_sorbed_fraction
-start
10 fraction_U_sorbed = (SYS("U") - TOT("U"))/SYS("U")
100 SAVE fraction_U_sorbed
-end

SOLUTION 1 COX porewater 473-475m
temp      80
pH        7.01
pe        3
redox     pe
units     mmol/l
density   1
Alkalinity 1.4 meq/l #2.2 meq/L #
Ca        7.9
Cl        40.4
K         1.1
Mg        5.3
Na        42.7 charge
S(6)     13.8
Sr        0.2
-water   1 # kg
SAVE SOLUTION 1
END
USE SOLUTION 1
SURFACE 1
#name; total num sites or density (mol/m2); surface are (m2/g); g of mineral (considering
100 g of rock and all mineral is reactive)
Surfill_s 2.26E-05 20 11.280; Surfill_w 4.51E-04; Surfill_z 4.51E-04;
Surfsm_s 1.34E-05 39 6.720; Surfsm_w 2.69E-04; Surfsm_z 2.69E-04
-no_edl
-equilibrate 1
```

```

EXCHANGE 1
-equilibrate 1
X 1.80E-03 #illite
Z 5.85E-03 #smectite
-equilibrate 1
SAVE SOLUTION 1
SAVE SURFACE 1
SAVE EXCHANGE 1
END
USE SOLUTION 1
USE SURFACE 1
USE EXCHANGE 1
EQUILIBRIUM PHASES 1
Fix_pH -7.01 NaOH 1
REACTION 1
UO2Cl2 1
1e-10 2e-10 5e-10 8e-10 1e-9 2e-9 5e-9 8e-9 1e-8 2e-8 5e-8 8e-8 1e-7 \
2e-7 5e-7 8e-7 1e-6 2e-6 5e-6 8e-6 1e-5 2e-5 5e-5 8e-5
END

```


Titre : Impact de l'élévation de la température jusqu'à 80 °C sur le comportement des radionucléides dans le Callovo-Oxfordien : application à l'uranium

Mots clés : Ca-U(VI)-CO₃ ; sorption ; température ; illite ; les argiles du Callovo-Oxfordien ; déchets radioactifs

Résumé : Ce travail vise à comprendre et quantifier le comportement de U(VI) dans les argilites du Callovo-Oxfordien (COx), prévues pour accueillir les déchets nucléaires de haute activité en France. L'effet de la température sur ce comportement est particulièrement étudié. La première partie du travail s'est concentrée sur les propriétés thermodynamiques des complexes ternaires Ca-U(VI)-CO₃ qui contrôlent la spéciation de U(VI) en solution. Ces dernières ont été mesurées par une méthode de compétition en présence d'une résine sous pCO₂ et pH contrôlés. Les résultats indiquent que la température ne favorise pas la formation de CaUO₂(CO₃)₃²⁻ ($\log_{10} \beta^{\circ}_{113} = 27,3 \pm 0,3$; $\Delta_r H^{\circ} = -27,4 \pm 8$ kJ/mol) et n'affecte pas la formation de Ca₂UO₂(CO₃)₃(aq) ($\log_{10} \beta^{\circ}_{213} = 29,7 \pm 0,3$; $\Delta_r H^{\circ} = 0 \pm 2$ kJ/mol).

Une approche « bottom-up » avec le modèle « 2SPNE SC / CE » publié dans la littérature a été suivie pour décrire les phénomènes de sorption, en considérant que la fraction argileuse du COx (Illite et I/S) gouverne la sorption de U(VI).

Ce modèle a été appliqué avec succès pour reproduire une multitude de données expérimentales obtenues avec l'illite, la fraction argileuse du COx et les argilites du COx en fonction de paramètres clés (pH, pCO₂, [U(VI)], [Ca]) à 20 °C. Le phénomène de rétention dans les conditions in-situ est principalement régi par la sorption des complexes U(VI)-carbonate et une nouvelle constante d'équilibre de réaction de complexation de surface est proposée pour l'illite.

Une augmentation de la température à 80 °C conduit à une augmentation de la rétention de U(VI) sur le COx. Cette augmentation est accompagnée d'un changement de pCO₂ et de pH. Le modèle de rétention testé à 20 °C combiné avec les paramètres thermodynamiques décrivant le comportement de U(VI) en solution expliquent cette augmentation sans pour autant obtenir un accord satisfaisant avec l'expérience. Le modèle est amélioré en intégrant des valeurs de $\Delta_r H^{\circ}$ obtenues pour les réactions de complexation de surface à partir du système U(VI)/illite.

Title: Impact of the increase in temperature up to 80 °C on the behaviour of radionuclides in the Callovo-Oxfordian formation: application to uranium

Keywords : Ca-U(VI)-CO₃; sorption; temperature; illite; Callovo-Oxfordian claystone; radioactive waste

Abstract : The aim of this study was to understand and quantify the behaviour of U(VI) on the Callovo-Oxfordian (COx) clay which is envisioned to host high-level radioactive waste in France. The temperature effect up to 80°C on this behaviour was particularly studied. The first part of the work focussed on the thermodynamic properties of the calcium uranyl carbonate aqueous complexes which govern U(VI) speciation in solution. They were measured indirectly by sorption-based methodologies under controlled pCO₂ and pH. The results indicate that the temperature does not favour the formation of CaUO₂(CO₃)₃²⁻ ($\log_{10} \beta^{\circ}_{113} = 27.3 \pm 0.3$; $\Delta_r H^{\circ} = -27.4 \pm 8$ kJ/mol) and does not affect the formation of Ca₂UO₂(CO₃)₃(aq) ($\log_{10} \beta^{\circ}_{213} = 29.7 \pm 0.3$; $\Delta_r H^{\circ} = 0 \pm 2$ kJ/mol).

A bottom-up approach with the published "2SPNE SC/CE" model was used for describing the sorption processes, with the assumption that the clay fraction of the COx (Illite, and I/S) governs U(VI) sorption.

The model was successfully applied to reproduce a wealth of experimental data obtained with illite, the COx clay fraction and the COx clay rock as a function of key parameters (pH, pCO₂, [U(VI)], [Ca]) at 20 °C. The sorption on COx conditions is mainly governed by the sorption of U(VI)-CO₃ complexes and a new sorption constant is proposed for illite.

An increase in temperature to 80 °C leads to an increase of U(VI) retention on COx. This increase is accompanied by a change of both pCO₂ and pH. The sorption model developed at 20 °C, together with the thermodynamic parameters describing U(VI) speciation in solution, can explain this increase but without obtaining a good agreement with the experiment. The model is improved by considering $\Delta_r H^{\circ}$ values for surface complexation reactions obtained for the U(VI)/illite system.